UC Berkeley

Title

Quantifying Links Between Fire and Water Cycles Across Time, Place and Processes, in California's Sierra Nevada

Permalink

https://escholarship.org/uc/item/5f63t9qg

Author

Rakhmatulina, Ekaterina

Publication Date

2020

Peer reviewed|Thesis/dissertation

Quantifying Links Between Fire and Water Cycles Across Time, Place and Processes, in
California's Sierra Nevada

by

Ekaterina Rakhmatulina

A dissertation submitted in partial satisfaction of the

requirements for the degree of

Doctor of Philosophy

in

Civil and Environmental Engineering

in the

Graduate Division

of the

University of California, Berkeley

Committee in charge:

Professor Sally E. Thompson, Co-chair
Professor Steven Glaser, Co-chair
Professor Scott Stephens
Professor Mark Stacey

Fall 2020

Quantifying Links Between Fire and Water Cycles Across Time, Place and Processes, in
California's Sierra Nevada

Abstract

Quantifying Links Between Fire and Water Cycles Across Time, Place and Processes, in California's Sierra Nevada

by

Ekaterina Rakhmatulina

Doctor of Philosophy in Civil and Environmental Engineering

University of California, Berkeley

Professor Sally E. Thompson, Co-chair

Professor Steven Glaser, Co-chair

Drought, elevated temperatures, and extended fire seasons combine with high fuel loads to increase the scale and severity of wildfires in California. Many of these fires occur in the forested montane watersheds that provide approximately 60% of the developed water supply of the state, creating a critical nexus between water and fire from a management perspective. However, the links between hydrological and fire processes go well beyond a common dependence on forests. Both water and fire cycles are impacted by, and impact upon the growth, spread, function, and disturbance of vegetation communities. This means there are multiple processes linking plants, fire and water. With climate change projected to warm temperatures, reduce snowpack, extend fire seasons, and increase drought stress on Californian watersheds, foresters are turning to alternative forest management strategies. One such strategy involves the re-introduction of frequent mixed-severity fire into the landscape to lower fuel loads and reduce the risk of catastrophic fires. Co-benefits of this strategy are anticipated to include greater water yields and storage, and increased landscape diversity and forest resilience. In my primary study site of the Illilouette Creek Basin (in Yosemite National Park, California), this strategy has proven to be successful to date. Many important knowledge gaps remain, however, including how the strategy of re-introduce fire will impact the water cycle as climates warm, how transferable this strategy is to other basin, the potential implications of frequent burning on erosion and water quality, and how changes in water storage in fire-treated landscapes, and specifically in soil moisture, might modify the resulting fire regime. To answer these questions, this dissertation draws on satellite and field collected data, laboratory experiments, and hydrological and statistical modeling to explore fire-vegetation-water-climate feedbacks and inform future forest management in California.

Contents

List of Figures

List of Tables

Acknowledgments

Chapter 1

Introduction

1.1 Motivation

Twenty-first century California (and much of the Western US) is experiencing a combination of extended droughts and large number of catastrophic wildfire events. The state is experiencing a number of extreme conditions each year; for example, years 2012-2016 were some of the driest years on record, followed by 2017 which had extremely wet conditions. Meanwhile, wildfire activity has greatly increased. In fact, five of the six largest fires in California's recorded history occurred in 2020 alone (CalFire, 2020b). With climate change projected to warm temperatures further, reduce snowpack, extend fire seasons, and increase drought stress on Californian watersheds (Goulden & Bales, 2019), a better understanding of the dynamic interactions of fire, water, vegetation, and climate is urgently needed. Although a growing literature addresses the interactions of many of the components of these systems individually, important knowledge gaps remain (Archibald et al., 2018). My dissertation addresses several of these knowledge gaps from two complementary perspectives: (i) understanding process interactions, and (ii) understanding how changes to fire dynamics influence the interactions of these processes leading to emergent, watershed scale environmental outcomes. Specifically, from a process perspective I investigate, in Chapters 2 and 3:

1. How soil moisture - dead fuel moisture interactions affect fire risks, a process that connects the water cycle with fire risks, but which has been almost unstudied to date; and

2. How climate cycles (namely wet-dry and freeze-thaw cycles) influence post-fire soil water repellency of the Sierra Nevada soils. Water repellent soils inhibit the infiltration of rainfall, pre-disposing fire-impacted landscapes to flooding and erosion.

Throughout the dissertation, I will also lean on observations made in two watersheds in the Sierra Nevada (Illilouette Creek and Sugarloaf Creek Basins) where the historical fire

management regime of "fire suppression" was replaced with a regime of "managed wildfire" in the 1970s. This change represents a shift from no fire occurrence for approximately 80 years, to frequent fire occurrence for the past 50 years. I investigate the effect of this policy shift on watershed processes in chapter 4 and 5 of my dissertation:

3. How altering fire management strategies from suppression to fire-management impacts the hydrological states and processes of the Illilouette Creek and Sugarloaf Creek Basins in the Sierra Nevada; and

4. How changing climate might influence the hydrological response to changes in fire management regimes in the well-characterized Illilouette Creek Basin.

.

In the remainder of this introduction, I outline my conceptual model for how fire, water, vegetation, and climate impact each other. This conceptual model is strongly influenced by processes in the major study region addressed in the thesis, namely California's Sierra Nevada Mountains. Multiple locations in the Sierra Nevada Mountains are featured in my analyses. I therefore provide a detailed introduction to this region in the next section of the introduction. Lastly I introduce contemporary wildfire management strategy in the Sierra Nevada and what we know about its impacts on the ecosystems and water resources.

Despite the place-based nature of my research, the results are likely to have relevance to fire and water management in seasonally dry, snow-dominated montane systems worldwide. Globally, these regions are unified by their importance as water sources, the prevalence of fire as a disturbance mechanism, and their vulnerability to climate change.

1.2 Background 1: Fire and water interactions mediated by vegetation

Fire-vegetation feedbacks

Ecosystems generate fuel that can be consumed by fire. Fuels comprise living and dead vegetation, litter and duff. Anything that has a potential to burn on the landscape is a fuel. Dead fuel properties, such as moisture content, loading (fuel mass per unit area), and spatial distribution throughout the landscape determine fire's probability of ignition, intensity, spread, and consequently its spatial pattern (C. Miller & Urban, 2000; Van Wagtendonk, 1977; Rothermel, 1983). Typically, fires are initiated by dead fuels, which enable fires to spread and increase in their intensity until they are hot enough to consume wetter live fuels, and eventually spread into the vegetation canopy (Parsons & DeBenedetti, 1979). If ignited, live vegetation further exacerbates fire severity by providing additional fuel and increasing fire spread via ember production (Graham & McCaffrey, 2003).

Vegetation influences fire properties, and in turn, fire influences the location, composition, structure and biomass of vegetation. Fires can induce major conversions in vegetation

type, in which dominant species are eliminated and cannot regrow either due unfavorable environmental conditions post-fire (Rother et al., 2015; Davis et al., 2019), or because fire has destroyed the seed-bank (Meng et al., 2015; Young et al., 2019). These conversions are often seen after severe wildfires, for example those which convert forest vegetation into shrubland (Tepley et al., 2018; Batllori et al., 2018; Lauvaux et al., 2016). Since shrub vegetation is more likely to burn under severe fire conditions, such conversions may be permanent (Karavani et al., 2018; Coppoletta et al., 2015; Stevens-Rumann et al., 2017). In montane environments, fire can also convert forests into meadows: for example, in Lassen National Forest, fire was deemed to be the primary factor mitigating tree encroachment into meadow edges (Norman & Taylor, 2005). If regular disturbance by fire shapes vegetation, removing fire disturbance has equally huge implications. Absence of fire in mixed conifer ecosystems leads to dense forested stands with heavy fuel loads which favor shade tolerant species, such as Incense cedar and White fir which can replace fire-prone but shade intolerant Ponderosa pines (Van Wagtendonk, 1977; Norman & Taylor, 2005).

Vegetation-water feedbacks

Ecosystems not only shape fire processes, but also act as major intermediaries in the terrestrial water cycle. In a simple water balance, water enters the basin as precipitation, and leaves the basin though streamflow and evapotranspiration. Plants take up water from the soil as they photosynthesize, and the water is lost through plants' stomata as transpiration. Living vegetation is one of the largest consumers of water with transpiration accounting for ∼39% of the terrestrial water budget (Schlesinger & Jasechko, 2014). Vegetation canopy intercepts precipitation (rain and snow), from where it can sublimate or evaporate. Furthermore, vegetation modifies the local energy balance by shading the ground surface and reducing wind speeds beneath the canopy (Cristea et al., 2013, 2017; Kostadinov et al., 2019). In snow-dominated systems, such as the Sierra Nevada Mountains, between 20 and 50% (depending on the topography) of yearly precipitation is stored as snowpack (Cooper et al., 2020; Hunsaker et al., 2012). Although direct shading of the snowpack from incoming shortwave radiation limits snowmelt, this can be confounded by vegetation inhibiting outgoing long-wave radiation, which increases air temperature and promotes snowmelt. Thus, snow water equivalent can be either lower or greater in forested vegetation in comparison to similar open areas, depending on which of these processes dominates (Hotovy & Jenicek, 2020; Revuelto et al., 2020; Kostadinov et al., 2019; Lundquist et al., 2013). Because of the impacts of fire disturbance on post-fire vegetation properties, fires can indirectly impact the water balance. For example, low to moderate severity fires can remove under-story vegetation which has high transpiration rates (Jayasuriya et al., 1993), leaving bigger and older species alive and reducing transpiration immediately post-fire. Recovery of understorey plants or re-sprouting, however, can cause transpiration rates to increase several years post fire (Tague et al., 2019). High-severity fires that remove all vegetation reduce transpiration, but may increase soil evaporation as the soil albedo is reduced (Quintano et al., 2019) and shading removed (Breshears et al., 1998).

Fire-water feedbacks

Fire processes are also influenced by water availability. As the landscape becomes water-limited, vegetation may die from inability to photosynthesize as stomata close due to water stress, or from vulnerability to insect attacks as a result of lowered sap flow rates (Raffa et al., 2008). As vegetation dies, landscape fire risks increase, since dead vegetation is both more flammable than live vegetation and creates a connected network of ground fuels, assisting fire propagation. Soil moisture can influence moisture levels of dead vegetation as well. C. Miller & Urban (2000) concluded that fuel moisture conditions (both wet and dry) can override the effect of fuel accumulation; if the fuels are dry, a risk of large fires will be present even if the fuel loads are low. The reverse is also true; if the fuels are wet, even dense and continuous fuel accumulations may not result in fire propagation. These fuel moisture effects may be particularly important in complex terrain, where valleys and poleward aspects may retain moisture longer than sun exposed terrain, creating natural fire breaks.

In addition to fire disturbance impacting the water cycle through its impacts on vegetation, fires also affect hydrology by modifying soil properties. In particular, heat can change soil bulk density and aggregate stability (Nimmo, 2005; Giovannini et al., 1983; Kořenková & Matúš, 2015). Heating can increase soil water repellency when soil organic matter gets vaporized during heating and condenses on soil particles during cooling, creating a hydrophobic coating (DeBano & Krammes, 1966). All of these factors contribute to a decrease in soil water infiltration, enhancing ponding of water on the soil surface, which can contribute to post-fire flooding and erosion (Keeley, 2009; Mataix-Solera et al., 2011; Stoof et al., 2011; Caon et al., 2014; Stoof et al., 2015). Where vegetation is removed by fire, flooding and erosion is likely to be more severe, since vegetation reduces rain splash erosion and retains surface water on the landscape, which can promote infiltration (Assouline & Mualem, 1997). Lastly, wildfires often create an ash layer which in some cases is associated with clogging of soil pores and reductions in infiltration (Woods & Balfour, 2010).

Climate

The fire-water-vegetation interactions above create a complex three-way feedback system which is likely to be further complicated by climate change. For example, increasing temperatures will elevate snowlines in montane watersheds (Hatchett et al., 2017), causing a shift to earlier snowmelt, peak streamflow, and the start of the growing season (Stewart et al., 2004; North et al., 2012). Prolonged droughts and the longer growing season will lead to drier fuel conditions and higher vegetation mortality, increasing fire risk (Nolan et al., 2020; Flannigan et al., 2015). Yet water stress could ultimately decrease vegetation density and therefore fuel loading, thus reducing the spread of fire (Hurteau et al., 2019). To manage the joint risks of fire and water stress under a warming climate, these interactions need to be understood.

1.3 Background 2: Sierra Nevada ecosystems

Fire-water-vegetation-climate feedbacks are important drivers of ecosystem processes in the Sierra Nevada mountain range in the western United States. The Sierra Nevada is a 63,100 km^2 mountain range primarily situated in the state of California, occupying 24% of the state's area, with portions extending into the state of Nevada. The range runs 640 km north-south, starting at the Mojave Desert in the south and terminating at the Cascade range in the north. The Sierra Nevada is about 105 km wide in the east-west direction and is bordered by the Central Valley of California to the west and the Great Basin to the east (Minnich & Padgett, 2003). At its foothills in the west, Sierra Nevada starts at ∼300 m, and reaches a maximum height of 4,396 m (Mount Whitney), with mean elevations being highest in the Southern portion of the range (Schoenherr, 2017a).

The mountain range is composed of a granitic block that was uplifted along the Sierra Nevada fault system. The uplift created gentle western slopes compared to the steeper eastern slopes (Minnich & Padgett, 2003). The soil across the Sierra Nevada is relatively young and shallow (Meyer et al., 2007), coarse grains and well-draining (E. Moghaddas & Hubbert, n.d.). At elevations above 1,543 m (5,000 ft), vegetated areas are often interspersed with granite outcrops (Rundel, 1975).

The Sierra Nevada is a crucial resource for California's economy (Klausmeyer & Fitzgerald, 2012; California Department of Food and Agriculture, 2019), human well-being, ecosystem health (Millar, 1996), and biodiversity (Richter et al., 2019). Sierra Nevada ecosystems are fire prone and dynamic, and experience a highly volatile climate characterized by extensive inter-annual variability in precipitation (Taylor & Beaty, 2005). Droughts are often relieved by precipitation-heavy years (Swain et al., 2018). Under natural conditions, wildfire is a ubiquitous component of this landscape, impacting local ecosystems, downstream communities and infrastructure (Millar & Stephenson, 2015).

Climate Trends

The Sierra Nevada mountain range experiences a Mediterranean climate with warm dry summers and cool wet winters. Climate varies with elevation and latitude across the Sierra Nevada; temperature drops ∼ 1°C per 100 m of elevation (Millar, 1996), while precipitation increases with elevation, reaching a peak of 180 cm/year on the western slope. The eastern slope is in the rain-shadow and much drier than the western, receiving an average of only 50 cm of precipitation a year (Schoenherr, 2017b). Additionally, precipitation increases with latitude; from 75 cm/yr in the south to 225 cm/yr in the north (for a common altitude of 1500 m Millar, 1996).

Precipitation form is also very important for ecosystems across the Sierra Nevada (Barbour et al., 1991). The transition between precipitation falling as rain and precipitation falling as snow is called the snowline (Erman, 1997). The snowline influences water storage dynamics and vegetation distributions across elevations. Above the snowline, up to 90% of Sierra Nevada's yearly precipitation occurs as snowfall (Millar, 1996; Dolanc et al., 2014),

compared to 47% for the entire Sierra Nevada range (Jepsen et al., 2016). The snowline is located around 1,500 m today, but is rising as fast as 72 m/yr (Hatchett et al., 2017) due to climate warming. Snowpack is predicted to decline by 20-90% by 2100 (North et al., 2012).

California has a large variation in inter-annual precipitation totals, which correlate with global patterns of El Niño-Southern Oscillation (ENSO) (Jong et al., 2016; Dettinger et al., 2011). During La Niña ocean cooling, California receives below average precipitation, and during the El Niño ocean warming counterpart, California receives above-average precipitation (Jong et al., 2016). In addition to inter-annual climate variations, climate change is projected to shift multi-decadal precipitation and temperature baselines; average temperatures in the Sierra Nevada are expected to increase by 1.1-2.2^{o}C in the winter and 2.2-4.4^o in the summer (North et al., 2012), and precipitation is likely to increase slightly (Dettinger, 2005; Pierce et al., 2013). Project precipitation is highly uncertain, but many models predict an increase in the number of extreme precipitation events (Gershunov et al., 2019).

Vegetation

There is a strong climatic gradient with elevation in the Sierra Nevada which leads to a distinct distribution of ecotones (Barbour et al., 1991). At low-elevations (<915 m) the climate is hot and dry, favoring drought tolerant vegetation. Oak woodland and chaparral vegetation dominate this lower elevation range (Erman, 1997).

At mid-elevations (760–1400 m in the north and 915–3050 m in the south of the western slope), the predominant vegetation is comprised of a mix of coniferous trees and black oaks. This band is referred to as the mixed-conifer forest (Minnich & Padgett, 2003; C. Chang, 1996), which is the most productive and widely distributed forest type across the Sierra Nevada, making up a least 5.7 million ha (Schoenherr, 2017b). Ponderosa pine, Jeffrey pine, and Incense cedar are drought-tolerant and tend to occupy drier, south-facing aspects. Meanwhile white fir and sugar pine occupy north-facing, wetter, and cooler portions of the mixed-conifer forest (Millar, 1996). Within the mixed conifer forest, Ponderosa and Jeffrey pines are shade intolerant but adapted to frequent fires, while white firs are shade tolerant though not well-adapted to survive fires (Tubbesing et al., 2020; Parsons & DeBenedetti, 1979; Safford & Stevens, 2017). These traits affect spatial distribution of species based on environmental conditions. Today mixed-conifer forest is the most vulnerable to disturbance and climate change (Dolanc et al., 2014).

At high-elevations (>1500 m), precipitation transitions from rain to snow and mixed conifer forest gives way to sub-alpine vegetation comprised mostly of white fir and then red fir forests (Erman, 1997). Upper elevation red fir forests receive 70-90% of precipitation as snow and historically experience little fire activity (Agee, 1993). Climate warming is predicted to increase the density of young trees while decreasing the number of older trees (McIntyre et al., 2015; Dolanc et al., 2014).

Mid to high elevation forests are the focus of the work presented throughout the dissertation.

Water

Water in the Sierra Nevada is an important resource not only to the local ecosystems, but also to downstream rural and urban communities (Bales, Battles, et al., 2011). Sierra Nevada watersheds provide between 60% and 90% of California's water supply (Madani & Lund, 2009) and 20% of the State's energy production (Cayan et al., 2008). The Sierra Nevada contain 24 major watersheds, 16 of which have major dams that cumulatively store between 12.3 and 43.1 thousand cubic meters of water (Dettinger & Anderson, 2015).

With most winter precipitation falling as snow, spring snowmelt is the main contributor to soil water storage that supports summer vegetation growth (Hunsaker et al., 2012; Bales, Hopmans, et al., 2011; Kurpius et al., 2003; Harpold et al., 2014). The length of the growing season and the water stress experienced by vegetation vary as a function of both snow water equivalent and melt timing (Lundquist & Loheide, 2011). The location of the snowline strongly controls soil moisture availability (Bales, Hopmans, et al., 2011): for example, in the upper-elevations of Stanislaus Forest, sites above the snowline had approximately double the May and August water content than sites located < 70m away that were below the snowline (Barbour et al., 1990). About two thirds of the precipitation is transpired and evaporated with the rest going into streamflow (Bales, Battles, et al., 2011).

Drought tolerant tree species in the Sierra Nevada are adapted to low soil water availability in the late summer season, having deep roots that can tap into water stores in the fractured bedrock (Bales, Hopmans, et al., 2011). Up to 70% of the water consumed during the growing season can come from weathered bedrock (Witty et al., 2003). Despite this adaptation, the effect of droughts on the Sierra Nevada forests is profound; during the 2012-2016 drought, an estimated 129 million trees died across the Sierra Nevada.

The downstream effects of the 2012-2016 drought were also acute: in 2015, reservoir storage dropped to as little as 18% and hydropower generation declined by 50% (Dettinger & Anderson, 2015). The economic cost of the drought reached 2.2 billion dollars in 2014 alone, with a loss of ∼17,100 jobs (Howitt et al., 2014). The five-year drought was followed by one of the wettest years on record; in 2017 precipitation was 150-400% of normal, causing flooding, threatening infrastructure and human life (Mount et al., 2018). Both intense drought and flooding are projected to increase by ∼50% by the end of the century (Yoon et al., 2015).

Fire

Historically (pre-1800), the Sierra Nevada experienced frequent fires, with 3.4 million ha (33% of Sierra Nevada) of mixed-conifer forest burning each year prior to European settlement (Stephens et al., 2007). Fire histories show a frequent and relatively steady areas burned by fire during this period, with fire-return period being consistently < 30 years (Stephens et al., 2007). In addition to lightning ignited fires, indigenous populations used fire as a tool for land management, burning frequently (Pyne, 1997; Skinner & Chang, 1996; Stephens et al., 2007; Anderson, 2005).

By the turn of the nineteenth century, European settlers had decimated indigenous populations, and in 1905, US Forest Service established a strict national policy of wildfire suppression (Stephens & Ruth, 2005; Agee, 1993). During this period, the area burned by wildfires was almost negligible. Indeed, the fire return interval for mixed-conifer forests during the fire suppression period was estimated as 640 years compared to < 30 years pre-European settlement (McKelvey et al., 1996; Scholl & Taylor, 2010; Stephens et al., 2007). At its peak in 1935, the fire suppression policy was one of strict control of all natural and man-made wildfires, with a "10:00 A.M. rule" stating that all fires should be put-out by 10 am the following day (Pyne, 1997). The fire suppression policy caused an upward of 430% densification of forests and a 25-49% increase of canopy and surface fuels (McKelvey et al., 1996; Vankat & Major, 1978; Parsons & DeBenedetti, 1979). Forests began to look drastically different: forests that one could easily walk through became so overgrown with vegetation and stacked with fuels, that they became completely impassible (Vankat & Major, 1978; Van Wagtendonk, 1977; Collins & Stephens, 2007).

Today, the area burned by wildfires in California is approaching pre-European Settlement statistics (1.8-4.8 million acres burned each year), with 4.5 million acres burned in 2020 alone (CalFire, 2020b). Contemporary wildfires, however, are much larger in size than historical fires were. Five of the largest fire complexes in 2020 represent 60% of the total area burned that year (CalFire, 2020a). Much of the increase in recent fire activity and fire severity is related to the combination of climate change and the legacy of fire suppression (J. D. Miller et al., 2012). Abatzoglou & Williams (2016) attributed a 4.2 million ha wildfire area during 1984-2015 in the US to Anthropogenic climate change, doubling the fire area that would have burned in its absence.

1.4   Background 3: Managed wildfire as a forest management strategy

By the 1960s, the negative effects of fire suppression on ecosystem diversity, forest health, and fire risk in the Sierra Nevada began to be better documented (Leopold, 1963). The National Park Service was the first Government agency to re-introduce wildfires to the landscape (Van Wagtendonk, 1977) in response to these impacts. In 1968, Sequoia-Kings Canyon National Park created a natural fire program for some of its remote watersheds, in which naturally ignited fires were allowed to burn unless they posed unacceptable threats to health, life or infrastructure. Sequoia-Kings Canyon National Park was soon followed by Yosemite National Park (Stephens & Ruth, 2005), although other National Forest lands continued fire suppression practices.

Today, scientists and policy-makers generally do agree that to have resilient forests, California needs to reduce forest density and fuel loads (Stephens et al., 2020). Resilient forests are those that can both resist and recover from disturbance. The re-introduction of wildfire to the Sierra Nevada forests is one tool being considered to promote such resilience. In this

dissertation, I will refer to such reintroduction interchangeably as a "fire use" or "managed wildfire" strategy. Managed wildfire entails allowing lightning-ignited wildfires to burn, subject to a strict management policy that calls for intervention to suppress fire when air quality, structures, or people are placed at risk (van Wagtendonk, 2007).

Managed wildfire requires time to reshape ecosystems. Yet only two watersheds in California - Illilouette Creek Basin (ICB) in Yosemite National Park and Sugarloaf Creek Basin (SCB) in Kings Canyon National Park - have been managed in this way for multiple decades. These sites are unique locations in which to study the interaction of managed wildfire, vegetation, and hydrology. Since the introduction of the managed wildfire strategy in 1972 in ICB and 1968 in SCB, 29 fires greater than 40 ha have burned in ICB (van Wagtendonk et al., 2012), and 10 in SCB. The mean fire return period for 1972-2005 was 6.8 years in ICB and 12 years in SCB, which is similar to the pre-suppression (1700-1900) fire return period of 6.3 and 9 years for ICB and SCB respectively (Collins & Stephens, 2007).

Of the two basins, ICB is the better characterized. In ICB, wildfire re-introduction had profound effects on landscape composition; since 1972, 75% of the vegetated area burned at least once in ICB, causing a 24% decline in conifer vegetation, while increasing shrub area by 35%, sparse meadows by 199%, and dense meadows by 155% (Boisramé et al., 2017). These vegetation conversions produced an upward of 7% increase in mean watershed soil moisture and increased landscape heterogeneity metrics (Boisramé et al., 2017). Meanwhile, watersheds surrounding the ICB have experienced greater tree mortality (47 trees per km^2) during the 2014-2016 drought than did the ICB (4 dead trees per km^2), suggesting that ICB is more resilient to disturbances than the surrounding areas experiencing similar climate (Boisramé et al., 2017).

Using a spatially-distributed ecohydrological model, Boisramé et al. (2019a) modeled wildfire effects in ICB on basin vegetation growth and water balance for the period 1972-2017. Boisramé et al. (2019a) predicted a 2.2% increase in watershed soil moisture storage, along with a 5% increase in streamflow production from reduced transpiration and a 1% increase in snow water equivalent attributed to the fire-altered vegetation structure. Boisramé et al. (2017) identified that approximately 19,100 km^2 of the Sierra Nevada region is topographically and climatically similar to ICB, making these areas potential candidates for wildfire management strategy. Yet extending such management to other locations remains fraught with open questions regarding fire, hydrology, vegetation and their coupled feedbacks.

1.5 Scope of the Dissertation

In this dissertation, I aim to fill some of the knowledge gaps in the fire-vegetation-hydrology-climate feedbacks discussed in the previous section. To do so, I use a broad range of tools, including remote sensing, field-based observations/data collection, laboratory-based experiments, and detailed hydrological modeling.

I begin with a broad exploration of how two-poorly understood fire-hydrological processes interact with each other; in Chapter 2, using field collected fuel and soil moisture data, I assess the impact of soil moisture on fire risk, both temporally and throughout space. Then, in Chapter 3, I design an experiment that measures the decay of post-fire soil hydrophobicity when exposed to different combinations of wetting/drying and freezing/thawing. By doing so, I quantify timescales and hydrological processes over which post-fire hydrophobicity decays. In Chapter 4, using satellite data, years of weather station record, thousands of soil moisture samples, and data collected from forestry plots, I compare hydrological outcomes of wildfire management strategy on soil storage and landscape structure in SCB to the ones observed in ICB. Lastly, I use a distributed ecohydrological model to quantify the outcomes of wildfire management strategy if it was implemented in ICB in the future climate (2030-2070) and compare those outcomes to the historically modeled climate from 1970-2010.

Figure 1.1 provides an overview of the specific feedbacks that each chapter addresses and how these feedbacks interact with other components of the fire-water-vegetation-climate feedback system.
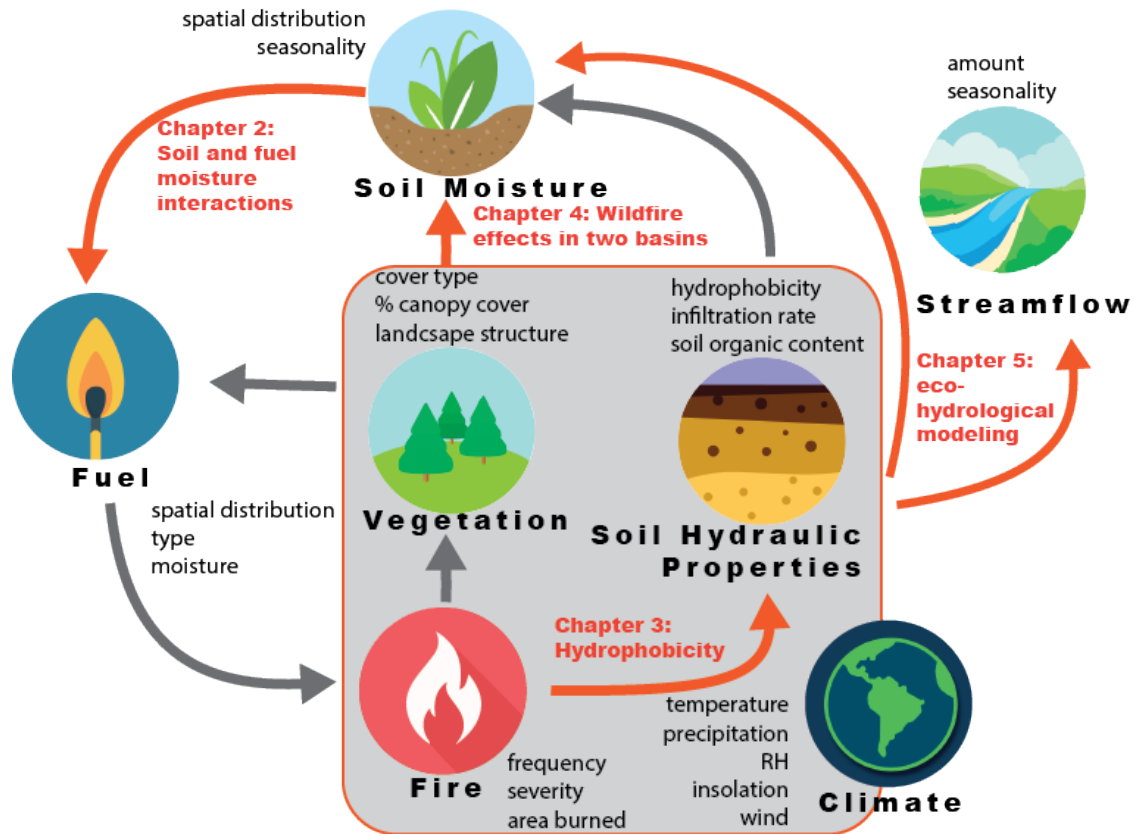
Figure 1.1: Overview of the relationships and variables involved in my systems thinking about wildfire and ecohydrology. Knowledge gaps are presented as red arrows and indicate dissertation work, blue arrows indicate work added to previous projects, and gray arrows indicate phenomena which have been well studied by the scientific community.

Chapter 2

Soil Moisture Influences on Sierra Nevada Dead Fuel Moisture Content and Fire Risks

2.1 Introduction

Fire behavior is strongly dependent on the availability and quality of living and dead fuels. Amongst dead fuels, which comprise duff, litter, dry grasses and non-living woody material, the moisture content (Fuel Moisture Content or FMC) has a profound influence on the probability of ignition, a fire's rate of spread and its burn intensity (Renkin & Despain, 1992; Chuvieco et al., 2004; Rothermel, 1983; Larjavaara et al., 2004; P. M. Fernandes et al., 2008). In fact, Van Wagtendonk (1977) cited dead fuel moisture to be "the principal factor influencing fire characteristics and subsequent effects on fuel and vegetation". Consequently, FMC is widely used as an input into fire risk assessment and fire modeling applications. Fine FMC is conventionally reported for fuels of two distinct sizes (1-hr and 10-hr fuels), corresponding to fuels with diameters of <0.64 cm and 0.64-2.54 cm, respectively. The size class names refer to the timescales over which the fuel moisture equilibrates with changing atmospheric conditions (M. Schroeder & Buck, 1970): finer fuels desorb and absorb moisture more rapidly than coarser fuels, resulting in distinct timelags (Cochrane, 2009). These fine dead fuel size classes are associated with the initial ignition and spread of fires, such that their moisture content is particularly relevant to the risk of fire occurrence (Bennett et al., 2010).

FMC for dead fuels is measured at numerous points across the United States - for example, ~60% of the 2,400 Remote Automated Weather Stations (RAWS) nationwide, and 85% of the 470 located in California, include continuous FMC readings of 10-hr wooden dowels. Moisture data from these readings forms the main input to the US National Fire Danger Rating System (NFDRS). Measured fuel moisture is interpolated to a 10 km grid over the continental US using atmospheric data to inform the interpolation (Wildland Fire Assesment

System, n.d.). These stations measure FMC using a standard 100 g pine dowel installed 10-12 inches above the ground (National Wildfire Coordinating Group, 2019). However, a study by Bovill et al. (2015), concluded that 10-hr fuel sticks were only able to accurately describe burning conditions (assuming that true burning conditions were represented by surface fuel measurements) about 50% of the time. Cawson et al. (2020) concluded that elevated fuel sticks report FMC values 3-fold lower than surface measured FMC. These finding suggest that RAWS stations on their own may not be sufficient for making FMC predictions, and that there may be important processes occurring at the ground surface that alter FMC. Field-sampled FMC is reported by the National Fuel Moisture Database (National Fuel Moisture Database, n.d.), but mostly on sparse (e.g. bi-monthly) time intervals, and at limited locations. For example, only 31 sites in California have 10-hr FMC records, and only 13 report 1-hr FMC. This suggests that no datasets in the U.S. have appropriate measurements on suitable temporal and spatial resolutions to accurately predict the FMC of surface fuels.

This relatively sparse measurement network means that fire predictions mostly rely on a range of empirical and mechanistic models to estimate FMC (Matthews, 2014). One of the most complete and widely used is the Nelson Dead Fuel Moisture Model (R. M. Nelson, 2000), a process-based model that forms a component of the FlamMap, BEHAVEPlus, and NFDRS fire behavior and management models used throughout the USA (https://www.firelab.org/applications). The Nelson model is forced using precipitation volume and time since precipitation, in conjunction with environmental conditions to describe heat and moisture transfer for an idealized 10-hr stick. The Nelson model performs well in many environmental conditions, but underestimates dead FMC predictions under wet conditions, when field sampled FMC exceeds 20% (Estes et al., 2012; Carlson et al., 2007). Errors in estimated FMC have real-world consequences: over-predicting FMC can result in escaped prescribed fires, higher severity fires, and less predictable fire behavior. Under-predicting FMC may cause unsuccessful prescribed fires (for example, 41% of interrupted burns in Portugal were due to high FMC, P. Fernandes & Botelho, 2004), due to exaggerated perceptions of risk (Quinn-Davidson & Varner, 2012; Bovill et al., 2015), or in failing to meet intended objectives, such as fuel hazard reduction or ecosystem restoration (Bovill et al., 2015; Johnson & Miyanishi, 1995; P. Fernandes & Botelho, 2004). In the context of modeling, reported uncertainty in FMC of +/- 50% (that is, ±2 percentage points around a mean of 4 percent FMC) can produce errors of up to 80% in output variables such as the rate of fire spread (Trevitt, 1988).

One possible explanation for errors in FMC, including the observed bias under wet conditions, is that soil moisture is excluded from model formulations predicting FMC (Hiers et al., 2019). Although FMC models attempt to account for antecedent wetness using precipitation data, these data may poorly represent soil moisture in topographically complex landscapes (Berryman et al., 2015; Holsinger et al., 2016), in snowmelt dominated systems where snowpack decouples the timing of precipitation from the input of moisture to soil (Harpold & Molotch, 2015; C. J. Williams et al., 2009; Bales, Hopmans, et al., 2011), or in other areas with heterogeneous moisture environments (McLaughlin et al., 2017; S. E. Thompson et al.,

2011; Kreye et al., 2018). Since surface fuels are often in direct contact with soil, heterogeneous soil moisture environments could produce variations in FMC - indeed, such variations are often implicitly assumed in fire management approaches when planning prescribed burns (Robert York, personal communication October 1, 2020).

Improved understanding of SMC - FMC relationships could be valuable for better interpolating FMC observations, for example using downscaled (e.g. Mascaro et al., 2019) remotely sensed observations of surface soil moisture from the Soil Moisture Active Passive (SMAP) radar (Chan et al., 2016) or NOAA's Soil Moisture Operational Products System (SMOPS) soil moisture product. The global availability of such products and a growing field of downscaling methodologies, coupled with *in situ* soil moisture measurements, would enable soil moisture to be viably used for continental-scale fuel moisture estimates.

To date only a handful of studies address the relationship between fuel moisture and soil moisture, but all suggest that FMC is likely to be related to underlying soil moisture. For example, Hatton et al. (1988) and Rothwell et al. (1991) found that soil moisture was a significant determinant of litter moisture content in Eucalyptus and Aspen forests. Pook & Gill (1993) showed that predictions of litter FMC were improved when incorporating soil moisture information, while Samran et al. (1995) concluded that precipitation and soil moisture account for 41% - 59% of the moisture content in the portion of the fuel bed in direct contact with soil.

Water transport processes in unsaturated soils include the flow of liquid water and the diffusion of water vapour. Both processes could transport water from soil to fuels. This transport would be expected to slow down under dry soil conditions which suppress hydraulic conductivity in both mineral soil and organic materials (e.g. $\approx 10^{-4} cm^{-1}$ for duff with $\approx 20\%$ water content, Raaflaub & Valeo, 2009), and also impeded evaporation fluxes (Gardner & Hillel, 1962; Kondo et al., 1990; Han et al., 2017). Consistent with these expectations, hydrologic modeling suggests dry conditions decoupled surface organic layers from underlying soil moisture content. This coupling was restored by increased liquid and vapour fluxes when soils became wetter (Keith et al., 2010). We therefore expect that FMC is likely to vary in how closely it is coupled to soil moisture content depending on how dry soils are.

In this study, we aim to expand the body of work addressing the connections between SMC and FMC by exploring the relationships between SMC and the FMC of fine (1-hr and 10-hr) woody fuels in the Sierra Nevada. We use the results to quantify the potential importance of accounting/failing to account for soil moisture variations when estimating fuel ignition probability in the mid-elevation mixed-conifer forests in the Sierra Nevada. Three research questions (RQs) guide the study:

(i) Is soil moisture content a significant driver of variation in fuel moisture content for 1-hr and 10-hr fuels?

(ii) How do predictions of 1-hr and 10-hr fuel moisture vary when soil moisture is included or excluded from predictive models?

(iii) What are the practical implications of inclusion or exclusion of soil moisture on the timing and spatial variation in ignition probability?

Throughout, we quantify soil moisture using the volumetric water content of the soil. This choice of a soil moisture metric is not necessarily obvious: arguably, if SMC-FMC relationships are primarily driven by fluxes of water from soil to fuels, soil water potential might provide a more direct physical control on FMC. Volumetric water content, however, offers several advantages over water potential, including spatially-scalable data (from remote sensing and geophysical models) and ease of field-sampling; soil water potential estimates require knowledge of soil textural properties and thus require much more extensive soil sampling. On the other hand, volumetric water content can be easily approximated using a portable TDR with minimal soil disturbance. Since either metric can introduce error into the inference of the SMC-FMC relationship, we have elected to work with water content as the independent variable throughout due to its ease of sampling and data availability.

2.2 Methods

Study Site

Blodgett Research Forest: Data Collection

Fuel moisture, soil moisture and other covariates were sampled from the 1,763 ha Blodgett Research Forest (lat: 38.91, lon: -120.66, elev: 1,200-1,500 m), located in the foothills of the Sierra Nevada. Tree species in this area include sugar pine (*Pinus lambertiana*), ponderosa pine(*Pinus ponderosa*), white fir (*Abies concolor*), incense-cedar (*Calocedrus decurrens*), Douglas-fir (*Pseudotsuga menziesii*), California black oak (*Quercus kelloggii*), tanoak (*Lithocarpus densiflorus*), bush chinkapin (*Chrysolepis sempervirens*), and Pacific madrone (*Arbutus menziezii*). Soils are well-draining, deep, weathered, sandy-loams overlain by an organic forest floor horizon. Common soil depths range from 85–115 cm (E. E. Y. Moghaddas & Stephens, 2007).

A variety of research activities take place within different compartments of this forest. Sampling took place in 15 out of 110 compartments (Appendix Figure A.1). Because some treatments associated with each compartment (treatments listed in Appendix Table A.1) had the potential to alter soil or fuel structure, which could bias the study results, we confined the sampling to locations in which no soil disturbance or recent prescribed fires had occurred. We selected compartments for sampling to get a wide representation of overstory cover, slope, aspect, and soil wetness conditions. Soil type, forest species composition, and fuel depths were comparable across locations. Because of similarities in soil texture, we were confident that soil moisture (rather than water potential) could be reasonably used as a fuel moisture predictor variable.

Blodgett Forest receives an average of 1340 mm of precipitation each year (2006-2019) of which 340 mm is snowfall. Average daily summer maximum temperatures are 30°C, and

average daily minimum winter temperatures are 2.6°C. A meteorological station (CDEC station BMT) located 2 kilometers from the Blodgett Research Forest perimeter measures wind speed, relative humidity, and temperature.

Data Collection

One hundred and one 1 and 10-hr fuel samples were taken in daylight hours between May 7th and May 12th, 2019. Sampling locations are plotted in the Appendix Figure A.1. Weather was sunny and clear throughout the sampling period, with an average wind speed of 4-6.5 km/h. The last precipitation events prior to sampling were 13 mm on April 15th and 20 mm on April 8th. At the time of sampling, the accumulated water-year precipitation was 1320 mm. Fuels were collected sufficiently late in the morning that no dew was observed on the fuel surface. Within a sampling compartment, fuels were collected along an elevation gradient or in transects following the profile of a stream. Samples were taken on slopes 0-35%. All topographic aspects were sampled, but south-facing aspects were most represented (54% of all samples).

At each sampling location, an average of 39 grams of 1-hr and 109 grams of 10-hr fuels were collected and weighed using a scale with a 0.01 gram resolution, then stored in paper bags. A standard fuel sizing gauge (<0.64 cm for 1-hr fuels, and 0.64-2.54 cm for 10-hr fuels) was used to standardize fuel collection. At the end of each day, fuels were oven dried at 105°C for 24 hours (Matthews, 2010). Dry fuel weight was recorded and FMC was calculated as the ratio of the difference between wet and dry fuel weight and dry fuel weight (Pollet & Brown, 2007). During sampling, temperature (T) and relative humidity (RH) were measured on 1 min intervals using a HOBO U23 Pro v2 data logger mounted at the top of a 2 m staff, which was moved to each sampling location. Temperature and humidity were reported as the 5-min average around sampling time. Vapor pressure deficit (VPD) was calculated as the difference between saturation vapor pressure (e_{sat}, computed following Buck, 1981) and vapour pressure of water in air ($e_a = e_{sat} * RH/100$). The presence/absence of wind was reported as a binary variable. Volumetric soil moisture was measured with a CS HydroSense II handheld probe across the top 12 cm of the mineral soil profile. At each sample site, 3 soil moisture readings were taken within 1-m radius of the fuel sampling location. Any duff and litter were cleared before measuring soil moisture.

To account for differences in fuel shading, at each sampling location, we took photographs of the canopy at the ground level using a phone camera (12 megapixel resolution). Canopy cover was calculated by binarizing photographs into canopy vs open sky by applying greyscale thresholds in *RStudio* (ver 1.3.1056), and the percentage canopy coverage was computed as the number of canopy pixels over the total number of pixels. Across the different sampled compartments, canopy cover ranged from 0-67% (Table 2.1). Additionally, we noted if fuel samples were shaded or in direct sunlight at the time of sampling. The time of day for each fuel collection was translated to solar elevation angle (sun angle from the horizon) using The National Renewable Energy Laboratory's Solar Position and Solar Intensity calculator (https://midcdmz.nrel.gov/solpos/solpos.html). Elevation,

Table 2.1: Summary of both field collected and topographically-derived variables collected
across one hundred and one sampling sites within the Blodgett Research Forest. Both 1-hr
and 10-hr fuels were collected at each location.

Continuous			
Variable	Abr.	Range	Unit
Fuel Moisture	FMC	2.8 - 46	%
Soil Moisture	SMC	6.3 - 53	%
Relative Humidity	RH	10 - 70	%
Temperature	T	14 - 27	^oC
Canopy Cover	C	0 - 67	%
Solar Elevation Angle §	SE	0 - 68	deg
Vapor Pressure Deficit†	VPD	0.6 - 3.0	kPa
Elevation ‡	$Elev$	1216 - 1382	m
Topographic Wetness Index †	TWI	3.7 - 17	-
Distance to stream		1 - 220	m
Slope †		0 - 34	%
Aspect †		0 - 360	deg
Discrete			
Wind	W	1 if there is wind/breeze; 0=otherwise	
Shade	Sh	1 if fuel is in shade; 0=otherwise	

§ : Calculated based on latitude/longitude and time of day
† : Calculated from temperature and relative humidity
‡ : Derived from 1/3 arc-second (10 by 8 meter)
spatial resolution digital elevation model

slope, aspect and topographic wetness index (TWI, K. J. Beven & Kirby, 1979) were cal-
culated for all sampling locations using a 1/3 arc-second DEM (10 m by 8 m) obtained
from USGS (https://www.sciencebase.gov/catalog/item/5aea899ee4b0860c0f70ed94). TWI
quantifies topographic controls on landscape wetness. Table 2.1 summarizes collected data
and sampling ranges.

Data Exploration

Before developing models to analyze the data, we scaled all data to have a mean of zero and
a standard deviation of 1, and visually inspected the form of the SMC-FMC relationships for
both 1-hr and 10-hr fuels. We expected that these relationships might have a nonlinear form,
weakest under dry soil conditions and stronger under wet soil conditions. Visual inspection
of the scaled data indicated that if such non-linearity was present in the 1-hr fuels, it was
weak, and that a more pronounced non-linearity was obvious in the 10-hr fuels, as shown in

Figure 2.1. These soils saturated at SMC of ∼53% and we collected only limited number of FMC samples (n=3) under saturated soil conditions.
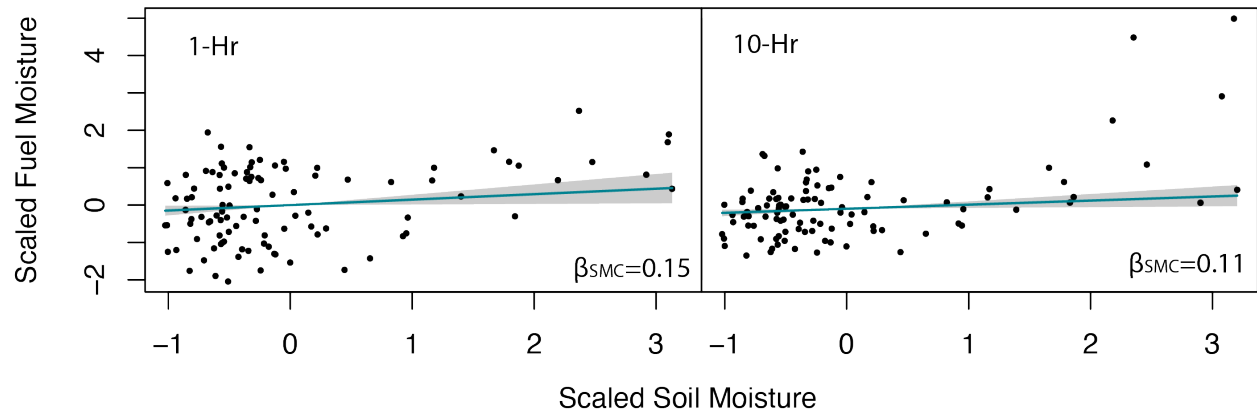
Figure 2.1: Relationship between field sampled SMC and FMC for 1-hr fuels (left) and 10-hr fuels (right). Regression fit between SMC and FMC is shown as a blue line. SMC coefficient, β_{SMC}, is the line's slope.

Research Question 1: Is soil moisture content a significant driver of variation in fuel moisture content for 1-hr and 10-hr fuels?

We addressed this question with a statistical modeling approach. An initial exploration of linear models for FMC showed that these models were heteroscedastic when applied to 10-hr fuels, but homoscedastic when applied to 1-hr fuels. Homoscedasticity was assessed by the Breusch–Pagan (BP) test on studentized residuals (Bischoff et al., 2006). Heteroscedasticity biases uncertainty estimates from linear models confounding the interpretation of the significance of SMC (and other variables) as drivers of FMC.

We employed several methods to account for heteroscedasticity in the 10-hr FMC linear models, including data transforms (logarithmic), robust errors (White, 1980; Huber, 1967), and weighted least squares (WLS) regression. Only WLS is capable at simultaneously addressing heteroscedasticity and non-linearity in the SMC-FMC relationship while avoiding variable transforms, which become difficult to interpret. Thus, WLS was chosen as the main method to assess the significance of the SMC-FMC relationship. Other statistical modeling results produced similar results to WLS across different modeling approaches (in terms of the relative ranking of coefficient strength across variables and the significance of SMC). We report the WLS results in the main text and the results from other methods are presented in Appendix C.2.

Multiple linear regression models were fit to explain variations in measured 1-hr and 10-hr FMC. Several field variables provided redundant information and were collinear with each

other - for instance, both TWI and soil moisture provide descriptions of landscape wetness. A correlation matrix for all variables is shown in the Appendix Figure A.2. To reduce the number of variables in the linear model and avoid multi-collinearity, we checked the partial correlation of the variables with FMC and used only the variables with the highest partial correlation for analysis (e.g. soil moisture was retained and TWI discarded).

Linear models were developed using backward stepwise selection (Chambers, 1992, *step.model* in *RStudio*) in order to identify the model with the lowest Akaike Information Criterion (Akaike, 1987, AIC). Weights for the 10-hr FMC WLS were assigned iteratively to maximise the p-value of Shapiro-Wilk (Shapiro & Wilk, 1965, SW) and Breusch–Pagan (Breusch & Pagan, 1979, BP) tests applied to studentized residuals (i.e. to maximise the normality and homoscedascity of the resulting model). We applied the weighting scheme separately to low values of SMC (where residual variance in the unweighted model was relatively low) and to high values of SMC (where residual variance was higher), using a SMC of 20.9% as a threshold. The weighting for low SMC was $1/\exp(\text{FMC})^{0.5}$ and for high SMC, $1/\exp(\text{FMC})^{1.3}$.

The final models (OLS for 1-hr fuels and WLS for 10-hr fuels) did not exhibit spatial autocorrelation (Moran's I test), and satisfied assumptions of linearity, normality (SW), and homoscedasticity (BP). Multicollinearity was not detected in 1-hr and 10-hr models, based on the variance inflation factor. Goodness-of-fit was assessed with root mean square error (RMSE).

The primary outcome of this analysis is a determination of whether SMC provides a significant contribution to variation in FMC. For the 1-hr FMC model, the strength of this contribution can also be evaluated relative to other variables. For the 10-hr FMC model, these comparisons are more problematic due to the apparently nonlinear SMC-FMC relationship, which could lead to linear coefficients over-estimating the importance of driving FMC variation at low soil moisture values, and under-estimating the response of FMC to SMC at higher soil moisture content. The linear model provides a stringent test of the significance of SMC as a linear predictor of FMC, given that heteroscedasticity must be accounted for. To predict the impact of soil moisture variations on FMC, however, we altered the regression strategy to piecewise linear regression (Toms & Lesperance, 2003).

Research Question 2: How do predictions of 1 and 10-hr fuel moisture vary when soil moisture is included or excluded from the predictive model?

To formulate predictive models for FMC, we used the OLS model for 1-hr fuels. To better represent the nonlinear relationship between SMC and 10-hr FMC, we developed a piecewise regression for the 10-hr fuels, with a single break-point based on SMC. We did not enforce model continuity at this break-point, allowing both the SMC coefficient and the intercept to change at the break-point. All other variables had a single coefficient (i.e. the coefficients on other variables did not change at the break-point). With these specifications, we repeatedly fit the piecewise model with different break-point locations, identifying the break-point that

minimized AIC, which was used to specify the final model. Since piecewise regression does not eliminate heteroscedasticity, we calculated robust errors (heteroscedasticity consistent errors or White-Huber standard errors) which allow for significance testing in the presence of heteroscedasticity (White, 1980; Huber, 1967). To enable us to compare the impact of including/excluding SMC on the FMC predictions, we refit both fuel models without SMC. For the 10-hr piecewise regression, we separated the dataset at the previously used SMC break-point, allowing us to compare the models with and without SMC directly; we split the data (as opposed to fitting a linear regression to the entire dataset) to allow for a more rigorous comparison between model with SMC and model without SMC. Because VPD has higher correlation to 10-hr FMC during wet conditions, we expected the split linear regression model to perform better at predicting high FMC, allowing for a more fair model comparison. All model summaries are provided in Appendix A.2.

We applied the resulting models with/without soil moisture to an environmental dataset obtained from the Upper Providence CZO weather station network in the Southern Sierra Nevada (Bales, Hopmans, et al., 2011, data: https://eng.ucmerced.edu/snsjho/files/MHWG/Field/SouthernSierraCZOKREW). To obtain soil moisture at 10-cm depth (the shallowest measured), we selected a node located on a flat aspect with an open canopy (elevation: 1982 meters, lat: 37.0626N, lon: -119.1823E). For other environmental variables such as snow-pack depth, temperature, relative humidity, and wind speed, we obtained data from the nearby base-station (data: https://www.fs.usda.gov/rds/archive/catalog/RDS-2018-0028). The base-station is located 40 meters from the soil moisture node and is also under an open canopy. Other nodes in the CZO network were used for data gap-filling, which was minimal.

We used the models to estimate FMC for each hour of the data record in three ways: (i) using daily soil moisture, (ii) using models that includes soil moisture, but holding SMC constant at its seasonal average value, and (iii) using the models that exclude soil moisture. We excluded periods when air temperature was below freezing, snow depth exceeded 1 cm, or solar angle was lower than 45 degrees in the morning and 1 degree in the evening - during these periods, the environmental conditions were too distant from the field sampled range for model validity. Given these constraints, we used the regressions to identify the lowest normalised fuel moisture for 1-hr and 10-hr daily FMC values for each of the three prediction models and each prediction day. To convert the normalised FMC values to absolute FMC estimates, we transformed the unit-less predicted to have the Blodgett field-collected statistics (mean and standard deviation of 11.3 % and 4.2% for 1 hr fuels; 13.4% and 6.6% for 10-hr fuels, respectively). These experiments enable evaluation of the consequences of including/excluding soil moisture on temporal variability when predicting FMC.

Research Question 3: What are the practical implications of inclusion or exclusion of soil moisture on the timing and spatial variation in ignition probability?

Temporal variation in ignition probability

Because of the long temporal weather and soil moisture record, we used the Upper Providence CZO weather station described above to explore the temporal fire risk dynamics at a single point and how they might be influenced by including or excluding soil moisture from the FMC predictions.

FMC estimated by each of the three regression models described in Section 2.2 applied at the Upper Providence CZO site from January 1, 2008 to January 1, 2018 was used to estimate the probability of ignition of 1-hr and 10-hr fuel classes. These predictions were based on probability of ignition tables adapted by Pat Andrews (Rothermel, 1983), which are derived based on a mechanistic model developed by M. J. Schroeder (1969), and are used in the field by fire managers. Predictions were made on hourly timescales, and the highest probability of ignition for each day is reported. Depending on the SMC-FMC model used, the time of day with the lowest FMC (highest ignition probability) may vary. The probability of ignition values were converted into an estimate of fire season start and end by finding the 5th and 95th percentile of all recorded days for each season with a probability of ignition of 30% or above, respectively. This threshold is partially based on the field sampled fuel moisture range, where relatively high minimum 10-hr FMC (4.5%-46.1%) results in a small number of days with high probabilities of ignition. Sampling during the entire growing season, may provide a greater range in FMC variability, and thus a different probability of ignition threshold might be more appropriate. Though the specific timing of the start and end of the fire season varies with the selected probability of ignition threshold, the relative relationship between predictions of fire season among different SMC models remained the same across different thresholds. We summarize the start and end of the fire season over a 10-year record using box and whisker plots (range, mean, and 90th percentile) for each model and fuel category. We compare the 10-year fire season start and end means derived from each model to determine the effect of SMC inclusion/exclusion on the fire season statistics.

Spatial variation in ignition probability

To assess the spatial variation in ignition probability, we used a soil moisture model for the Illilouette Creek Basin (ICB) developed by Boisramé et al. (2017) to explore spatial variations in fire risk at two points in time (spring and fall), again when including/excluding SMC from FMC predictions. ICB was chosen for spatial analysis of fire risk, because of extensive soil moisture measurement campaigns across many years and vegetation types in addition to having a fine weather station record. This weather record spans four years, which is why we did not use it for the temporal assessment of fire risk described in Section 2.2.

We compare the effect of SMC inclusion/exclusion on the spatial distribution of fire prob-

ability in the ICB over a snapshot in time in the spring of 2017 and fall of 2017. ICB is a well characterized 150 km^2 basin located in Yosemite National Park, USA, spanning elevations of 1,270-3,600 meters. Like Blodgett Research Forest, the soils are sandy and well-drained and vegetation is a mix of coniferous forest. ICB also has large areas of shrub/grassland and meadow vegetation (Boisramé et al., 2017). Although we do not alter the SMC-FMC model for different vegetation cover types, we use a percent canopy map for ICB from LANDFIRE for 2016 (USGS, 2016) to separately estimate percent canopy for forest and shrubland. We set percent canopy for non-forest landcover to 0%, because we do not expect sufficient shading to affect FMC. A spatial 30 m resolution SMC map of the top 12 cm soil profile was derived based on the random forest model developed by Boisramé et al. (2017). The SMC values in this map are representative of a two week interval close to the dates of field sampling of SMC used to train and cross-validate the random forest model (May 23-24th in the spring and August 5-9th 2017 in the fall). Three temporary weather stations are installed in ICB (lat -119.57, lon 37.68, elevation 2,136 m) recording volumetric SMC at 10 cm depth along with climatic variables at 10-min resolution for years 2016-2020. We used the weather station record to determine a data point at the lowest VPD within each two week period. We use this lowest VPD value to make spatial FMC predictions which represent high fire risk periods, meteorologically, for both fall and spring seasons. Temperature (used to calculate VPD) was spatially scaled from the weather station location to the rest of the basin based on temperature lapse rate of -0.0007^{0}C/m of elevation (following Boisramé et al., 2019b). The actual vapor pressure was not scaled in calculating VPD. The wind binary was set to 1 (presence of wind) for the entire basin, and the solar angle was determined based on the weather station time, day, and location. The solar angle was not corrected for slope (i.e. this variable measures sun elevation, not the inclination of light onto the land surface).

We then calculated FMC at all 30 m pixels in the basin using the changing SMC model and the no SMC model for 10-hr fuels only, and converted these to probability of ignition (Rothermel, 1983), using the air temperature, and LANDFIRE derived percent canopy values. Finally, we report the differences in the probability of ignition between the two models for both spring and fall soil moisture scenarios.

2.3 Results

Research Question 1: Is soil moisture content a significant driver of variation in fuel moisture content for 1-hr and 10-hr fuels?

Table 2.2 summarizes the fitted regression coefficients for 1-hr OLS regression and 10-hr WLS regression. Both 1 and 10-hr FMC regressions satisfy homoscedasticity, linearity, and normality tests (Table 2.2 and Figure A.2 in the Appendix). For both regressions, SMC variations contributed significantly ($p < 0.05$) to variability in FMC. This finding is robust to the specific methodology used to control for heteroscedasticity in the 10-hr regression, as shown in Appendix C.2: all methods used indicate that SMC is a significant predictor of

Table 2.2: Scaled regression coefficients for 1-hr FMC regression (top), and 10-hr FMC regression (bottom). Regression intercept is α and regression residuals are represented by ϵ. The significance level of each coefficient is reported using p-values. Normalized partial r^2 (sum of all partial r^2 coefficients=1) values are used to assess relative importance of each variable. Model performance is assessed by AIC and RMSE. P-values of homoscedasticity test (BP) and residuals' normality (SW) test are provided, where the null hypothesis is the assumption of homoscedasticity and normality of the studentized residuals. Lastly, expected value of studentized residuals is reported as $E[\epsilon]$

Coefficient (β)	Estimate	p-Value	Partial r^2	Significance
$FMC_{1-hr} = \alpha + \beta_{SM}SM + \beta_{VPD}VPD + \beta_C C + \beta_{SE}SE + \beta_W W + \epsilon$				
α	-0.000	1.000		
SMC	0.146	0.032	0.058	*
VPD	-0.329	0.000	0.258	***
C	0.580	0.000	0.560	***
SE	0.189	0.005	0.099	**
W	-0.089	0.167	0.024	
AIC=199 RMSE= 0.61				
SW: p-value=0.70 BP: p-value= 0.85 E[ϵ]= 0.00				
$FMC_{10-hr} = \alpha + \beta_{SMC}SMC + \beta_{VPD}VPD + \beta_C C + \beta_{SE}SE + \beta_W W + \epsilon$				
α	-0.098	0.009		**
SMC	0.109	0.018	0.098	*
VPD	-0.126	0.001	0.173	**
C	0.290	0.000	0.629	***
SE	0.071	0.071	0.057	.
W	-0.086	0.167	0.045	
AIC=117 RMSE=0.76				
SW: p-value=0.40 BP: p-value= 0.24 E[ϵ]=0.00				
Significance Level: ·0.1, *0.05, **0.01, ***0.001				

FMC.

The use of scaled variables in the models allows the importance of SMC as a driver of FMC to be evaluated between 1-hr and 10-hr fuels and between different variables. All coefficients in Table 2.2 are unit-less, with a mean of zero and a standard deviation of 1, facilitating such comparisons.

In making such comparisons we note that the heteroscedasticity corrections (WLS or other methods outlined in the Appendix C.2) under-predict FMC under high SMC conditions. This is illustrated in Figure 2.1, which shows both the 1-hr and 10-hr SMC-FMC data and the fitted linear regression for the SMC-FMC relationship. The under-prediction of 10-hr FMC during wet soil conditions suggests that comparing SMC coefficients to others within the WLS regression framework may underestimate the effect size of SMC on FMC

when soils are wet. With this caveat, the models show that 1-hr and 10-hr fuels respond to similar environmental factors, since both "final" forms of the regression include the same variables. The AIC of 1-hr regression is 199, higher than the AIC of 117 for the 10-hr WLS regression. The AIC of the 10-hr regression is lower due to the weighting factors which put less weight on high FMC/SMC values which show large variation. On the other hand, the root mean squared error (RMSE) is lower for the 1-hr OLS compared to 10-hr WLS (0.61 vs 0.76), meaning that on average, we would have more accurate 1-hr FMC predictions than 10-hr FMC predictions. The wind variable (indicating binary presence or absence of wind) was not significant, but was also not eliminated from the model using stepwise model selection.

Table 2.2 shows two measures of variable importance in addition to significance: 1) the partial r^2 (aka partial correlation) which measures the degree of association of each predictor with FMC, while controlling for correlation with all other predictors, and 2) the regression coefficients, which measure the sensitivity of change in FMC to a change in each variable. Canopy cover is the most important environmental control on FMC in terms of both goodness of fit and coefficient strength for both 1-hr and 10-hr fuels, with FMC increasing with canopy cover. VPD is the next most important predictor for both fuel categories, again in terms of both goodness of fit and coefficient size. As VPD increases, FMC decreases. For 1-hr fuels, sun elevation is the next most important predictor, followed by SMC. For 10-hr fuels, SMC is more important than sun elevation. In all cases, the presence/absence of wind is the least important variable in the model.

We conclude that SMC is a significant predictor of FMC; that it is somewhat important for 1-hr fuels (similar in importance to solar angle), and may be more important in controlling 10-hr fuel variations.

Research Question 2: How do predictions of 1 and 10-hr fuel moisture vary when soil moisture is included or excluded from the predictive model?

We first address this question in the context of model fit and coefficient values, before turning to the implications in terms of predicted FMC time-series based on observational data.

We find that in general, excluding SMC from predictions of the linear models for 1-hr fuels slightly worsens the model fit (AIC increased by 2.9, the adjusted r^2 dropped slightly by 0.015, and the RMSE increased by 0.1). The linear model continued to meet all linear regression assumptions (homoscedasticity, normality, and with residual expectation of ~ 0). In the absence of SMC, the coefficients on the other predictor variables all increased, and the significance of the variables was unchanged. This suggests that in the absence of SMC, the model accounts for temporal changes in FMC primarily by increasing the sensitivity to VPD (since percentage canopy is static). The summary of the linear model fit without SMC is provided in Appendix A.2.

The piecewise regression used to explore predictions of 10-hr FMC in response to research

question 2 is reported in Table 2.3. In Table 2.3, p-values are based on robust standard errors. AIC was minimized (AIC=206) by situating the regression break-point at 20.9% SMC. We interpret this value as a degree of soil wetness required to enable hydraulic continuity between soil and fuels, as shown in Figure 2.2. Within this model, SMC does not significantly influence FMC below the break-point, but significantly influences FMC for wet soils. The break-point also introduces a large increase in the SMC coefficient, from 0.26 for dry soils (implying that a +1% increase in SMC increases FMC by +0.18%), to 0.85 above the break-point (implying that a +1% increase in SMC increases FMC by +0.58%). By comparison, the VPD coefficient is -0.15 (implying that a 1 kPa increase in VPD, decreases FMC by -1.6%). As postulated, this model suggests that SMC is not an important control of FMC under dry soil conditions, but is an important - in fact, the most important predictor of FMC under wet soil conditions.

The piecewise model with SMC was compared to a model that fit linear regressions on the other variables separately below and above 20.9% SMC. Under dry soil conditions, the scaled VPD coefficient was -0.15 (implying that a 1 kPa decrease in VPD decreases FMC by -1.6%) and at higher SMC, the scaled VPD coefficient was -0.42 (implying that a 1 kPa decrease in VPD decreases FMC by -4.4%). A full summary of the linear models fit without SMC is provided in Appendix A.2.

Overall, removing SMC as a predictor of 1-hr FMC, decreased RMSE from 2.53% to 2.49%. Removing SMC as a predictor of 10-hr FMC, decreased RMSE from 2.18% to 0.70% for data below SMC of 20.9% and from 9.77 to 4.32% for data above SMC of 20.9%.

In summary, during dry conditions, inclusion/exclusion has little impact on 10-hr FMC predictions, and VPD, which is the main FMC driver, remains unchanged. Under wet conditions, however, excluding SMC means the model relies more heavily on VPD to approximate the changes in FMC. However, since the correlation coefficient, r, between scaled SMC and VPD under wet soil conditions is 0.38, this worsens the model fit relative to incorporating SMC directly.

Table 2.3: Scaled regression coefficients for 10-hr piecewise FMC regression with a break-point (b) at scaled SMC value f 0.29 (or non-scaled 20.1%). Upper and lower bound estimates provide a 95% confidence interval for the slope coefficients. Confidence intervals are calculated using robust standard errors which can be trusted in the presence of heteroscedasticity in the residuals. Significance level of each coefficient is based on p-values. Model performance is assessed by AIC.

Coefficient (β)	Estimate	p-Value	Significance
$\alpha_{<b}$	-0.016	0.024	*
$\alpha_{\geq b}$	-0.868	0.010	*
$SMC_{<b}$	0.263	0.089	.
$SMC_{\geq b}$	0.835	0.006	**
VPD	-0.153	0.004	**
C	0.431	0.000	***
SE	0.102	0.058	.
W	-0.121	0.72	

AIC=206   RMSE=0.63

SW: p-value=4.8e^{-8} BP: p-value=3.8e^{-7} E[ϵ]=0.00

Significance Level: $\cdot 0.1$, $*0.05$, $**0.01$, $***0.001$

The effects of including/excluding SMC as a predictor of FMC based on observational data from the Upper Providence CZO are summarized in Figure 2.3. Panels A-F of this figure show predicted 1-hr (left-hand column) and 10-hr (right-hand column) FMC time-series using 1) daily observed SMC (A, D), 2) season-averaged SMC (B,E) where the average was taken over the snow-free period within which the fire season could feasibly occur, and 3) regressions excluding SMC (C,F). At this site, SMC is >20.9% for approximately 8.3% of the data record, and these wet conditions are responsible for the elevated predictions of 10-hr fuel moisture at the beginning and end of the snow-free period. We note that the high FMC predictions in the Fall are subject to an assumption of stationarity in the fitted SMC-FMC relationship under drying conditions (when measurements were made) compared to wetting conditions (when first winter rains arrive on a dry landscape), and may overestimate FMC during these periods.

For both 1-hr and 10-hr fuels, inclusion of the daily SMC increases the variability in predicted FMC, although this is much more pronounced for 10-hr than 1-hr fuels. Comparing Panels F and E in Figure 2.3 shows that where soil moisture is included but held constant, the other variables produce little FMC variability. Because seasonally averaged SMC is <20.9%, only the dry-soil regression values are being used to predict 10-hr FMC. Unsurprisingly, this means that the predictions do not indicate increases in 10-hr FMC during early spring and late fall. Comparing Panels D and F indicates that when daily SMC is included, both the predicted peak FMC and the within-season variability in predicted FMC is greater. Additionally, the predicted decline in early season FMC, and increase (where present) in late season FMC is less dramatic for the model including SMC (panel F) vs the one that
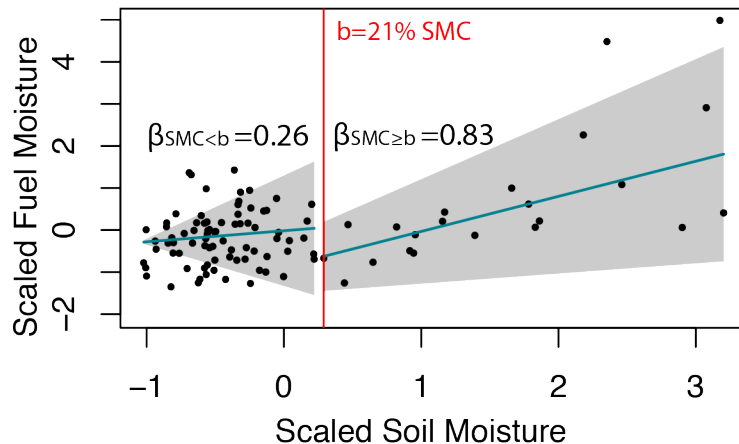
Figure 2.2: Relationship between field sampled SMC and FMC of 10-hr fuels. Piecewise regression fit between SMC and FMC is shown as a blue line, 95% confidence interval around SMC/FMC slope coefficients is shown in gray.

excludes FMC (panel D).

We conclude that the use of SMC in FMC predictions marginally improves model fit using the Blodgett Forest data and marginally increases predictions of peak FMC and within-season FMC variability for 1-hr fuels, relative to models that omit SMC when fitting, or that hold SMC constant. The use of SMC in FMC predictions for 10-hr fuels has a large impact on the model fit of Blodgett Forest data, and increases predicted FMC peaks in spring and fall based on the 10-year Providence Creek CZO data.

Research Question 3: What are the practical implications of inclusion or exclusion of soil moisture on the timing of fire season and spatial variation in fire risk?

Temporal Effects of including Soil Moisture on predicted Fire Season timing

First, we consider the implications of SMC variations on the the yearly timing of the season when ignition probabilities are > 0.3 for each fuel type. In our results we refer to this as the 'fire season', recognizing that this is somewhat arbitrary, but is useful for analysis.

Associating a 'fire season' with 1-hr and 10-hr FMC reflects their high surface area to volume ratio, which promotes ignition, fire spread and propagation (Bennett et al., 2010; Gould, 2003).

Figure 2.3-G illustrates how the dates associated with the start and end of the fire season varied in 2009 depending on the use of daily SMC, or season-averaged SMC, or the complete exclusion of SMC from the FMC model. As illustrated, the higher FMC in the early spring and late fall greatly curtail the period of time of elevated ignition probabilities for the 10-hr fuels. Meanwhile the predictions based solely on weather/topographic variables or season-averaged soil moisture only, tend to predict lower FMC during these times, and thus earlier starts and later ends to this fire season. Notice, however, that during the height of the fire season (August - October), the predicted FMC is actually lowest in the daily SMC model, illustrating the potential for FMC predictions based on SMC inclusion to also be lower than those that exclude SMC as a predictor variable. If dry conditions arrive in the early spring or late fall, it is possible that SMC based predictions could extend the fire season relative to predictions that fix or neglect SMC.

Indeed, as summarized in box-and-whisker plots for both 1-hr and 10-hr fuels in Figure 2.4, the shrinking of the fire season is not universal; the inclusion of soil moisture barely alters the timing of the fire season for 1-hr fuels (which starts 4 days later and ends 2 days earlier if SMC is considered in the regression, compared to the other models), but tends to significantly delaying the onset of the fire season and the timing of its end for the 10-hr fuels. In particular, dry soil conditions may prolong the fire season, even when meteorological conditions suggest fire risks are lower (whisker on the end of fire season changing soil moisture plot extends beyond the whiskers on the other models). At this site, snowmelt saturates spring soils and retains wet soil conditions well into the warm season, accounting for soil moisture significantly delays the predicted timing of the season start, by approximately 35 days. Although there is more variation at the end of the dry season, accounting for soil moisture increases FMC enough to lower ignition probabilities some 2-3 weeks earlier than predictions based on average or lack of SMC. The total length of the predicted fire season in any specific year, however, can be greater or lesser when SMC is included in predicting FMC (data not shown). Furthermore, the predicted fire season may also change depending on the probability of the ignition threshold chosen to represent fire risk conditions.
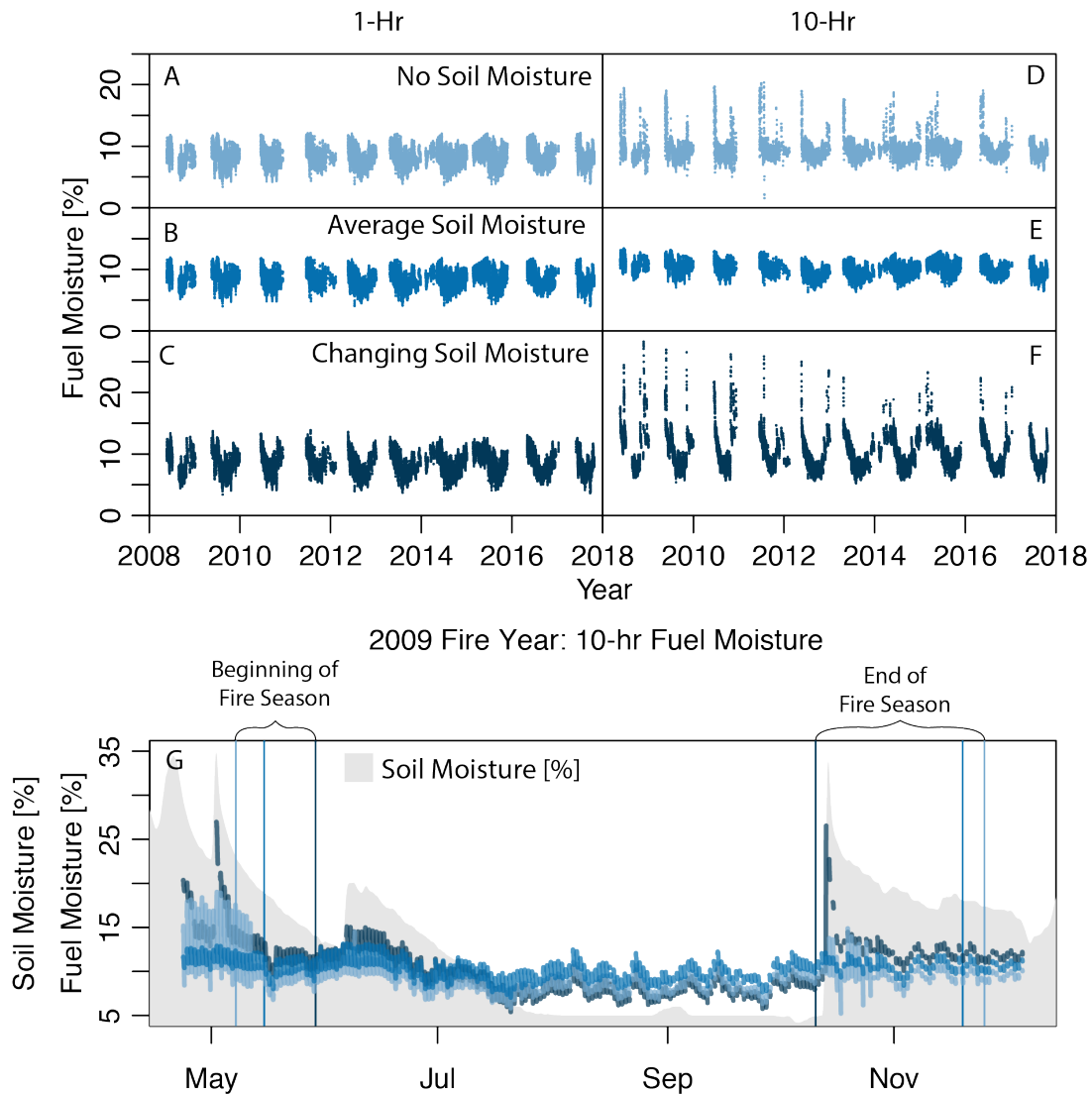
Figure 2.3: 1-hr FMC at Upper CZO Providence site from 2008-2018 predicted by: A) a
linear regressions trained on data without SMC; E) OLS regression with season-averaged
SMC values, and F) OLS regression with daily soil moisture values. 10-hr FMC at Upper
CZO Providence site from 2008-2018 predicted by: D) two linear regressions trained on
data points below and above fuel moisture content of 20.9%, but excluding soil moisture;
E) segmented linear regression with season average soil moisture values, and F) segmented
linear regression with daily soil moisture values. G) Ten-hour FMC, SMC, start, and end of
the 2009 fire season (vertical lines) are shown in dark blue based on changing soil moisture
model, blue for average soil moisture model, and light blue for the model that excludes soil
moisture. Start of the fire season was determined as the 5th percentile of days of the year
with the recorded probability of ignition of 30% or greater. End of the fire season corresponds
to the 95th percentile.
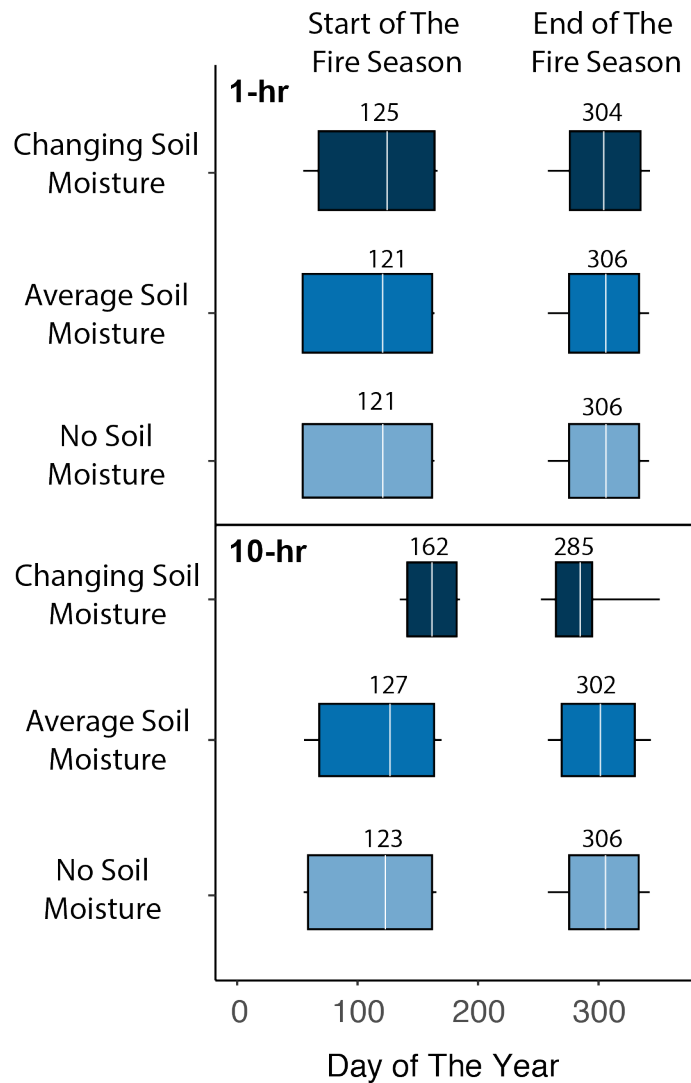
Figure 2.4: Box-and-whisker plot of the start and end of the fire season based on 1-hr (top) and 10-hr (bottom) FMC. The min and max of the start and end of the fire season are summarized as vertical lines, 25th and 75th percentiles as boxes, and mean as vertical white line with a numerical summary above. Fire season was calculated as a function of air temperature, shading, and fuel moisture. The beginning and end of the fire season is defined as the 10th and 90th percentiles of the number of days since January 1st of each year where probability of ignition is greater or equal to 30%.

Spatial Effects of including Soil Moisture on predicted ignition probabilities

Spatially distributed probability of ignition maps for the Illilouette Creek Basin were derived for 10-hr fuels in the spring and fall of 2017 using the changing soil moisture FMC model and the no SMC model (see Appendix A.3). Differences in the resulting predicted probability of ignition for both periods are shown in Figure 2.5. In this map, red colors indicate that probability of ignition is higher at a given location if the model accounts for SMC, and blue colors mean that the probability of ignition is lower if the model accounts for SMC (Figure 2.5).

During spring conditions, including SMC in predictions tends to reduce predicted ignition probability in mid elevations of the basin, particularly along the riparian areas, meadows and creeks. Even during spring, however, low elevation areas in the basin, particularly those with no shading, and some higher-elevation locations with high slope gradients, had sufficiently low soil moisture and/or warm temperatures, that the model including SMC predicted high ignition probability than SMC-excluding models. In the fall, areas predicting lower probability of ignition if SMC is included expand around riparian corridors which retain elevated soil moisture conditions into the fall. Though the difference between fire ignition probabilities (with SMC and without SMC) is less drastic than in the spring. Some high elevation and steep-slope areas predict higher probability of ignition when SMC is accounted for.

These temporal (Providence Creek) and spatial (Illilouette Creek) analyses indicate that including SMC variability in FMC predictions can have large impacts on how models might predict the probability of ignition through time and space, in response to heterogeneous soil moisture conditions.
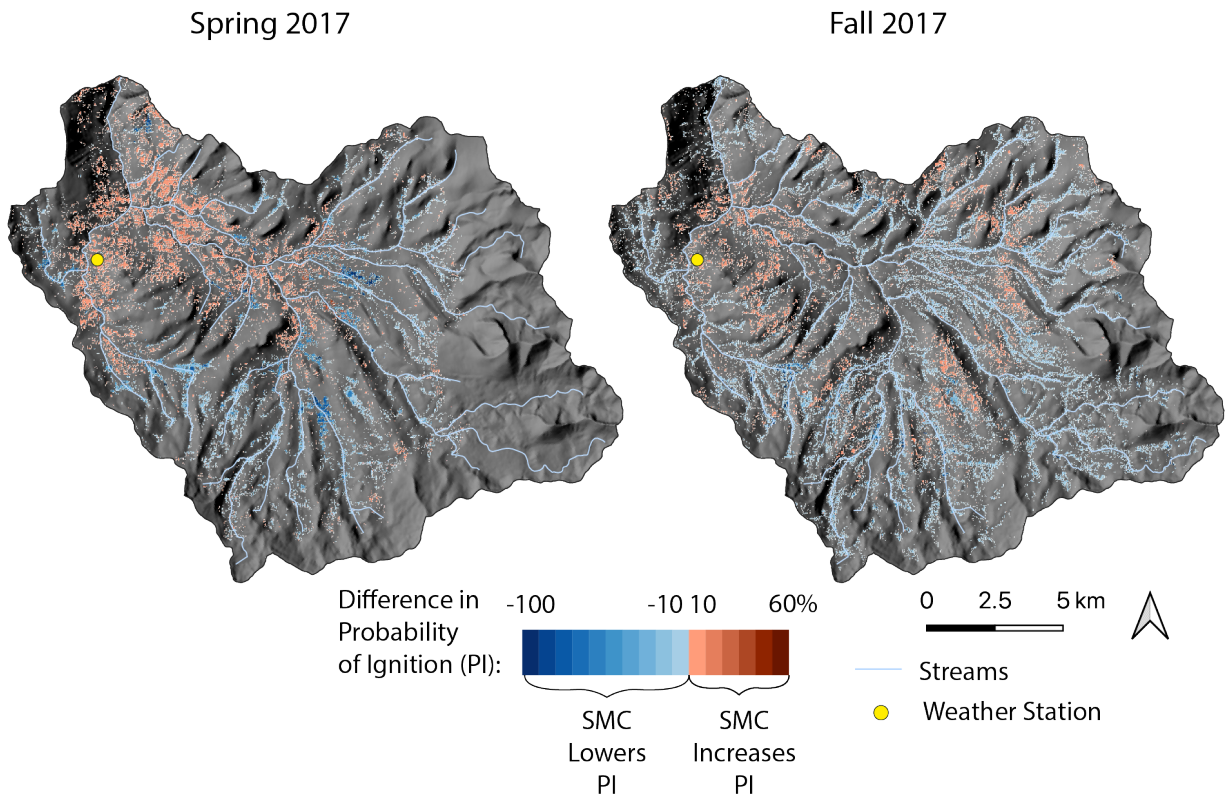
Figure 2.5: Difference in the probability of ignition between regression model trained with soil moisture and model that was trained without soil moisture. VPD (one of the FMC predictors) is calculated using temperature lapse rate of -0.007ºC/m. Temporal weather station (yellow dot) record was used to calculate VPD. Soil Moisture was calculated based on Boisramé et al. (2017). Canopy cover was obtained from LANDFIRE for year 2016 (USGS, 2016) .

2.4 Discussion

The data from Blodgett Forest suggest that both 1-hr and 10-hr fuel moisture contents vary with soil moisture, but with different sensitivities which we attribute to differences in the rate at which these fuels dry out via evaporation. In this interpretation, the relatively weak response of 1-hr fuels to SMC reflects the larger surface-to-volume area of these finer fuels, which enables rapid loss of water in response to increasing atmospheric water demand. The flow of water from wet soils to fuels is expected to be comparatively slow, meaning that atmospheric and radiative conditions impose a stronger influence on the variation in FMC than does the soil water - that is, FMC in the 1-hr fuels appears to be mostly controlled by

the 'demand' for evaporation. By contrast, the smaller surface-to-volume area of coarser fuels slows the rate of drying due to evaporation (R. M. Nelson, 2000; Matthews, 2014), reducing the sensitivity of 10-hr FMC to atmospheric and radiative conditions, and increasing the importance of slower and more consistent water fluxes provided by soil moisture. FMC in the coarser fuels therefore seems to be more controlled by water 'supply' than demand. A dependence on supply would be consistent with the observed increase in sensitivity of FMC to SMC under wet soil conditions, which would tend to increase the rate of supply.

The sensitivity of 10-hr FMC to wet soil conditions is likely to be important under a variety of conditions. In the snow-driven Mediterranean climates of the Sierra Nevada, wet soil conditions following spring snowmelt can co-exist with other-wise fire-prone atmospheric conditions. Excluding soil moisture from FMC predictions could result in an under-estimation of FMC and over-estimation of fire risk at these times. Similar effects could take place following fall rainfall. That said, it must be recognised that the measurements made in this study took place in the context of a wet landscape that was drying in the spring. There is a potential for the SMC-FMC relationships to be hysteretic (to differ under wetting versus drying conditions), which may alter the non-linearity or strength of the SMC-FMC relationship. Further field and laboratory experimentation to better characterise SMC-FMC relationship in drying versus wetting conditions would be useful to resolve this issue. It would also be valuable to increase the observations made in wet soil conditions from the n=22 obtained in this analysis.

The time-series analysis of the SMC and meteorological data from the Upper Providence CZO suggests that changes in the inferred fire season attributable to inclusion of SMC were greatest under drying conditions in the spring. Unsurprisingly, the impacts of SMC inclusion on FMC predictions were minimal for 1-hr fuels (shortening the fire season by 6 days overall). However, for the 10-hr fuels, the greatest impact was to shorten the fire season on average by 39 days. Impacts in the fall were smaller, with the fire season predicted to end 21 days earlier - assuming that the association between FMC and SMC was the same under wetting conditions in the fall as it was under drying conditions in the spring. While it is difficult to anticipate how much the FMC-SMC relationship might change when fuels and soils were both originally dry, we would expect originally dry conditions to weaken the relationship between FMC and SMC, so that the regression model would overestimate the reduction in fire season length in fall. However, even discounting the SMC-FMC behavior in fall, inclusion of SMC in the models increases FMC and is likely to reduce ignition probability in the shoulder seasons. The specifics of how much ignition probabilities change are specific to the minimum FMC used to scale the time-series of FMC from the regression model predictions. If local FMC observations were lower than the minimum observed during field observations at Blodgett, predicted FMC would be lower overall, and the inclusion of SMC would result in a less dramatic change in ignition probabilities.

Spatially, SMC influences the distribution of 10-hr FMC as well. Inclusion of SMC in the models caused both increases and decreases of the probability of ignition relative to a model that excludes SMC completely. In the spring, there are areas that predict much lower probability of ignition (relatively to models that exclude changing SMC) around riparian

areas due to heightened SMC. These wet areas may be crucial as fire-breaks by preventing extensive fire spread throughout the landscape, an inference supported by observations that early spring prescribed fires in the Sierra Nevada produced only patchy fuel consumption (Knapp et al., 2005). However, in mid summer when soil moisture is at its lowest, these dry soils tend to lower FMC predictions, increasing the predicted probability of ignition in some areas of the landscape.

While this study suggests that there is potential to improve the understanding of the spatial and temporal variations in fire risk by incorporating observations/predictions of SMC into FMC predictions, many challenges remain before SMC-FMC relations could be generalised for the purpose of such predictions. These challenges include: (i) characterising SMC-FMC relations across different soil types, which are expected to influence the strength and non-linearity of the SMC-FMC relation, (ii) characterising SMC-FMC relationships for other fine fuel types, notably litter, which often comprises the bulk of fuel loads (Burrows et al., 2006) and could have a different dependence on soil moisture than fine woody fuels (Keith et al., 2010; Raaflaub & Valeo, 2009). In the present study, sampling was confined to locations with low litter content. However, in areas with heavy litterfall and accumulation, it is likely that soils, litter and woody fuels could interact to modify evaporation and water fluxes, and consequently litter and fuel moisture content (Mahdavi et al., 2017; Matthews, 2005). Additionally, (iii) the physical processes associated with movement of water from wet soils to woody fuels remain poorly characterised, and could be productively explored in a laboratory settings. Potentially, such process characterisation could enable physical modeling of the water and energy balance of the surface soil, litter and fuel layers, which could be helpful for generalising relationships across distinct soil and vegetation conditions. Finally, (iv), one of the most powerful avenues for incorporating SMC into FMC predictions at landscape scales is the growing number of satellite remote sensing products that are sensitive to soil moisture (i.e. SMAP, SMOS, MWRI, AMSR-E, AMSR2 and many others Kim et al., 2019). However, the spatial resolution of these products is considerably coarser than the point measurements used to derive the current relationship. Resolving these scale mismatches for the purpose of FMC and fire risk prediction could usefully draw on recent advances in scaling of soil moisture observations (Montzka et al., 2018; Peng et al., 2017; Guevara & Vargas, 2019), but the optimal scale for FMC prediction, and how to inform such predictions with satellite SMC observation, remain essentially open questions.

2.5 Conclusion

This study demonstrated that under soil, weather and vegetation conditions broadly representative of Sierra Nevada mixed conifer forests, fuel moisture covaries meaningfully with soil moisture, and that this covariation is particularly strong for 10-hr fuels under wet soil conditions. Neglecting the relationship between soil moisture and fuel moisture when predicting fire risk is likely to over-estimate ignition probabilities under wet soil conditions, particularly in the spring, and to mis-characterise spatial patterns in ignition risk. More research

is required to understand fuel moisture relations to soil moisture under: wet soil conditions specifically, wetting and drying conditions separately, different soil types, and in the presence of leaf litter layers. Such observational studies would be usefully complemented and informed by a better characterisation of the physical processes governing water and energy balances at the soil surface and between mineral soil, litter and fuel layers. Nevertheless, the results, albeit preliminary, indicate that resolving the effects of soil moisture on fuel moisture could meaningfully improve fuel moisture predictions relative to the status quo of neglecting soil moisture variations. These improvements are most likely to arise under situations where soil moisture variations are not well correlated with variations in fire weather conditions - for instance in transitions between seasons, following snowmelt, and in wet locations in heterogeneous landscapes. With fire and water cycles both changing rapidly in mountainous areas like the Sierra Nevada, better characterising and understanding their influences on each other will be helpful for predicting and responding to changing risk profiles.

Chapter 3

Freeze-Thaw Processes Degrade Post-Fire Water Repellency in Wet Soils

The contents of this chapter were originally published in Horological Processes Journal in 2020, as an article titled "Freeze-Thaw Processes Degrade Post-Fire Water Repellency in Wet Soils", DOI: 10.1002/hyp.13931. Sally Thompson is the co-author.

3.1 Introduction

A century-long policy of fire suppression in California's Sierra Nevada Mountains, like much of the rest of the Western United States, has favored the growth of dense forests with high fuel loads that lead to more frequent catastrophic fires (Collins et al., 2011; Collins, 2014; J. Miller et al., 2009). Catastrophic fires are large in extent and also include large areas of high severity burn, (Keyser & Westerling, 2017; Schweizer et al., 2020), which dramatically changes landscapes, soils and hydrological processes (Robinne et al., 2016; Martin, 2016). Increased runoff generation and elevated erosion rates are well known consequences of severe fire (Tiedemann, 1979; Burch et al., 1989; Kinoshita & Hogue, 2015; Moody & Martin, 2001b, e.g.). For example, fires are responsible for up to 60% of long-term sediment production rates in some regions (Robichaud, 2000). In the Sierra Nevada, up to 3 orders of magnitude increases in annual sediment yield (up to 120 tonnes ha^{-1} per year) have been reported following fires (Moody & Martin, 2009). Post-fire debris flows can be immediate and acute, moving rapidly over large areas, threatening lives and costing hundreds of millions of (US) dollars (e.g. the 2018 Thomas Fire in coastal CA, Cui et al., 2018). Extensive infrastructure damage due to sediment mobilization into water systems is also reported. For example, the 2002 Hayman Fire in the Rocky Mountains deposited $\approx 765,000$ m^3 of sediment into water supply reservoirs, requiring $30 million worth of dredging (Bladon et al., 2014). Post-fire erosion impacts can also be chronic; in the 1996 Buffalo Creek wildfire in Colorado, the

immediate sediment input into reservoirs was only a fraction of the total sediment load from the fire, 67% of which was deposited in stream beds and is expected to be exported gradually over a 300-year period (Moody & Martin, 2001a).

Both vegetation loss and physicochemical changes in topsoil after fires contribute to elevated runoff and erosion rates (Keeley, 2009; Mataix-Solera et al., 2011; Stoof et al., 2011; Caon et al., 2014; Stoof et al., 2015). Vegetation canopies, roots, litter, and duff mitigate runoff and erosion by reducing throughfall volumes via canopy interception (e.g. Ahlgren, 1981), maintaining higher infiltration rates by protecting the soil surface from rain splash and soil seal formation (Assouline & Mualem, 1997), mechanically increasing soil cohesion (Gyssels et al., 2005), and slowing flow and trapping suspended sediments (Stoof et al., 2015). Loss of vegetation cover thus contributes to increased runoff and erosion through multiple pathways (Larsen et al., 2009b). The impacts of these process changes are enhanced when fire also produces physiochemical changes to topsoils, including inducing soil water repellency (DeBano, 2000). Soil water repellency is attributed to the volatilization and subsequent condensation of organic chemical species on soil grains (DeBano & Krammes, 1966), which are derived from the complex humic fraction of the soil (S. H. Doerr et al., 2000; DeBano, 2000). The deposition of these chemicals coats on soil grains results in a mixture of nonpolar (insoluble in water) and amphiphilic (partially soluble in water) compounds that tend to inhibit infiltration. By cementing soil grains together, decreasing porosity and increasing the stability of soil aggregates (coherent units formed by chemically or physically bound soil particles, Nimmo, 2005; Giovannini et al., 1983; Kořenková & Matúš, 2015), hydrophobic compounds can further inhibit water entry into soil. Hydrophobicity usually manifests as a spatially heterogeneous water repellent layer within the top 8 cm of the soil (DeBano et al., 1970; Ebel & Moody, 2020), with its precise depth and extent depending on the vegetation type and properties of the fire (DeBano, 2000; DeBano et al., 1970). Many techniques are available to measure hydrophobicity, all of which assess the physics of water interaction with soils (e.g. the time taken to infiltrate a droplet of water (Letey, 1969), the contact angle of water on the soil surface (Bachmann et al., 2000), or the extent of capillary rise within the soil (Letey et al., 1962)). In this study, hydrophobicity was measured with Molarity of Ethanol Test (MED), which relates soil hydrophobicity to an ethanol concentration of a water drop used to infiltrate soil over a set time (King, 1981).

Post-fire soil hydrophobicity is not a permanent soil property, but decreases at a variable rate, typically returning to pre-fire levels within 1 to 6 years (Shakesby, 2011; Leelamanie & Karube, 2007). There are some clear associations between hydrophobicity levels and the environmental conditions experienced by soil, including temporary increases in wettability with increasing soil moisture content (S. H. Doerr et al., 2000), more permanent increases following repeated cycles of wetting and drying (Quyum et al., 2002; S. H. Doerr et al., 2000), and increases in wettability following soil agitation (Horne & McIntosh, 2000; Mashum & Farmer, 1985; King, 1981). The underlying mechanisms responsible for degradation via these environmental drivers remain unclear, with chemical leaching (S. Doerr & Thomas, 2003), chemical transformation of hydrophobic compounds (Simkovic et al., 2008), destruction of aggregates (Horne & McIntosh, 2000; Mashum & Farmer, 1985; King, 1981), and creation of

preferential flow paths all finding inconsistent support across studies (Leelamanie & Karube, 2007; Jordan et al., 2017). Additionally, several studies suggest that complex surface chemical processes, such as changes in isomer configuration or ion exchange states could cause reversible changes to hydrophobicity (S. H. Doerr et al., 2000; Horne & McIntosh, 2000; Kleber et al., 2007).

In the Sierra Nevada (and much of the western US), the fire season is followed by a cold, wet winter. In these environments, the wet-dry cycling that is linked to the reduction of soil hydrophobicity also involves freeze-thaw cycles at the soil surface. Freeze-thaw processes in soils are known to generate a range of physical (Ferrick & Gatto, 2005; Fitzhugh et al., 2001, e.g. frost heave), chemical (DeLuca et al., 1992; Herrmann & Witter, 2002, e.g. enhanced mineralization), and biological (Yanai et al., 2004, e.g. depression of enzyme reaction kinetics and degradation rates) changes (Marion, 1995; Henry, 2007). In particular, freeze-thaw cycles have been repeatedly shown to reduce soil aggregate stability (Oztas & Fayetorbay, 2003; Kværnø & Øygarden, 2006; Zhang et al., 2016), a reduction often associated with the degradation of soil hydrophobicity (Giovannini et al., 1983; Kořenková & Matúš, 2015; Horne & McIntosh, 2000; Mashum & Farmer, 1985; King, 1981). To date, however, there is almost no information measuring how soil hydrophobicity degrades following exposure to freeze-thaw cycling, and how this degradation compares to that induced by the better known process of soil wetting and drying. One study reported that *freeze-drying* converted a severely water-repellent soil into a readily wettable soil, although rewetting and oven drying restored water repellency (Mashum & Farmer, 1985). No *in situ* or laboratory studies have been undertaken to explore freeze-thaw cycling effects on hydrophobicity in contexts similar to those in the field (e.g. repeated freezing, thawing, wetting, and drying processes).

To begin to fill this knowledge gap, we tested the effects of freeze-thaw cycles on the degradation of heat induced soil hydrophobicity in a laboratory study. Hydrophobicity was measured using MED on soil samples subjected to repeated and varied combinations of wet-dry and freeze-thaw cycles. To constrain potential degradation mechanisms, the soil samples were characterized chemically, physically, and at the granular level (via electron microscopy) under contrasting MED conditions. The relationships obtained between soil hydrophobicity and soil exposure to different freeze-thaw and wet-day cycles were then used to estimate the timescale over which post-fire hydrophobicity would decay in the field under Sierra Nevada climate conditions, and to assess the significance of freeze-thaw processes for recovery of soil wettability in this area.

3.2   Methods

Soil Preparation

Soil samples were obtained from the Jennie Lakes Wilderness (36.71403°N, -118.75708°E) located in the Californian Sierra Nevada at an elevation of 2530 m. Soils were sampled from beneath a canopy mix of Jeffrey pine (*Pinus jeffreyi*), lodgepole pine (*Pinus contorta*), white

fir (*Abies concolor*), and red fir (*Abies magnifica*). No fires were recorded in the sampling location since local records for the Sequoia Kings Canyon National Park began in 1910 (see fire perimeter data at https://frap.fire.ca.gov/mapping/gis-data). Soil samples were taken from the top 5 cm of mineral soil after first removing the surface litter layer, which consisted of pine needles and duff. Approximately 5 gallons of soil were collected, and air dried at room temperature (25 °C) in a laboratory at UC Berkeley, until the soil weight stabilized. The dry soil was sieved at 2 mm and homogenized (Figure 3.1-A). In previous studies, sieving had no significant impacts on soil hydrophobicity (Badía et al., 2013; King, 1981). The soil was sandy (75% sand, 6% clay, and 19% silt).

The MED test was used to assess the hydrophobicity of soil. The test identifies the molarity of ethanol in water needed for a drop of the solution to infiltrate into the soil in a fixed 10 second time period (King, 1981; Watson & Letey, 1970). We implemented MED tests using ethanol solutions ranging from 0% to 22% molarity, in increments of 0.5%. Soil is deemed moderately hydrophobic above 5.5% (King, 1981). The MED of the field sampled soil was 6.5%, indicating that a low level of hydrophobicity was present in the native soil. Even in the absence of wildfires, hydrophobicity is observed in many sandy soils, especially under *Pinus* species (S. Doerr et al., 2009; Zavala et al., 2014).

To determine optimal heating conditions, soil sub-samples were held in a furnace at temperatures ranging from 150 to 285 °C for 15 and 20 min. Once cooled, their hydrophobicity was assessed with the MED test. The highest MED value of 16% ('very hydrophobic') was achieved for soils that were heated for 15 minutes at 260°C (data not shown). Then, sixty aluminum baking trays, each containing 6 separate pans, were filled with 8-12 g of soil in each pan. Each tray was heated once for 15 minutes at 260°C (3.1-B). Throughout heating, the furnace (*Fisher Scientific Isotemp Muffle Furnace 650-14*) fluctuated ± 1°C. The soil was cooled before any further treatments were applied.

Reference samples of both hydrophobic and hydrophilic soils were also prepared. We considered two kinds of hydrophilic soils: the original, sieved and homogenized field soils, which are referred to as 'non-heated' soils, and hydrophilic soils prepared by heating the soil until soil hydrophobicity was minimized, referred to as 'heated hydrophilic' soils. Heated hydrophilic soil was prepared by heating field soil at 260^0C until smoke was generated and for at least 20 min. The MED for these soils was 0% with pure water droplets infiltrating instantly. Finally, reference samples of heated hydrophobic soils were also prepared, similarly to the treatment soils, by holding field-collected soil (homogenized and sieved) at 260^0C for 15 min.

Experimental Treatments

The hydrophobic soils were subjected to different treatments (Figure 3.1-C), comprising different, physically plausible, combinations of wet-dry and freeze-thaw cycling. These treatments are:

- repeated wet/dry cycles (WD)

- repeated wet/freeze/thaw/dry cycles (WFTD)

- repeated wet/dry/freeze/thaw (WDFT)

- repeated freeze/thaw cycles on dry soils (DFT)

- repeated freeze/thaw on wet soils (WFT).

To wet the soil (as required in the WD, WFTD, WDFT, WFT cycles), de-ionized water
was applied using a misting spray bottle. The mist application was selected to minimize the
impact of drop splash on the soil surface. Water was sprayed onto the surface until free water
ponded to a depth of approximately 1 cm on the soil surface, after which the sample was
left undisturbed for 12 hours. Perforation in the aluminum baking pans allowed for water
to drain if it fully infiltrated the soil column. Any remaining ponded water was removed
from the soil surface with a pipette after 12 hours. This situation often occurred in the first
treatment cycles while soils were highly hydrophobic. For the WFT treatment, soil samples
were wetted once and the trays with soil were stored in sealed plastic bags to prevent drying.
Each sample was allowed to dry once only, immediately before the MED measurement. To
dry the soil (as required to measure MED for the WFT treatment, and as part of the regular
treatment cycle for the WD, WFTD, WDFT, DFT treatments), soil samples sat for twelve
hours at room temperature ($\sim 25^0$C). To freeze the soil (as required for the WFTD, WDFT,
DFT, WFT treatments), soil samples were placed in a temperature stable freezer at -20^0C
for at least 6 hours. To thaw the soil, frozen soil samples were left at room temperature for
at least 6 hours. The time periods used were determined following experimental pilots which
found that the soil samples dried (to the point where no further weight change was recorded
with further drying) after 12 hours, and that water without soil would freeze and thaw in
the freezer and at room temperature within 6 hours.

Each treatment was applied to 12 separate soil samples (i.e. 2 of the aluminum trays).
For each treatment, one sample was used to measure MED after induction of hydrophobicity
and before treatment application. The remaining 11 samples were subject to between 1 and
11 repeated treatment applications referred to as "cycles" (Figure 3.1-C). Each treatment
was replicated six times. After each treatment cycle, MED was measured for one sample.
The location of the samples used for each cycle was randomized across all treatments to avoid
any systematic biases associated with location within the trays. Figure 3.1-B illustrates this
schematically for one treatment.
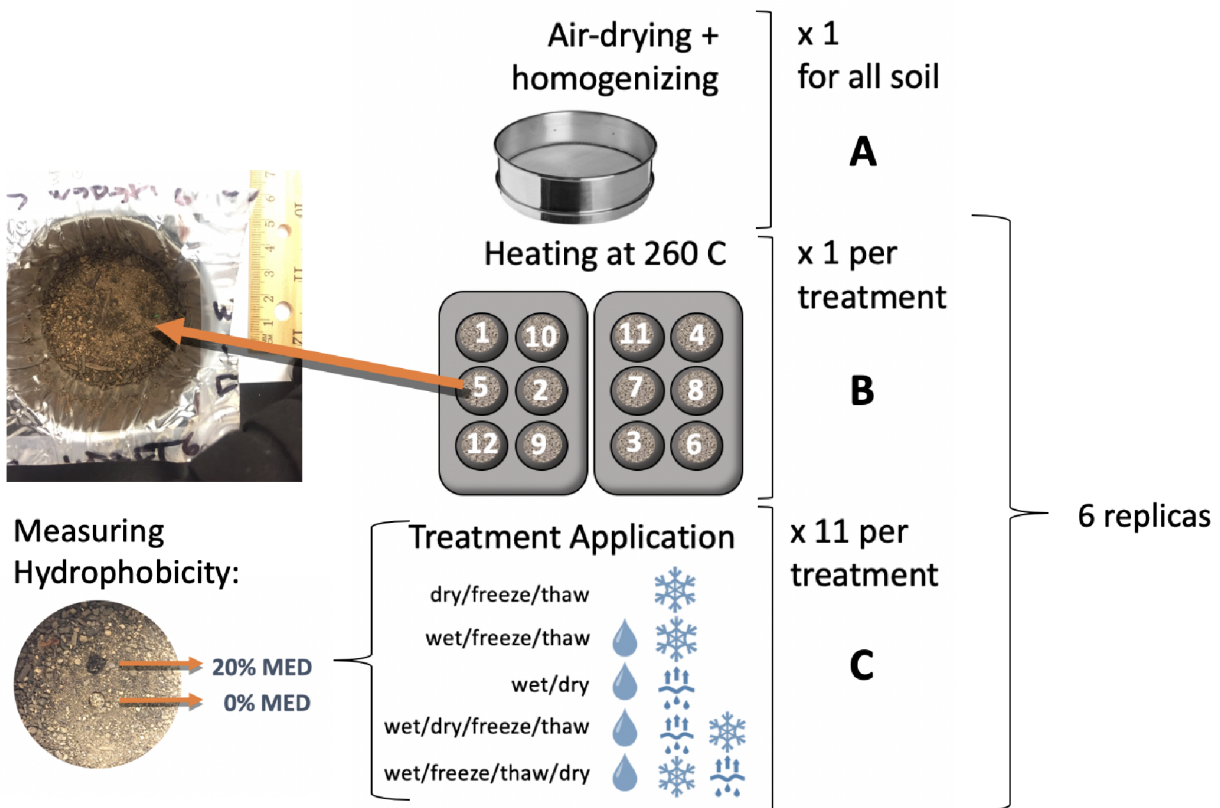
Figure 3.1: All soil was first air dried at room temperature until its weight stopped changing, then sieved with a 2 mm sieve, and homogenized through mixing (A). Prior to heating, soil was divided between treatment trays. There were 2 trays per treatment with space for 12 samples. Each sample represented one cycle of a given treatment and was assigned a random location within the treatment trays. Each set of treatment trays was heated once at 260 °C for 15 min (B). Five different treatments cycles were then applied 11 times, and MED measurements made between each cycle (C).

Total Organic Carbon

Three replicas from each cycle and treatment were used to assess changes in total organic carbon content via the Walkley-Black test according to a standard protocol following D. W. Nelson & Sommers (1965) at UC Davis Analytical Laboratory (https://anlab.ucdavis.edu/). The Walkley-Black method was chosen because it is accurate on soils with low total organic matter (<15%). The entire soil sample was analysed in each case. In total, 180 samples were measured, including 20 duplicates used to check reproducibility.

Scanning Electron Microscopy

Scanning Electron Microscopy (SEM) was used to visualise the surface topography of non-heated soil, heated hydrophobic soil, and heated hydrophilic soil. We also made one opportunistic measurement of a soil sample that went through seven cycles of wet/dry/freeze/thaw (WDFT): this was the only undisturbed treated sample available for SEM scanning. Untreated soil samples were evenly sprinkled on a mount while surface soil from the WDFT sample was carefully removed and placed on a mount: the SEM imagery of the WDFT soil therefore imaged the undisturbed soil surface.

All samples were sputter coated with a thin gold/palladium film. Subsequently, samples were examined with a Hitachi TM4000 microscope. Imagery of samples was taken using backscattered electrons (BSE), second electrons (SE), and Mix (mixture of SE and BSE) detection modes with an acceleration potential of 15 kV at resolutions of 100, 300, 400, 500, and 1000 times. We present images at $\times 100$ resolution in the BSE mode, in which individual aggregates are most distinguishable. In this analysis, aggregates are identified as individual particles, or collections of particles clumped together and including not only the mineral substrate but also the organic matter.

Using ImageJ software (Rasband & Ferreira, 2012), aggregate size analysis was performed for $\times 100$ BSE and Mix images of non-heated, heated hydrophobic, heated hydrophilic, and 7th cycle of WDFT soil samples. First, each image was binarized into aggregates and void space using a grayscale threshold (image intensity value from a range of 0-256). All void pixels enclosed within aggregate pixels were reclassified as aggregate pixels using the "Fill Holes" tool. The "Watershed" tool was used to separate individual aggregates. The tool successfully separated adjacent particles, but in some cases erroneously broke down aggregates into smaller pieces. We manually examined all images and removed watershed lines that incorrectly separated parts of an aggregate, focusing on the largest aggregates. Finally, the "Particle Size Analysis" tool was used to calculate an area for individual aggregates and generate the cumulative aggregate size curve, showing the percentage of aggregates smaller than a given area.

Following this methodology, the aggregate area is sensitive to the threshold used to binarize the image. To standardize, we selected thresholds as the 40%, 50%, and 60% percentiles of the grayscale intensity distribution of each image. Although we did not have multiple images to compare the analysis across, we tested for sampling bias and variability

by repeating the analysis (with the 50% threshold level) on three random, non-overlapping sub-samples of each image. We report both the cumulative aggregate size distribution curves and the percentage the largest ten particles occupy out of the total aggregate area based on the analysis of the four ×100 BSE images using 50% threshold.

Time frame of hydrophobicity decay in the Sierra Nevada

The laboratory experiment relates changes in MED to the application of successive treatment cycles. To relate these cycles to an estimate of time-since-fire, we used a nine year climate and soil moisture record (October 1, 2008 through October 1, 2017) from the Providence Critical Zone Observatory (CZO) site located in the Southern Sierra (Bales, Hopmans, et al., 2011). We obtained air temperature, snowpack depth, and shallow soil moisture measurements at 10 cm depth from the Upper Providence sensor node located on flat aspect and having open canopy (elevation: 1982 meters, lat: 37.0626N, lon: -119.1823E, data: https://eng.ucmerced.edu/snsjho/files/MHWG/ Field/SouthernSierraCZOKREW). The reported soil texture at this site is very similar to the soil collected for the main experiment at Jennie Lakes Wilderness, with 79% sand, 6% silt, and 15% clay (Bales, Hopmans, et al., 2011). Vegetation around the Providence CZO instrumentation site is also very similar to our soil sampling location, with 76-99% of the Providence watershed cover comprising of mixed-conifer forest of white fir (*Abies concolor*), ponderosa pine (*Pinus ponderosa*), Jeffrey pine (*Pinus jeffreyi*), sugar pine (*Pinus lambertiana*), and incense cedar (*Calocedrus decurrens*) (Bales, Hopmans, et al., 2011).

Daily precipitation data were obtained from the neighboring (within 40 m) Upper Providence Weather Station (data: https://www.fs.usda.gov/rds/archive/catalog/RDS-2018-0028). Missing air temperature records ($\approx 10\%$) were gap filled from the neighboring weather station, and remaining gaps ($< 0.2\%$ of the record) were linearly interpolated. Hourly air temperature data were averaged to a 6 hour resolution to correspond to the timescales of freeze/thaw used in the laboratory cycles. The hourly soil moisture record was smoothed using a cubic smoothing spline function (*smooth.spline* in R) to generate a 6 hour record.

We classified the smoothed soil moisture data, identifying drying events when the volumetric water content fell below 6%, and wetting events when the volumetric water content rose above 6%. The 6% cutoff is based both on the CZO time-series at 10 cm depth of minimum soil moisture threshold and studies stating that the critical soil moisture for a transition between hydrophobic and hydrophilic soil state can range anywhere between 2-28% at surface (Dekker et al., 2001; S. Doerr & Thomas, 2003; S. H. Doerr et al., 2000).

Where smoothed soil moisture at 10 cm was $< 6\%$ but a precipitation event of > 1cm was recorded, we assumed that the surface soil was wetted and then dried, but that the wetting fronts had not reached the sensor at 10cm. We assumed, however, that these events represented a wet-dry cycle at the soil surface that would impact hydrophobicity. If dry conditions were maintained through repeated days of precipitation, these were treated as a single wet/dry event. Precipitation events were assumed not to contribute to wet/dry cycles when the snowpack was over 10 cm, regardless of the soil condition.

To account for the effect of the thermal insulating properties of snowpack, we assumed that no freeze-thaw cycles could be induced in the soil when the snowpack depths exceeded 10 cm. Above this depth, snowpack acts as an insulator that de-couples air temperature from soil surface temperature (K. L. Thompson et al., 2018; Zhao et al., 2018; J. Chang et al., 2014). Provided snow depth was < 10cm, then a freeze event was identified when air temperature dropped below 0°C (on 6 hour timescales). Thaw events occurred when sub-zero temperatures then rose above 0°C. Dry freeze/thaw cycles were identified as freeze-thaw cycles occurring when the soil was dry (soil moisture at 10 cm below 6%). Wet freeze/thaw cycles required either a wet soil or a freeze/thaw cycle that occurred within 24 hours of a precipitation event on dry soil.

For the nine year data record (2008-2017), we calculated the time taken for each cycle to occur following a hypothetical fire that stopped burning on October 1st. The final hypothetical fire ended in October 2015; this was the last date for which sufficient climate data were available to resolve all 11 cycles. Finally, the different cycles were converted into an estimate of hydrophobicity decline, with drops in hydrophobicity estimated based on the different rates of decline (and the uncertainties in these rates across the experimental replicates) associated with each of the different kinds of wetting-drying or freeze-thaw cycles experienced.

3.3   Results

Soil Water Repellency Degradation Mechanisms

After heating soil at 260^0C for 20 min, the mean MED for the soil samples was 16.6% (cycle 0 in Figure 3.2), classified as very severely hydrophobic (King, 1981). Hydrophobicity remained the same after one cycle of treatments that included a freeze/thaw component of wet soil (WFT, WFTD), and increased by 1.6% MED for cycles with a wet/dry component (WD and WDFT). After 3 cycles of treatment, the MED of the treated samples other than the DFT treatment all declined below a reference condition given by the 'heated hydrophobic' soil. The MED values of the DFT treatment were statistically indistinguishable from the 'heated hydrophobic' reference across all treatment cycles. Freeze-thaw cycles applied to wet soil, however, lead to declines in hydrophobicity, whether or not the soil was allowed to dry between the freeze-thaw cycles. All cycles containing a wetting component lead to similar rates of hydrophobicity decline. However, the wet/freeze/thaw cycles exhibit greater MED variability across replications than the other cycles involving a wet soil phase (standard deviation of 3.1% MED vs 1.7% MED respectively). The soil water repellency returned to conditions similar to the non-heated hydrophobic native soils (MED=6.5%) after the 6th cycle for all treatments other than DFT. By the end of the 11th cycle, the mean MED across treatments (other than DFT) dropped to 1.9%, much lower than the MED of the non-heated soil from the field.
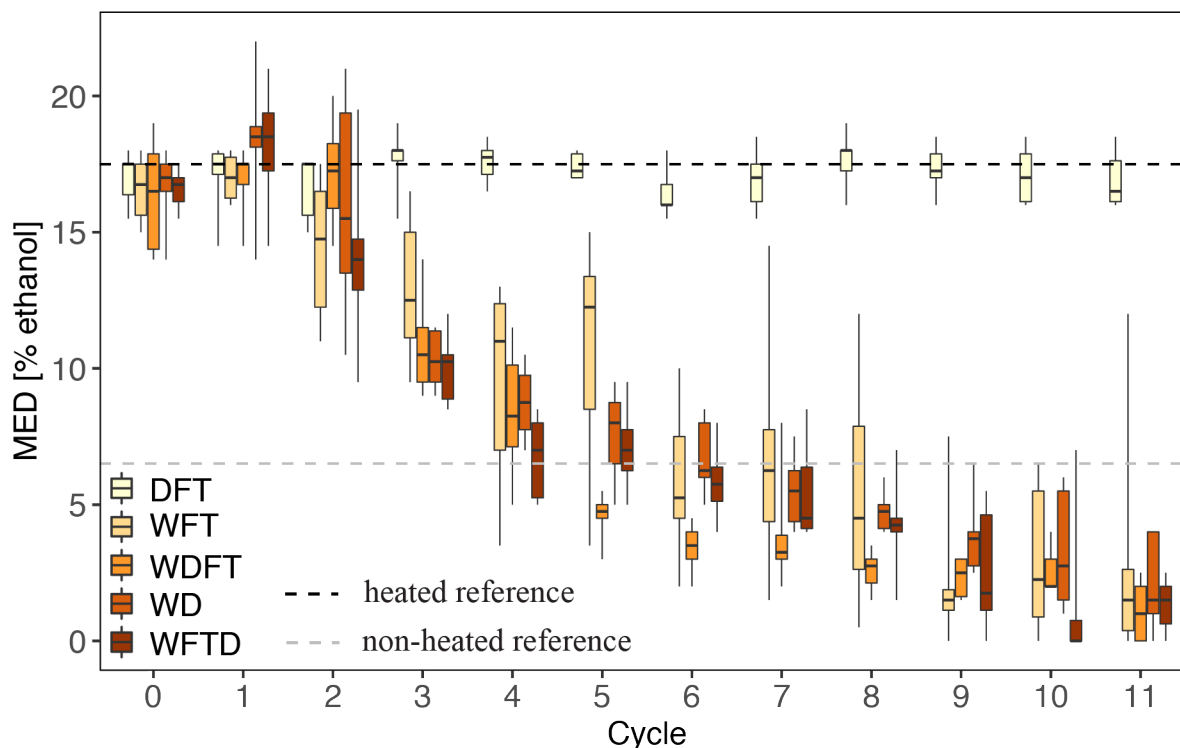
Figure 3.2: Box and whisker plots of hydrophobicity as measured by the MED test for eleven
cycles of five treatments, each replicated six times; the treatments are dry/freeze/thaw
(DFT), wet/freeze/thaw (WFT), wet/dry (WD), wet/dry/freeze/thaw (WDFT), and
wet/freeze/thaw/dry (WFTD). MED of heated, but not treated soils is shown by Cycle
0. Average MED of non-burned soil is indicated by a gray dash line. Average MED for a
reference soil that was burned but without treatment application measured throughout the
experiment is indicated by a black dashed line.

As multiple treatment cycles progressed, the soil surface became visually different. Pho-
tographs of the soil surface for one of the replicas of the wet/freeze/thaw cycles are shown
in Figure 3.3. Small fissures that appeared in the soil surface following treatment are high-
lighted in white. Fissures developed after 2 cycles, and their number and length increased
as treatment applications increased. Similar patterns were observed in all treatments that
involved a wetting component. No fissures formed on the soil surface of dry/freeze/thaw
cycles (images not shown).
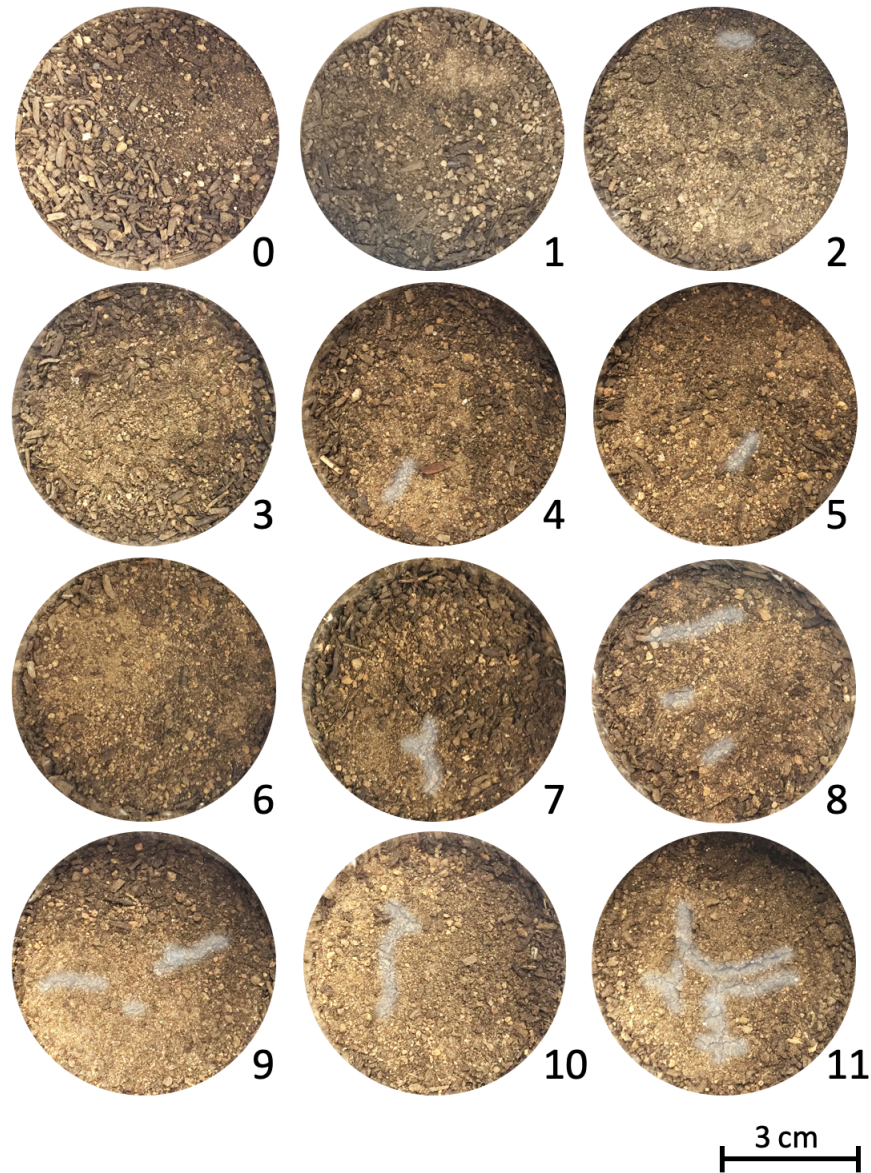
Figure 3.3: Images of eleven cycles of wet/freeze/thaw treatment. Cycle "0" is heated but untreated soil sample. Each image is of a different soil sample that went through an assigned number of cycles within one replica of the WFT treatment. Visible racking on soil surface is highlighted in white.

Soil Organic Matter

Soil organic matter (SOM) measured for all cycles and treatments with three replicas is presented in Figure 3.4. Prior to treatment applications, the mean SOM (cycle 0) was 10.9%±0.68 (1.2%±0.54); here, the standard deviation across treatments is shown in brackets, and errors are based on the differences between 20 replicate samples. By the 11th cycle, SOM had decreased by 1.8% SOM which is significantly different from the pre-treatment (cycle 0) SOM, based on a 2-sided Kolmogorov-Smirnov test. The overall change, however, is small. There is a weak correlation of 0.27 (data not shown) between treatments' SOM content and measured MED. There is no significant difference in SOM between treatment types. Potentially these SOM results were diluted by measuring SOM for the whole soil sample, rather than the soil surface only. We estimate that the soil surface represents $\sim 10\%$ of the entire soil sample.
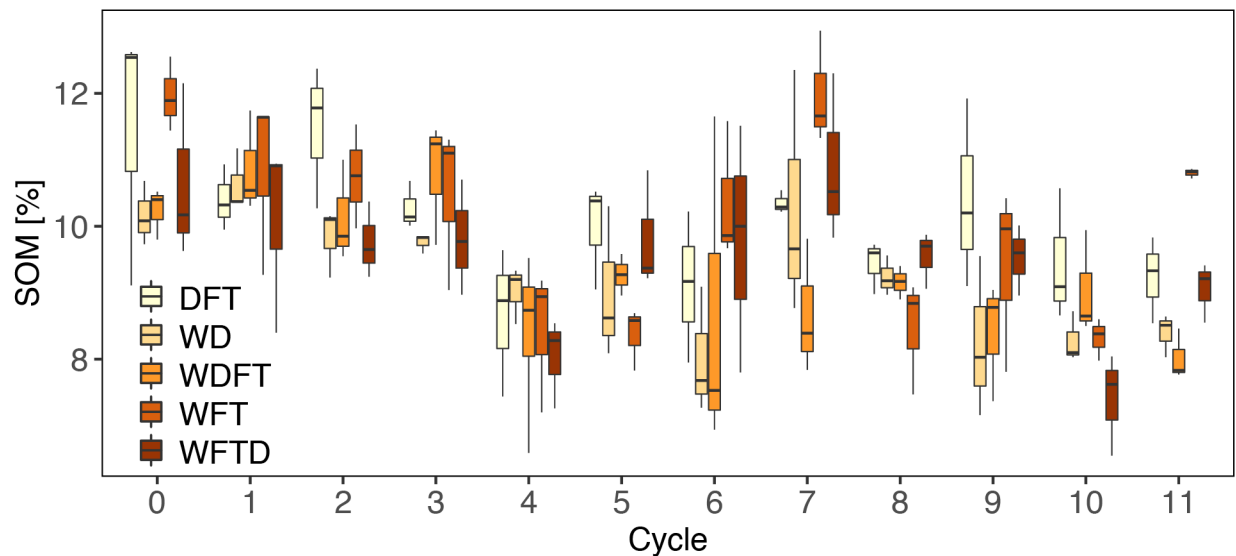
Figure 3.4: Box plot of the total organic matter as determined by Walkley-Black test for eleven cycles of five treatments, each with three replicas; the treatments are dry/freeze/thaw (DFT), wet/freeze/thaw (WFT), wet/dry (WD), wet/dry/freeze/thaw (WDFT), and wet/freeze/thaw/dry (WFTD). Cycle 0 is SOM of heated, but untreated soil samples. The variability in Cycle 0 measurements encompasses both measurement error and potential variability of SOM in soil.

Scanning Electron Microscopy

The SEM images in Figure 3.5 did not reveal any differences in the organic matter matrix that has been reported by others (Jiménez-Morillo et al., 2017). This may be due to the organic coating being too thin for the SEM to detect (S. H. Doerr et al., 2000). Though at ×100 resolution, there were differences in aggregate size distribution between soils of different MED (Figure 3.6).
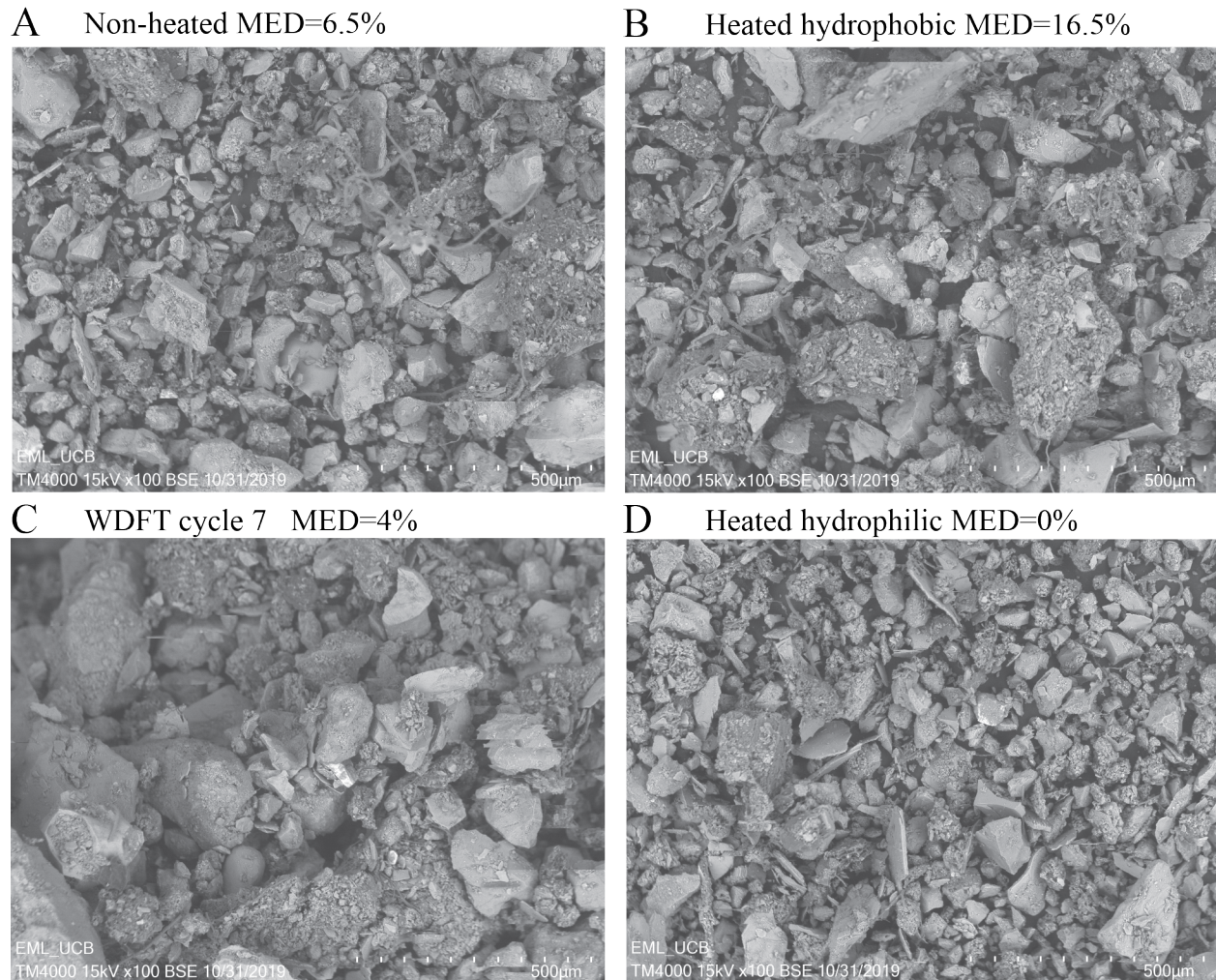
Figure 3.5: Scanning Electron Microscopy images at x100 magnification and BSE mode of soil surface of non-heated (A), heated hydrophobic (B), cycle 7 of WDFT (C), and heated hydrophilic (D) soil samples. A, B, and D were prepared by sprinkling soil samples on a mount, while C by placing an undisturbed portion of soil crust on a mount. Mean soil aggregate size from smallest to largest is D, A, B, C.

Based on the aggregate size distribution curves, the ten largest aggregates make up 58% of the total aggregate area for cycle 7 of WDFT, followed by 44% for the heated hydrophobic soil, 33% for the non-heated soil, and 21% for the heated hydrophilic soil samples. The aggregate size below which 50% of the aggregates are finer is 2.9, 0.9, 0.5, and 0.3 cm^2 for the 7th WDFT cycle, heated hydrophobic, non-heated hydrophobic, and heated hydrophilic respectively. Based on these two metrics, there is a positive correlation between MED and aggregate size among non treated samples. However, this relationship does not hold when the treated (7th cycle of WDFT) sample is included; even though its MED of 4% is relatively low, cycle 7 of WDFT treatment has larger aggregates among all of the samples.

Analysis using different grayscale thresholds and image sub-sampling (data not shown) produced aggregate size distribution curves with the same relative relationship as in Figure 3.6, making our analysis robust.
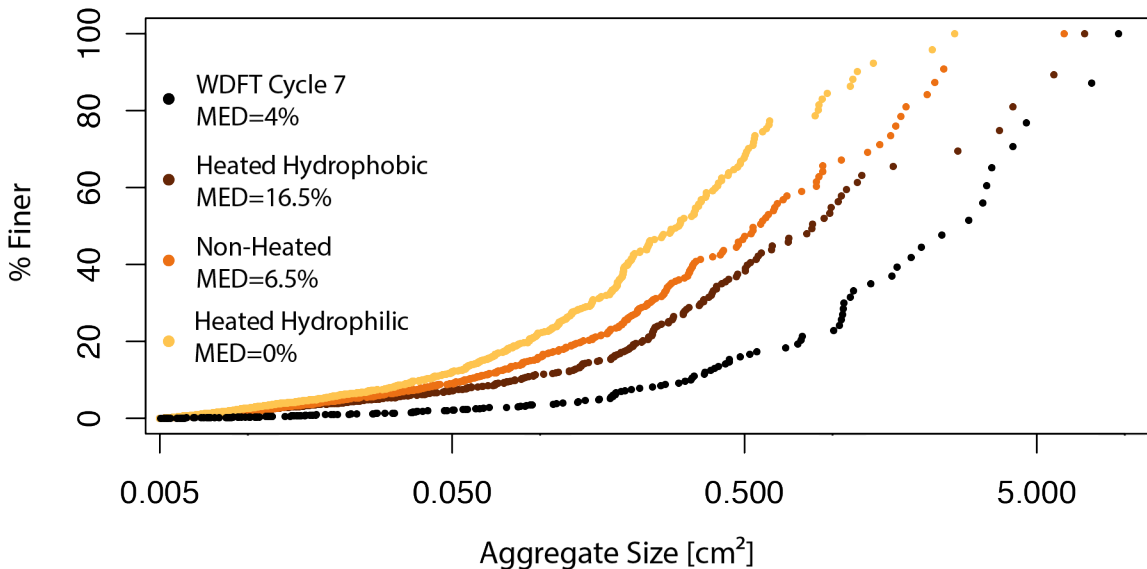
Figure 3.6: Aggregate size (area) distribution curve of heated hydrophobic, heated hydrophilic, non-heated, and cycle 7 of WDFT soil samples. Aggregate sizes were calculated from SEM images at x100 resolution and BSE detection mode. Minimum particle size was cutoff at 0.005 cm^2

Sierra Nevada Climate and Hydrophobicity Decay

Fifty-nine freeze-thaw events and 38 wet-dry events were identified in the nine year climate and soil moisture record from Upper Providence CZO, as shown in Figure 3.7-A,C. The identification of these events for the 2013 water year is shown in Figure 3.7-B and -D.

Figure 3.8-A shows the timing of the first eleven successive WFT, WDFT, or WD cycle relative to October 1st over the eight analysed years. In Figure 3.8-B, the hydrophobicity distribution associated with each cycle is shown as a function of the median number of days since October 1st when that cycle occurred. Seventy-one percent of the first eleven cycles over eight years were wet/freeze/thaw cycles. The most rapid reduction of hydrophobicity during the analysed period was for winter 2011-2012, when all eleven cycles occurred in 79 days and were primarily wet freeze/thaw cycles. The longest duration of hydrophobicity was associated with the severe warm California drought from 2014-2015: hydrophobic soils induced prior to that winter would have persisted for 562 days. On average, the eleven cycles considered occurred within 350 days. Hydrophobicity was typically reduced to the
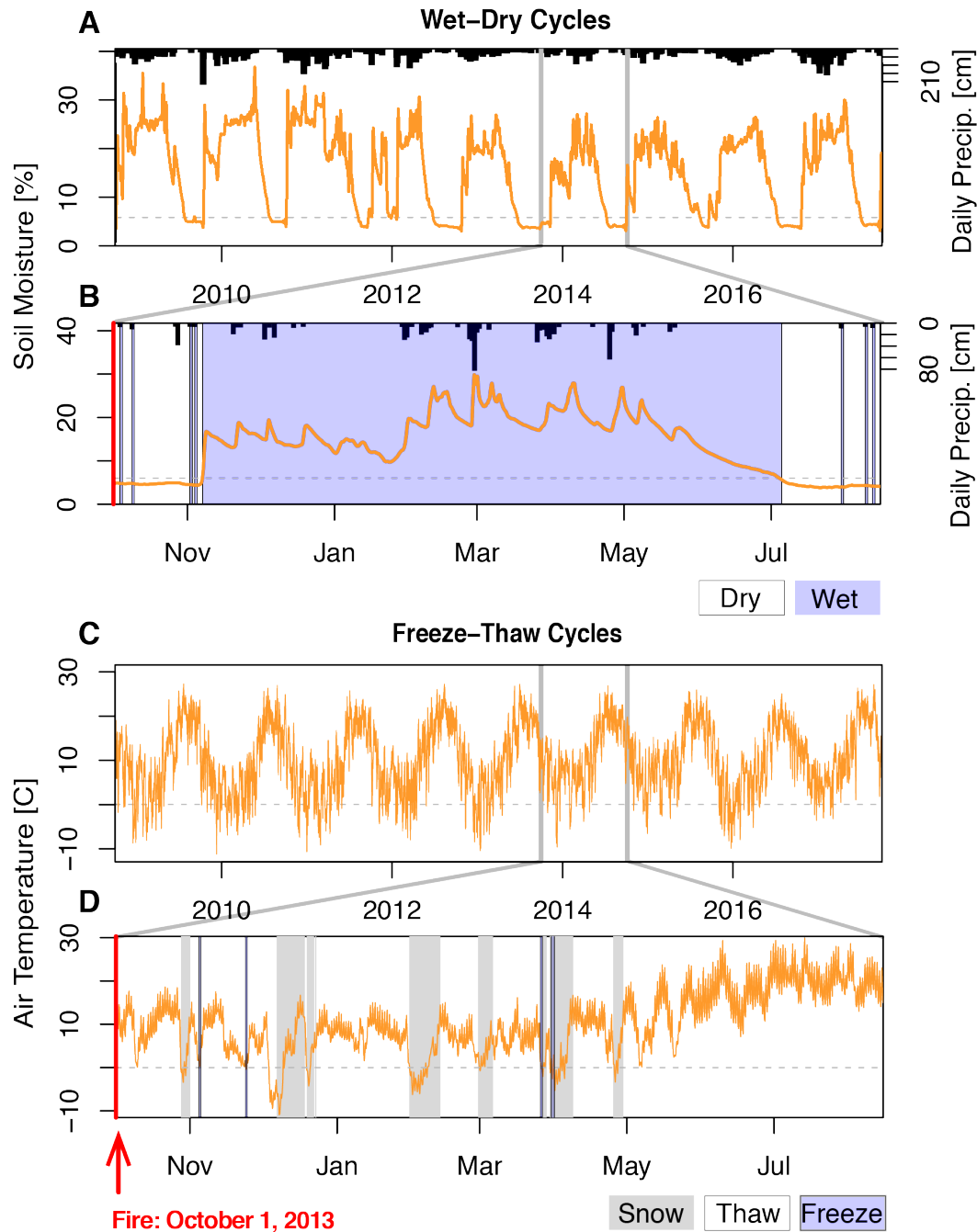
Figure 3.7: Soil moisture at 6 hour resolution and precipitation at daily resolution time series for the entire nine year record (A), and October-April 2013-2014 (B). Shading in the the zoomed-in soil moisture and precipitation time series shows occurrence of wet and dry periods; each vertical bar represents a wet/dry cycle (B). Air temperature time series at 6 hour resolution for the entire nine year record (C), and October-April 2013-2014 (D). Purple shading in the zoomed-in in events shows freezing events when snowpack is below 10 cm. Periods of time when snowpack is above 10 cm is shaded in gray (D).
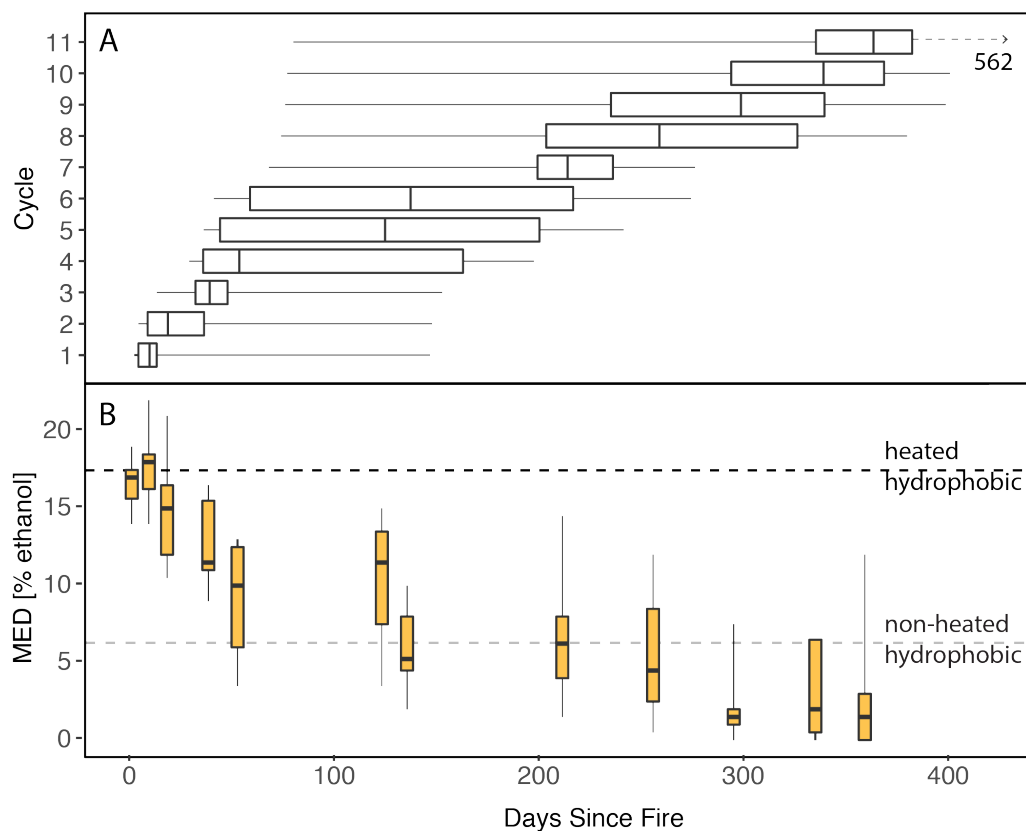
Figure 3.8: Box-and whisker plot of the number of days after October 1st that each cycle occurs over an eight year climate and soil moisture time series (A). Soil MED distribution for each cycle as a function of median number of days since October 1st (B) The MED distribution is based on the type of cycles recorded and the replicas of the MED measurements for each cycle.

'non-heated hydrophobic' reference condition within six cycles, requiring a mean of 144 days.

3.4   Discussion

The experimental results indicate that freeze-thaw cycling on wet soils resulted in a similar magnitude and rate of hydrophobicity reduction as did more conventionally considered wet-dry cycling, or wet-dry cycling combined with freeze-thaw cycling; suggesting the potential for freeze-thaw processes to be important mechanisms of soil physico-chemical recovery following fire.

Analysis of climate and soil moisture data to identify the occurrence of freeze/thaw and wet/dry cycles in surface soils of a well-monitored mid-elevation Sierra Nevada site confirmed

that freeze-thaw processes are likely to have pragmatic importance in post-fire soil recovery. Most of the area burned by fires in the Sierra Nevada burns in the period from October to December (A. P. Williams et al., 2019); these late-season wildfires occur under low fuel and soil moisture conditions, which are conducive to soil heating and the generation of hydrophobic soil layers. It is the arrival of winter rain and low temperatures that typically ends the Sierra Nevada fire season: as represented in this analysis by a hypothetical October 1st end-of-fire date. Over the eight-years of data analysed, hydrophobic soils generated by this hypothetical fire would return to pre-fire wettability conditions over a mean period of 144 days. This relatively rapid rate of degradation of hydrophobicity would be mostly attributed to freeze-thaw cycling, representing approximately 80% of the soil changes that contributed to hydrophobicity reduction. Thus, it is likely that freeze-thaw cycling is of practical importance in regulating the recovery of soils from post-fire hydrophobicity in the Sierra Nevada.

The experimental results do not clearly identify the mechanisms by which soil hydrophobicity is lost as repeated wetting, drying, freeze and thaw cycles are imposed on the soil. They do, however, constrain some of the possibilities. First, it is clear that degradation is not simply a function of time, given that no change in hydrophobicity of the dry freeze-thaw samples was observed. Second, it seems unlikely that removal of hydrophobic compounds via leaching was the main mechanism responsible. Two strands of evidence contradict this. Firstly, although leaching was possible in treatment cycles that involved repeated wetting and drying, it was not possible in the freeze-thaw cycles applied to a wet soil. Yet the decay in hydrophobicity in the wet freeze-thaw cycling was comparable, if more variable across replicates, to that in other treatment cycles involving repeated wetting and drying. Secondly, although soil organic matter declined in all treatments, this decline was modest in magnitude (less than 2 percentage points decline relative to an initial mean SOM of 10.9%), only weakly correlated to MED, and not statistically different between the hydrophobic samples from the dry freeze/thaw cycle (MED=16.9%) and the hydrophilic samples across all samples following eleven treatment cycles (MED=1.9%). Third, there is suggestive if inconclusive evidence that physical changes in the soil structure at macro- and micro-scales. Fissure length and number increased as MED decreased over repeated wet/dry (or wet freeze/thaw) cycles. In the absence of chemical changes, these fissures may have provided flow pathways that were less influenced by surface hydrophobicity (e.g. due to smaller surface area to volume ratios) than the original soil pores. Similarly, the SEM images indicated that soil surfaces with distinct MED patterns were also distinguished by different aggregate sizes. Amongst untreated soils, there was a clear trend towards increasing MED and hydrophobicity with aggregate size. The opportunistic measurement made on the treated soil sample suggests that its distribution of surface aggregate sizes was also distinct from the untreated soils. However, due to its different treatment history, and the fact that this sample was an intact soil surface rather than a homogenised soil sample, makes a direct comparison of aggregate size distributions between the untreated and treated soils impossible. It is, however, again suggestive that differences in soil wettability were, to some extent, reflected in differences in soil aggregate structures at the microscopic level.

Therefore, based on the preliminary evidence collected here, it seems likely that the degradation of hydrophobicity is associated with similar processes amongst the wet/dry and wet freeze/thaw cycles. These processes depend upon water, and may have a physical component, potentially associated with macroscopic and microscopic changes to soil structure induced by drying of wet soil (e.g. shrink-swell behavior) or by expansion of frozen water (e.g. frost-heave processes). From a soil physics perspective, freezing and thawing cycles are physically similar to drying and wetting cycles since both cycles eliminate liquid water from the soil. It is also possible that other chemical mechanisms, not tested here, could be associated with changing hydrophobicity. For example, changes in the orientation of amphipathic (partially polar) molecules could be induced by varying environmental conditions, leading to changes in hydrophobicity that do not require changes in bulk soil chemistry (Horne & McIntosh, 2000; Kleber et al., 2007; Mao et al., 2018).

Regardless of the microscopic mechanisms involved, the significance of freeze/thaw cycling for post-fire soil hydrophobicity in the Sierra Nevada and other montane or seasonally frozen environments suggests the potential for complex feedbacks between fire and hydrological processes subject to climatic warming. As climate warms, the duration and mean depth of snowpack will decline, as will the length of the season in which freeze-thaw cycling occurs. This is likely to have confounding effects on freeze/thaw cycling, which may be more frequent with a shallower snowpack (Decker et al., 2003): in the dataset analysed here, freeze thaw cycles would increase in importance for degrading hydrophobicity (from 79% of cycles to 91% of cycles) in the absence of a snowpack. However, the shorter snow season would tend to reduce the number of such events. The effect of climatic warming will also alter the elevation of the snowline: currently moving upward from its current elevation between 800 and 2800 m across the Sierra Nevada (Lundquist et al., 2008) by as much as 72 m/yr (Hatchett et al., 2017). Below the snowline, warmer temperatures would tend to reduce freeze-thaw cycling. Near the snowline, warmer mean temperatures might be expected to increase the frequency with which air temperatures fluctuate around 0°C while reducing the insulating effect of the snowpack itself (Templer et al., 2017). While well above the snowline, climate warming will probably not greatly alter the frequency of freeze/thaw events. The loss of snowpack and freeze-thaw dynamics along with the increased fire risk anticipated with warming and drying at low elevations may also exacerbate the risks to soil and water quality degradation following fires, due to the loss of freeze/thaw mechanisms to restore soil wettability. Other energy drivers, such as slope, aspect, and canopy shading may also influence the post-fire rate of hydrophobicity decay.

Unfortunately, we have been unable to identify field studies documenting the timescales of hydrophobicity reduction after fires in the Sierra Nevada. Field studies that do document hydrophobicity reductions do not generally report wet-dry and freeze-thaw cycle occurrences in enough detail to determine if a geographic signal of freeze-thaw processes on hydrophobicity reduction can be found. There is a general pattern of more rapid reductions of hydrophobicity in cooler and wetter regions - e.g. significant declines post-fire occurred within a year in Michigan (Reeder & Jurgensen, 1979), less than two winter months in southern California's San Gabriel Mountains, and less than 13 months in a temperate pine forest in

Poland (Hewelke et al., 2018); compared to persistence of hydrophobicity at least 15 months after fire in Spain (Rodríguez-Alleres et al., 2012), and over two-year timescales in Southeastern Australia (S. Doerr et al., 2006). However, this pattern is not universal, and despite the Bobcat and Crosier Mountain Fires occurring near each other in the Colorado Front Range (Huffman et al., 2001), at one of these sites hydrophobicity was negligible after a year (MacDonald & Huffman, 2004), but persisted for over 22 months at the other (Huffman et al., 2001). Thus, field studies that can separate freeze-thaw and wet-dry cycles (rather than solely using precipitation as a climate descriptor) would be useful to determine the importance of the different hydrophobicity reduction mechanisms in the field.

We conclude that freeze-thaw cycling could be an important factor mitigating against long-term water quality, erosion, and flood risks from fire in the Sierra Nevada. These cycles, which do not in themselves produce risks of erosion or flood exacerbation, appear to enable substantial soil wettability recovery in the first winter after late summer fires. Of course, this mechanism does not prevent flooding and erosion impacts from fire in the Sierra Nevada and other Western US montane watersheds, as the effects of vegetation loss remain (Berg & Azuma, 2010; Larsen et al., 2009b). The potential relevance of freeze-thaw cycles for post-fire soil recovery merits further investigation, both to resolve the underlying mechanisms by which hydrophobicity is degraded, and to quantify the importance of freeze/thaw processes *in situ* for recovery of soil hydraulic properties post fire. The latter may be particularly important to an improved understanding of fire impacts in the Sierra Nevada and similar mountain ecosystems as climate continue to warm.

Chapter 4

Forest Vegetation Change and Its Impacts on Soil Water Following 47 Years of Managed Wildfire

The contents of this chapter were originally published in Ecosystems in 2020, as an article titled "Forest Vegetation Change and Its Impacts on Soil Water Following 47 Years of Managed Wildfire," DOI: 10.1007/s10021-020-00489-5. The co-authors are Jens Stevens, Gabrielle Boisramé, Sally Thompson, Brandon Collins, and Scott Stephens.

4.1   Introduction

Many forests in California's Sierra Nevada, like other dry mixed-conifer forests of the western United States, have experienced fire exclusion since the end of the 1800s, and were managed under an active policy of fire suppression throughout the Twentieth Century (McKelvey et al., 1996). The consequences of fire exclusion for the vegetation of the Sierra Nevada are well known and include increases in forested area, increases in forest stem density and uniformity of stands, and reductions in landscape heterogeneity (Collins et al., 2011; Safford and Stevens, 2017). By creating large connected patches of dense fuels, fire exclusion and suppression have also set the stage for a dramatic escalation in the frequency and extent of severe fires (Westerling and Swetnam, 2003; Stephens et al., 2013; North et al., 2015; Stephens et al., 2016) – for example, five of the ten largest and most destructive fires in California (as of fall 2018), occurred after 2010 (CalFire, 2018a, 2018b). The scale of fire-caused tree mortality in these and many other contemporary fires is well outside the historical range of variability in Sierra Nevada forests (Collins et al., 2011; Safford and Stevens, 2017). Recent large-scale stand-replacing fire effects, combined with the densification and homogenization brought about by widespread fire suppression, have negatively impacted some animal taxa, water resources and forest resilience (Grant et al., 2013; Ponisio et al., 2016). Such negative impacts have motivated the adoption of a broad suite of forest management practices ranging

from mechanical forest thinning to prescribed fire (Stephens et al., 2016) to restore a forest structure resilient to future fires. An additional forest restoration strategy, managed wildfire, is drawing increased attention (North et al., 2012; Boisramé et al., 2017a). Managed wildfire involves allowing naturally ignited wildfires to burn unimpeded unless specific predefined criteria (for example relating to hazard or air quality) are met and trigger intervention. In the Sierra Nevada, two wilderness areas, the Illilouette Creek and Sugarloaf Creek Basins - in Yosemite and Sequoia-Kings Canyon National Parks, respectively - have used managed wildfire for nearly 50 years. The resulting wildfire regime in these basins has near-historical fire frequencies for at least a portion of the past 50 years (Collins and Stephens, 2007). In addition, the emergence of non-overlapping fire extents in these basins suggests self-limiting behavior as the fuel distribution becomes more fragmented in space (Collins et al., 2007; Collins et al., 2009; Collins et al., 2011; Parks et al., 2015; Collins et al., 2016). While these outcomes suggest that managed wildfire has had a positive effect in restoring historical fire regimes and mitigating fire hazard, its co-benefits on other ecosystem services remain less certain. The influence of managed wildfire on water supply, given the importance of these forests for water resources in California and the western US more generally, is of particular interest. Although there is a well-established literature in fire hydrology (e.g., Stoof et al., 2012; Ebel, 2013; Wine and Cadol, 2016; Atchley et al., 2018), studies that explore longer-term hydrological responses (e.g. over decadal scales) are rare (but see Kinoshita and Hogue, 2015). The sites in question here allow the investigation of not only a longer-term set of hydrological responses to fire, but more interestingly again, the responses to a change in fire regime and the imposition of multiple disturbance events on a catchment. In the Illilouette Creek Basin (ICB), the imposition of managed wildfire led to large (24%) decreases in forested area and the replacement of forests with new areas of shrubland, grassland and dense meadows/wetlands (Boisramé et al., 2017b). Field measurements in ICB showed that vegetation type is a strong predictor of soil moisture: for example dense meadows indicate wet soil conditions, in comparison to the dry soils conditions associated with shrublands or sparse meadows (Boisramé et al., 2018). With sufficient information relating soil moisture, vegetation cover and other landscape predictors of soil moisture, statistical models can be trained to predict soil moisture based on mapped vegetation (Boisramé et al., 2018). Such models suggest that the fire-induced changes to vegetation cover in ICB (less forest cover, but more meadows and shrublands) are associated with an overall increase in water storage and plant available water resources (Boisramé et al., 2018). This finding is consistent with comparisons to similar but fire-suppressed Sierra Nevada river basins (Boisramé et al., 2017a), and with mechanistic ecohydrological modeling of ICB (Boisramé et al., 2019), which suggest that soil moisture and streamflow have increased, and plant water stress decreased, in response to the changed fire regime. Model results showed that these hydrologic changes could be explained by reductions in forest cover causing a combination of reduced interception, reduced transpiration, and deeper peak snowpacks (Boisramé et al., 2019). These results suggest a promising co-benefit for water resources associated with restoration of a near-natural fire regime in the ICB. However, it is unclear how the effects of managed wildfire will play out in other Sierra Nevada forests. ICB is a relatively wet, mid-elevation watershed

containing productive forests. Basins with different climates, soils or vegetation types found at other elevations and locations in the Sierra Nevada could exhibit different responses to a changed fire regime, as could subtle differences in how a managed wildfire regime is operated. Sugarloaf Creek Basin (SCB) in Sequoia-Kings Canyon National Park offers a chance to explore the impact of managed wildfire beginning in 1973 in a slightly less productive, drier, and less-frequently burned watershed than ICB. In this study, we draw on historical (1970) and contemporary forest plot surveys, historical (1973) and contemporary aerial photography and vegetation classifications, and contemporary soil moisture and meteorological observations within SCB to address four questions:

1. How has forest composition and structure at the survey plot scale changed from 1970-present, and how are these changes associated with fire?

2. Has vegetation cover changed in the SCB from 1973-present at the landscape scale, and if so, how are these changes associated with fire? Are different vegetation cover types in the SCB associated with differences in soil moisture, and what does this imply about hydrologic response to wildfire in the SCB?, and finally

3. How do changes in landscape vegetation cover (2) and soil moisture (3) compare with those previously described in the Illilouette Creek Basin, a wetter and more productive basin that has burned more frequently over the same period?

4.2 Methods

Study site and climate

The Sugarloaf Creek Basin (SCB) covers 125 km2, spanning elevation ranges of 2000 – 3200 m in Sequoia and Kings Canyon National Parks. Average daily temperatures range from 10o C to 31o C, with the annual average being 14.5o C (Global Historical Climate Network, station USR0000CSUG). Vegetation in this region varies with elevation, topography, and soil type (Stephenson, 1998; Caprio and Graber, 2000). The dominant tree species found in SCB are Jeffrey pine (*Pinus jeffreyi*), lodgepole pine (*Pinus contorta*), white fir (*Abies concolor*), and red fir (*Abies magnifica*), which occur interspersed with meadows and shrublands. There is no evidence of logging in SCB. Based on fire scar reconstructions, fire was common in this area prior to 1900, with a mean fire interval of 9 years for the period 1700-1900 (Collins and Stephens, 2007). Fire exclusion and suppression appears to have started in SCB shortly before 1900, resulting in an anomalously long fire-free period lasting until the early 1970's (Collins and Stephens, 2007).

In 1968 the National Park Service changed its fire policy and began to use prescribed fires and managed lightning fires to meet ecological goals; previously all fires had been suppressed (van Wagtendonk, 2007). Yosemite National Park (including the 150 km2 ICB) is the only other place in the Sierra Nevada that has had a policy of allowing lightning-ignited wildfires

to burn for as long as Kings Canyon National Park (van Wagtendonk, 2007). The first notable fire in SCB under the fire use policy was the Ball Dome Fire in 1971, which burned nearly 100 ha. In total, 10 fires over 40 ha in size burned partially or completely in SCB between 1970 and 2016, the largest of which was over 4000 ha (Appendix A, Table A.1). For comparison, ICB had 27 fires >40 ha between 1970 and 2016 (Collins et al., 2016).

We obtained fire perimeters for all SCB fires between 1952 and 2016 from a statewide database maintained by the California Department of Forestry and Fire Protection (FRAP, 2017). These perimeters were corroborated with those maintained by park staff (personal communication, A. Caprio, Sequoia and Kings Canyon National Park). Because our historical imagery dates to 1973 (see below), we removed four small (<100 ha) fires that burned between 1952-1972 from our imagery analyses (Figure 4.1; Table A1). Our historical forestry plots date to 1970 (see below), but none were located within the perimeters of these four fires (Figure 4.1). We also removed two fires, from 2004 and 2006, that were both <5 ha and located on the margins of the watershed (not shown in Figure 4.1). Of the 12 fires included for analysis, the mean fire size was 830 ha (median 248 ha).
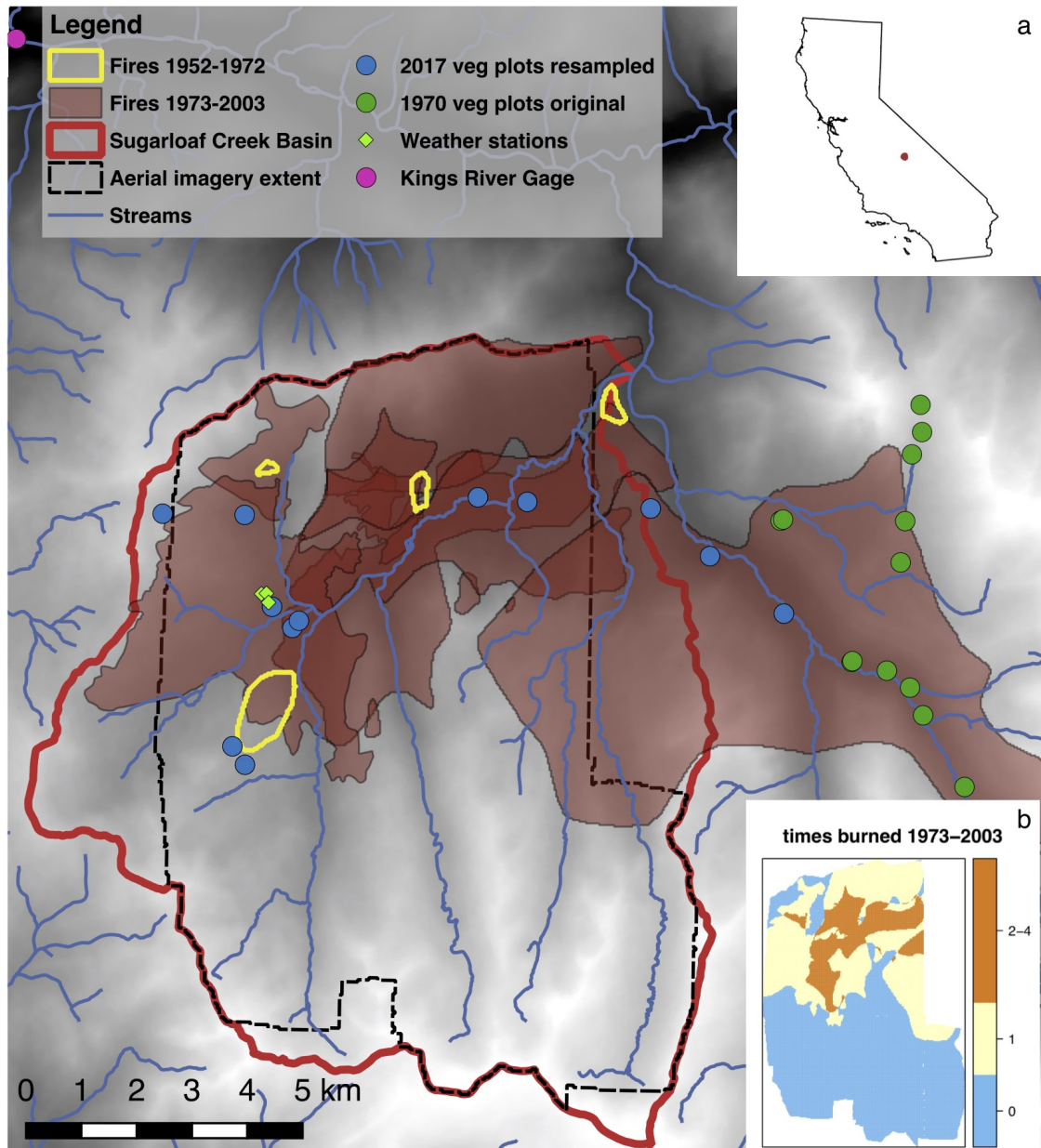
Figure 4.1: Sugarloaf Creek Basin (SCB) shown in red (and in panel a). Base layer DEM ranges from 1480 m (black) to 3375 m (white; Data source: ASTER GDEM, a product of METI and NASA). Overlapping fire perimeters since 1973 shown in transparent red. Inset (b) shows composite of overlapping fires from 1973-2003, with colors indicating number of times burned, over the extent represented by the 1973 aerial imagery. Green points in main figure indicate main vegetation (forestry) plots installed in 1970, a subset of which (blue) were re-sampled in 2017. The pink point is the approximate location of the Kings River streamflow gage near Cedar Grove; USGS gage 11212500 (exact coordinates given in Table A2).

In addition to the increased fire frequency at ICB compared to SCB since 1970 (27 compared to 10 large fires), differences in water balance and site productivity between the basins may influence vegetation response to the reintroduction of fire. ICB and SCB have similar mean elevation (2500 m and 2700 m respectively) and forest types (Collins et al., 2016), but three lines of evidence suggest that ICB is the wetter and more productive basin. First, temporary weather stations (Appendix B.2) at both sites showed greater precipitation (Figure 4.1) at ICB than SCB for the duration of our field data collection (2016-2018). Second, specific discharge (total streamflow divided by watershed area) measured downstream of ICB is greater (0.65-0.66 m/yr) than that measured downstream of SCB (0.48-0.55 m/yr) over a time period through the 1950's where data from both basins were available (Table A2).

Third, these differences in water inputs are reflected in slightly higher productivity in ICB than SCB (Figure 4.2). To assess productivity, we used the LANDSAT-derived Normalized Difference Vegetation Index (NDVI) product during the early-mid growing season at both basins, available at https://ndvi.ntsg.umt.edu/ (Robinson et al., 2017). To minimize the effect of recent fires on productivity estimates, we used the earliest available data from 1984 and 1985, prior to the 1985 Sugarloaf Fire (Table A1), and at least 3 years after the most recent fire in either basin. We filtered out any region of either watershed that was likely granite or water (NDVI <0.15) or cloud cover (filtered out during image processing), and only compared the vegetated portions of each watershed that had data for every image date.
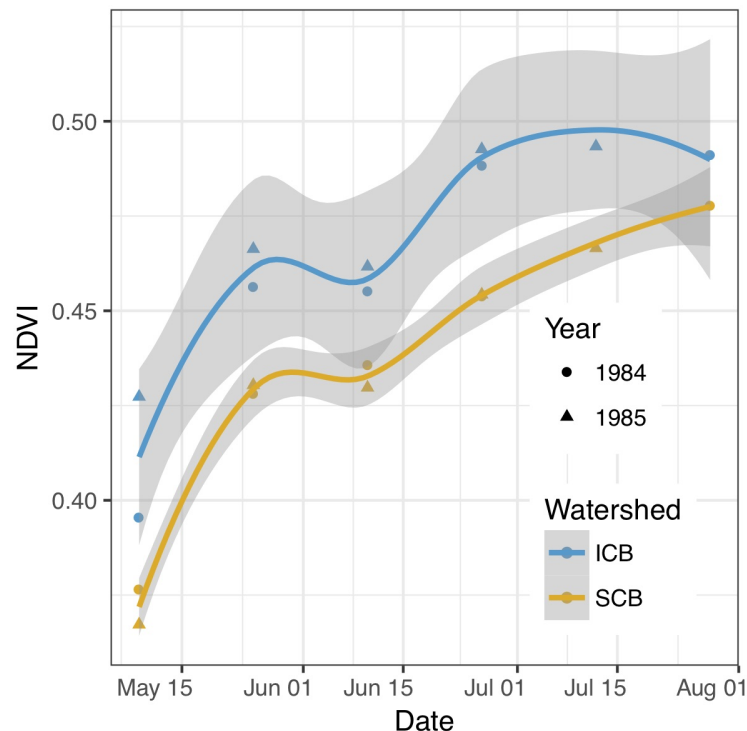
Figure 4.2: Normalized Difference Vegetation Index (NDVI; averaged across a given basin for a given date), a proxy for productivity, was consistently higher in Illilouette Creek Basin (ICB; Boisramé et al. 2017a) than Sugarloaf Creek Basin (SCB; this study). Curves with error bands represent loess smoothing estimates of mean NDVI across the two years.

Question 1: Forest composition and structural change

In areas of SCB that did not convert to alternative vegetation patches (Question 2 below), we explored the question of how forest structure has changed over time in response to fire by resampling a historic forest plot dataset. Forest surveys were conducted in Sugarloaf Creek Basin in July 1970 by Hammond, Jensen Wallen Mapping and Forestry Services, Oakland CA. Surveyors measured 25 plots (Figure 4.1), which consisted of five 0.2 ac (0.08 ha) subplots each. Each subplot was surveyed for conifer trees (stems > 7.6 cm DBH), saplings (stems 0.6 m tall up to 7.6 cm DBH, where DBH was not recorded), and seedlings (stems <0.6 m tall). The surveyors estimated representative tree heights and woody (shrub) ground cover within the plots. All shrubs and trees were identified to species level. Subplots were arranged along linear transects with generally 40 m spacing between them, from an anchor point and a given transect azimuth that was described in the field notes. We re-surveyed 12 of these plots in 2017 (Figure 4.1) following the same methods, leading to a total of 57 subplots sampled in both 1970 and 2017, which constituted our sample size for

analysis.

For each subplot, we used the collection of fire perimeters from Sugarloaf Creek Basin to identify the number of times each subplot had burned since fire was reintroduced in 1973 (0, 1, or 2-4). We calculated density of all trees (>7.6 cm DBH), medium trees (>15.2 cm DBH), large trees (>61 cm DBH), and very large trees (>100 cm DBH), and calculated basal area of each of these size classes by species as well. For each size class we compared the change in density and basal area over time, using linear mixed-effects models that assigned a random intercept to subplot ID, accounting for repeated sampling of the same plots over time by allowing a given plot to have higher or lower overall values of the response variables, using the R package *lme4* (Bates et al., 2015). We evaluated the significance of these trends using the Kenward-Rodgers approximation to estimate degrees of freedom in the mixed-effects models, via the R package *pbkrtest* pbkrtest.

Question 2: Vegetation cover change

In order to assess potential impacts of vegetation change on soil moisture (Question 3 below), we mapped the change in larger vegetation patches in SCB since the first large fire in 1973. We created these maps by classifying aerial photographs into granite (exposed rock), water, sparse meadows (areas dominated by bare ground, with sparse shrub and/or herbaceous cover), dense meadows (wetlands and other areas of dense herbaceous cover), conifer forest, and shrublands, following the methods used by Boisramé et al. (2017b). We obtained the earliest set of aerial photographs available for the region from Sequoia Kings Canyon National Park. These black and white photos were dated to 1973, prior to the first large fires occurring in SCB, scanned at 600 dpi, and covered 10,120 ha (81%) of the 12,500-ha watershed (Figure 4.1). Contemporary cover was represented by color imagery from the 2014 National Agriculture Imagery Program, and clipped to the same extent as the 1973 imagery. The 1973 images were orthorectified using ERDAS IMAGINE software, using approximately 15-20 control points per image. We used the eCognition object-oriented software package (produced by Trimble, www.ecognition.com) to classify the images into objects of similar color band values, texture and shape (Blaschke et al., 2014). Our supervised classification approach produced objects in the following categories: mixed-conifer forest, shrub, sparse meadow, dense meadow, rock and open water. Following classification, the 1973 images (representing approximately 16.7 km2 each) were mosaicked together in ArcGIS, as were the 2014 images (representing approximately 39 km² each).

During post-processing, the vector-object layers produced by eCognition were converted to raster layers in ArcGIS, with a 40-m pixel resolution, ensuring alignment of the 1973 and 2014 rasters to enable a change detection analysis. Because the rasterization process created single isolated pixels of a given class derived from polygon slivers, we smoothed the resulting raster surface using the *adjacent* function in the R library *raster* (Hijmans and van Etten 2014). We removed isolated pixels surrounded by other vegetation in the four cardinal directions, changing the pixel in question to the most common vegetation type surrounding it. We used the spatial layers from 1973 and 2014 to determine the direction

and proportionality of vegetation change in the intervening 41 years. We then analyzed the relationship between these changes and the number of times each pixel had burned. We overlaid the fire perimeter polygons on the two vegetation raster layers to extract a "times burned" attribute for each pixel. Due to subsequent chi-squared tests not converging for analyses of pixels burned 3 times (218 ha) and 4 times (15 ha), we combined these categories into a single "2-4 times burned" category, in addition to analyses conducted for once-burned pixels, unburned pixels, and the entire mapped area. We excluded pixels classified as granite or water from this analysis, leaving four vegetation classes which could transition from one to another: shrubs, sparse meadow, mixed conifer and dense meadow. We assessed which types of vegetation transitions were overrepresented relative to a null expectation of no difference in transition types, for the entire watershed and based on number of times burned, using a chi-squared analysis (Appendix B.3). As a basis for comparing the post-fire vegetation landscapes at SCB and ICB (Question 4), we assessed landscape metrics (Appendix B.3) to describe the heterogeneity of the landscape and spatial distribution of individual vegetation classes in SCB, in both 1973 and 2014, using FRAGSTATS (McGarigal et al., 2012), and compared these to values calculated for ICB (Boisram'e et al., 2017b). At the landscape level, these metrics included the evenness index and the aggregation index, and at the vegetation class level they included mean, standard deviation, and maximum of patch area, and mean patch fractal dimension.

Question 3: Soil moisture variability

Spatially-distributed soil moisture measurements

To assess the drivers of spatial variability in shallow soil moisture, we sampled soil moisture in the field at 40 sites in 2016, 2017, and 2018, which included three sites where we installed temporary weather stations (see below). We measured soil moisture in the top 12 cm of soil using Hydrosense 2 Time-Domain Reflectometer (TDR) probes (campbellsci.com/hs2). We measured most of these sites in both early and late summer of 2016 and 2017. Twenty-nine of these sites were re-measured in June of 2018. In most sites, 25 evenly-spaced measurements of soil moisture were made within a 30m by 30m grid, with additional measurements made in heterogeneous sites in order to better capture variability. One-meter spaced measurements were made across a 30 m transect in sites with obvious strong gradients in soil moisture (e.g. wetland sites bordered by dry uplands).

At each site, we categorized the vegetation of the site into one of the four classes used in our imagery analysis (n = 3 plots for shrub only, 1 plot for sparse meadow only, 2 plots for dense meadow only, 28 plots for mixed-conifer only, 2 plots split between sparse meadow and dense meadow, and 4 plots split between mixed-conifer and dense meadow). We also quantified slope, aspect, and recorded the presence of burned snags or fire-scarred trees. Sites were georeferenced using handheld Garmin GPSMAP 62st and 64st devices (horizontal accuracy 3–10 m). We used these geographic positions to extract additional topographic variables that could predict soil moisture (below) from raster grids created using a digital

elevation model (DEM) in ArcMap. These variables include topographic position index (TPI; a continuous variable ranging from concave to convex), upslope area (i.e. area contributing drainage to the plot), and topographic wetness index (TWI; ln[upslope area / tan[slope]]). In order to aggregate the 25-30 point moisture measurements made within a sampling site to a scale more consistent with our DEM-created maps of topographic variables, we grouped the within-site measurements for a given sampling date and vegetation cover type, and calculated the mean values within each group. These aggregated means were used for all data training and validation, so there is only one measured soil moisture value for any unique combination of site, vegetation, and date.

We analyzed how soil moisture varied across SCB among sampling dates, vegetation types, and other environmental variables, using a random forest model implemented in the R package *RandomForest* (Liaw and Wiener, 2002). Specifically, we created the model to predict continuous soil moisture using the following site characteristics: 2014 vegetation type, 1973 vegetation type, measurement year, day of year, elevation, slope, aspect, TPI, upslope area, TWI, year since fire, number of times burned since 1973, maximum fire severity (only available for fires after 1984, from the US Forest Service Pacific Southwest Region Fire Severity Mapping Program) (J. D. Miller et al., 2009), and distance from nearest stream. This model used the same methods as Boisramé et al. (2018). The drivers of soil moisture distribution vary with time since precipitation, with certain local topographic and soil texture factors being more important predictors under dry conditions compared to wet (Grayson et al., 1997; Famiglietti et al., 1998). Accordingly, our method includes a variety of local (e.g., vegetation cover, slope, aspect) and nonlocal (e.g. distance from nearest stream, upslope area) controls, and the use of the day of year as a predictor allows the model to account for late-summer changes in dominant controls, as suggested by Grayson et al. (1997).

While information on soil type may have increased this model's accuracy (Famiglietti et al., 1998), we did not include soil properties since we did not have verifiable basin-wide soils data that would have allowed us to upscale the measurements to the rest of the watershed. Since random forest is a statistical model, rather than a physically-based model, it does not require information about physical soil parameters in order to represent soil moisture, as long as the covariates used are correlated with soil moisture state. Statistical models such as random forest provide multiple benefits, including their ability to fit nonlinear relationships without needing to make (potentially erroneous) assumptions about the relationship between a predictor and the modeled variable (Grömping, 2009). However, the model may not perform well when being used to infer conditions outside the range of observations, since there is no guarantee that the fitted relationships hold true for predictor values not included in the model fitting. While it was not possible to capture the complete range of predictors and their combinations present throughout the watershed, we selected our measurement sites in order to cover as broad a range of conditions as possible (in terms of fire history, vegetation type, water year type, and topography) in order to make the model validation applicable to a wide range of conditions. We cross-validated the model by selecting a subset of measured sites as training data and using the resulting model to predict soil moisture at the remaining measured sites. To compare the drivers of soil moisture at SCB and ICB

(Question 4), we examined the ability of a similar soil moisture model trained on ICB data (Boisramé et al., 2018) to explain soil moisture variation observed at SCB. We also used the random forest model to extrapolate our soil moisture measurements to unmeasured areas of the watershed and estimate soil moisture changes due to fire changes. We modeled soil moisture on a 40m grid across the entire area of the watershed where vegetation was mapped. At each grid point, we used our vegetation maps, fire maps, and the DEM to extract the needed covariates to run the model. To estimate soil moisture levels in the absence of fire, we modeled soil moisture on the same 40m grid, with the same covariates, except that we set times burned and fire severity to zero, time since fire to 100 years, and replaced 2014 vegetation cover with 1973 vegetation (since this vegetation represents the watershed's state after years of fire suppression). We then compared these two modeled soil moisture datasets - one with "unburned" conditions and one using contemporary vegetation and fire histories – in order to quantify the change in soil moisture due to fire. This technique assumes that only a negligible amount of vegetation change between 1973 and the present is due to causes other than fire, which is supported by the fact that the largest patches of changed vegetation occur in burned areas (Figure 4.5d). This method also assumes that our model is able to capture pre-fire conditions accurately, despite the observational data being from burned areas. Although we could not access any completely unburned areas of the watershed for measuring soil moisture, we measured sites that had not burned since 1974 and/or burned only at very low severity; we believe such sites provide reasonable proxies for unburned areas and are therefore appropriate for fitting a model that is meant to simulate both burned and unburned conditions.

Continuous soil moisture measurements

In addition to low-frequency, spatially-distributed moisture sampling described above, we addressed Question 3 by measuring in-situ, continuous soil moisture dynamics in soils at three weather stations installed in September 2016. The three weather stations are located within 250m of each other, in an area that was burned once since 1973, by the Williams fire in 2003 (Figure 4.1), with one weather station each in dense meadow, mixed conifer regeneration and shrubs, and mature mixed conifer vegetation types (see details and visuals in Appendix B.2). For simplicity, the dense meadow site is referred to as the "wetland", the shrub/conifer regeneration site as the "shrub" site, and the mixed conifer site as the "forest" site hereafter.

At these weather stations, we collected data on soil moisture, soil texture, and precipitation (Appendix B.2). The precipitation record includes rainfall and snowmelt, but not solid-phase snow. Therefore, we augmented our information on snowpack dynamics by recording four visual images of the stations and surrounding area per day using time-lapse cameras (Brinno TLC200), allowing us to estimate snow depth at each station and derive equivalent water depth (Appendix B.2). The weather station soil moisture record is substantially complete for the period September 2016-September 2018, with no more than 1.3% of data points missing for a given weather station. However, up to 32% of the precipitation

time series was missing in the 2016-2018 period, due to a combination of snowmelt run-off outside of the precipitation gauge, a frozen tipping mechanism, and/or external damage to the tipping bucket and associated wiring from wildlife and extreme weather. To gap-fill missing precipitation data, we used multiple imputation via predictive mean matching (Little, 1988) on precipitation observations from the neighboring stations (Appendix B.2). We also calculated cumulative shallow soil moisture gain between 12 and 60 cm using depth- and time-integrated soil moisture timeseries (Appendix B.2). Cumulative soil moisture is a useful metric to gauge how much water shallow soils have received, and to approximate precipitation amounts in unsaturated soils (in combination with snowmelt estimates; Appendix B.2) when the tipping bucket record is missing or not reliable. However, in saturated wetland sites and during periods of steady-state infiltration, cumulative water gain cannot be calculated.

The weather station soil moisture record provides important context for interpreting the spatially-distributed soil moisture measurements. Specifically, it allows us to explore relationships between soil moisture at very shallow depths (the top 12 cm as measured in our spatially-distributed measurements) and soil moisture throughout the top 1m. Since soil moisture could behave idiosyncratically across the depth profile (Bales et al., 2011), this comparison helped determine whether the spatially-distributed measurements across the watershed are reasonable proxies for soil moisture storage and plant available water at greater soil depths. Furthermore, these stations were built and sited in a similar manner to three weather stations at ICB (Table B3) and provide an additional point of comparison between the two basins (Question 4).

4.3 Results

Question 1: Forest composition and structural change

Within the 10,120 ha of the SCB watershed where we classified vegetation via remote sensing imagery, 1,240 ha (12%) burned 2-4 times, 3,173 ha (31%) burned once, and 5,707 ha (57%) did not burn between 1973 and 2014 (Figure 4.1 inset). Among our 57 forestry subplots, 18 (32%) burned 2-4 times, 27 (47%) burned once, and 12 (21%) did not burn. Increased fire occurrence did not lead to decreases in basal area or density in most size classes (Figure 4.3). Only for large trees >61 cm DBH was there a significant influence of fire frequency, where density and basal area decreased from 1970 to 2017 only when burned 2 or more times (Figure 4.3 g, h). This effect of number of times burned was likely driven by trees in the 61-100 cm size class, because for very large trees >100 cm DBH, there was a significant decrease in density and basal area regardless of fire occurrence (Figure 4.3 j, k). Furthermore, even in plots that had burned twice, total tree density increased, possibly due to post-fire density increases of the fire-intolerant Pinus contorta, which increased in basal area over the 47 years (Figure 4.3c).

The number of times a plot burned was not independent of the forest species composi-

tion: even prior to the reintroduction of large managed wildfires in 1973, plots that would eventually burn twice were located in predominantly *Pinus jeffreyi* forest. Plots that would eventually burn once were located in mixed-conifer forest with comparable proportions of *P. jeffreyi, P. contorta, Abies magnifica and A. concolor.* Finally, plots that did not burn in the 47 years were located in A. magnifica-dominated forest (Figure 4.3c). There was also a strong difference in initial abundance of shrubs in the different forest types, with shrubs being absent in 1970 from all subplots in A. magnifica forest that did not burn in the subsequent 47 years, but present in about 50% of the plots that eventually burned (Figure 4.4). The reintroduction of even a single wildfire was sufficient to increase shrub abundance to 80% of subplots in 2017 (Figure 4.4).
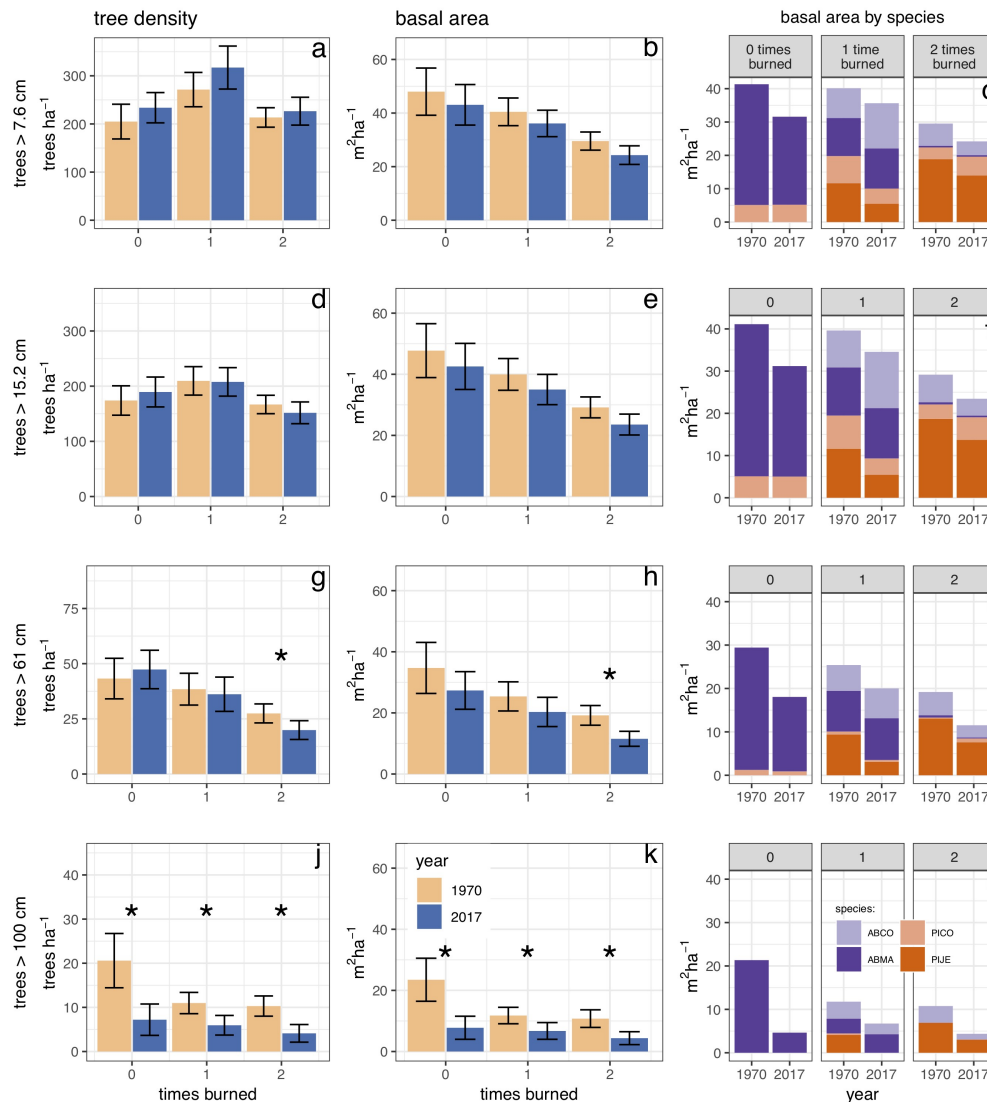
Figure 4.3: Change in forest structure based on forestry plots. Column 1 shows changes in density, column 2 shows changes in basal area, and column 3 shows changes in composition of the four most common species by basal area fraction (the minor presence of additional species in some plots accounts for the minor height differences between columns 2 and 3). Row 1 is for all trees >7.6 cm, row 2 is for trees>15.2 cm, row 3 is for trees >61 cm, and row 4 is for trees >100 cm. Asterisks in columns 1 and 2 indicate significant differences in the response variable between 1970 (gold) and 2017 (blue). Note the different axis scaling in panels (g) and (j).
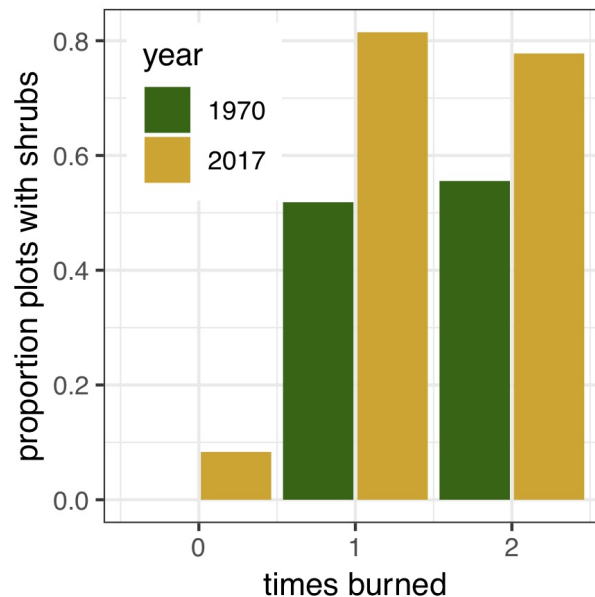
Figure 4.4: Change in the proportion of subplots where shrubs were detected, from 1970 to 2017, by number of times burned. These data apply to all plots across vegetation type, as in Figure 4.3.

Question 2: Vegetation cover change

The dominant types of vegetation transitions we observed in the watershed were generally observed similarly across all three burn classes (0, 1, and 2-4 times burned; Figure 4.5). In particular, transitions from shrub to sparse meadow, mixed-conifer to sparse meadow, and mixed-conifer to shrub were overrepresented compared to the null expectation of no change, both in the watershed as a whole ($X^2 = 236$, df = 15, P <0.001) and in unburned, once-burned and 2-4 times burned areas ($X^2 = 47$, 272, and 88 respectively; all df = 15, all P <0.001). However, transitions towards earlier-seral vegetation types, particularly shrub to sparse meadow and mixed conifer to sparse meadow, were more strongly overrepresented in the burned areas than in the unburned areas (Figure C1c-d). Dense meadows did not show a consistent response to fire but in general there was limited dense meadow area to begin with and limited expansion or contraction of this vegetation type in absolute terms (Figure C1).

The magnitude of vegetation type change in SCB was much less than in ICB over a similar period of time (Figure 4.6). Over roughly four decades, net cover of mixed-conifer at SCB only decreased from 83% to 82%, while at ICB it decreased from 81% to 62% (Figure 4.6). Landscape-scale indices of heterogeneity increased slightly in 2014 compared to 1973, though the changes were much less pronounced than those that occurred in the ICB over

a similar time period of repeated wildfires (Appendix B.3). The major differences in land cover patterns for SCB were that the mean size of conifer patches decreased from 15ha to 13ha (Figure C5a), and sparse meadows experienced small increases in mean patch size (0.38 ha to 0.52 ha; Figure C5c).
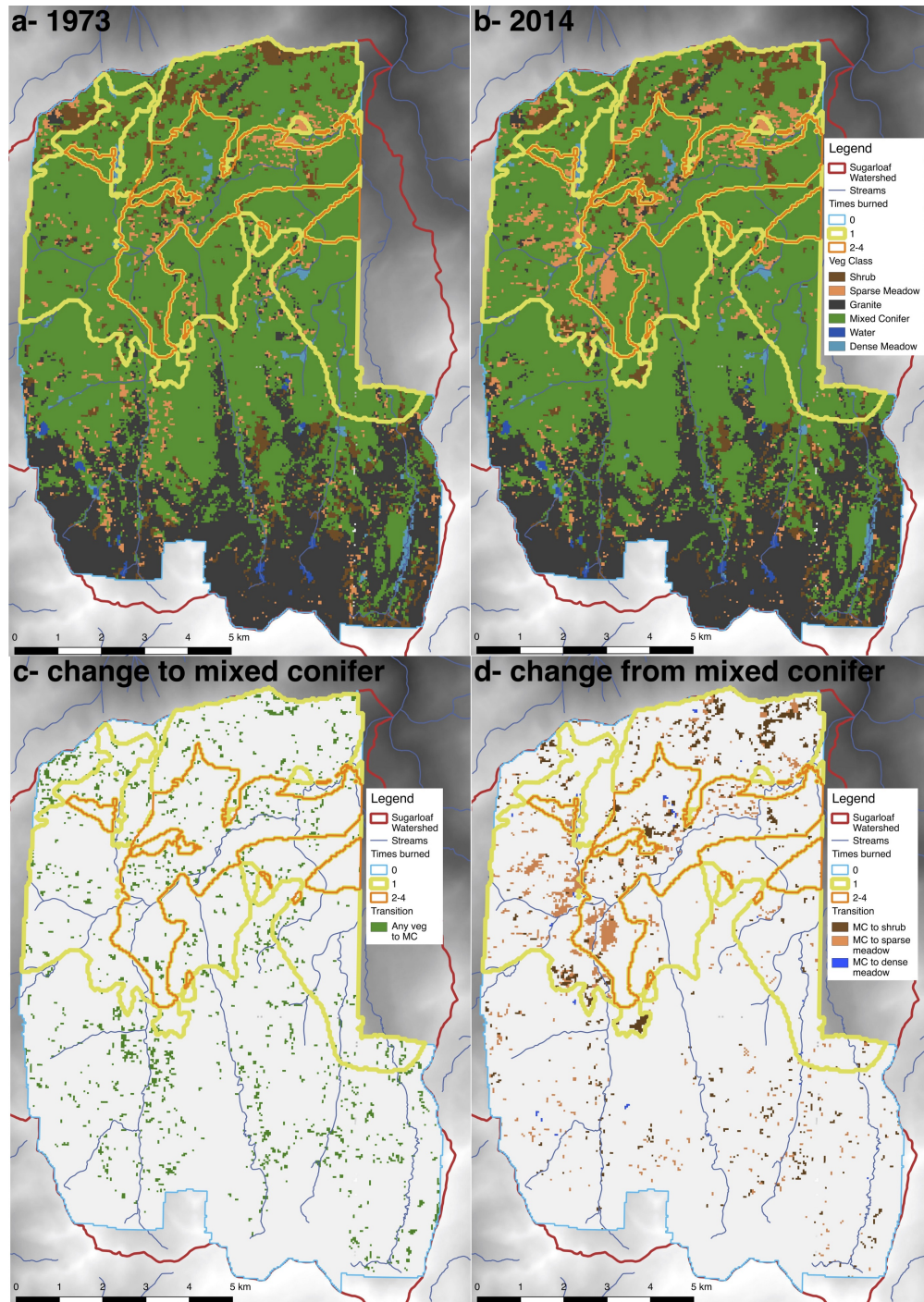
Figure 4.5: Comparison of classified aerial images from 1973 (a) and 2014 (b) in Sugarloaf
Creek Basin. Perimeters of fires that burned between 1973 and 2014 are shown, aggregated
by number of times burned. Four vegetation classes (shrub, sparse meadow, mixed conifer
(MC), and dense meadow) are shown, along with granite and water. Transitions from non-
forest to MC (c) and from MC to non-forest (d) are highlighted.
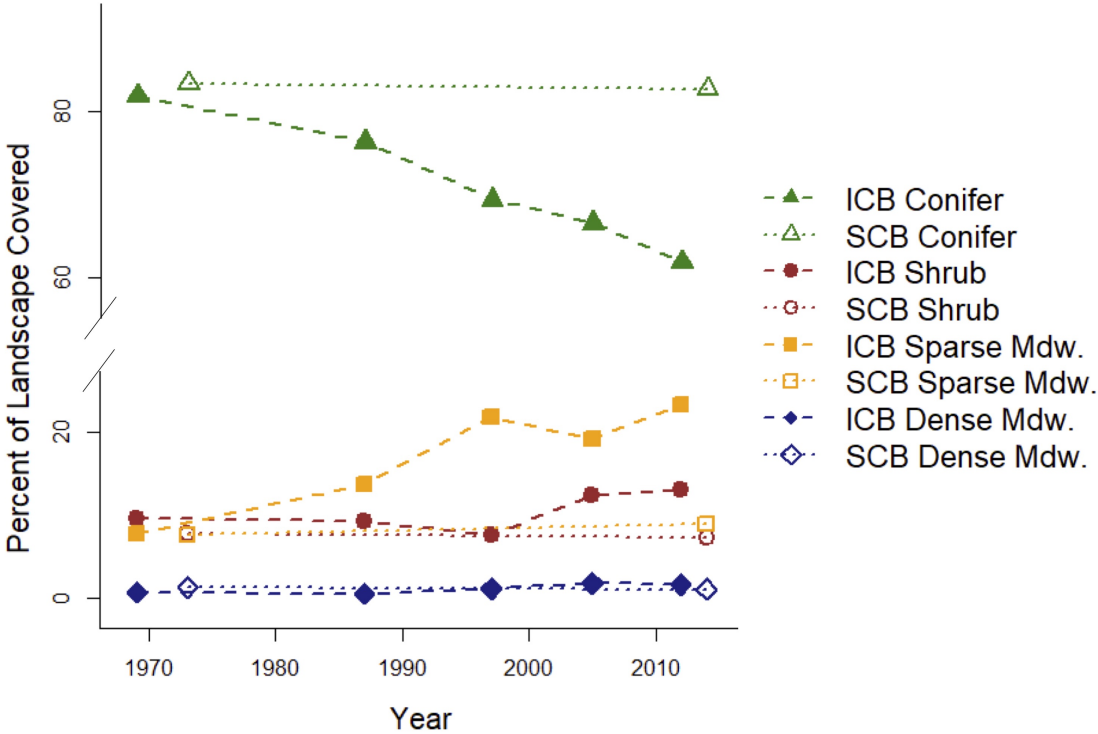
Figure 4.6: Percent of the total vegetated area covered by each vegetation class for both Illilouette Creek Basin (ICB) and Sugarloaf Creek Basin (SCB).

Question 3: Soil moisture variability

There was variability in spatially-distributed soil moisture measurements in SCB, both among vegetation types and to a lesser degree among site visits (Figure 4.7). Specifically, soil moisture in dense meadows was over 3 times higher than in the other vegetation types (Figure 4.7). Furthermore, soil moisture in 2017 was higher than in 2016 or in 2018 across all vegetation types (Figures 7, 9), consistent with measurements that 2017 was the wettest year of the three at our study site and in the southern Sierra Nevada in general (Tables 1, B3).
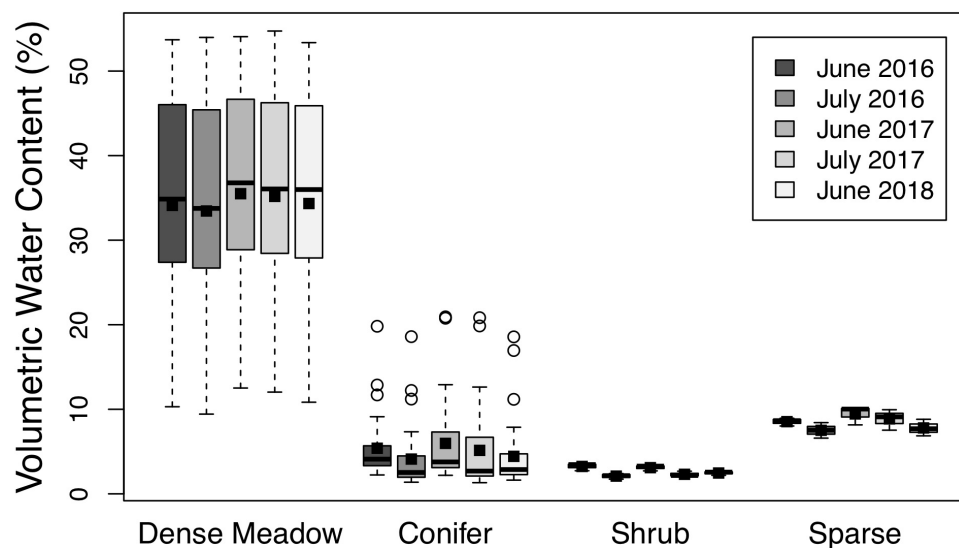
Figure 4.7: Distribution of modeled soil moisture (in terms of volumetric water content) for each site-date-vegetation class combination, based on the random forests model but not controlling for site-specific variation in topography and other covariates which also influence these modeled values (see Figure D3). Modeled values are binned by date (either June or July of each measurement year) as well as by vegetation class: dense meadow (n=9), conifer (n=32), shrub (n=3), and sparse meadow (n=3). Within each box, the dark horizontal bar denotes the median while the box spans the 25th to the 75th percentile and dotted bars show the full range of the data. Circles show outliers, black squares show the mean within each bin.

Table 4.1: Weather station data from Sugarloaf Creek Basin (SCB) and Illilouette Creek Basin (ICB). Gap-filled precipitation totals measured by rain gauge; cumulative shallow soil water gain was calculated from shallow soil moisture timeseries (Appendix B.2). End of water year (WY) deep soil moisture (Volumetric Water Content [VWC]) and number of saturation days were based on the 100 cm soil moisture probe record. Pearson's correlation coefficient was calculated between daily average 12 cm and 100 cm soil moisture for months of June - August.

Weather Station Vegetation Type		Total precipitation [mm]		Cumulative shallow (12-60 cm) soil water gain [mm]		End of WY VWC [%] at 100 cm		Days Saturated at 100 cm		Correlation coeff. between 12 & 100 cm VWC for Jun-Aug	
	WY:	2017	2018	2017	2018	2017	2018	2017	2018	2017	2018
SCB	Wetland	680	429	477	469	34	14	155	81	0.85	0.97
ICB		1067	537	56	30	43	43	365*	365	0.88	0.54
SCB	Shrub	842	546	362	287	16	10	88	0	0.93	0.67
ICB		1137	590	940	378	10	5.6	86*	0	0.87	0.84
SCB	Forest	577	397	834	184	4.7	3.4	56	0	0.99	0.97
ICB		769	450	776	334	3.5	3.4	31*	0	0.90	0.87

* Approximated due to missing data as a result of the 2017 Empire Fire

A random forest model fit to the measured soil moisture (expressed as % volumetric water content; VWC) was able to predict the data with an RMSE of 3.6% VWC and a Pearson correlation coefficient of 0.98. We tested the model's ability to extrapolate beyond training data: on average, when the model was trained on only 70% of the measured locations, it was able to predict soil moisture at the remaining 30% of locations with an RMSE of 10 and a correlation of 0.82. The relationship between soil moisture and site properties was similar for ICB and SCB, but not identical. In both watersheds, current vegetation type was the most important predictor of soil moisture (Appendix B.4; Figure B.10). The random forest model trained on ICB measurements fit the SCB soil moisture measurements with a correlation coefficient of 0.82, whereas the model fit to SCB data was able to predict them with a correlation of 0.98 (Figures B.13, B.14).

The random forest model showed small, but generally positive, changes in modeled June soil moisture as a result of fire in SCB (Figure 4.8). These results did not vary with year, but changes were slightly greater earlier in June compared to July or August (data not shown). The largest modeled changes in volumetric water content were less than 5 percentage points (Figure 4.8 inset), whereas in ICB a similar model predicted fire-related changes of up to 30 percentage points (Figure D6). Figure 4.8 also suggests that all areas that transitioned from conifer to dense meadow already had relatively high soil moisture prior to fire, and areas where forests encroached on meadows were relatively dry areas of meadow.
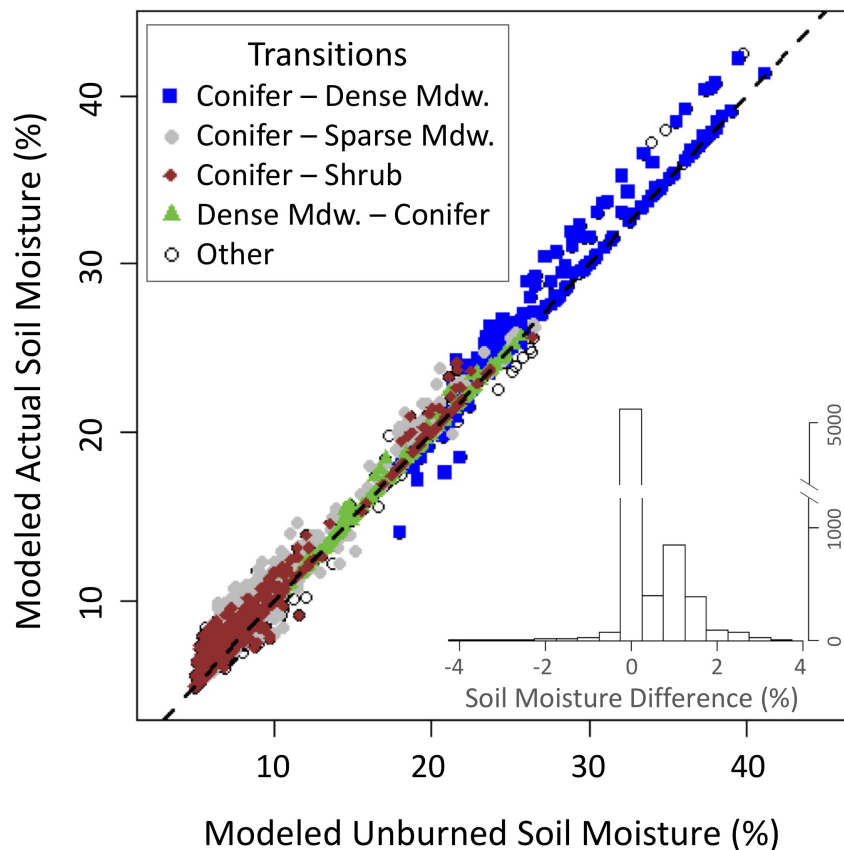
Figure 4.8: Modeled actual soil moisture (current vegetation cover and fire history) compared to modeled soil moisture assuming the same climatology (date set to early June) but no fire or vegetation change since 1973. The inset shows a histogram of the point-wise differences between these two sets of modeled values. Only locations where vegetation type changed between 1973 and 2014 are shown (see Figure 4.5). Locations that transitioned from conifer to dense meadow (mdw.) are shown as blue squares, conifer to sparse meadow as grey circles, conifer to shrub as red diamonds, and dense meadow to conifer as green triangles. Other types of transitions are rare (open black circles). Points above the dashed one-to-one line represent locations where the model predicts soil moisture is higher than it would have been without fire (positive numbers in the inset histogram).

Consistent with the data from spatially-distributed soil moisture measurements (Figure 4.7), continuous weather station records (Figure 4.9; Appendix B.2) indicated that the wetland site was associated with the highest soil moisture among the three weather stations, followed by the shrub and forest sites, at all three soil depths measured (12, 60, and 100 cm). All sites experienced greater and more persistent soil moisture during the 2017 WY than the 2018 WY, as a result of large precipitation differences (SCB weather stations were installed in September 2016 at the end of the 2016 WY, so data were not available for that period). The forest stations tended to measure the least amount of precipitation (Figure 4.1) and experience the earliest snowmelt (Figure B3), and had the greatest interannual soil moisture differences (Figure 4.9). Cumulative shallow soil water gain showed idiosyncratic trends among sites and years (Figure 4.1), although soil type and texture were generally similar between ICB and SCB for each vegetation type (Appendix B.2). Cumulative soil water gain reflects any detectable increase in VWC of shallow soil, however it does not always reflect change in storage or availability of water for vegetation uptake. At SCB, cumulative soil moisture gain was greatest at the forest site in 2017 but greatest at the wetland site in 2018 (Figure 4.1). Soil moisture gain at the forest site may be explained by rapid wetting and drying during the snowmelt period in 2017 (Figure 4.9), possibly due to relatively shallow snowpack (compared to the shrub and wetland sites) experiencing diurnal fluctuations in freezing and thawing. Low values of cumulative soil moisture gain may also be attributable to saturation and/or steady-state infiltration at certain sites, as such conditions preclude additional moisture gains. During the wet 2017 WY, all sites were saturated at 1-meter depth for some period of the year, yet during the drier 2018 WY, only soils at wetland stations experienced saturation. In ICB, the wetland site remained fully saturated for both 2017 and 2018 WYs, while in SCB the wetland site was saturated only for a portion of each year (Figure 4.1). In general, deeper soils contained more water and were saturated longer than shallow soils, while shallow soil moisture was more responsive to precipitation, though water input pulses were apparent at 60 and 100 cm depths as well (Figure 4.9). Very shallow (12 cm) soil moisture was positively correlated with deep (100 cm) soil moisture across sites and years (Figure 4.1).
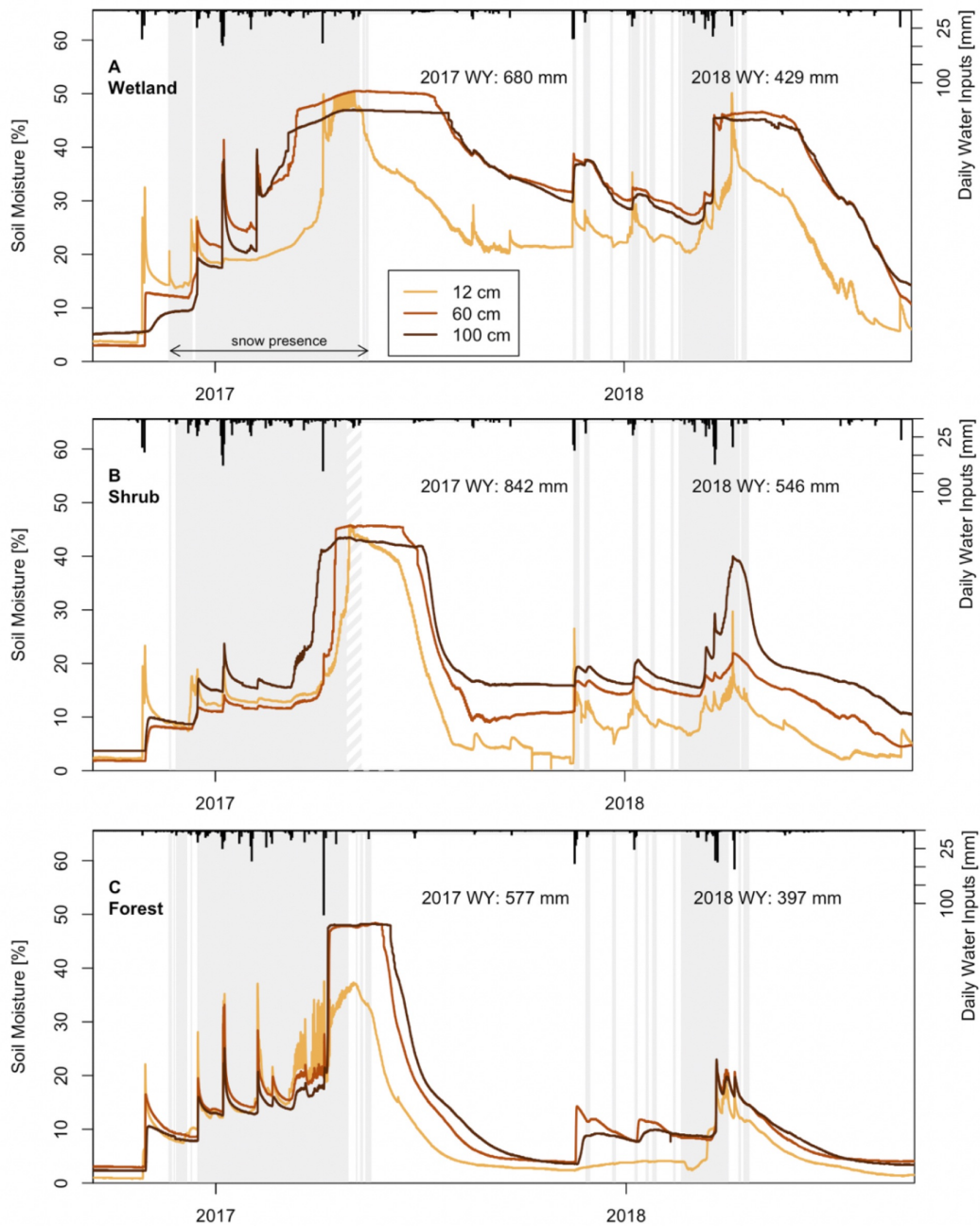
Figure 4.9: Volumetric water content [%] in shallow (12 cm), mid (60 cm), and deep (100 cm) soils as measured by weather stations located in dense meadow (a), shrub (b), and forest (c) sites. Data were measured at 10 minute intervals for 2017 and 2018 water years. Vertical bars at top of panels indicate daily water inputs in the form of rain and snow melt. Grey regions represent periods of time when snow is present around the base of the weather station (at the shrub station camera data were not available in spring 2017, shown by grey hatching). Water year (WY) summaries are also provided for total water inputs recorded at each station. Refer to Appendix B.2 for visuals of each site.

4.4 Discussion

Fire-driven changes in dominant vegetation type (from aerial imagery analysis; Figure 4.5) and forest structure (from forestry plot data; Figure 4.3) were minimal at Sugarloaf Creek Basin (SCB), despite over 40 years of managed wildfire and ten fires greater than 40 ha over that time period in the basin. The minimal changes are a notable contrast from the nearby Illilouette Creek Basin (ICB; Fig. 6), which had a similar duration of a restored semi-natural fire regime yet saw much greater vegetation turnover (even within the first 20 years), heterogeneity of vegetation patches, and soil moisture response (Boisramé et al., 2017a; Boisramé et al., 2017b; Boisramé et al., 2018). A number of potential explanations for this discrepancy exist, including differences in the fire history of the two basins, and differences in water balance and vegetation productivity between the two basins.

Approximately 5,500 ha (44%) of the 12,500 ha SCB watershed burned at least once and approximately 1,300 ha (10%) of the watershed burned 2-4 times since 1973. Fires were more active in ICB, with 52% of the ICB burning at least once in the same period, and 25% burning 2-4 times. The number of fires >40 ha from 1973 to 2016 was also much higher in ICB (n=27) than SCB (n=10), and particularly in recent decades, with ICB experiencing 12 fires >40 ha after 1985 (https://frap.fire.ca.gov/mapping/gis-data/) and SCB only experiencing 4 (Table A1). Despite a marked increase over the fire exclusion and suppression period (Mallek et al., 2013), this comparison with ICB demonstrates that the amount of fire activity in SCB since 1970 may represent a relative lack of fire compared to an expected historical fire return interval (and what is possible under a managed fire regime) over this period, since both ICB and SCB had pre-suppression fire return intervals <10 years (Collins and Stephens, 2007). This low fire return interval may partially reflect recent changes in how the managed wildfire policy has been applied: only 1 ha has burned in the SCB between 2004 and 2017, with 59% of active ignitions suppressed, compared with 7,289 ha burned and only 23% of ignitions suppressed between 1969 and 2003 (Table A1; A. Caprio, personal communication).

The greater emphasis on fire suppression in recent years suggests that additional changes in vegetation cover and forest structure might have been observed had a historical fire return interval been more closely approximated. This is especially true given that the last large fires across the central and eastern portions of SCB were in 1977 and 1985. While the 2003 fire reburned a portion of the 1985 fire, much of the area affected by the 1985 and 1977 fires has not reburned. This means there is considerable area for which the time since last fire exceeds the historical fire return interval by 3- to 4-fold. In addition, the proportion of area burned at high severity (since 1984) is quite small at only 2% of burned area or 69 ha total (Table A1). For comparison ICB had 1129 ha of area burned at high severity (13% of burned area) from 1984-2016 (B. Collins, unpublished data). Taken together these points all demonstrate that fires in SCB had much less potential to manipulate vegetation structure and composition relative to ICB.

The predominantly low-severity fires that burned in SCB by definition caused relatively little conversion to alternative vegetation patches (Figures 3, 6), due in part to the range of acceptable fire management conditions. Two of the most recent fires in SCB, the 1997

Sugarloaf Fire and the 2003 Williams Fire, were responsible for the bulk of the larger patches of overstory tree mortality that we detected in our vegetation change analysis (Figure 4.5; Table A1). These two fires are also in a database of fire weather indices that enable comparison to 475 other fires across California in similar mixed-conifer and fir forest (Stevens et al., 2017). For maximum high temperature during the burn window, which was the number one climatic predictor of burn severity in this database (Stevens et al. 2017), the Williams Fire was in the 9th percentile (23.4ºC) and the Sugarloaf Fire was in the 4th percentile (21.7ºC), indicating mild fire weather conditions.

While weather conditions for many SCB fires may have been mild, it is also possible that there was reduced fuel accumulation in SCB relative to ICB in the fire-suppression period, potentially due to lower precipitation and productivity in SCB. Three lines of evidence support wetter and more productive conditions in ICB vs SCB: first, in-situ weather station data (Figure 4.1) and interpolated PRISM data (Table B3) show higher annual precipitation in ICB; second, streamflow per watershed area is greater in ICB and its encompassing watersheds (Table A2); third, remote sensing analysis revealed greater vegetation productivity in ICB compared with SCB (Figure 4.2), which is generally correlated with fuel accumulation (Collins et al., 2016).

Climatically-driven reductions in fuel accumulation rates in SCB could explain differences in alternative vegetation patch sizes post-fire (Appendix C.3) if tree densities were reduced and less continuous in the drier SCB (e.g., Stephens et al., 2018). Although similar proportions of both basins were dominated by conifers prior to the reintroduction of managed wildfire (Figure 4.6), our analysis did not account for potential differences in forest density. Forest densities in the more productive ICB may have increased more during fire exclusion than in SCB, which could have led to larger patches of alternative vegetation once fire was reintroduced. Besides reducing productivity, drier conditions may make the SCB less hydrologically-responsive to wildfire-induced changes (Saksa et al., 2020). This is because any additional water that becomes available in a water-limited forest (e.g., due to fire-caused tree mortality reducing canopy interception and competition for soil water) is likely to be taken up by the remaining water-stressed vegetation rather than contributing to increased streamflow or soil moisture. For example, Roche et al. (2018) found that the Kings Watershed had less post-fire reductions in ET than the American River Watershed, which had higher precipitation and greater post-fire basal area.

While it is not possible from this study to disentangle the relative contributions of low fire frequency and low productivity to the minimal changes observed in SCB relative to ICB, we found clear evidence of those minimal ecosystem changes from our vegetation patch analysis, our forestry plot analysis, and our soil moisture analysis in response to the restoration of managed wildfire to SCB. With respect to the vegetation patch analysis, the proportional area (Figure 4.6) and the maximum patch size of areas (Figure C4) converted from forest to non-forest was higher in ICB. For larger high-severity patches to develop, there needs to be a confluence of topography, weather and fuels sufficient to cause complete tree mortality (Collins et al., 2007). Relatively small patches of alternative vegetation are one of the primary goals of managed wildfire (Hessburg et al., 2016), so in that respect the fires within

SCB may have met some management objectives with respect to the fine-scale heterogeneity on the landscape to improve resilience to future fires.

With respect to the forestry plot analysis, we did not observe the changes in forest structure from our re-measurement of forestry plots (Figure 4.3) that we would have expected under managed wildfire (Larson et al., 2013). For instance, we observed a uniform decrease in large (>61 cm) and very large (>100 cm) trees, even in unburned red fir forest (Figure 4.3). This is consistent with long-term trends that have been observed across the western US (van Mantgem & Stephenson, 2007; van Mantgem et al., 2009; Das et al., 2016), and may be indicative of climate or pest/pathogen influences in addition to fire, which we would not expect to disproportionately target large fire-resistant trees in low-severity burns.

While large tree density in the forestry plots decreased over time, we observed a slight increase in small (7.6 – 15.2 cm dbh) tree density regardless of number of times burned (Figure 4a). One of the objectives of managed wildfire is the removal of smaller understory trees, particularly of fire-sensitive species (North et al., 2012; North et al., 2015), an outcome that has been observed with managed wildfire in other wilderness areas (Larson et al., 2013). However in SCB in twice-burned plots, we saw an increase in species more easily killed by fire (e.g. *Pinus contorta*) in smaller size classes (Figure 4.3c). The four plots that burned twice (Figure 4.1) were all classified as low to moderate burn severity in the second fire (the initial fire in each case pre-dated remotely sensed burn severity maps). Given the absence of recent fire in the watershed discussed above (Table A1), the regeneration we observed in the smallest size class (Figure 4.3a) may have filled in since the fires of the 1980's and late 1990's even if those fires did consume much of the previous regeneration layer, highlighting the importance of repeated fires to continue to regulate fuels and the spatial heterogeneity of fire-prone forests (North et al., 2012). The increase in shrubs at all burn frequencies (Figure 4.4) was expected, as the dominant shrub species of Arctostaphylos and Ceanothus in this system have fire-cued seed germination (Safford and Stevens 2017).

With respect to the soil moisture analysis, the lack of a strong watershed-wide signal of changing soil moisture is primarily due to 1) minimal detectable differences between forest, shrub, and dry meadow soil moisture profiles when accounting for other moisture drivers (Figure D3c), and 2) the relatively low initial abundance and minimal post-fire expansion of the dense meadow vegetation class (the vegetation type associated with the highest soil moisture; Figures 7, D3c). Both of these factors could be attributable to soil and topographic properties of the watershed as well as precipitation and productivity effects as discussed above. In contrast, within the more productive ICB (Appendix B.2), pronounced increases in the dense meadow vegetation type were observed following fire (Boisramé et al., 2017a; Boisramé et al., 2017b). In ICB, there may have been a greater encroachment of trees, particularly *Pinus contorta*, into meadows during the late 19th century fire exclusion period. This higher encroachment could be due to the ICB's higher productivity relative to SCB, greater consistency in soil saturation of the SCB meadows (this limiting conifer growth), or a combination of both. Alternatively, climate, topography and soil type may be constraining meadow locations at SCB more than at ICB, as we observed little dense meadow encroachment into the margins of existing dense meadows on the rare occasions where those

meadow margins burned (Figure 4.3). It is possible that fire might have greater impacts on soil moisture at shorter time scales; our hydrologic data collection all took place at least a decade following the most recent fire, which could be sufficient time for ET processes (which impact soil moisture) to recover to pre-fire conditions (Roche et al. 2018) and highlights the need for repeated fires to truly restore fire-adapted forests.

High correlations between shallow and deep soil moisture during summer months (Figure 4.1) suggest that our spatially-distributed soil moisture measurements can reflect conditions in deeper soils. However, this correlation only captures relative changes over time, not absolute values. In late summer, there was a greater difference between deep and shallow soil moisture at the shrub and wetland stations than there was at the forest station (Figure 4.9). Therefore, it is possible that transitions from mature forest to more open vegetation cover might lead to greater increases in deeper soil moisture than would be suggested by shallow soil moisture. This could mean that the modeled surface soil moisture changes in Figure 4.8 may underestimate the total change in plant-available moisture. Findings from the ICB also suggested that the soil moisture impact of forest removal might be larger in deeper soils (Boisramé et al., 2018). However, there is high uncertainty regarding the changes to deeper soil water storage, since we cannot determine how broadly these relationships between deep and shallow soils extent beyond the weather station locations.

Similarities in the random forest models trained on ICB and SCB moisture data show that certain variables are consistently strong predictors of soil moisture. For example, vegetation cover type and TWI were within the top 4 most important predictors of soil moisture for both ICB and SCB, with years since fire, times burned, and year of measurement being the least important predictors in both watersheds (Figure D1). However, the relatively poor ability of the ICB-trained model to predict SCB moisture values indicates that the relative importance of these factors for controlling summer soil moisture varies between the watersheds. The extent to which this variation should be attributed to physical and ecological factors in the watershed, and the extent to which it reflects features of the random forest methodology, is not clear given the information available.

Conclusion

Our characterization of vegetation change and the hydrological response following the implementation of a natural fire program in SCB demonstrates the contextual nature of landscape-level fire-ecosystem interactions. While the nearby ICB is similar to SCB in size, elevation, forest types, and time since establishment of a managed wildland fire policy, assuming similar fire-related changes in SCB would have overestimated fire-driven change in vegetation and in water availability. This discrepancy highlights the importance of the place-based field and imagery datasets that we used in our analysis here. While the direction of change and predictors of soil moisture were similar for the two watersheds, the magnitude of change was much lower in SCB, likely due to the interaction between watershed-level productivity and fire effects. In SCB, the lower overall productivity, the reduced fire frequency, and the lesser proportions of high severity fire effects relative to ICB led to greater stability in vege-

tation over time and a more muted hydrological response to managed wildfire in SCB. More landscape-level experimentation in other watersheds, including lower elevation sites more productive than ICB, would further clarify the range of possible landscape and hydrologic responses to natural fire regimes.

Chapter 5

Hydrological Benefits of Restoring Wildfire Regimes in the Sierra Nevada Persist in a Warming Climate

The contents of this chapter are accepted to the Journal of Hydrology in 2020, as an article titled "Hydrological Benefits of Restoring Wildfire Regimes in the Sierra Nevada Persist in a Warming Climate", Gabrielle Boisramé, Scott Stephens, and Sally Thompson is the co-author. The article is going through the publishing process.

5.1   Introduction

Mountain watersheds represent a locus of environmental change and vulnerability in the Western US. The Sierra Nevada, for example, produce 9-30% of California's electricity, and 60-90% of California's water supply (Madani & Lund, 2009), "provisioning" ecosystem services (Stephens et al., 2020) that supply water to 30 million of the state's residents and support agricultural industries with an estimated value of $50 billion/year (Klausmeyer & Fitzgerald, 2012; California Department of Food and Agriculture, 2019). These watersheds, however, experience a naturally volatile climate, are expected to warm and dry due to climate change, and are at increasing risk of disturbance, particularly from wildfire, which is also expected to increase in severity and frequency in a warmer climate (Goulden & Bales, 2019; Westerling & Bryant, 2008). This volatility, warming, drying, and increase in fire risk present significant risks to power production (Tarroja et al., 2016), water supply (Dahm et al., 2015; Writer et al., 2014), human lives (CalFire, 2019b), health and infrastructure (CalFire, 2019c), biodiversity (Richter et al., 2019), ecosystem services (Wood & Jones, 2019; Stephens et al., 2020), and amenity of the montane landscape (Millar & Stephenson, 2015). Conventional management approaches are unlikely to be able to address these joint threats: for example, the costs of fire suppression and firefighting in California are growing exponentially, reaching $950 million USD in 2018 (CalFire, 2019a) with reparation costs in the

billions of dollars (Thomas et al., 2017).

Consequently, foresters and catchment managers are seeking alternative management paradigms for fire-prone montane forests (Stephens et al., 2020). One option is to adopt a "fire use" policy, also known as "managed wildfire", for watershed management. Fire use policies allow lightning-ignited wildfires to burn, subject to a strict management policy that calls for intervention to suppress fire when air quality, structures, or people are placed at risk (van Wagtendonk, 2007). In part, this policy attempts to restore the natural fire-regime in Western US forests, reversing the more than one hundred years of fire suppression in the region. Fire suppression has altered contemporary forests relative to their pre-European settlement condition, such that fuel loads, the prevalence of shade-tolerant and fire-intolerant species, and density of forest vegetation have all increased relative to historical baselines (Collins & Stephens, 2007; van Wagtendonk et al., 2012; Scholl & Taylor, 2010; Stephens et al., 2015). Although interest in adopting fire use strategies is growing (Stephens et al., 2016), there have been relatively few locations where they have been implemented for long enough to assess their effects. Within the Sierra Nevada, the Illilouette Creek Basin (ICB) in Yosemite National Park, CA (Collins & Stephens, 2007), has experienced 29 fires larger than 40 ha since 1972, when 100 years of fire exclusion and suppression in the Basin ended (van Wagtendonk et al., 2012). ICB is located in proximity to long-term weather stations and is gauged shortly downstream of its confluence with the Upper Merced River. These unique characteristics have made it the subject of ongoing research to establish the ecological and hydrological effects of fire use policies (e.g. Collins & Stephens, 2007; Ponisio et al., 2016; Boisramé et al., 2017; Boisramé et al., 2018; Boisramé et al., 2019a).

Hydrologically, the impact of fire use strategies in the ICB has been to increase streamflow production and expand wet environments (Boisramé et al., 2017, Boisramé et al., 2019a). Changes to the water balance of the basin inferred using the Regional Hydro-Ecological Simulation System (RHESSys) suggest that annual transpiration has decreased by up to 30 mm, peak snowpack depth increased by up to 10 mm of snow water equivalent (SWE), annual discharge has increased by up to 40 mm/year in the fire-affected section of the watershed or approximately 5% (25 mm/year) overall, and storage of water in the soil and groundwater (referred to as subsurface storage hereafter) has increased by an average of 60 mm (Boisramé et al., 2019a). These changes, although modest, are comparable to inference of increased streamflow, subsurface storage and snowpack, and decreased evapotranspiration, following wildfires in the Consumnes Watershed in the Sierra Nevada (Maina & Siirila-Woodburn, 2019). Such post-fire wetting occurs against a background of warming and drying in the Sierra Nevada, and could represent a positive hydrological co-benefit relevant to the social and economic case for fire-use policies (c.f. González-Sanchis et al., 2019).

Expanding wildland fire use policies to other locations involves confronting the long timescales on which the forests adjust to changed fire regimes (Stevens, Boisramé, et al., 2020). These timescales mean that changes in fire management policy implemented in the near future would impact forests and their hydrology during the mid-21st century, in comparison to the late 20th century when most of the changes occurred in the ICB. Thus, before attempting to use the hydrological insights gained from the ICB to inform contemporary

forest management decisions, it is pertinent to ask whether the hydrological outcomes of wildland fire use are sensitive to the changes in climate expected by the mid-21st century. Although assessments of the hydrological impact of climatic extremes on watersheds in the Western US suggest that the increases in streamflow due to wildfire dwarf the reductions predicted due to climate change by 2050 (Wine et al., 2018), many uncertainties surround these predictions, including variable effects of post-fire vegetation growth rates and the impact of different fire regimes on water balance (Tague et al., 2019), poorly understood post-fire vegetation successional trajectories in a changed climate, and uncertainties surrounding the future fire regime itself.

By the mid-21st Century, the Sierra Nevada region is projected to be warmer, to experience similar or slightly elevated precipitation inputs (Dettinger, 2005; Pierce et al., 2013), and more frequent fires than in the 1972-present period (Westerling & Bryant, 2008; Yue et al., 2013; Geos Institute, 2013). Multiple studies agree that warmer conditions will dry fuels and increase fire frequency, severity, and extent (e.g. Westerling & Bryant, 2008; Westerling, 2018; Littell et al., 2009), but recent re-appraisals of this work in the Sierra Nevada suggest that fire frequency in future climates is over-estimated because projections have ignored the effects of fuel limitation (Hurteau et al., 2019). Additional complexities, including non-stationary relationships between drought and fire occurrence across climate gradients (McKenzie & Littell, 2017), and feedbacks between fire extent, vegetation dynamics and distributions (Syphard et al., 2018), mean there is considerable uncertainty regarding the future fire regime; so much that Syphard et al. (2018) concluded that there was "no way to ascertain which projections of fire are most feasible".

Compounding uncertainties about future fire regimes is the hard-to-predict successional trajectory of vegetation post-fire, and the interaction of these trajectories with a non-stationary climate (Lenihan et al., 2003; Steel et al., 2015; Cornwell et al., 2012; Batllori et al., 2015). Rapid vegetation transitions from conifer forests to shrubland are associated with the loss of tree seed banks, which limits forest regeneration within large patches of high severity fire (Meng et al., 2015; Young et al., 2019), and with arid post-fire conditions that create unfavorable growth conditions for many forest species (Davis et al., 2019). Shrublands regenerate rapidly after a fire and have a greater tolerance for arid conditions (Lauvaux et al., 2016; Serra-Diaz et al., 2018; Baudena et al., 2019). In the absence of high severity fires, forest succession occurs on timescales of multiple decades (Halofsky et al., 2018; Liang et al., 2016), and fire excluded forests are hypothesized to lie near tipping points where disturbances could cause significant changes in vegetation composition (Batllori et al., 2018). This literature suggests that the potential range of post-fire vegetation transitions is poorly bounded.

Fully predicting the effects of wildland fire use on hydrologic regimes under future climates would require unraveling these uncertain processes to specify the feedbacks between vegetation, water, fire risk and successional dynamics, a highly challenging problem (Brotons & Duane, 2019; Riley et al., 2019). We therefore do not directly address this problem for the specific case of the ICB, but instead adopt a set of simplifying assumptions which are further developed and justified in the methods section: (i) we use standard approaches to

predicting future climate in ICB by downscaling and bias correction of an ensemble of global circulation models (Lanzante et al., 2019; Luo et al., 2018), (ii) we assume that the characteristics of the fire regime that would arise if applied to fire-suppressed forests in 2030-2070 are well represented by the severity - area distribution of the historical fires that occurred in ICB from 1972-2010, and we allow for the frequency of these fires to increase across a set of scenarios drawn from the literature and considering climate impacts on frequency only (see Section 5.2 for details). Specifically, the assumptions keep severity and fire area constant, and therefore do not account for possible feedbacks between these aspects of fire, climate, and vegetation. Finally (iii) we assess the hydrological implications of climate change on fire impacts under two vegetation scenarios: one in which post-fire vegetation transitions match those which occurred in the historical period (a scenario which might arise if, for example, topography and geological context primarily drive vegetation community types), and one "bounding case" scenario in which we force all post-fire vegetation regeneration to occur as a single plant type (conifers, shrublands, or wet meadows), assuming that reality would lie in between these extreme limits of vegetation change. With these assumptions, we use an existing RHESSys model parameterization for the ICB (Boisramé et al., 2019a) to answer three questions:

i) How would the hydrology of the ICB respond to climate change in the absence of the fire use policy, where vegetation remains in a fire excluded state?

ii) How do the hydrological outcomes of fire use strategies in ICB differ under future climate conditions (2030-2070; RCP 4.5 and RCP 8.5), relative to those outcomes under the observed climate (1970-2010)?

and

iii) How sensitive are the hydrological outcomes of fire use strategies for the 2030-2070 period to potential increases in fire frequency?

5.2   Methods

Study Site

Illilouette Creek Basin (ICB) is located within Yosemite National Park, California, USA (Figure 5.1). The 150 km^2 basin spans an elevation range of 1,270-3,600 meters, with a mean elevation of 2,500 meters. About 41% of the ICB is forested with *Pinus jeffreyi*, *Abies concolor*, *Abies magnifica*, and *Pinus contorta*, interspersed with meadows (16%) and shrubland (9%). About 34% of the basin is high elevation granite, which acts to confine fires to the basin (Boisramé et al., 2017; Collins et al., 2009).

ICB experiences a Mediterranean climate with warm dry summers and cool wet winters. The nearest weather station is located in Yosemite Valley (1,240 meters, 37.74 lat, -119.59 lon, CDEC station YYV), and has operated since 1926. Over 1970-2010, this station recorded a mean annual precipitation of 92.0 cm, mean daily minimum January temperature of -2 °C and mean daily maximum July temperature of 27°C. The ICB has similar precipitation
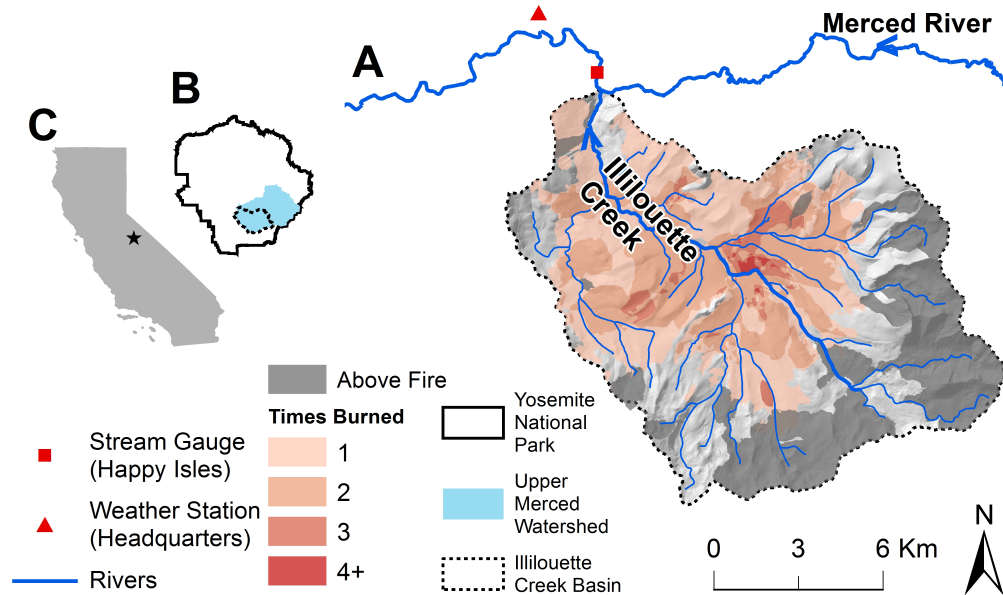
Figure 5.1: Study site location: Illilouette Creek Basin (A), within Yosemite National Park (B), California (C). Stream gauging station (Happy Isles) and weather station are displayed along with major rivers and tributaries.

totals to Yosemite Valley, but is approximately 7 °C cooler (January 2015 to December 2017, Appendix Figure C.1), leading to a greater fraction of precipitation falling as snowfall. While streamflow data for the ICB itself are limited, the basin comprises 33% of the Upper Merced River Basin, which has a century-long streamflow record at the Happy Isles gauge located downstream of the confluence of the Illilouette Creek with the Upper Merced River (Figure 5.1; Boisramé et al., 2019a). The mean flow at Happy Isles was 10 m^3/sec (71 cm/year) for 1970-2010 (USGS gauge # 11264500, data from waterdata.usgs.gov).

During the period from 1700-1900, prior to fire suppression, ICB had a fire return interval of 6.3 years. Following the initiation of fire use strategies, the fire return interval was 6.8 years (from 1972-2005), similar to the pre-exclusion era (Collins & Stephens, 2007). From 1972 to 2019, there were 29 fires greater than 40 ha in ICB, of which 1 was human caused (1986, burned 291 ha), 1 was prescribed (1999, 54 ha), and the other 27 fires were lightning ignited (van Wagtendonk et al., 2012). Of the 8187 ha burned in ICB (75% of the watershed's vegetated area), 4463 ha (55%) burned twice, 767 ha (9%) three times, 72 ha (1%) four times, and 4 ha (<1%) five times (Figure 5.1). As shown in Figure 5.2, this high wildfire activity in ICB has doubled the area of dense and sparse meadows in the basin (Boisramé et al., 2017, Boisramé et al., 2018), increased landscape heterogeneity and habitat for multiple plant and animal species, and is associated with increased biodiversity (Ponisio et al., 2016; Campos et al., 2017; Stephens et al., 2019).
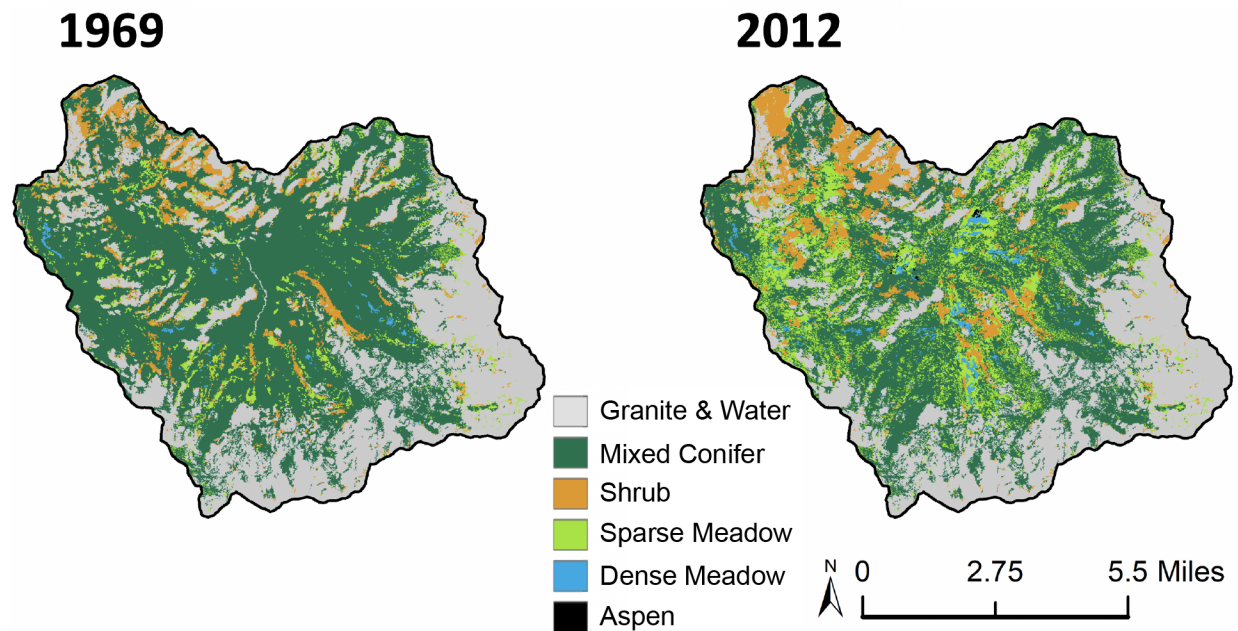
Figure 5.2: Vegetation classification of ICB based on satellite imagery for 1969 (left) and 2012 (right). 1969 landscape signifies over 100 years of fire suppression, while 2012 represents 40 years of fire use strategies.

The contemporary (1972-present) fire regime in the ICB has been relatively stationary (Figure 5.3). Following the initiation of fire use strategies, the fires were relatively small in area with low to moderate burn severities, as assessed by Landsat-derived indices, where the Relative difference Normalized Vegetation Index (RdNDVI) was used prior to 1984, and the Relative difference Normalized Burn Ratio (RdNBR) post 1984 (Collins et al., 2009). Both burn severities (Figure 5.3-A) and burn areas (Figure 5.3-B) in the ICB are more stable in the contemporary period than in the surrounding Sierra Nevada, where fire severity and area have both increased. Fire perimeters in the ICB indicate that fires in the basin are self-limiting (Collins et al., 2009).
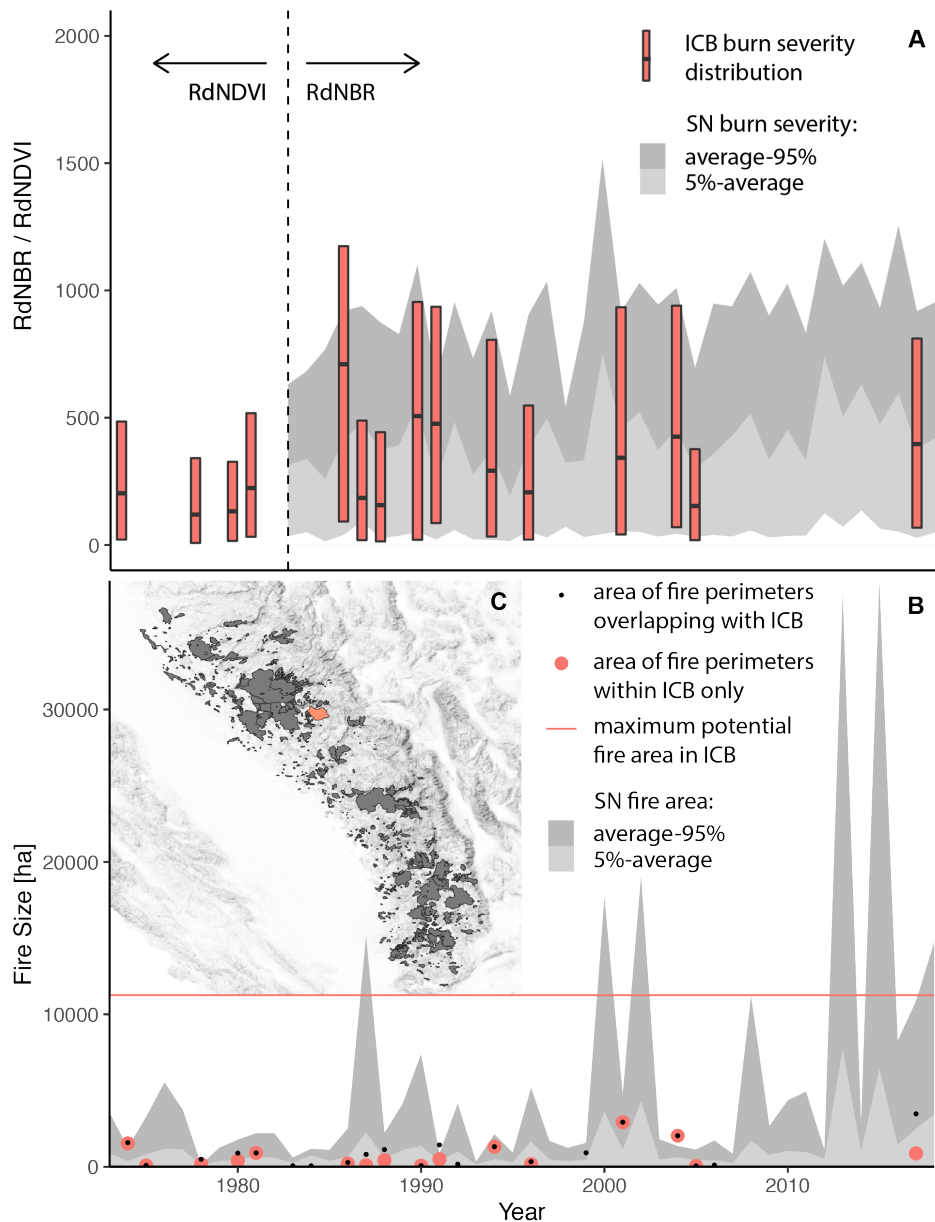
Figure 5.3: Burn severity for fires that occurred within ICB (red in C) and the surrounding
Sierra Nevada (SN) region (SN fires are dark gray in C) were assessed using Landsat-derived
RdNBR index for years after 1983 and RdNDVI prior to 1983 (A). For the SN, a 90%
confidence interval is provided along with the average fire size for the years 1984-2018. Fire
severity in ICB is shown as a box and whisker plot in red, where the range is the 5th
through 95th percentile, and the average is shown as a horizontal dash. In B, mean and 90th
percentile fire size from 1974-2018 is shown for fires in the SN (gray colors). Red dots in B
are fire areas within the ICB only, and black dots are full fire perimeters of which at least a
portion was within the ICB. The maximum fire size within ICB (vegetated area of ICB) is
shown as a horizontal red line. Fires less than 40 hectares were excluded from both the SN
and ICB analyses.

RHESSys Model

The Regional Hydro-Ecological Simulation System (RHESSys, version 5.20.1) is a spatially distributed ecohydrological model that simulates water, energy, and vegetation growth processes. It represents landscapes through a hierarchy of spatial units: small areas of uniform soil and vegetation are represented as patches, water is routed between patches within hillslopes, and basin-scale processes arise from water fluxes and stores aggregated across hillslopes. The ability of RHESSys to simulate climatic, hydrological and vegetation growth processes at a basin scale makes it well suited to simulating the effects of disturbance (such as fire) on water balance.

At the patch scale, RHESSys resolves a detailed vertical energy and water balance. The energy balance is forced by shortwave radiation inputs, varied to account for slope, aspect, topographic shading, and seasonality. Other energy flux terms, and wind speeds, are attenuated through vegetation canopies as a function of leaf area index (LAI), which itself changes dynamically as the vegetation grows. Incoming precipitation is intercepted by canopy and litter layers, and is partitioned between infiltration (via Green & Ampt, 1911) and surface detention storage (which contributes to runoff if sufficiently large) at the soil surface. Vapor fluxes include evaporation or sublimation from all vertical layers, and transpiration separately computed from sunlit and shaded canopy layers, all computed using the Penman-Monteith approach (Monteith, 1965). Infiltrated water is routed between a root zone, an unsaturated and saturated zone based on Darcy relationships and soil parameters, and lateral fluxes of water between spatially explicit patches are resolved based on surface topography and calibrated drainage parameters. In addition to specifying LAI growth rates, species-specific plant properties control maximum stomatal conductance values and their response to changing soil water. A more detailed description of the RHESSys model is provided in Tague & Band (2004).

Boisramé et al. (2019a) implemented RHESSys in the ICB, drawing on LiDAR elevation data at 10m resolution (Kane et al., 2015), a vegetation analysis (Boisramé et al., 2017) that used aerial photos and the Yosemite National Park vegetation mapping to delineate six cover types, daily weather data from the Yosemite Headquarters Weather Station, and flow records at Happy Isles Gauge and a short flow record within the Illilouette Creek. The six cover types are conifer forest, aspen (*Populus tremuloides*), shrub (primarily *Ceanothus cordulatus*), wet meadow (dense grasses and forbs), dry grassland (sparsely vegetated areas dominated by grasses), or unvegetated (exposed rock or sand). The model was calibrated to identify behavioral parameter ensembles consisting of (i) temperature and precipitation lapse rates (ii) decay of hydraulic conductivity with depth, (iii) saturated hydraulic conductivity at the land surface, (iv) depth of hydrologically active water storage across soil and saprolite layers, (v) the proportion of saturated soil water routed directly (via preferential flow paths) to deeper groundwater stores below plant root access, and (vi) the proportion of these deeper groundwater stores draining to the stream each day. RHESSys captures spatial variations in subsurface properties across soil types by scaling them using mapped soil categories for the ICB. Calibration was performed against Happy Isles flow data and identified

an ensemble of 93 behavioral parameter sets (assessed across a multi-objective set of criteria aiming to capture volume and timing of streamflow on monthly, seasonal and annual scales) that were used to constrain model uncertainty using the Generalized Likelihood Uncertainty Estimation (GLUE) approach (K. Beven & Binley, 1992). More details regarding the parameterization, calibration, and validation of RHESSys for the ICB are provided in Boisramé et al. (2019a).

Modeling the Effect of an Individual Fire

Individual fires in RHESSys were defined based on fire perimeter and severity maps. Fires were treated as having an instantaneous effect on vegetation biomass, on the thickness of the litter layer, and on the species-specific properties of the vegetation (to represent post-fire vegetation transitions): these factors drive subsequent hydrological responses in RHESSys. Wildfires can, however, have other hydrologically-relevant effects that were omitted from the model, including reduced albedo from charred surfaces (Burles & Boon, 2011, Gleason et al., 2013, Gleason et al., 2019), changes in the size and distribution of canopy gaps (Stevens, 2017; Kostadinov et al., 2019; Lundquist et al., 2013), reduced soil infiltration capacity due to ash clogging or soil hydrophobicity (Neary et al., 2005; Ebel & Moody, 2020; S. Doerr et al., 2006), and increased erosion rates (Larsen et al., 2009a). In the ICB, low-moderate severity fires are most common (rather than the high severity fires that generate persistent changes in soil properties S. Doerr et al., 2006), and water quality monitoring at the Happy Isles' gauge indicates no increases in turbidity or flow peaks post-fire (results not shown). The reliance of our modeling on spatially uniform daily precipitation, although necessary given lack of more resolved precipitation data for the Merced River Basin (Henn et al., 2018) would likely prevent the model from resolving surface-flow events that might arise due to soil changes. Consequently, the model, which was calibrated to optimize long timescale water balance predictions, may under-estimate peak flow occurrences, particularly immediately post-fire.

Fire severity was used to determine the degree of biomass and litter loss in each fire-affected patch. The threshold approach of J. D. Miller & Thode (2007) was used to relate RdNDVI/RdNBR observations to fire severity in ICB following Collins et al. (2009). We considered three classes of change: (i) for RdNBR and RdNDVI values between 69 and 315 (low severity), only litter stores were removed; (ii) for values between 315 and 640 (moderate severity), in addition to litter removal, plant carbon stores were reduced 50%; (iii) for values greater than 640 (high severity), all carbon and litter layers were removed within the fire perimeter. Additionally, if analysis of aerial photos indicated a change in vegetation cover type following a fire, we mapped these patches also as high severity burn areas.

Where high severity fire occurred, all above-ground vegetation carbon and litter stores were set to zero and modeled vegetation was allowed to immediately regrow dynamically. To account for the possibility of a post-fire cover-type transition, we reset the vegetation parameters in these patches to represent one of two scenarios. In one scenario, individual pixels followed the observed historical successional trajectory that occurred in the 1972-2010

setting. In the other scenario, pixels that burned at high severity were forced to regenerate with a single vegetation type: all forest, all shrub, or all wetland. This "bounding cases" scenario was used to constrain the uncertainty in the hydrological projections that arises due to unknown patterns of future post-fire regeneration, under the assumption that enforcing a single vegetation type provides a limiting case. The bounding case scenarios were run for the historical fire regime only.

Using 1972-2010 Fire Data to Define Potential Future Fire Regimes

The characteristics of the fire regime that has prevailed in ICB since 1972 are illustrated in Figure 5.3 which shows RdNDVI and RdNBR distributions, fire return interval, and area of all fires over 40 ha. Note that the most recent fire, the Empire Fire of 2017 (the only fire after 2010) is not shown on this figure. It was omitted from this study due to a lack of data about post-fire vegetation type and condition. However, as illustrated in the Appendix Section C.3, the Empire Fire was similar to previous fires in size and severity. These data are suggestive of a relatively stable fire regime, consistent with the self-limiting behavior of fire in the ICB.

Defining the spatial, temporal, and severity characteristics of potential future fire regime is, as the literature reviewed in the introduction suggests, inherently uncertain. In light of these uncertainties and the stability of the fire regime in the ICB over five decades of climatic and vegetation change, we use the observed fire perimeters and severity maps to define potential future fire areas and severities. With the historical fire perimeters providing some control on fuel limitation, warmer temperatures are expected to increase the probability of ignition by decreasing fuel moisture, leading to increased fire occurrence (Riley & Loehman, 2016; Westerling & Bryant, 2008; Lauvaux et al., 2016). To explore the effects of changing fire frequency, we shortened the time interval (in days) between historical fires by 30% and 60% in line with predictions for the Sierra Nevada based on climatic warming (Riley & Loehman, 2016; Westerling & Bryant, 2008; Lauvaux et al., 2016). This had the effect of some fire perimeter/severity combinations being imposed twice in the modeled record – for the 30% increase in fire frequency scenario("+30%"), these were the fires from 1974 and 1978; for the 60% scenario, the fires from 1974, 1978, 1980, 1981, 1986, 1988, and 1990 were imposed twice. As can be seen visually in Figure 5.3, these fires are broadly representative of the range of fires in the ICB (i.e. we did not repeat extreme cases). We checked if these increases were reasonable in light of the minimum time needed to allow fuel to build up and reburn in the ICB - estimated as approximately 9 years (Collins et al., 2009). For a 60% increase in fire frequency scenario ("+60%"), the average interval between reusing a given fire perimeter is 24 years, and the average interval between pixels reburning is 7 years, suggesting that this increase represents a reasonable fuel-limited maximum for the basin.

Using a historical fire occurrence record as a basis for increasing fire frequency can lead to a situation where a fire is predicted to occur outside the fire season (historically observed

to be June-September in the ICB). If this projected timing was such that the fire occurred in the window of April 1st to October 31st (a period that we confirmed is snow-free in all modeled future climate scenarios), we allowed the fire to burn on that projected date, in line with the expected lengthening of the regional fire season (Yue et al., 2013). If, however, the projected fire date lay outside this seasonal range, it was assigned a random date from the nearest fire season.

The approach of using historical fire perimeters to define the future fire regime omits exploration of other future fire scenarios - for example, scenarios in which the severity/area of fires changes dramatically. Using historical fire perimeters does not allow a fully comprehensive analysis of the uncertainty in hydrological predictions associated with the specific sequence of fires. It does not explore a situation in which fire frequency is reduced in the basin relative to historical conditions; although the fact that three fires were suppressed during the California Drought (2011-2016, this is likely responsible for the large fire-free interval before the Empire Fire in 2017) suggests that reduced fire frequency regime could be a possible outcome within the future climate. Given these limitations our goal is not to be predictive, but rather to determine if the hydrological responses to this sequence of historically managed fires, or to a "sped up" version of this sequence of fires, are the same as they were under historical climate conditions.

Future Climate Data and Bias Correction

Ensembles of climate model predictions are widely recognized as being essential to characterize the uncertainty surrounding future climates (Pierce et al., 2009; Hagedorn et al., 2005; P. D. Thompson, 1977). Since too few regional climate models are available over the ICB to generate such an ensemble, we downscaled the minimum and maximum temperature and precipitation output of 10 GCMs, using data from the cell (ranging from 0.75-2.8 degrees latitude and longitude) containing the ICB, for the 2030-2070 period. In selecting 10 models, we followed the recommendations of Pierce et al. (2009), who suggested that climate ensembles became stable after 5 or more models are included. The GCMs we selected were: ACCESS1.3, CanESM2, CMCC-CM, CSIRO-Mk3.6.0, GFDL-ESM2M, INM-CM4, IPSL-CM5A-MR, MIROC5, MRI-CGCM3, and NorESM1-M (Appendix Figure C.2 provides additional descriptions of each model). These models were chosen to maximize model skill and model independence as computed by Sanderson et al. (2017), and to cover a range of predicted future climate extremes (i.e. to include models that predict both cooler/wetter futures in the region, and those that predict hotter/drier conditions). All model data were obtained from the Coupled Model Intercomparison Project Phase 5, CMIP5 (https:/esgf-node.llnl.gov/projects/cmip5), and have the same initializations, realizations, and parameterization states (abbreviated as "r1i1p1" in CMIP5). We obtained future climate timeseries from both RCP 4.5 and RCP 8.5 climate scenarios, where RCP 4.5 scenario represents a decline in greenhouse emissions around year 2040 and RCP 8.5 is a "business-as-usual" scenario with a continuous rise in greenhouse emissions. Both scenarios predict a global rise in temperature.

Choosing temperature and precipitation data of the single GCM grid point containing ICB, we used quantile delta mapping (QDM) ("MBC" package in R) to bias correct the GCM data and downscale it to the location of the Yosemite Headquarters weather station. QDM is a non-parametric method to correct systematic modeled biases with respect to observed values while preserving model-projected relative changes in precipitation and temperature quantiles (Cannon et al., 2015). In addition to modeled, observed, and future climate time-series, QDM requires observed climate observations, which we obtained from the Yosemite Headquarters weather station and gap filled via multivariate imputation ('MICE' package in R) and data from adjacent weather stations (see Appendix Section C.2). We bias-corrected the daily precipitation and the daily maximum and minimum temperatures for 2030-2070, treating the historical period (1970-2010) as static. During a static period, the distribution of climatic variables does not change significantly for any decade. QDM was then used to superimpose the modeled quantile trends ("delta changes") onto the observed static period. The delta changes were applied multiplicatively to the precipitation correction and additively to the temperature corrections (Cannon et al., 2015). The resulting bias-corrected model timeseries form the climate ensemble were used to drive RHESSys modeling. The timeseries were summarized in terms of rainfall, temperature, snowfall, and snow season statistics across the ensemble: these quantities are important determinants of the length of the fire season and basin hydrology.

Although CO_2 concentrations are predicted to rise in the future climate, due to model limitations, they are held constant across all model simulations.

Model Experiments

The model experiments were set up to answer the Research Questions. Prior to conducting the model experiments, RHESSys was initialized with the 1969 fire-excluded vegetation map, which was spun-up for a few hundred years using observed historical climate (repeated time-series), starting from no carbon stores, and until LAI reached a steady-state (Boisramé et al., 2019a). Then, prior to the future climate simulations (2030-2070), for each RCP scenario, the 1969 fire-excluded and spun-up vegetation was further spun-up using the 2020-2030 climate.

Research Question (i) asks how changing climate would alter the hydrology of the fire-excluded ICB, assuming vegetation was initialized in the same state as was observed in 1969. To answer this question, we held vegetation type constant and ran RHESSys for 40 years using the observed 1970-2010 climate, and for the RCP 4.5 and 8.5 future 2030-2070 climates (see Figure 5.4). Differences in the predictions can be interpreted as the impact of climate on vegetation and hydrology in the absence of changes imposed by fire.

Research Question (ii) addresses the differences in how wildland fire use affects ICB hydrology under future versus observed climates. To answer this question we ran RHESSys for a 40 year period using the observed 1970-2010 climate, and for the future climate ensemble for the period 2030-2070 under RCP 4.5 and RCP 8.5 scenarios.

For each of these climates we ran a control model representing fire excluded conditions based on the 1969 vegetation map (Figure 5.2-A) with no fire disturbance imposed ("fire ex-
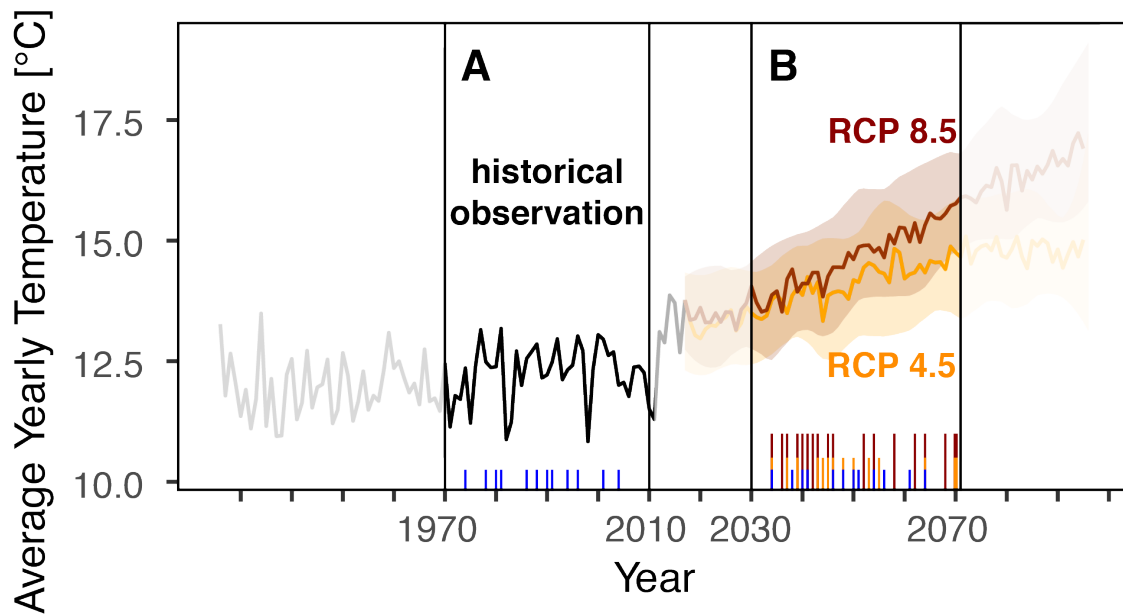
Figure 5.4: Historical modeling time period from 1970 to 2010 (A), denoting observed 40 years since the end of fire exclusion policies in the ICB. Future modeling time period from 2030 to 2070 (B) is compared to the historical one. An ensemble of 10 different CMIP5 general circulation models (GCMs) was used as future climate inputs for two different representative concentration scenarios (RCP 4.5 and RCP 8.5). Blue vertical lines denote historical frequency fire events. Orange vertical lines denote 30% increase in fire frequency from historical observations, and dark red vertical lines denote 60% increase in fire frequency.

cluded"). We also ran a treatment model in which fire disturbance was imposed based on the observed historical (1970-2010) fire regime ("historical frequency") and updated vegetation maps after fires (using both the observed post-fire vegetation transitions and the bounding cases where all vegetation transitions to specific cover types). The differences in hydrological predictions between control and treatment models can be attributed to the effects of fire on vegetation and litter. The differences in these differences (sensu Angrist & Pischke, 2008) can be attributed to the role of different climates interacting with the fires.

Research Question (iii) is addressed by repeating this analysis using the higher frequency fire regimes in combination with the future climate scenarios (Figure 5.4), however, in this case, only historical vegetation transitions were modeled. Again, the fire excluded landscape was modeled across all climate regimes as a control. Differences between control and treatment can again be attributed to the role of fire.

RHESSys output was generated on daily timescales at the scale of the entire Illilouette Creek Basin. The analysis focuses on streamflow, vertically aggregated depth of saturated and unsaturated groundwater storage ("subsurface storage"), snow water equivalent (SWE),

snow sublimation, LAI, evaporation, and transpiration. These variables were aggregated to water year to visualise long-term fire effects. All results were reported as a depth of water, with basin-scale fluxes normalized by the basin area (150 km^2). However, in interpreting these results, it is important to recall that all changes in basin-scale hydrology were derived from fire-induced changes that occurred in at most 75% (112 km^2) of the watershed. If considering how the observed changes in ICB might play out in other watersheds, it may be more appropriate to weigh these changes by fire-affected area in each basin. Heterogeneity in hydrological processes should also be considered: for example, only approximately 52% of the streamflow in ICB is generated in the area that burned (and the remaining 48% is generated on high elevation rock and is largely uninfluenced by downgradient vegetation condition). Snowpack dynamics are also highly spatially variable, with these spatial patterns shifting greatly between climate scenarios. These variations are masked in the whole-of-basin averaging used to present hydrological change in this study, but analysis of heterogeneity in hydrological response to fire is beyond the scope of this manuscript.

Uncertainty Analysis

Recognizing that the scenarios modeled do not fully bound the range of possible fire-climate-vegetation interactions, our uncertainty analysis follows the GLUE approach to constrain the combination of uncertainty due to climate projections and hydrological parameter uncertainty. Each hydrological model experiment consisted of running the 93 highest performing calibration parameter ensembles, in conjunction with the 10 climate model ensemble members. Thus each combination of a future climate scenario (RCP 4.5 or RCP 8.5) and a fire scenario (exclusion, observed historical, +30%, or +60%) generated an ensemble of 930 modeled timeseries for each variable (93 RHESSys model parameterizations times 10 climate models). This ensemble formed the basis for uncertainty analyses. In general, the question we were asking was related to the significance (relative to parameter and climate model uncertainty) of differences in predicted values of any hydrological variable between two scenarios. To compute this significance, we differenced model output from equivalent ensemble members (having the same combination of driving climate model and RHESSys model parameters) from the two scenarios of interest. This generated a set of 930 differences (except in the case where fire scenarios were compared for the observed climate, when 93 differences result). The 95% confidence interval was then specified as the interval between the 2.5 and 97.5 percentiles for these 930 differences. If this interval excluded zero, the difference was considered significant at the 95% confidence level. See Appendix D for a mathematical formulation of how the ensemble of differences was calculated.

5.3 Results

Future Climate

Table 5.1 shows climate statistics aggregated by decade for the 4 decades of simulation, where decades 1, 2, 3, and 4 correspond to the historical time periods of 1971-1980, 1981-1990, 1991-2000, 2001-2010, and future time periods of 2031-2040, 2041-2050, 2051-2060, 2061-2070 respectively. By considering output on this decadal basis, we can better compare between climates based on the common time since first fire (first fire occurs in 1974 for the historical modeling and 2034 for future model scenarios). Each decadal value shown is based on the average of the 10 GCM models following downscaling and bias correction. All results discussed below refer to comparisons between 1970-2010 historical averages, and 2030-2070 future climate simulations. By 2060-2070, ICB will warm by 2.2°C under RCP 4.5 and by 3.1°C under RCP 8.5 climate scenarios. Predicted annual precipitation totals in both scenarios are slightly wetter than the historically observed record. The 2030-2070 RCP 4.5 climate, on average, receives 159 mm more precipitation per year than the 1970-2010 period, while RCP 8.5 receives 32 mm more. The historically observed precipitation lies within the 95% uncertainty bounds of both future climate ensembles, meaning that some models predict a drier and others a wetter future climate. Ensemble-averaged precipitation under both RCP 4.5 and 8.5 scenarios exhibits much less inter-annual variability than do historical observations (see Appendix Figure C.3-A), which is a result of averaging over the ensemble. The RCP 8.5 climate ensemble distributions of daily precipitation show an increase in extreme events when compared to the historically observed precipitation distribution (see Appendix Figure C.4). Higher average temperatures, with similar total precipitation, result in a shorter snow season. On average, by 2060-2070, the snow season length drops by 26 days for RCP 4.5 and 43 days for RCP 8.5 climates. Additionally, and again due to the warmer temperatures, the snow fraction of precipitation (% precipitation falling as snow) declines for future climates. Historically, 60-70% of precipitation in ICB occurred as snowfall, and this percentage falls to 49% (RCP 4.5) and 42% (RCP 8.5) by 2060-2070.

Table 5.1: Bias-corrected yearly average temperature data and precipitation yearly sums are averaged decadaly and presented as an average of all 10 GCM models for both RCP 4.5 and RCP 8.5 scenarios. Decades 1, 2, 3, and 4 refer to the historical time periods of 1971-1980, 1981-1990, 1991-2000, 2001-2010, and future time periods of 2031-2040, 2041-2050, 2051-2060, 2061-2070 respectively. Temperature and precipitation data were used as RHESSys model inputs while maximum snow depth, snow season length, and % of precipitation as snow are based on RHESSys fire excluded model outputs. Gray shading indicates that the variable in the future climate scenario is statistically different from the observed climate scenario at the 95% confidence level.

	Decade			
Climate	1	2	3	4
Temperature [°C]				

Climate	Decade 1	2	3	4
Observed	12.0	12.3	12.4	12.3
RCP 4.5	13.7	14.0	14.4	14.5
RCP 8.5	14.0	14.3	14.9	15.4
Precipitation [mm]				
Observed	929	937	1071	745
RCP 4.5	1125	1026	1059	1106
RCP 8.5	914	987	976	933
Snow Season Length [days]				
Observed	213	213	212	208
RCP 4.5	182	174	173	176
RCP 8.5	180	180	171	158
% Precipitation as Snow				
Observed	66	63	67	70
RCP 4.5	54	54	48	48
RCP 8.5	54	49	45	42

Hydrological Outcomes of Wildfires

To understand the hydrological outcomes of wildfire, we considered multiple hydrological variables at the annual scale (transpiration, evaporation, streamflow, subsurface storage, and maximum snow water equivalent) and their mean values across all model parameter sets and climate ensemble members. We averaged the value of these variables on decadal timescales, and Table 5.2 shows these decadal averages for the observed, RCP 4.5, and RCP 8.5 climate scenarios for the four fire regimes: fire excluded, historical fire frequency, and +30% and +60% fire frequency. The analysis of the results is broken down based on the model scenarios, showing the changes in hydrology due to: 1) climate only, 2) climate in combination with the historical wildland fire use regime, and 3) climate combined with hypothetical, higher-frequency fire regimes.

Climate Only

Answering Research Question (i) isolates the influence of climate on hydrology if vegetation was to remain in a fire-excluded state. Overall, other than expected but statistically non-significant decreases in snowpack, the different climate scenarios cause only minimal changes in predicted ICB hydrology at annual timescales. To discuss these changes we focus on the final decade of simulation (i.e. 2000-2010 and 2060-2070). Trends in all water balance components across the climate scenarios are shown in Figure 5.5-A as a fraction of annual precipitation. Streamflow is always the largest component of the water balance, representing 83.4% (observed), 86.1% (RCP 4.5) and 86.7% (RCP 8.5) of precipitation. Independent of the climate scenario, transpiration represents 6% of annual precipitation, meaning it increased

in absolute terms in the slightly wetter climate projections (by 19 mm for RCP 4.5 and 10 mm for RCP 8.5). The small projected increases in streamflow as a fraction of the water balance in RCP 4.5 and 8.5 can be attributed to reduced evaporation (litter, canopy, and soil evaporation, excluding transpiration, plus snow sublimation), which declines from 10.4% of precipitation (observed climate) to 7.7% (RCP 4.5), and 6.8% (RCP 8.5), almost entirely due to lower snowpack - and thus sublimation - in the warmer climates. Unsurprisingly, the maximum basin-averaged snow water equivalent decreases in future climates, by 42 mm (RCP 4.5) and 146 mm (RCP 8.5) relative to observed climate conditions ("Fire Excluded" in Table 5.2). Lower snowfall and snowpack also reduce the fraction of streamflow derived from snowmelt and move the month of peak streamflow earlier. For example, peak snowmelt occurs in May for 2000-2010, but in April for 2060-2070, in both RCP 4.5 and RCP 8.5 scenarios. In this peak snowmelt month, the proportion of streamflow derived from snowmelt declines from a historical maximum of 95% (2000-2010), to 83% and 79% (2060-2070, RCP 4.5 and RCP 8.5 respectively, see Appendix Figure C.8-A and B). Notably, in this final decade there are no observed trends in subsurface storage (ΔS in Figure 5.5-A, where ΔS is the net change in storage over one water year, is near zero). This means that the differences in water balance across the climate scenarios are exogenously driven, rather than arising from non-stationarity associated with interannual trends of wetting or drying of the basin.

Lastly, the only significant changes in future climate when compared to the observed climate (gray shading in Table 5.2) is a 19 mm/year increase in transpiration (RCP 4.5 climate) and a 18 mm/year decrease in evaporation (RCP 8.5). This lack of significance is associated with high uncertainty of both climate models and hydrological parameters which is a common phenomenon in hydrological models (Her et al., 2019; Najafi et al., 2011). Even if they are not statistically significant, there are clear trends in hydrological variables across climate scenarios; particularly there is higher transpiration, increased streamflow, and decreased maximum snow water equivalent for RCP 4.5 and 8.5 climate scenarios compared to the historical baseline (Table 5.2).

Climate + Historical Fire regime

This section addresses Research Question (ii), which asks how the hydrological outcomes of fire use strategies in ICB would differ under future climate conditions (2030-2070, RCP 4.5 and RCP 8.5), relative to those outcomes under the observed climate (1970-2010). Answering this question repeats the analysis above, but including fire under the "historical frequency" model scenario, enabling us to compare the differences in hydrology associated with fire between different climate scenarios. These model runs were conducted for both the observed post-fire vegetation succession and for bounding cases where all post-fire vegetation in high severity burn areas was forced to transition to a single vegetation type. These "bounding" cases suggest that the hydrological changes predicted have low sensitivity to the type of vegetation regrowing in high severity burn areas (Figure 5.2). Subsurface storage and streamflow were almost entirely insensitive to the vegetation transitions prescribed, regardless of the future climate scenario, and variations in the predicted change in other hy-

drological variables across vegetation types were on the order of $< 10\%$, being largest where vegetation was forced to regenerate as conifers. A more detailed analysis of the uncertainty due to the prescribed successional trajectories is provided in Appendix C.6, but considering this limited sensitivity, we focus here on the models using the observed vegetation transitions only.

Detailed results, showing water balance components for each scenario, are provided in Table 5.2. Timeseries results showing how the historical fire regime influenced the trajectory of hydrological variables in the different climates are shown in the first column of Figure 5.6. Again we focus the discussion here on the final simulated decade and discuss the magnitude of the differences in the fire-induced changes that arise in the different components of the water balance across the climate scenarios for this decade.

Similarly to the fire-excluded condition described in Section 5.3, there are few statistically significant differences between future climate conditions and observed climate under a historical fire regime; comparing future climate of 2060-2070 to observed climate of 2000-2010, the only statistically significant differences (gray shading in "Historical Frequency" rows in Table 5.2) were observed for RCP 4.5 transpiration (16 mm/year greater than observed climate) and RCP 8.5 evaporation (18 mm/year decrease). In this paragraph we compare ICB's hydrology under historical fire frequency to ICB's hydrology under fire excluded conditions. Though there is little significant difference across climate regimes in a basin experiencing historical fire frequency, many changes induced by fire - compared to a fire excluded scenario - are significant (asterisks in Table 5.2). For RCP 4.5, by the final decade of simulation, statistically significant declines in transpiration (15 mm/year) and evaporation (9 mm/year) are associated with a statistically significant increase in subsurface water storage (34 mm/year), a statistically-significant but small increase in peak snow water equivalent (3.2 mm/year), and a non-significant 23 mm/year increase in streamflow. For RCP 8.5, historical frequency fire regime results in statistically significant decreases in transpiration (15 mm/year) and evaporation (6 mm/year), increases in subsurface water storage (35 mm/year) and peak snow water equivalent (2.9 mm/year), and a non-significant increase in streamflow (19 mm/year). The results do suggest that fire management could slow the climatically driven loss of snowpack in the ICB; although climate warming reduces snowpack, there is more snowpack in a given future climate in the context of wildfire compared to fire exclusion (Table 5.2).

The overall effect of the historical frequency fire regime across all climates is to decrease the relative importance of transpiration and evaporation, where transpiration declines by 1.4%, 1.2%, and 1.5% and evaporation declines by 0.7%, 0.8%, and 0.6% for observed, RCP 4.5, and RCP 8.5 climates respectively (Figure 5.5-B). The decline in precipitation-normalized evaporation and transpiration results in an increase of the runoff ratio by 1.91%, 1.85%, and 1.82% for observed, RCP 4.5, and RCP 8.5 climates respectively. Fire-induced change in annual soil storage gain/loss is <1% across all climates.

Other indicators of hydrological function in the basin are also similar across the climate scenarios - for example, most streamflow increases due to fire occur during peak snowmelt, regardless of climate scenario (see Appendix Figure C.8). The increases in peak snow water

equivalent due to the imposition of fire use are caused by decreases in sublimation and canopy interception (see Appendix Figures C.9 and C.6), again mostly independently of the climate scenario. Fire use causes snowmelt to become less important as a driver of streamflow; snowmelt explains at most 38%, 47%, and 31% of the fire-induced change in streamflow for observed, RCP 4.5, and RCP 8.5 climates, respectively, by 2060-2070 (see Appendix Figure C.8-D,E,F).

The impacts of fire use policies on hydrology are more apparent amongst climate scenarios when considering intra-annual responses. Under the observed climate, wildfire use causes the greatest change to streamflow (relative to fire exclusion) during the peak snowmelt months of March through May. However, wildfire use under future climates significantly increases streamflow relative to fire excluded conditions for the period of October through May (for the final decade of simulation). Little change in streamflow is modeled during the summer months (June-September) in any fire/climate scenario (Appendix Figure C.8-D,E,F). The maximum change in transpiration due to fire occurs one month earlier (June) under the RCP 4.5 and RCP 8.5 climate scenarios than it does under observed climate (see Appendix Figure C.7).

Overall, these results suggest that the changes associated with fire use in the ICB during the 1970-2010 period are highly comparable to those that would be predicted if the same set of fires and vegetation changes occurred under future climate conditions. This is visually evident in the right-hand column of Figure 5.6, where trajectories of hydrological change and its confidence interval under different climate scenarios track each other closely for most variables.

Climate + Changing Fire Regimes

Research Question (iii) asks how sensitive the hydrological outcomes of fire use strategies for the 2030-2070 period were to potential increases in fire frequency. Again, we focus on the results for the observed vegetation transitions only. Detailed results, showing water balance components for each scenario, are provided in Table 5.2. Different fire regimes influence the trajectory of hydrological variables in the different climates as shown in the left hand columns of Figure 5.6. These plots show that the most dramatic effect of the increasing fire frequency is to reduce the time needed to approach a pseudo-steady condition, which itself is very similar across the climate scenarios. Since the first wildfire occurrence, it takes approximately 13, 22, and 30 years to observe maximum changes in most water balance components under the +60%, +30%, and historical fire frequency scenarios respectively. These distinctions in timing are most easily observed in the subsurface storage and streamflow plots of Figure 5.6. Increasing fire frequency increases the maximum observed changes slightly in the hydrological variables, where +60% fire frequency scenario generally results in greatest hydrological change across climate scenarios.

With the exception of streamflow, all water balance variables experience significant change due to fire, across all climate and fire regimes, by the final simulated decade. Streamflow increases relative to fire excluded conditions under all scenarios, although the increases

are significant only for certain climate and fire scenarios: for the RCP 4.5 climate scenario streamflow is significantly higher in the final simulated decade of the +30% fire frequency scenario and the last two decades of the +60% fire frequency scenario, and in the RCP 8.5 climate scenario streamflow increase is only significant in the third decade (2050-2060) of the +60% fire frequency scenario. The decades with significant increases in streamflow due to fire correspond to decades with greater precipitation and decades in which many fire events occur. Averaging across the final simulated decade, the greatest changes between fire scenarios compared to the fire excluded scenario for the same climate are: an 18 mm decrease in transpiration (RCP 4.5, +30%), and 11 mm decrease in evaporation (RCP 4.5, +30%), a 29 mm increase in streamflow (RCP 4.5, +30%), a 44 mm increase in subsurface storage (RCP 4.5, +60%), and a 4.1 mm increase in maximum snow water equivalent (RCP 4.5, +30%). With the exception of maximum snowpack, the historical fire regime always produced the smallest changes in hydrological variables for each climate type (Figure 5.2). The different pace of change across the scenarios is closely related to the rate of change of LAI: more frequent fires cause a more rapid decline in LAI (see Appendix Figure C.6). In the final simulated decade, LAI had declined by 0.07 and 0.08 for RCP 8.5 and 4.5 climate scenarios respectively (historical fire regime), by 0.10 and 0.11 (30% increase), and 0.08 and 0.09 (+60%), relative to the fire excluded cases (see Appendix Table C.2).

One possible risk associated with fire use strategies is that by removing vegetation from the ICB, the peak flow and flood risks might increase. Noting that the model calibration was not optimized to predict peak flows (Boisramé et al., 2019a), we nonetheless examined the largest daily streamflows for each year, and how these varied with fire regime and climate forcing. The maximum daily flow increased by about 3.2% due to fire in the final simulated decade - an increase that did not vary across the different climate and wildfire scenarios, and which was not statistically significant relative to model uncertainty (see Appendix Figure C.10).

Table 5.2: Hydrological variables averaged decadally for all climate and fire scenarios. Decades 1, 2, 3, and 4 refer to the time periods 1971-1980, 1981-1990, 1991-2000, and 2001-2010 for the observed climate, while for future climate scenarios (RCP 4.5 and 8.5) these decades refer to 2031-2040, 2041-2050, 2051-2060, and 2060-2070 respectively. Grey highlighting indicates a significant difference between modeled variables in the future climate and the historically observed climate (Using Equation C.2). An asterisk indicates that wildfires significantly affected the modeled hydrological variable (Using Equation C.1). Change is reported as significant if the 95% confidence interval for the difference between two fire-climate model scenarios does not include zero.

Scenario		Decade			
Fire	Climate	1	2	3	4
		Transpiration [mm/year]			

Scenario		Decade			
Fire	Climate	1	2	3	4
Fire Excluded	Observed	59	60	65	53
	RCP 4.5	71	67	70	72
	RCP 8.5	60	62	63	63
Historical Frequency	Observed	58*	57*	59*	41*
	RCP 4.5	70	65	64*	57*
	RCP 8.5	59*	59	56*	48*
+30%	RCP 4.5	70	62*	57*	54*
	RCP 8.5	59	56*	49*	45*
+60%	RCP 4.5	69*	56*	54*	54*
	RCP 8.5	59*	50*	45*	45*
Evaporation [mm/year]					
Fire Excluded	Observed	88	79	76	81
	RCP 4.5	89	89	87	89
	RCP 8.5	70	68	66	63
Historical Frequency	Observed	87*	78*	74*	75*
	RCP 4.5	89*	88*	84*	80*
	RCP 8.5	69*	67*	64*	57*
+30%	RCP 4.5	89*	86*	79*	78*
	RCP 8.5	69*	66*	60*	56*
+60%	RCP 4.5	88*	82*	78*	79*
	RCP 8.5	69*	64*	59*	56*
Streamflow [mm/year]					
Fire Excluded	Observed	957	974	1133	752
	RCP 4.5	1162	1072	1111	1181
	RCP 8.5	963	1012	1024	991
Historical Frequency	Observed	957	977	1141	769
	RCP 4.5	1164	1075	1120	1204
	RCP 8.5	964	1016	1033	1010
+30%	RCP 4.5	1164	1080	1130	1210*
	RCP 8.5	964	1020	1042	1016
+60%	RCP 4.5	1164	1088	1136*	1209*
	RCP 8.5	964	1027	1048*	1015
Subsurface Storage [mm]					
Fire Excluded	Observed	1711	1708	1700	1707
	RCP 4.5	1701	1700	1700	1694
	RCP 8.5	1708	1705	1706	1705
Historical Frequency	Observed	1712	1714	1713*	1740*
	RCP 4.5	1702	1707	1716*	1730*
	RCP 8.5	1709	1712	1722*	1740*

Scenario		Decade			
Fire	Climate	1	2	3	4
+30%	RCP 4.5	1702	1712	1732*	1737*
	RCP 8.5	1709	1717*	1737*	1746*
+60%	RCP 4.5	1703	1726*	1742*	1738*
	RCP 8.5	1710	1730*	1747*	1748*
		Max Snow Water Equivalent [mm]			
Fire Excluded	Observed	600.1	572.9	743.5	513.6
	RCP 4.5	569.3	523.9	463	471.8
	RCP 8.5	491.1	458.3	415.4	367.8
Historical Frequency	Observed	600.2*	573.4*	744.4*	517.1*
	RCP 4.5	569.4	524.3	463.8	475.0*
	RCP 8.5	491.2	458.6	416.1	369.7*
+30%	RCP 4.5	569.5	525.2*	465.6	475.9*
	RCP 8.5	491.2	459.3	417.4*	370.0
+60%	RCP 4.5	569.6	526.4	466.2*	475.3*
	RCP 8.5	491.2	460.0	418.0*	370.1

* : Difference between burned and fire excluded scenarios is statistically significant at 5% level

Grey Shading : Future fire-climate scenario is statistically different from observed fire-climate scenario at 5% level
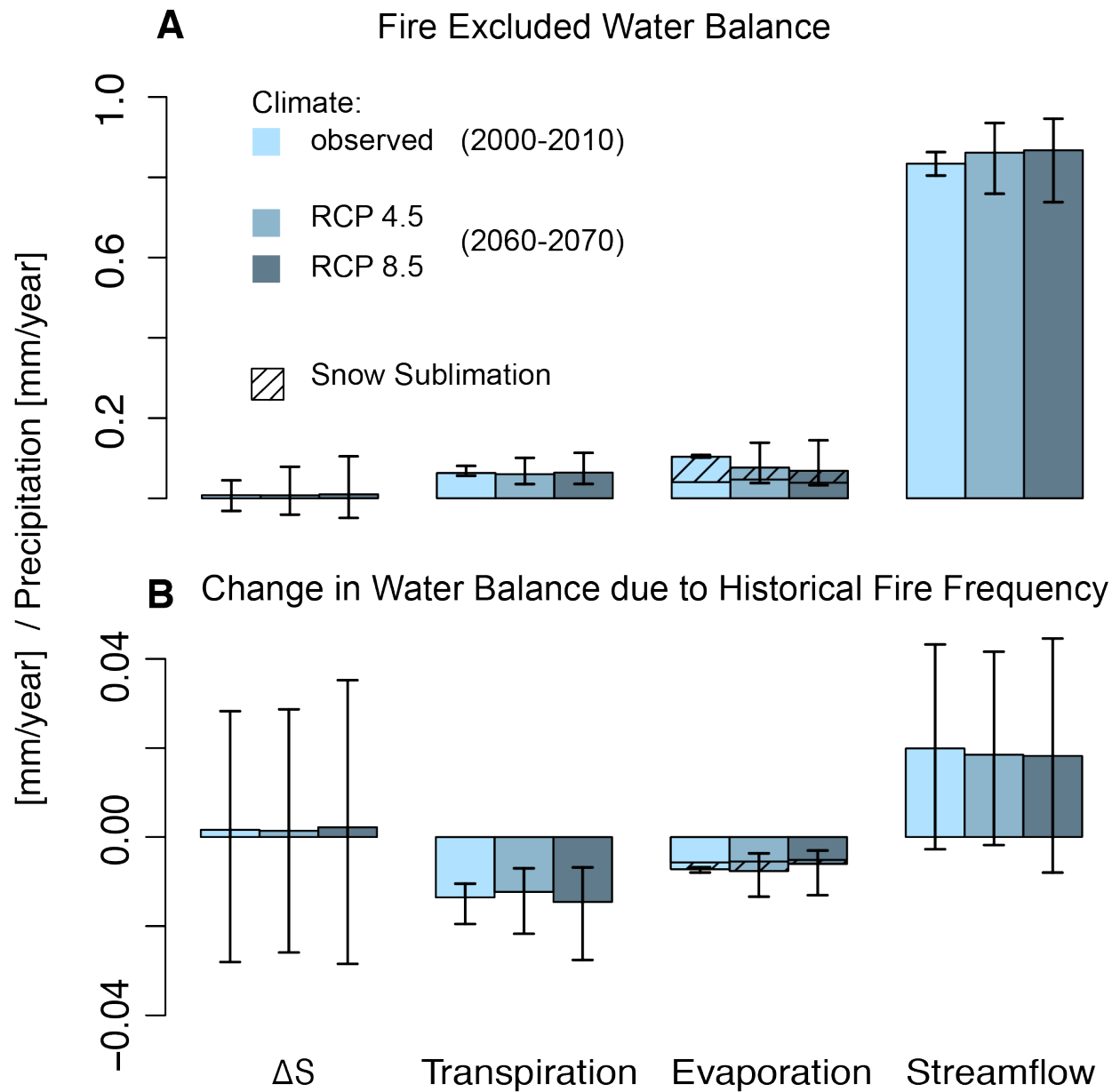
Figure 5.5: A: Water balance for the fire-excluded scenario. Subsurface storage change (ΔS; the change in subsurface water storage from one water year to the next), transpiration, evaporation, and streamflow are normalized to precipitation. B: Modeled average change in water balance variables due to fires normalized to precipitation. In both A and B, results are shown for the final simulated decade (resulting in most change). Historically observed fire frequency scenario is used for the difference in B. Error bars represent 95% confidence interval across all climate scenarios, parameter sets, and years within the final simulated decade.
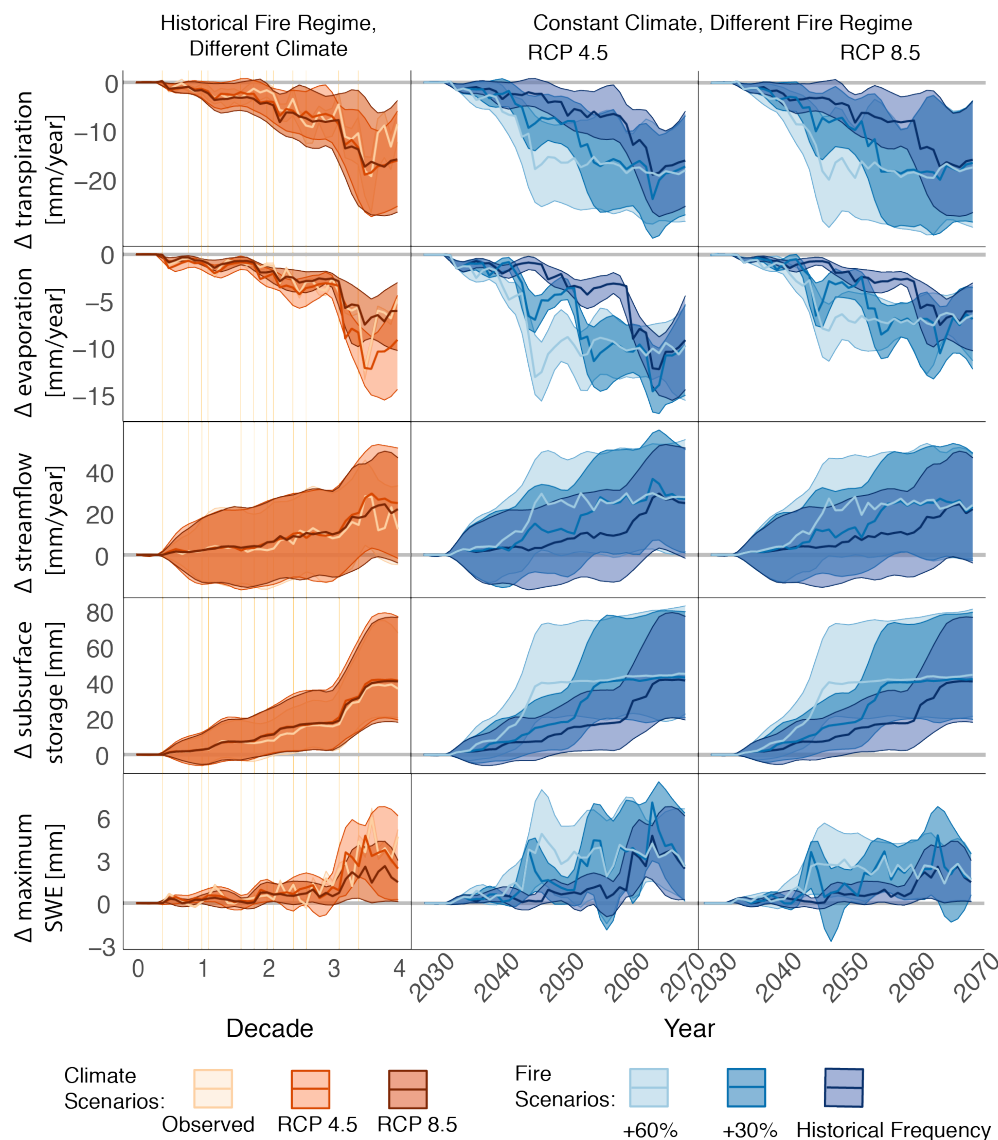
Figure 5.6: All plots show the difference between the burned and fire excluded ICB. Plots in blue have constant climate (RCP 4.5 in left panel and RCP 8.5 in middle panel), but vary the fire frequency scenario. Plots in red keep the fire frequency constant (historical), but vary the climate scenario. Vertical orange lines in the right panel indicate a historical fire occurrence. Shading indicates 95% confidence interval of the 93 observed climate or 930 future climate model runs (93 parameter sets for each of the 10 GCMs or 1 observed climate), while thick lines represent average difference. Vertical axis has the same scale for each hydrological variable. Decade 0, 1, 2, 3, and 4 refer to years 1970, 1980, 1990, 2000, and 2010 for observed climate and years 2030, 2040, 2050, 2060, and 2070 for RCP 4.5 and RCP 8.5 climates.

5.4 Discussion

Impacts of Fire Use on ICB Hydrology Under Future Climates

The modeling efforts presented here suggest that fire use strategies will have a similar impact on the hydrology of the ICB under future climates to that which occurred due to the historical fire management from 1972 - present - namely modest increases in streamflow, driven primarily by reductions in vapor fluxes, particularly sublimation and evaporation (see Boisramé et al. (2019a) for additional detail on fire-induced decreases in evaporation), and increased subsurface water storage. The broad similarity in these outcomes is perhaps unsurprising given the modest changes in water balance predicted for fixed, fire-suppressed, vegetation cover when climate change alone is considered. These differences may be increased in models that are able to consider variation in CO_2 concentration across the future climate scenarios, unlike the present model which held CO_2 constant in all scenarios.

Initiating a fire use strategy in 2030 is predicted to increase streamflow by an average of 19-29 mm/year by 2070, relative to maintaining fire exclusion (c.f. a 17 mm/year historical increase). Although the predicted streamflow increases are not always statistically significant given the uncertainties associated with future climate and the hydrological model parameters, the drivers of this increase - greater snowpack and subsurface storage and reductions in evaporation and transpiration due to fire use relative to fire suppressed conditions, are significant in all climate and fire frequency scenarios. Future applications of fire use strategies in the ICB would therefore be likely to increase natural water storage in the basin, and may result in increased streamflow. Increasing fire frequency, while maintaining similar spatial fire severity distributions to the historical period, has the primary effect of speeding up the rate of change, without altering the final hydrological state of the basin greatly. The final hydrological state predicted for the ICB was largely robust to changes in the post-fire vegetation transitions used in the model; model scenarios in which highly burned regions transitioned to coniferous forests, shrublands or wetlands diverged minimally from each other.

We did not quantitatively explore the robustness of these final states to our modeling decision to use historical fire areas and severities to represent these elements of future climate, but the consequences of these decisions can be qualitatively explored. For example, the similarity in the final hydrological state of the basin across fire frequency scenarios may be partly attributable to the re-use of the same fire perimeters in all scenarios - all cases converged on a similar basin-averaged LAI independently of the fire frequency. These fire perimeters do, however, cover 75% of the vegetated area of ICB, so that the modeled fires affected most of the area of the ICB that can burn. However, by preventing fire from burning into areas that did not experience a fire in 1970-2010, the modeled fire perimeters may under-estimate the maximum vegetation changes which could be induced in ICB, thus also underestimating the extremes of vegetation and hydrological changes that could be induced by fire. On the other hand, a scenario where the historical perimeters over-estimate fire extent and severity seems probable due to additional fuel reductions. Consideration of this fuel limitation means the use of historical fire severity in the models is likely an upper

bound on future fire severity. Therefore, it is likely that uncertainties in the future fire regime associated with our fire modeling choices are opposite in sign and likely to mitigate each other.

Our work has focused on representing known fire impacts of a frequently-burned watershed rather than modeling them and thus introducing additional uncertainty. However, there is promising work being done coupling RHESSys to a fire spread model (WMFire) which uses RHESSys fuel loads and water deficits to model fire spread for a given location (Kennedy et al., 2017; Bart et al., 2020). Both studies have demonstrated that such coupling can re-produce realistic historical fire regime characteristics across different eco-systems and stand-ages without being specifically tuned to do so. Further validation of this coupled model is needed, especially its representation of the sensitivity of fire-vegetation feedbacks to a changing climate. Future work will explore the potential of RHESSys-WMFire to study fire-hydrology-vegetation feedbacks in ICB.

While the eco-hydrological model used in this study has been successfully validated using a number of streamflow metrics, it was not configured to capture high flow events (important for flood and erosion management) due to the lack of high-resolution precipitation and streamflow observations. The model also ignores post-fire changes to soil properties which could lead to greater overland and streamflow from heightened soil water repellency. Within these limitations, modeling suggests that fire use in the ICB would increase peak streamflow by at most 3.2% from fire excluded conditions for all climate and fire regime scenarios. This increase is likely under-predicted.

In spite of the limitations on the modeling, which mean that results should not be interpreted as a forecast of absolute hydrological behavior in fire-affected watersheds like the ICB, it is important to recognise that the limitations also affect the historical baseline estimates of hydrological change from 1970-2010 similarly to future modeled scenarios. Thus, we can conclude that fire use policies implemented in fire-suppressed basins similar to ICB and generating similar or more frequent fire regimes, would generate similar hydrological co-benefits to those experienced to date.

Management Implications

These hydrological co-benefits may be an essential component of building an economic case for forest management, because the economic investment needed to implement forest management strategies remains an impediment to their uptake (González-Sanchis et al., 2019). For instance, although the streamflow gains predicted from ICB to date are modest on a per-area basis in the watershed, the additional streamflow gains from ICB alone could produce $1.5-2.3 million of hydropower revenue per year, and represent a volume equivalent to approximately 5.1% of the city of San Francisco's annual water use, which itself is worth approximately $6.0-9.2 million in water sales from the San Francisco Public Utility Commission (detailed calculations in Appendix-C.7). Although the ICB does not directly feed the Hetch Hetchy reservoir that forms San Francisco's water supply, these figures provide an indication of the potential economic value of even modest local changes in water balance,

which could be driven by fire use policies. Of course, this value would be offset by the costs of the negative impacts of wildfire on watersheds, such as increased erosion and declines in water quality (Tiedemann, 1979; Smith et al., 2011), which should also form part of any economic analysis of wildfire use policies. To date, there is no evidence of extensive erosion or downstream water quality declines in response to ICB wildfires, but work to better establish the potential scope of such problems remains needed.

The ICB remains a unique long term experiment on the effects of fire restoration on forests and water balance, but policy is shifting to extend fire restoration across the Sierra Nevada. For example, current revisions to the Land and Resource Management Plans for National Forests (NF) in the southern Sierra Nevada emphasize fire use for resource benefit over some 69 to 84% of National Forest land. Boisramé et al. (2017) estimated that approximately 19,100 km^2 of the Sierra Nevada region is topographically and climatically similar to ICB, and may be suitable for similar fire use strategies. However, to achieve similar hydrological outcomes as in ICB, fire use in other basins would also need to achieve the substantial changes in forest cover that occurred in that Basin. In the only other basin in the Sierra Nevada with a multi-decadal history of fire use policies, Sugarloaf Creek Basin in Sequoia-Kings Canyon National Park, greater fire suppression activity in the recent decades and lower productivity forests have led to a much more modest impact of fire on vegetation than observed in ICB (Stevens, Boisramé, et al., 2020). The relatively limited sensitivity of predicted hydrological outcomes to climate, however, suggests that extension of the fire use policy beyond ICB to other productive and topographically suitable forests could produce modest but valuable increases in streamflow.

5.5   Conclusion

Downscaling and bias correction of climate projections for ICB and their use in the RHESSys hydrological model suggest that the modest increases in streamflow estimated to have occurred due to fire use policies in the late 20th - early 21st Century are likely to be robust to the warmer future climate. Although the timing and provenance of streamflow shifts earlier in the year and towards rainfall rather than snowmelt, these changes are not projected to result in large alterations in annual water balance partitioning. To summarize our response to the posed questions:

i) In the absence of fire use policy, hydrology of the ICB is relatively similar during RCP 4.5 and RCP 8.5 2030-2070 climates and under the observed historical climate of 1970-2010 (in terms of annual volumes of various fluxes). One notable difference is the reduction of snowpack which leads to lower total evaporation (due to a reduction in sublimation) in the future climate scenarios.

ii) The hydrological outcomes of fire use strategies in ICB under future climate conditions are similar to those under observed climate. The historical fire frequency regime produces similar reductions in evaporation and transpiration and gains in streamflow across

all climates. Fire-induced increase in snowpack partially counteracts climate change induced reductions in snowpack.

iii) Considering fuel-limited conditions in ICB, anticipated increases in fire frequency (due to ignitions and not fuel availability) in the future climate of 2030-2070 will lead to similar hydrologic changes as historic fires, but in a shorter timeframe.

Though we provide a broad range of possible fire regime outcomes, future work should focus on fully coupling post-fire vegetation transitions to climate and hydrology and consequent fire-regime. More advanced modeling of fire effects on hydrology may be needed as well; in addition to wildfire impacts on vegetation removal, changes to soil properties are needed to accurately model high intensity precipitation events that have an impact on erosion, flooding, and water quality.

Rising temperatures and a naturally volatile hydroclimatic setting present ongoing challenges to California's water supply security and forest resilience. This study suggests that where self-limiting fire behavior, as per ICB, can be anticipated, the hydrological co-benefits should be considered as part of future fire policy development and cost-benefit analysis.

Chapter 6

Conclusion

6.1 Summary of Findings

Wildfire activity in California and worldwide is increasing as a consequence of fire suppression legacy and the warming climate. This increase is occurring in tandem with a social change, in which wildfires are increasingly appreciated as a natural disturbance agent and a potential tool for managing healthy forests. Both the benefits and risks of fires require improved understanding across spatial and temporal scales and in the context of their feedbacks to vegetation and water cycling.

This dissertation has contributed to such understanding by revealing the importance of interactions between fire and hydrological processes. I showed that the negative consequences of fires in promoting flooding and erosion, in part through causing water repellency in soils, are not necessarily long-lived or problematic for wildfire management in the middle and high elevation zones in the Sierra Nevada. In these regions, freeze-thaw processes, a novel mechanism for degradation of water repellency, mean that soils would largely recover their hydraulic properties within six months of most fires. This suggests that the negative impacts of wildfires on hydrology may be short-lived in climates that experience frequent freeze/thaw events. This is an important consideration for cost-benefit analysis of wildfire management decisions, and supports greater use of fire in the Sierra Nevada.

I also showed that soil moisture variation influences the risk of fire through a coupling between soil water content and dead fuel moisture content. Although fuel-moisture values are integral to fire modeling and risk forecasting, to date no studies explored the impact of soil moisture on dead fuel moisture. My field observations and statistical analysis showed that soil moisture had a small but significant effect on fuel moisture across all sampled conditions, and was greatest for wet soil conditions and 10-hr fuels. Incorporating soil moisture into predictions of fuel moisture based on a nine-year weather and soil moisture timeseries from a Sierra Nevada observatory increased fuel moisture predictions in the spring and fall shoulder seasons, and reduced periods in which fuels had a high probability of ignition by 60 days for 10-hr fuels and 6 days for 1-hr fuels. Similarly, inclusion of soil moisture into

spatially-distributed fuel moisture predictions in Illilouette Creek Basin produced a more heterogeneous distribution of probability of ignition through space, compared with similar models that did not incorporate soil moisture information. These findings are important as they suggest that fire management decisions could be sensitive to the inclusion of soil moisture information in modeling - which itself is becoming increasingly feasible with the availability of remotely sensed soil moisture datasets.

Feedbacks between fire, water and vegetation can lead to distinct outcomes for different basins. Comparing fire management within basins is generally difficult given the prevalence of fire suppressed conditions in the Western US. Using Illilouette Creek and Sugarloaf Creek Basins as case studies, I was able to show that distinct outcomes can arise depending on how dramatically wildfires impact dominant vegetation cover. In Illilouette Creek Basin, large changes in vegetation cover were associated with meaningful increases in Basin wetness and streamflow. Conversely, in Sugarloaf Creek basin, the 47-year period of wildfire management lead to minimal vegetation cover conversion, and a relatively subdued change in soil moisture. In Sugarloaf Creek basin, fire occurrence was limited to drier mixed-conifer sites, with small patches of overstory tree mortality. This had little effect on removing mid- and lower strata trees. Few dense meadow areas were created by fire, with most forest conversion leading to sparse meadow and shrub areas, which had similar soil moisture profiles to nearby mixed-conifer vegetation. These findings are important as they suggest that a range of hydrological responses to wildfire restoration should be expected, mediated by the extent of tree cover conversion, and potentially also by the environmental properties of treated basins.

Conversely, my final chapter demonstrated that wildfire management hydrological outcomes may be relatively insensitive to projected climate change in the Sierra Nevada. Using a distributed ecohydrological model and a statistically downscaled climate ensemble, I showed that the hydrological impacts of fire use are comparable under observed climate and projected future climates through year 2070, and are largely insensitive to the significant uncertainties regarding post-fire successional trajectories for vegetation. While expected increases in fire frequency cause minor changes in the basin hydrology, the main impact of more frequent fires is to cause the basin to reach peak hydrological change more rapidly. These findings are important because they offer managers confidence that co-benefits of wildfire restoration activities are likely to persist even in the face of the changes expected in the 21st century.

6.2   Future Work

There appears to be considerable scope for productive future work exploring the coupling of fire, water and vegetation and its implications of modeling and watershed management. In particular, there is a need to confront methods for upscaling the relationship I uncovered between fuel and soil moisture so that it can be applied at scales relevant for fire forecasting, there is a need to improve the representation of fire within ecohydrological models so that simulation of coupled fire, vegetation and water regimes can be undertaken. Finally, as the benefits and negatives associated with managed wildfire become more clearly delineated

scientifically, the time is becoming ripe for an economic analysis to explore the costs and benefits of different wildfire management policies in the Sierra Nevada.

Upscaling and Generalizing Findings

My plot scale measurements of fuel moisture and soil moisture demonstrated that there is a link between hydrological and fire processes. However, the study can only be understood as an initial exploration of these links. It will be essential to further characterise these relationships across multiple soil types, and under wetting and drying conditions. With an improved understanding of the functional form of such relationships, satellite imagery that is sensitive to soil moisture can be interpreted in terms of likely fuel moisture states, and current fuel moisture models can incorporate soil moisture information. Linking updated models with satellite inference of fuel/soil moisture offers the potential for estimation (or data assimilation) to map fuel moisture and fire risk at continental scales. Similarly, characterizing post-fire hydrophobicity decay for other soil types and organic matter will allow for a better inference of post-fire flooding and erosion hazards in other ecosystems.

Modeling Feedbacks

RHESSys ecohydrological model was used in Chapter 5 to assess the impacts of wildfires on basin ecohydrology. There were many limitations imposed by the model, with the main one being RHESSYs' inability to directly couple wildfire processes to vegetation and hydrology. Through recent advances coupling VMFire, a fire spread model of intermediate complexity, to RHESSYs, it is now becoming possible to simulate a fire regime based on hydrological and vegetation states (Kennedy et al., 2017; Bart et al., 2020). However, RHESSys-VMFire does not account for post-fire vegetation transitions, which themselves have an important role on watershed fire risks and hydrological states. As climate change is expected to speed-up vegetation transitions, especially after disturbance, modeling this relationship is urgently needed.

The findings from Chapter 2 and 3 could be incorporated into fire-water-vegetation modeling frameworks. In Chapter 3, I related soil moisture to fuel moisture and fire risks. Since RHESSys models subsurface water stores and vapor pressure deficit along with fuel production, it is possible to further couple hydrological fluxes to fire risk by incorporating the effect of soil moisture on fuel moisture. Currently VMFire relies only on vapor pressure deficit to model probability of ignition.

Similarly, at present, RHESSys cannot account for transient changes in soil properties such as those observed post fire. This could be readily changed, allowing better approximations of post-fire overland flow and subsurface water stores. RHESSys downscales temperature and precipitation to modeled topography and can identify wetting/drying and freezing/thawing events. Using hydrophobicity decay curves from Chapter 3 can improve the representation of post-fire hydrological processes in RHESSys.

Economic Analysis

To date, the economic assessment of wildfire use as a management strategy has been limited. Yet sufficient information is now available to address - at least for Illilouette Creek Basin - the net economic costs and benefits of implementing wildfire management on hydropower production, water yield, timber and carbon stocks, flooding and erosion damage, water quality, air pollution, and recreation. With most indicators suggesting significant benefits and relatively minimal negatives, such an assessment has the potential to shift policy and increase funding towards increased wildfire management programs. Not all areas within Sierra Nevada will be able to support a safe implementation of wildfire management policy due to vegetation structure, proximity to structures, and topography. A comprehensive suitability analysis that identifies such areas and accounts for a changing climate can inform the distribution of areas suitable for wildfire management strategy. With both a spatial and economic case in hand, this dissertation, the science it builds on, and the science that will build on it, has the potential to meaningfully shift the management practice of western montane forested watersheds, hopefully to the benefit of both people and the environment.

References

Abatzoglou, J. T., & Williams, A. P. (2016, October). Impact of anthropogenic climate change on wildfire across western US forests. *Proceedings of the National Academy of Sciences*, *113*(42), 11770–11775. Retrieved from `https://doi.org/10.1073/pnas.1607171113` doi: 10.1073/pnas.1607171113

Agee, J. (1993, 01). Fire ecology of pacific northwest forests. *The Bark Beetles, Fuels, and Fire Bibliography*.

Ahlgren, C. E. (1981). Seventeen-year changes in climatic elements following prescribed burning. *Forest Science*, *27*(1), 33–39.

Akaike, H. (1987). Information Theory and an Extension of the Maximum Likelihood Principle. In E. Parzen, K. Tanabe, & G. Kitagawa (Eds.), *Selected papers of hirotugu akaike* (pp. 199–213). New York, NY: Springer New York. Retrieved from `https://doi.org/10.1007/978-1-4612-1694-0` 15 doi: 10.1007/978-1-4612-1694-0_15

Anderson, M. K. (2005). *Tending the wild: Native american knowledge and the management of california's natural resources* (1st ed.). University of California Press. Retrieved from `http://www.jstor.org/stable/10.1525/j.ctt1ppfn4`

Angrist, J. D., & Pischke, J.-S. (2008). *Mostly harmless econometrics: An empiricist's companion*. Princeton university press.

Aquafornia. (2008). *Where does California's water come from?*

Archibald, S., Lehmann, C. E. R., Belcher, C. M., Bond, W. J., Bradstock, R. A., Daniau, A.-L., . . . Zanne, A. E. (2018, March). Biological and geophysical feedbacks with fire in the earth system. *Environmental Research Letters*, *13*(3), 033003. Retrieved from `https://doi.org/10.1088/1748-9326/aa9ead` doi: 10.1088/1748-9326/aa9ead

Assouline, S., & Mualem, Y. (1997). Modeling the dynamics of seal formation and its effect on infiltration as related to soil and rainfall characteristics. *Water Resources Research*, *33*(7), 1527–1536.

Bachmann, J., Ellies, A., & Hartge, K. (2000, May). Development and application of a new sessile drop contact angle method to assess soil water repellency. *Journal of Hydrology*, *231-232*, 66–75. Retrieved from `https://doi.org/10.1016/s0022-1694(00)00184-0` doi: 10.1016/s0022-1694(00)00184-0

Badía, D., Aguirre, J., Martí, C., & Márquez, M. (2013, September). Sieving effect on the intensity and persistence of water repellency at different soil depths and soil types from NE-spain. *CATENA*, *108*, 44–49. Retrieved from `https://doi.org/10.1016/j.catena.2012.02.003` doi: 10.1016/j.catena.2012.02.003

Bales, R. C., Battles, J. J., Chen, Y., Conklin, M. H., Holst, E., O'Hara, K. L., . . . Stewart, W. (2011). Forests and water in the sierra nevada: Sierra nevada watershed ecosystem enhancement project. *Sierra Nevada Research Institute report*, *11*.

Bales, R. C., Hopmans, J. W., OGeen, A. T., Meadows, M., Hartsough, P. C., Kirchner, P., . . . Beaudette, D. (2011, August). Soil moisture response to snowmelt and rainfall in a sierra nevada mixed-conifer forest. *Vadose Zone Journal*, *10*(3), 786–799. Retrieved from `https://doi.org/10.2136/vzj2011.0001` doi: 10.2136/vzj2011.0001

Barbour, M. G., Berg, N. H., Kittel, T. G. F., & Kunz, M. E. (1991, March). Snowpack and the distribution of a major vegetation ecotone in the sierra nevada of california. *Journal of Biogeography*, *18*(2), 141. Retrieved from `https://doi.org/10.2307/2845288` doi: 10.2307/2845288

Barbour, M. G., Pavlik, B. M., & Antos, J. A. (1990, July). Seedling growth and survival of red and white fir in a Sierra Nevada ecotone. *American Journal of Botany*, *77*(7), 927–938. Retrieved from `https://doi.org/10.1002/j.1537-2197.1990.tb15187.x` doi: 10.1002/j.1537-2197.1990.tb15187.x

Bart, R. R., Kennedy, M. C., Tague, C. L., & McKenzie, D. (2020, January). Integrating fire effects on vegetation carbon cycling within an ecohydrologic model. *Ecological Modelling*, *416*, 108880. Retrieved from `https://doi.org/10.1016/j.ecolmodel.2019.108880` doi: 10.1016/j.ecolmodel.2019.108880

Bates, D., Mächler, M., Bolker, B., & Walker, S. (2015). Fitting linear mixed-effects models using lme4. *Journal of Statistical Software*, *67*(1), 1–48. doi: 10.18637/jss.v067.i01

Batllori, E., Ackerly, D. D., & Moritz, M. A. (2015, March). A minimal model of fire-vegetation feedbacks and disturbance stochasticity generates alternative stable states in grassland–shrubland–woodland systems. *Environmental Research Letters*, *10*(3), 034018. Retrieved from `https://doi.org/10.1088/1748-9326/10/3/034018` doi: 10.1088/1748-9326/10/3/034018

Batllori, E., Cáceres, M. D., Brotons, L., Ackerly, D. D., Moritz, M. A., & Lloret, F. (2018, December). Compound fire-drought regimes promote ecosystem transitions in

mediterranean ecosystems. *Journal of Ecology*, *107*(3), 1187–1198. Retrieved from `https://doi.org/10.1111/1365-2745.13115` doi: 10.1111/1365-2745.13115

Batllori, E., Parisien, M.-A., Krawchuk, M. A., & Moritz, M. A. (2013). Climate change-induced shifts in fire for mediterranean ecosystems. *Global Ecology and Biogeography*, *22*(10), 1118-1129. doi: 10.1111/geb.12065

Baudena, M., Santana, V. M., Baeza, M. J., Bautista, S., Eppinga, M. B., Hemerik, L., . . . Rietkerk, M. (2019, November). Increased aridity drives post-fire recovery of mediterranean forests towards open shrublands. *New Phytologist*, *225*(4), 1500–1515. Retrieved from `https://doi.org/10.1111/nph.16252` doi: 10.1111/nph.16252

Bennett, M., Fitzgerald, S., Parker, B., Main, M. L., Perleberg, A., Schnepf, C., . . . Extension, P. N. C. (2010). Reducing fire risk on your forest property..

Berg, N. H., & Azuma, D. L. (2010). Bare soil and rill formation following wildfires, fuel reduction treatments, and pine plantations in the southern sierra nevada, california, USA. *International Journal of Wildland Fire*, *19*(4), 478. Retrieved from `https://doi.org/10.1071/wf07169` doi: 10.1071/wf07169

Berryman, E. M., Barnard, H. R., Adams, H. R., Burns, M. A., Gallo, E., & Brooks, P. D. (2015, April). Complex terrain alters temperature and moisture limitations of forest soil respiration across a semiarid to subalpine gradient. *Journal of Geophysical Research: Biogeosciences*, *120*(4), 707–723. Retrieved from `https://doi.org/10.1002/2014jg002802` doi: 10.1002/2014jg002802

Beven, K., & Binley, A. (1992). The future of distributed models: Model calibration and uncertainty prediction. *Hydrological Processes*, *6*(3), 279–298. doi: 10.1002/hyp.3360060305

Beven, K. J., & Kirby, M. J. (1979, March). A physically based, variable contributing area model of basin hydrology / un modèle à base physique de zone dappel variable de lhydrologie du bassin versant. *Hydrological Sciences Bulletin*, *24*(1), 43–69. Retrieved from `https://doi.org/10.1080/02626667909491834` doi: 10.1080/02626667909491834

Bischoff, W., Heck, B., Howind, J., & Teusch, A. (2006, mar). A procedure for estimating the variance function of linear models and for checking the appropriateness of estimated variances: A case study of GPS carrier-phase observations. *Journal of Geodesy*, *79*(12), 694–704. Retrieved from

Bladon, K. D., Emelko, M. B., Silins, U., & Stone, M. (2014, July). Wildfire and the future of water supply. *Environmental Science & Technology*, *48*(16), 8936–8943. Retrieved from `https://doi.org/10.1021/es500130g` doi: 10.1021/es500130g

Blaschke, T., Hay, G. J., Kelly, M., Lang, S., Hofmann, P., Addink, E., . . . Tiede, D. (2014, January). Geographic object-based image analysis – towards a

new paradigm. *ISPRS Journal of Photogrammetry and Remote Sensing*, *87*, 180–191. Retrieved from `https://doi.org/10.1016/j.isprsjprs.2013.09.014` doi: 10.1016/j.isprsjprs.2013.09.014

Blodgett Forest Research Station. (2012). *A brief guide to recreational pyromania.* Available at `https://forests.berkeley.edu/sites/forests.berkeley.edu/files/184038.pdf` (2020/10/16).

Boisramé, G., Thompson, S., Collins, B., & Stephens, S. (2017). Managed Wildfire Effects on Forest Resilience and Water in the Sierra Nevada. *Ecosystems*, *20*(4), 717–732. doi: 10.1007/s10021-016-0048-1

Boisramé, G., Thompson, S., Collins, B., & Stephens, S. (2017). Managed wildfire effects on forest resilience and water in the sierra nevada. *Ecosystems*, *20*(4), 717–732.

Boisramé, G., Thompson, S., Kelly, M., Cavalli, J., Wilkin, K., & L. Stephens, S. (2017, 10). Vegetation change during 40 years of repeated managed wildfires in the Sierra Nevada, California. *Forest Ecology and Management*, *402*, 241-252.

Boisramé, G., Thompson, S., & Stephens, S. (2018, February). Hydrologic responses to restored wildfire regimes revealed by soil moisture-vegetation relationships. *Advances in Water Resources*, *112*, 124–146. doi: 10.1016/j.advwatres.2017.12.009

Boisramé, G. F. S., Thompson, S. E., Tague, C. N., & Stephens, S. L. (2019a, July). Restoring a natural fire regime alters the water balance of a Sierra Nevada catchment. *Water Resources Research*, *55*(7), 5751–5769. Retrieved from `https://doi.org/10.1029/2018wr024098` doi: 10.1029/2018wr024098

Boisramé, G. F. S., Thompson, S. E., Tague, C. N., & Stephens, S. L. (2019b, July). Restoring a natural fire regime alters the water balance of a sierra nevada catchment. *Water Resources Research*, *55*(7), 5751–5769. Retrieved from `https://doi.org/10.1029/2018wr024098` doi: 10.1029/2018wr024098

Bovill, W., Hawthorne, S., Radic, J., Baillie, C., Ashton, A., Lane, P., & Sheridan, G. (2015). Effectiveness of automated fuelsticks for predicting the moisture content of dead fuels in Eucalyptus forests..

Breshears, D. D., Nyhan, J. W., Heil, C. E., & Wilcox, B. P. (1998, November). Effects of woody plants on microclimate in a semiarid woodland: Soil temperature and evaporation in canopy and intercanopy patches. *International Journal of Plant Sciences*, *159*(6), 1010–1017. Retrieved from `https://doi.org/10.1086/314083` doi: 10.1086/314083

Breusch, T. S., & Pagan, A. R. (1979, September). A simple test for heteroscedasticity and random coefficient variation. *Econometrica*, *47*(5), 1287. Retrieved from `https://doi.org/10.2307/1911963` doi: 10.2307/1911963

Brotons, L., & Duane, A. (2019, February). Correspondence: Uncertainty in climate-vegetation feedbacks on fire regimes challenges reliable long-term projections of burnt area from correlative models. *Fire*, *2*(1), 8. Retrieved from `https://doi.org/10.3390/fire2010008` doi: 10.3390/fire2010008

Buck, A. L. (1981, December). New equations for computing vapor pressure and enhancement factor. *Journal of Applied Meteorology*, *20*(12), 1527–1532. Retrieved from `https://doi.org/10.1175/1520-0450(1981)020<1527:nefcvp>2.0.co;2` doi: 10.1175/1520-0450(1981)020¡1527:nefcvp¿2.0.co;2

Burch, G. J., Moore, I. D., & Burns, J. (1989, July). Soil hydrophobic effects on infiltration and catchment runoff. *Hydrological Processes*, *3*(3), 211–222. Retrieved from `https://doi.org/10.1002/hyp.3360030302` doi: 10.1002/hyp.3360030302

Bureau of Labor Statistics. (2018, 2). *Average energy prices, san francisco-oakland-hayward – january 2018.* `https://www.bls.gov/regions/west/news-release/2018/pdf/averageenergyprices_sanfrancisco_20180220.pdf`. ((Accessed on 12/29/2019))

Burles, K., & Boon, S. (2011). Snowmelt energy balance in a burned forest plot, Crowsnest Pass, Alberta, Canada. *Hydrological Processes*. Retrieved from `https://doi.org/10.1002/hyp.8067` doi: 10.1002/hyp.8067

Burrows, N., Ward, B., Robinson, A. D., & Behn, G. (2006). Fuel dynamics and fire behaviour in spinifex grasslands of the western desert..

CalFire. (2019a). *Emergency fund fire suppression expenditures.* `https://www.fire.ca.gov/media/8641/suppressioncostsonepage1.pdf`. ((Accessed on 12/11/2019))

CalFire. (2019b). *Top 20 deadliest CA wildfires.* `https://www.fire.ca.gov/media/5512/top20_deadliest.pdf`. ((Accessed on 12/11/2019))

CalFire. (2019c). *Top 20 destructive California wildfires.* `https://www.fire.ca.gov/media/5511/top20_destruction.pdf`. ((Accessed on 12/11/2019))

CalFire. (2020a). *Stats and events.* Retrieved from `https://www.fire.ca.gov/stats-events/`

CalFire. (2020b). *Top 20 largest California wildfires.* `https://www.fire.ca.gov/media/11416/top20_acres.pdf`. ((Accessed on 11/27/2020))

California Department of Food and Agriculture. (2019). California Agricultural Statistics Review 2018-19. , 1–121. Retrieved from `www.cdfa.ca.gov/statisticsACKNOWLEDGEMENTS`

California Energy Commission. (2019a). *Power plant statistical information.* `https://ww2.energy.ca.gov/almanac/electricity_data/web_qfer/plant_stats_2_cms.php?PlantValue=H0274`. ((Accessed on 12/29/2019))

California Energy Commission. (2019b). *Power plant statistical information.* `https://ww2.energy.ca.gov/almanac/electricity_data/web_qfer/plant_stats_2_cms.php?PlantValue=H0601`. ((Accessed on 12/29/2019))

Campos, B., Burnett, R., & Steel, Z. (2017). Bird and bat inventories in the storrie and chips fire areas 2015—2016: Final report to the lassen national forest.

Cannon, A. J., Sobie, S. R., & Murdock, T. Q. (2015). Bias correction of GCM precipitation by quantile mapping: How well do methods preserve changes in quantiles and extremes? *Journal of Climate*, *28*(17), 6938-6959. doi: 10.1175/JCLI-D-14-00754.1

Caon, L., Vallejo, V. R., Ritsema, C. J., & Geissen, V. (2014). Effects of wildfire on soil nutrients in mediterranean ecosystems. *Earth-Science Reviews*, *139*, 47–58.

Carlson, J. D., Bradshaw, L. S., Nelson, R. M., Bensch, R. R., & Jabrzemski, R. (2007). Application of the nelson model to four timelag fuel classes using oklahoma field observations: model evaluation and comparison with national fire danger rating system algorithms. *International Journal of Wildland Fire*, *16*(2), 204. Retrieved from `https://doi.org/10.1071/wf06073` doi: 10.1071/wf06073

Cawson, J. G., Nyman, P., Schunk, C., Sheridan, G. J., Duff, T. J., Gibos, K., ... Menzel, A. (2020). Corrigendum to: Estimation of surface dead fine fuel moisture using automated fuel moisture sticks across a range of forests worldwide. *International Journal of Wildland Fire*, *29*(6), 560. Retrieved from `https://doi.org/10.1071/wf19061_co` doi: 10.1071/wf19061_co

Cayan, D. R., Maurer, E. P., Dettinger, M. D., Tyree, M., & Hayhoe, K. (2008, January). Climate change scenarios for the california region. *Climatic Change*, *87*(S1), 21–42. Retrieved from `https://doi.org/10.1007/s10584-007-9377-6` doi: 10.1007/s10584-007-9377-6

Chambers, J. M. (1992). Statistical models in s. In J. M. Chambers & T. J. Hastie (Eds.), (chap. Linear models). Wadsworth Brooks/Cole.

Chan, S. K., Bindlish, R., ONeill, P. E., Njoku, E., Jackson, T., Colliander, A., ... Kerr, Y. (2016, August). Assessment of the SMAP passive soil moisture product. *IEEE Transactions on Geoscience and Remote Sensing*, *54*(8), 4994–5007. Retrieved from `https://doi.org/10.1109/tgrs.2016.2561938` doi: 10.1109/tgrs.2016.2561938

Chang, C. (1996). Ecosystem responses to fire and variations in fire regimes. In *Sierra nevada ecosystem project: final report to congress* (Vol. 2, pp. 1071–1099).

Chang, J., xu Wang, G., heng Gao, Y., & bo Wang, Y. (2014, May). The influence of seasonal snow on soil thermal and water dynamics under different vegetation covers in a permafrost region. *Journal of Mountain Science*, *11*(3), 727–745. Retrieved from `https://doi.org/10.1007/s11629-013-2893-0` doi: 10.1007/s11629-013-2893-0

Chuvieco, E., Aguado, I., & Dimitrakopoulos, A. P. (2004, November). Conversion of fuel moisture content values to ignition potential for integrated fire danger assessment. *Canadian Journal of Forest Research*, *34*(11), 2284–2293. Retrieved from `https://doi.org/10.1139/x04-101` doi: 10.1139/x04-101

Cochrane, M. A. (2009). *Tropical fire ecology: climate change, land use and ecosystem dynamics.* New York: Springer. Retrieved from `http://site.ebrary.com/id/10383015`

Collins, B. M. (2014). Fire weather and large fire potential in the northern sierra nevada. *Agricultural and Forest Meteorology*, *189*, 30–35.

Collins, B. M., Everett, R. G., & Stephens, S. L. (2011). Impacts of fire exclusion and recent managed fire on forest structure in old growth sierra nevada mixed-conifer forests. *Ecosphere*, *2*(4), 1–14.

Collins, B. M., Miller, J. D., Thode, A. E., Kelly, M., van Wagtendonk, J. W., & Stephens, S. L. (2009, November). Interactions among wildland fires in a long-established Sierra Nevada natural fire area. *Ecosystems*, *12*(1), 114–128. Retrieved from `https://doi.org/10.1007/s10021-008-9211-7` doi: 10.1007/s10021-008-9211-7

Collins, B. M., & Stephens, S. L. (2007, December). Managing natural wildfires in Sierra Nevada wilderness areas. *Frontiers in Ecology and the Environment*, *5*(10), 523–527. doi: 10.1890/070007

Cooper, A. E., Kirchner, J. W., Wolf, S., Lombardozzi, D. L., Sullivan, B. W., Tyler, S. W., & Harpold, A. A. (2020, September). Snowmelt causes different limitations on transpiration in a sierra nevada conifer forest. *Agricultural and Forest Meteorology*, *291*, 108089. Retrieved from `https://doi.org/10.1016/j.agrformet.2020.108089` doi: 10.1016/j.agrformet.2020.108089

Coppoletta, M., Merriam, K. E., & Collins, B. M. (2015, September). Post-fire vegetation and fuel development influences fire severity patterns in reburns. *Ecological Applications*. Retrieved from `https://doi.org/10.1890/15-0225.1` doi: 10.1890/15-0225.1

Cornwell, W. K., Stuart, S. A., Ramirez, A., Dolanc, C. R., Thorne, J. H., & Ackerly, D. D. (2012). *Climate change impacts on California vegetation: physiology, life history, and ecosystem change.* UC Davis: Information Center for the Environment. Retrieved from `https://escholarship.org/uc/item/6d21h3q8`

Cristea, N. C., Breckheimer, I., Raleigh, M. S., HilleRisLambers, J., & Lundquist, J. D. (2017, August). An evaluation of terrain-based downscaling of fractional snow covered area data sets based on LiDAR-derived snow data and orthoimagery. *Water Resources Research*, *53*(8), 6802–6820. Retrieved from `https://doi.org/10.1002/2017wr020799` doi: 10.1002/2017wr020799

Cristea, N. C., Lundquist, J. D., Loheide, S. P., Lowry, C. S., & Moore, C. E. (2013, July). Modelling how vegetation cover affects climate change impacts on streamflow timing and magnitude in the snowmelt-dominated upper tuolumne basin, sierra nevada. *Hydrological Processes*, *28*(12), 3896–3918. Retrieved from `https://doi.org/10.1002/hyp.9909` doi: 10.1002/hyp.9909

Cui, Y., Cheng, D., & Chan, D. (2018, December). Investigation of post-fire debris flows in montecito. *ISPRS International Journal of Geo-Information*, *8*(1), 5. Retrieved from `https://doi.org/10.3390/ijgi8010005` doi: 10.3390/ijgi8010005

Dahm, C. N., Candelaria-Ley, R. I., Reale, C. S., Reale, J. K., & Horn, D. J. V. (2015, March). Extreme water quality degradation following a catastrophic forest fire. *Freshwater Biology*, *60*(12), 2584–2599. Retrieved from `https://doi.org/10.1111/fwb.12548` doi: 10.1111/fwb.12548

Das, A. J., Stephenson, N. L., & Davis, K. P. (2016, September). Why do trees die? characterizing the drivers of background tree mortality. *Ecology*, *97*(10), 2616–2627. Retrieved from `https://doi.org/10.1002/ecy.1497` doi: 10.1002/ecy.1497

Davis, K. T., Dobrowski, S. Z., Higuera, P. E., Holden, Z. A., Veblen, T. T., Rother, M. T., . . . Maneta, M. P. (2019, March). Wildfires and climate change push low-elevation forests across a critical climate threshold for tree regeneration. *Proceedings of the National Academy of Sciences*, *116*(13), 6193–6198. Retrieved from `https://doi.org/10.1073/pnas.1815107116` doi: 10.1073/pnas.1815107116

DeBano, L. F. (2000). The role of fire and soil heating on water repellancy in wildland environments: a review. *Journal of Hydrology*, *231-232*, 195–206. doi: 10.1016/S0022-1694(00)00194-3

DeBano, L. F., & Krammes, J. S. (1966). Water repellent soils and their relation to wildfire temperatures. *International Association of Scientific Hydrology. Bulletin*, *11*(2), 14–19. doi: 10.1080/02626666609493457

DeBano, L. F., Mann, L. D., & Hamilton, D. A. (1970, January). Translocation of hydrophobic substances into soil by burning organic litter. *Soil Science Society of America Journal*, *34*(1), 130–133. Retrieved from `https://doi.org/10.2136/sssaj1970.03615995003400010035x` doi: 10.2136/sssaj1970.03615995003400010035x

Decker, K., Wang, D., Waite, C., & Scherbatskoy, T. (2003, September). Snow removal and ambient air temperature effects of forest soil temperatures in northern vermont. *Soil Science Society of America Journal*, *67*(5), 1629–1629. Retrieved from `https://doi.org/10.2136/sssaj2003.1629` doi: 10.2136/sssaj2003.1629

Dekker, L. W., Doerr, S. H., Oostindie, K., Ziogas, A. K., & Ritsema, C. J. (2001, November). Water repellency and critical soil water content in a dune sand. *Soil Science Society of America Journal*, *65*(6), 1667–1674. Retrieved from `https://doi.org/10.2136/sssaj2001.1667` doi: 10.2136/sssaj2001.1667

DeLuca, T., Keeney, D., & McCarty, G. (1992). Effect of freeze-thaw events on mineralization of soil nitrogen. *Biology and Fertility of Soils*, *14*(2), 116–120.

Dettinger, M. D. (2005, March). From climate-change spaghetti to climate-change distributions for 21st century California. *San Francisco Estuary and Watershed Science*, *3*(1). Retrieved from `https://doi.org/10.15447/sfews.2005v3iss1art6` doi: 10.15447/sfews.2005v3iss1art6

Dettinger, M. D., & Anderson, M. L. (2015). Storage in California's reservoirs and snowpack in this time of drought. *San Francisco Estuary and Watershed Science*, *13*(2). Retrieved from `http://pubs.er.usgs.gov/publication/70159664` doi: 10.15447/sfews.2015v13iss2art1

Dettinger, M. D., Ralph, F. M., Das, T., Neiman, P. J., & Cayan, D. R. (2011, March). Atmospheric rivers, floods and the water resources of california. *Water*, *3*(2), 445–478. Retrieved from `https://doi.org/10.3390/w3020445` doi: 10.3390/w3020445

Doerr, S., Shakesby, R., Blake, W., Chafer, C., Humphreys, G., & Wallbrink, P. (2006, March). Effects of differing wildfire severities on soil wettability and implications for hydrological response. *Journal of Hydrology*, *319*(1-4), 295–311. Retrieved from `https://doi.org/10.1016/j.jhydrol.2005.06.038` doi: 10.1016/j.jhydrol.2005.06.038

Doerr, S., & Thomas, A. (2003). Soil moisture: a controlling factor in water repellency? In *Soil water repellency* (pp. 137–149). Elsevier. Retrieved from `https://doi.org/10.1016/b978-0-444-51269-7.50016-3` doi: 10.1016/b978-0-444-51269-7.50016-3

Doerr, S., Woods, S., Martin, D., & Casimiro, M. (2009, June). 'natural background' soil water repellency in conifer forests of the north-western USA: Its prediction and relationship to wildfire occurrence. *Journal of Hydrology*, *371*(1-4), 12–21. Retrieved from `https://doi.org/10.1016/j.jhydrol.2009.03.011` doi: 10.1016/j.jhydrol.2009.03.011

Doerr, S. H., Shakesby, R. A., & Walsh, R. P. (2000). Soil water repellency: Its causes, characteristics and hydro-geomorphological significance. *Earth Science Reviews*, *51*(1-4), 33–65. doi: 10.1016/S0012-8252(00)00011-8

Dolanc, C. R., Safford, H. D., Thorne, J. H., & Dobrowski, S. Z. (2014, August). Changing forest structure across the landscape of the sierra nevada, CA, USA, since the 1930s. *Ecosphere*, *5*(8), art101. Retrieved from `https://doi.org/10.1890/es14-00103.1` doi: 10.1890/es14-00103.1

Ebel, B. A., & Moody, J. A. (2020, July). Parameter estimation for multiple post-wildfire hydrologic models. *Hydrological Processes*. Retrieved from `https://doi.org/10.1002/hyp.13865` doi: 10.1002/hyp.13865

Erman, D. C. (Ed.). (1997). *Status of the sierra nevada: the sierra nevada ecosystem project.* US Geological Survey. Retrieved from `https://doi.org/10.3133/ds43` doi: 10.3133/ds43

Estes, B. L., Knapp, E. E., Skinner, C. N., & Uzoh, F. C. C. (2012). Seasonal variation in surface fuel moisture between unthinned and thinned mixed conifer forest, northern california, USA. *International Journal of Wildland Fire*, *21*(4), 428. Retrieved from `https://doi.org/10.1071/wf11056` doi: 10.1071/wf11056

Famiglietti, J., Rudnicki, J., & Rodell, M. (1998, September). Variability in surface moisture content along a hillslope transect: Rattlesnake hill, texas. *Journal of Hydrology*, *210*(1-4), 259–281. Retrieved from `https://doi.org/10.1016/s0022-1694(98)00187-5` doi: 10.1016/s0022-1694(98)00187-5

Fernandes, P., & Botelho, H. (2004, January). Analysis of the prescribed burning practice in the pine forest of northwestern portugal. *Journal of Environmental Management*, *70*(1), 15–26. Retrieved from `https://doi.org/10.1016/j.jenvman.2003.10.001` doi: 10.1016/j.jenvman.2003.10.001

Fernandes, P. M., Botelho, H., Rego, F., & Loureiro, C. (2008, February). Using fuel and weather variables to predict the sustainability of surface fire spread in maritime pine stands. *Canadian Journal of Forest Research*, *38*(2), 190–201. Retrieved from `https://doi.org/10.1139/x07-159` doi: 10.1139/x07-159

Ferrick, M., & Gatto, L. W. (2005). Quantifying the effect of a freeze–thaw cycle on soil erosion: laboratory experiments. *Earth Surface Processes and Landforms: The Journal of the British Geomorphological Research Group*, *30*(10), 1305–1326.

Fitzhugh, R. D., Driscoll, C. T., Groffman, P. M., Tierney, G. L., Fahey, T. J., & Hardy, J. P. (2001). Effects of soil freezing disturbance on soil solution nitrogen, phosphorus, and carbon chemistry in a northern hardwood ecosystem. *Biogeochemistry*, *56*(2), 215–238.

Flannigan, M. D., Wotton, B. M., Marshall, G. A., de Groot, W. J., Johnston, J., Jurko, N., & Cantin, A. S. (2015, October). Fuel moisture sensitivity to temperature and precipitation: climate change implications. *Climatic Change*, *134*(1-2), 59–71. Retrieved from `https://doi.org/10.1007/s10584-015-1521-0` doi: 10.1007/s10584-015-1521-0

Gardner, W. R., & Hillel, D. I. (1962, October). The relation of external evaporative conditions to the drying of soils. *Journal of Geophysical Research*, *67*(11), 4319–4325. Retrieved from `https://doi.org/10.1029/jz067i011p04319` doi: 10.1029/jz067i011p04319

Geos Institute. (2013, December). Future climate, wildfire, hydrology, and vegetation projections for the sierra nevada, California: A climate change synthesis in support of the vulnerability assessment/adaptation strategy process. `https://climatewise.org/images/projects/sierra-nevada-report-projections.pdf`. (online: https://climatewise.org/images/projects/sierra-nevada-report-projections.pdf)

Gershunov, A., Shulgina, T., Clemesha, R. E. S., Guirguis, K., Pierce, D. W., Dettinger, M. D., . . . Ralph, F. M. (2019, July). Precipitation regime change in western north america: The role of atmospheric rivers. *Scientific Reports*, *9*(1). Retrieved from `https://doi.org/10.1038/s41598-019-46169-w` doi: 10.1038/s41598-019-46169-w

Giovannini, G., Lucchesi, S., & Cervelli, S. (1983). Water-repellent substances and aggregate stability in hydrophobic soil. *Soil Science*, *135*(2).

Gleason, K. E., McConnell, J. R., Arienzo, M. M., Chellman, N., & Calvin, W. M. (2019, May). Four-fold increase in solar forcing on snow in western u.s. burned forests since 1999. *Nature Communications*, *10*(1). Retrieved from `https://doi.org/10.1038/s41467-019-09935-y` doi: 10.1038/s41467-019-09935-y

Gleason, K. E., Nolin, A. W., & Roth, T. R. (2013, September). Charred forests increase snowmelt: Effects of burned woody debris and incoming solar radiation on snow ablation. *Geophysical Research Letters*, *40*(17), 4654–4661. Retrieved from `https://doi.org/10.1002/grl.50896` doi: 10.1002/grl.50896

González-Sanchis, M., Ruiz-Pérez, G., Campo, A. D. D., Garcia-Prats, A., Francés, F., & Lull, C. (2019, February). Managing low productive forests at catchment scale: Considering water, biomass and fire risk to achieve economic feasibility. *Journal of Environmental Management*, *231*, 653–665. Retrieved from `https://doi.org/10.1016/j.jenvman.2018.10.078` doi: 10.1016/j.jenvman.2018.10.078

Gould, J. (2003). *Fire behavior: integrating science and management.* CSIRO Publishing. Retrieved from `https://ebooks.publish.csiro.au/content/9780643090965/9780643090965` doi: 10.1071/9780643090965

Goulden, M., & Bales, R. (2019, 07). California forest die-off linked to multi-year deep soil drying in 2012–2015 drought. *Nature Geoscience*, 1. doi: 10.1038/s41561-019-0388-5

Graham, R. T., & McCaffrey, S. (2003). Influence of forest structure on wildfire behavior and the severity of its effects.

Grayson, R. B., Western, A. W., Chiew, F. H. S., & Blöschl, G. (1997, December). Preferred states in spatial soil moisture patterns: Local and nonlocal controls. *Water Resources Research*, *33*(12), 2897–2908. Retrieved from `https://doi.org/10.1029/97wr02174` doi: 10.1029/97wr02174

Green, W. H., & Ampt, G. (1911). Studies on soil phyics. *The Journal of Agricultural Science*, *4*(1), 1–24.

Gregory Flato, J. M. (2013). *Climate change 2013: The physical science basis. contribution of working group i to the fifth assessment report of the intergovernmental panel on climate change.* `https://www.ipcc.ch/site/assets/uploads/2018/02/WG1AR5_Chapter09_FINAL.pdf`. ((Accessed on 01/08/2020))

Grömping, U. (2009, November). Variable importance assessment in regression: Linear regression versus random forest. *The American Statistician*, *63*(4), 308–319. Retrieved from `https://doi.org/10.1198/tast.2009.08199` doi: 10.1198/tast.2009.08199

Guevara, M., & Vargas, R. (2019, September). Downscaling satellite soil moisture using geomorphometry and machine learning. *PLOS ONE*, *14*(9), e0219639. Retrieved from `https://doi.org/10.1371/journal.pone.0219639` doi: 10.1371/journal.pone.0219639

Gyssels, G., Poesen, J., Bochet, E., & Li, Y. (2005). Impact of plant roots on the resistance of soils to erosion by water: a review. *Progress in physical geography*, *29*(2), 189–217.

Hagedorn, R., Doblas-Reyes, F. J., & Palmer, T. (2005, January). The rationale behind the success of multi-model ensembles in seasonal forecasting — i. basic concept. *Tellus A: Dynamic Meteorology and Oceanography*, *57*(3), 219–233. doi: 10.3402/tellusa.v57i3.14657

Halofsky, J. S., Conklin, D. R., Donato, D. C., Halofsky, J. E., & Kim, J. B. (2018, December). Climate change, wildfire, and vegetation shifts in a high-inertia forest landscape: Western washington, u.s.a. *PLOS ONE*, *13*(12), e0209490. Retrieved from `https://doi.org/10.1371/journal.pone.0209490` doi: 10.1371/journal.pone.0209490

Han, J., Lin, J., & Dai, Y. (2017). Numerical modeling of soil evaporation process and its stages dividing during a drying cycle. *Geofluids*, *2017*, 1–11. Retrieved from `https://doi.org/10.1155/2017/5892867` doi: 10.1155/2017/5892867

Harpold, A. A., & Molotch, N. P. (2015, October). Sensitivity of soil water availability to changing snowmelt timing in the western u.s. *Geophysical Research Letters*, *42*(19), 8011–8020. Retrieved from `https://doi.org/10.1002/2015gl065855` doi: 10.1002/2015gl065855

Harpold, A. A., Molotch, N. P., Musselman, K. N., Bales, R. C., Kirchner, P. B., Litvak, M., & Brooks, P. D. (2014, December). Soil moisture response to snowmelt timing in mixed-conifer subalpine forests. *Hydrological Processes*, *29*(12), 2782–2798. Retrieved from `https://doi.org/10.1002/hyp.10400` doi: 10.1002/hyp.10400

Hatchett, B., Daudert, B., Garner, C., Oakley, N., Putnam, A., & White, A. (2017, November). Winter snow level rise in the northern sierra nevada from 2008 to 2017. *Water*, *9*(11), 899. Retrieved from `https://doi.org/10.3390/w9110899` doi: 10.3390/w9110899

Hatton, T. J., Viney, N. R., Catchpole, E., & De Mestre, N. J. (1988). The influence of soil moisture on eucalyptus leaf litter moisture. *Forest Science*, *34*(2), 292–301.

Henn, B., Clark, M. P., Kavetski, D., Newman, A. J., Hughes, M., McGurk, B., & Lundquist, J. D. (2018, January). Spatiotemporal patterns of precipitation inferred from streamflow observations across the Sierra Nevada mountain range. *Journal of Hydrology*, *556*, 993–1012. Retrieved from `https://doi.org/10.1016/j.jhydrol.2016.08.009` doi: 10.1016/j.jhydrol.2016.08.009

Henry, H. A. (2007). Soil freeze–thaw cycle experiments: trends, methodological weaknesses and suggested improvements. *Soil Biology and Biochemistry*, *39*(5), 977–986.

Her, Y., Yoo, S.-H., Cho, J., Hwang, S., Jeong, J., & Seong, C. (2019, March). Uncertainty in hydrological analysis of climate change: multi-parameter vs. multi-GCM ensemble predictions. *Scientific Reports*, *9*(1). Retrieved from `https://doi.org/10.1038/s41598-019-41334-7` doi: 10.1038/s41598-019-41334-7

Herrmann, A., & Witter, E. (2002). Sources of c and n contributing to the flush in mineralization upon freeze–thaw cycles in soils. *Soil Biology and Biochemistry*, *34*(10), 1495–1505.

Hessburg, P. F., Spies, T. A., Perry, D. A., Skinner, C. N., Taylor, A. H., Brown, P. M., ... Riegel, G. (2016, April). Tamm review: Management of mixed-severity fire regime forests in oregon, washington, and northern california. *Forest Ecology and Management*, *366*, 221–250. Retrieved from `https://doi.org/10.1016/j.foreco.2016.01.034` doi: 10.1016/j.foreco.2016.01.034

Hewelke, E., Oktaba, L., Gozdowski, D., Kondras, M., Olejniczak, I., & Górska, E. (2018, August). Intensity and persistence of soil water repellency in pine forest soil in a temperate continental climate under drought conditions. *Water*, *10*(9), 1121. Retrieved from `https://doi.org/10.3390/w10091121` doi: 10.3390/w10091121

Hiers, J. K., Stauhammer, C. L., O'Brien, J. J., Gholz, H. L., Martin, T. A., Hom, J., & Starr, G. (2019, March). Fine dead fuel moisture shows complex lagged responses to environmental conditions in a saw palmetto (serenoa repens) flatwoods. *Agricultural and Forest Meteorology*, *266-267*, 20–28. Retrieved from `https://doi.org/10.1016/j.agrformet.2018.11.038` doi: 10.1016/j.agrformet.2018.11.038

Holsinger, L., Parks, S. A., & Miller, C. (2016, November). Weather, fuels, and topography impede wildland fire spread in western US landscapes. *Forest Ecology and Management*, *380*, 59–69. Retrieved from `https://doi.org/10.1016/j.foreco.2016.08.035` doi: 10.1016/j.foreco.2016.08.035

Horne, D., & McIntosh, J. (2000, May). Hydrophobic compounds in sands in new zealand—extraction, characterisation and proposed mechanisms for repellency expression. *Journal of Hydrology*, *231-232*, 35–46. Retrieved from `https://doi.org/10.1016/s0022-1694(00)00181-5` doi: 10.1016/s0022-1694(00)00181-5

Hotovy, O., & Jenicek, M. (2020, October). The impact of changing subcanopy radiation on snowmelt in a disturbed coniferous forest. *Hydrological Processes*. Retrieved from `https://doi.org/10.1002/hyp.13936` doi: 10.1002/hyp.13936

Howitt, R., Medellín-Azuara, J., MacEwan, D., Lund, J. R., & Sumner, D. (2014). *Economic analysis of the 2014 drought for california agriculture.* Center for Watershed Sciences University of California, Davis, CA.

Huber, P. J. (1967). The behavior of maximum likelihood estimates under nonstandard condition. In N. LeCam & J. Neyman (Eds.), *Proceedings of the fifth berkeley symposium on mathematical statistics and probability.* Berkeley, CA, USA: University of California Press.

Huffman, E. L., MacDonald, L. H., & Stednick, J. D. (2001). Strength and persistence of fire-induced soil hydrophobicity under ponderosa and lodgepole pine, Colorado Front Range. *Hydrological Processes*, *15*(15), 2877–2892. doi: 10.1002/hyp.379

Hunsaker, C. T., Whitaker, T. W., & Bales, R. C. (2012, February). Snowmelt runoff and water yield along elevation and temperature gradients in california's southern sierra nevada1. *JAWRA Journal of the American Water Resources Association*, *48*(4), 667–678. Retrieved from `https://doi.org/10.1111/j.1752-1688.2012.00641.x` doi: 10.1111/j.1752-1688.2012.00641.x

Hurteau, M. D., Liang, S., Westerling, A. L., & Wiedinmyer, C. (2019, February). Vegetation-fire feedback reduces projected area burned under climate change. *Scientific Reports*, *9*(1). Retrieved from `https://doi.org/10.1038/s41598-019-39284-1` doi: 10.1038/s41598-019-39284-1

Jayasuriya, M., Dunn, G., Benyon, R., & OShaughnessy, P. (1993, October). Some factors affecting water yield from mountain ash (eucalyptus regnans) dominated forests in south-east australia. *Journal of Hydrology*, *150*(2-4), 345–367. Retrieved from `https://doi.org/10.1016/0022-1694(93)90116-q` doi: 10.1016/0022-1694(93)90116-q

Jepsen, S., Harmon, T., Meadows, M., & Hunsaker, C. (2016, February). Hydrogeologic influence on changes in snowmelt runoff with climate warming: Numerical experiments on a mid-elevation catchment in the sierra nevada, USA. *Journal of Hydrology*, *533*, 332–342. Retrieved from `https://doi.org/10.1016/j.jhydrol.2015.12.010` doi: 10.1016/j.jhydrol.2015.12.010

Jiménez-Morillo, N. T., Spangenberg, J. E., Miller, A. Z., Jordán, A., Zavala, L. M., González-Vila, F. J., & González-Pérez, J. A. (2017, November). Wildfire effects on lipid composition and hydrophobicity of bulk soil and soil size fractions under quercus suber cover (SW-spain). *Environmental Research*, *159*, 394–405. Retrieved from `https://doi.org/10.1016/j.envres.2017.08.022` doi: 10.1016/j.envres.2017.08.022

Johnson, E. A., & Miyanishi, K. (1995, December). The need for consideration of fire behavior and effects in prescribed burning. *Restoration Ecology*, *3*(4), 271–278. Retrieved from `https://doi.org/10.1111/j.1526-100x.1995.tb00094.x` doi: 10.1111/j.1526-100x.1995.tb00094.x

Jong, B.-T., Ting, M., & Seager, R. (2016, May). El niños impact on california precipitation: seasonality, regionality, and el niño intensity. *Environmental Research Letters*, *11*(5), 054021. Retrieved from `https://doi.org/10.1088/1748-9326/11/5/054021` doi: 10.1088/1748-9326/11/5/054021

Jordan, C. S., Daniels, J. L., & Langley, W. (2017, August). The effects of temperature and wet-dry cycling on water-repellent soils. *Environmental Geotechnics*, *4*(4), 299–307. Retrieved from `https://doi.org/10.1680/envgeo.14.00032` doi: 10.1680/envgeo.14.00032

Kane, V. R., Lutz, J. A., Cansler, C. A., Povak, N. A., Churchill, D. J., Smith, D. F., . . . North, M. P. (2015, February). Water balance and topography predict fire and forest structure patterns. *Forest Ecology and Management*, *338*, 1–13. Retrieved from `https://doi.org/10.1016/j.foreco.2014.10.038` doi: 10.1016/j.foreco.2014.10.038

Karavani, A., Boer, M. M., Baudena, M., Colinas, C., Díaz-Sierra, R., Pemán, J., . . . de Dios, V. R. (2018, January). Fire-induced deforestation in drought-prone mediterranean forests: drivers and unknowns from leaves to communities. *Ecological Monographs*, *88*(2), 141–169. Retrieved from `https://doi.org/10.1002/ecm.1285` doi: 10.1002/ecm.1285

Keeley, J. E. (2009). Fire intensity, fire severity and burn severity: a brief review and suggested usage. *International Journal of Wildland Fire*, *18*(1), 116–126.

Keith, D. M., Johnson, E. A., & Valeo, C. (2010, May). A hillslope forest floor (duff) water budget and the transition to local control. *Hydrological Processes*, *24*(19), 2738–2751. Retrieved from `https://doi.org/10.1002/hyp.7697` doi: 10.1002/hyp.7697

Kennedy, M. C., McKenzie, D., Tague, C., & Dugger, A. L. (2017). Balancing uncertainty and complexity to incorporate fire spread in an eco-hydrological model. *International Journal of Wildland Fire*, *26*(8), 706. Retrieved from `https://doi.org/10.1071/wf16169` doi: 10.1071/wf16169

Keyser, A., & Westerling, A. L. (2017). Climate drives inter-annual variability in probability of high severity fire occurrence in the western united states. *Environmental Research Letters*, *12*(6), 065003.

Kim, S., Zhang, R., Pham, H., & Sharma, A. (2019, November). A review of satellite-derived soil moisture and its usage for flood estimation. *Remote Sensing in Earth Systems Sciences*, *2*(4), 225–246. Retrieved from `https://doi.org/10.1007/s41976-019-00025-7` doi: 10.1007/s41976-019-00025-7

King, P. M. (1981). Comparison of methods for measuring severity of water repellence of sandy soils and assessment of some factors that affect its measurement. *Australian Journal of Soil Research*, *19*(3), 275–285. doi: 10.1071/SR9810275

Kinoshita, A. M., & Hogue, T. S. (2015). Increased dry season water yield in burned watersheds in southern california. *Environmental Research Letters*, *10*(1), 014003.

Klausmeyer, K., & Fitzgerald, K. (2012). Where Does California's Water Come From? Land conservation and the watersheds that supply California's drinking water. (online: https://www.nature.org/media/california/california $drinking-water-sources-2012.pdf$)

Kleber, M., Sollins, P., & Sutton, R. (2007, June). A conceptual model of organo-mineral interactions in soils: self-assembly of organic molecular fragments into zonal structures on mineral surfaces. *Biogeochemistry*, *85*(1), 9–24. Retrieved from `https://doi.org/10.1007/s10533-007-9103-5` doi: 10.1007/s10533-007-9103-5

Knapp, E. E., Keeley, J. E., Ballenger, E. A., & Brennan, T. J. (2005, April). Fuel reduction and coarse woody debris dynamics with early season and late season prescribed fire in a sierra nevada mixed conifer forest. *Forest Ecology and Management*, *208*(1-3), 383–397. Retrieved from `https://doi.org/10.1016/j.foreco.2005.01.016` doi: 10.1016/j.foreco.2005.01.016

Knutti, R., Masson, D., & Gettelman, A. (2013). Climate model genealogy: Generation CMIP5 and how we got there. *Geophysical Research Letters*, *40*(6), 1194–1199. doi: 10.1002/grl.50256

Kolden, C. A., Abatzoglou, J. T., Lutz, J. A., Cansler, C. A., Kane, J. T., Wagtendonk, J. W. V., & Key, C. H. (2015, August). Climate contributors to forest mosaics: Ecological persistence following wildfire. *Northwest Science*, *89*(3), 219–238. Retrieved from `https://doi.org/10.3955/046.089.0305` doi: 10.3955/046.089.0305

Kondo, J., Saigusa, N., & Sato, T. (1990, May). A parameterization of evaporation from bare soil surfaces. *Journal of Applied Meteorology*, *29*(5), 385–389. Retrieved from `https://doi.org/10.1175/1520-0450(1990)029<0385:apoefb>2.0.co;2` doi: 10.1175/1520-0450(1990)029¡0385:apoefb¿2.0.co;2

Kořenková, L., & Matúš, P. (2015, July). Role of water repellency in aggregate stability of cultivated soils under simulated raindrop impact. *Eurasian Soil Science*, *48*(7), 754–758. Retrieved from `https://doi.org/10.1134/s1064229315070054` doi: 10.1134/s1064229315070054

Kostadinov, T. S., Schumer, R., Hausner, M., Bormann, K. J., Gaffney, R., McGwire, K., . . . Harpold, A. A. (2019, March). Watershed-scale mapping of fractional snow cover under conifer forest canopy using lidar. *Remote Sensing of Environment*, *222*, 34–49. Retrieved from `https://doi.org/10.1016/j.rse.2018.11.037` doi: 10.1016/j.rse.2018.11.037

Kreye, J. K., Hiers, J. K., Varner, J. M., Hornsby, B., Drukker, S., & O'Brien, J. J. (2018, November). Effects of solar heating on the moisture dynamics of forest floor litter in humid environments: composition, structure, and position matter. *Canadian Journal of Forest Research*, *48*(11), 1331–1342. Retrieved from `https://doi.org/10.1139/cjfr-2018-0147` doi: 10.1139/cjfr-2018-0147

Kurpius, M., Panek, J., Nikolov, N., McKay, M., & Goldstein, A. (2003, July). Partitioning of water flux in a sierra nevada ponderosa pine plantation. *Agricultural and Forest Meteorology*, *117*(3-4), 173–192. Retrieved from `https://doi.org/10.1016/s0168-1923(03)00062-5` doi: 10.1016/s0168-1923(03)00062-5

Kværnø, S. H., & Øygarden, L. (2006, November). The influence of freeze–thaw cycles and soil moisture on aggregate stability of three soils in norway. *CATENA*, *67*(3), 175–182. Retrieved from `https://doi.org/10.1016/j.catena.2006.03.011` doi: 10.1016/j.catena.2006.03.011

Lanzante, J. R., Adams-Smith, D., Dixon, K. W., Nath, M., & Whitlock, C. E. (2019, September). Evaluation of some distributional downscaling methods as applied to daily maximum temperature with emphasis on extremes. *International Journal of Climatology*. Retrieved from `https://doi.org/10.1002/joc.6288` doi: 10.1002/joc.6288

Larjavaara, M., Kuuluvainen, T., Tanskanen, H., & Venäläinen, A. (2004). Variation in forest fire ignition probability in finland. *Silva Fennica*, *38*(3). Retrieved from `https://doi.org/10.14214/sf.414` doi: 10.14214/sf.414

Larsen, I. J., MacDonald, L. H., Brown, E., Rough, D., Welsh, M. J., Pietraszek, J. H., . . . Schaffrath, K. (2009a). Causes of post-fire runoff and erosion: water repellency, cover, or soil sealing? *Soil Science Society of America Journal*, *73*(4), 1393–1407.

Larsen, I. J., MacDonald, L. H., Brown, E., Rough, D., Welsh, M. J., Pietraszek, J. H., . . . Schaffrath, K. (2009b, July). Causes of post-fire runoff and erosion: Water repellency, cover, or soil sealing? *Soil Science Society of America Journal*, *73*(4), 1393–1407. Retrieved from `https://doi.org/10.2136/sssaj2007.0432` doi: 10.2136/sssaj2007.0432

Larson, A. J., Belote, R. T., Cansler, C. A., Parks, S. A., & Dietz, M. S. (2013, September). Latent resilience in ponderosa pine forest: effects of resumed frequent fire. *Ecological Applications*, *23*(6), 1243–1249. Retrieved from `https://doi.org/10.1890/13-0066.1` doi: 10.1890/13-0066.1

Lauvaux, C. A., Skinner, C. N., & Taylor, A. H. (2016, March). High severity fire and mixed conifer forest-chaparral dynamics in the southern Cascade Range, USA. *Forest Ecology and Management*, *363*, 74–85. Retrieved from `https://doi.org/10.1016/j.foreco.2015.12.016` doi: 10.1016/j.foreco.2015.12.016

Leelamanie, D. A. L., & Karube, J. (2007, December). Effects of organic compounds, water content and clay on the water repellency of a model sandy soil. *Soil Science and Plant Nutrition*, *53*(6), 711–719. Retrieved from `https://doi.org/10.1111/j.1747-0765.2007.00199.x` doi: 10.1111/j.1747-0765.2007.00199.x

Lenihan, J. M., Drapek, R., Bachelet, D., & Neilson, R. P. (2003, December). Climate change effects on vegetation distribution, carbon, and fire in California. *Ecological Applications*, *13*(6), 1667–1681. Retrieved from `https://doi.org/10.1890/025295` doi: 10.1890/025295

Leopold, A. S. (1963). *Wildlife management in the national parks.* US National Park Service.

Letey, J. (1969). Measurement of contact angle, water drop penetration time and critical surface tension..

Letey, J., Osborn, J., & Pelishek, R. E. (1962). *Measurement of liquid-solid contact angles in soil and sand.* (Vol. 93) (No. 3). doi: 10.1097/00010694-196203000-00001

Liang, S., Hurteau, M. D., & Westerling, A. L. (2016, November). Response of Sierra Nevada forests to projected climate-wildfire interactions. *Global Change Biology*, *23*(5), 2016–2030. Retrieved from `https://doi.org/10.1111/gcb.13544` doi: 10.1111/gcb.13544

Littell, J. S., McKenzie, D., Peterson, D. L., & Westerling, A. L. (2009). Climate and wildfire area burned in western us ecoprovinces, 1916–2003. *Ecological Applications*, *19*(4), 1003–1021.

Little, R. J. A. (1988, July). Missing-data adjustments in large surveys. *Journal of Business & Economic Statistics*, *6*(3), 287. Retrieved from `https://doi.org/10.2307/1391878` doi: 10.2307/1391878

Lundquist, J. D., Dickerson-Lange, S. E., Lutz, J. A., & Cristea, N. C. (2013, October). Lower forest density enhances snow retention in regions with warmer winters: A global framework developed from plot-scale observations and modeling. *Water Resources Research*, *49*(10), 6356–6370. Retrieved from `https://doi.org/10.1002/wrcr.20504` doi: 10.1002/wrcr.20504

Lundquist, J. D., & Loheide, S. P. (2011, March). How evaporative water losses vary between wet and dry water years as a function of elevation in the sierra nevada, california, and critical factors for modeling. *Water Resources Research*, *47*(3). Retrieved from `https://doi.org/10.1029/2010wr010050` doi: 10.1029/2010wr010050

Lundquist, J. D., Neiman, P. J., Martner, B., White, A. B., Gottas, D. J., & Ralph, F. M. (2008, April). Rain versus snow in the sierra nevada, california: Comparing doppler profiling radar and surface observations of melting level. *Journal of Hydrometeorology*, *9*(2), 194–211. Retrieved from `https://doi.org/10.1175/2007jhm853.1` doi: 10.1175/2007jhm853.1

Luo, M., Liu, T., Meng, F., Duan, Y., Frankl, A., Bao, A., & Maeyer, P. D. (2018, August). Comparing bias correction methods used in downscaling precipitation and temperature from regional climate models: A case study from the Kaidu River Basin in Western China. *Water*, *10*(8), 1046. Retrieved from `https://doi.org/10.3390/w10081046` doi: 10.3390/w10081046

MacDonald, L. H., & Huffman, E. L. (2004). Post-fire soil water repellency: Persistence and soil moisture thresholds. *Soil Science Society of America Journal*, *68*(5), 1729–1734. doi: 10.2136/sssaj2004.1729

Madani, K., & Lund, J. R. (2009, November). Estimated impacts of climate warming on California's high-elevation hydropower. *Climatic Change*, *102*(3-4), 521–538. Retrieved from `https://doi.org/10.1007/s10584-009-9750-8` doi: 10.1007/s10584-009-9750-8

Mahdavi, S. M., Neyshabouri, M. R., Fujimaki, H., & Heris, A. M. (2017, April). Coupled heat and moisture transfer and evaporation in mulched soils. *CATENA*, *151*, 34–48. Retrieved from `https://doi.org/10.1016/j.catena.2016.12.010` doi: 10.1016/j.catena.2016.12.010

Maina, F. Z., & Siirila-Woodburn, E. R. (2019, August). Watersheds dynamics following wildfires: Nonlinear feedbacks and implications on hydrologic responses. *Hydrological Processes*, *34*(1), 33–50. Retrieved from `https://doi.org/10.1002/hyp.13568` doi: 10.1002/hyp.13568

Mallek, C., Safford, H., Viers, J., & Miller, J. (2013, December). Modern departures in fire severity and area vary by forest type, sierra nevada and southern cascades, california, USA. *Ecosphere*, *4*(12), art153. Retrieved from `https://doi.org/10.1890/es13-00217.1` doi: 10.1890/es13-00217.1

Mao, J., Nierop, K. G. J., Dekker, S. C., Dekker, L. W., & Chen, B. (2018, December). Understanding the mechanisms of soil water repellency from nanoscale to ecosystem scale: a review. *Journal of Soils and Sediments*, *19*(1), 171–185. Retrieved from `https://doi.org/10.1007/s11368-018-2195-9` doi: 10.1007/s11368-018-2195-9

Marion, G. M. (1995). *Freeze-thaw processes and soil chemistry.* (Tech. Rep.). Cold Regions Research and Engineering Lab, Hanover NH.

Martin, D. A. (2016). At the nexus of fire, water and society. *Philosophical Transactions of the Royal Society B: Biological Sciences*, *371*(1696), 20150172.

Mascaro, G., Ko, A., & Vivoni, E. R. (2019, November). Closing the loop of satellite soil moisture estimation via scale invariance of hydrologic simulations. *Scientific Reports*, *9*(1). Retrieved from `https://doi.org/10.1038/s41598-019-52650-3` doi: 10.1038/s41598-019-52650-3

Mashum, M., & Farmer, V. (1985). Origin and assessment of water repellency of a sandy south australian soil. *Soil Research*, *23*(4), 623. Retrieved from `https://doi.org/10.1071/sr9850623` doi: 10.1071/sr9850623

Mataix-Solera, J., Cerdà, A., Arcenegui, V., Jordán, A., & Zavala, L. (2011, November). Fire effects on soil aggregation: A review. *Earth-Science Reviews*, *109*(1-2), 44–60. Retrieved from `https://doi.org/10.1016/j.earscirev.2011.08.002` doi: 10.1016/j.earscirev.2011.08.002

Matthews, S. (2005, December). The water vapour conductance of eucalyptus litter layers. *Agricultural and Forest Meteorology*, *135*(1-4), 73–81. Retrieved from `https://doi.org/10.1016/j.agrformet.2005.10.004` doi: 10.1016/j.agrformet.2005.10.004

Matthews, S. (2010). Effect of drying temperature on fuel moisture content measurements. *International Journal of Wildland Fire*, *19*(6), 800. Retrieved from `https://doi.org/10.1071/wf08188` doi: 10.1071/wf08188

Matthews, S. (2014). Dead fuel moisture research: 1991–2012. *International Journal of Wildland Fire*, *23*(1), 78. Retrieved from `https://doi.org/10.1071/wf13005` doi: 10.1071/wf13005

McGarigal, K., Cushman, S., & Ene, E. (2012). Spatial pattern analysis program for categorical and continuous maps. *Computer software program produced*

by the authors at the University of Massachusetts, Amherst. FRAGSTATS v4. See http://wwwumassedu/landeco/research/fragstats/fragstatshtml.

McIntyre, P. J., Thorne, J. H., Dolanc, C. R., Flint, A. L., Flint, L. E., Kelly, M., & Ackerly, D. D. (2015, January). Twentieth-century shifts in forest structure in california: Denser forests, smaller trees, and increased dominance of oaks. *Proceedings of the National Academy of Sciences*, *112*(5), 1458–1463. Retrieved from `https://doi.org/10.1073/pnas.1410186112` doi: 10.1073/pnas.1410186112

McKelvey, K. S., Skinner, C. N., Chang, C., Erman, D. C., Husari, S. J., Parsons, D. J., . . . Weatherspoon, C. P. (1996). An overview of fire in the Sierra Nevada. In *Sierra nevada ecosystem project: Final report to congress, volume ii* (Vol. Chapter 37). Davis, CA: University of California-Davis, Wildland Resources Center. Retrieved from `http://pubs.er.usgs.gov/publication/70006799`

McKenzie, D., & Littell, J. S. (2017). Climate change and the eco-hydrology of fire: Will area burned increase in a warming western USA? *Ecological applications*, *27*(1), 26–36.

McLaughlin, B. C., Ackerly, D. D., Klos, P. Z., Natali, J., Dawson, T. E., & Thompson, S. E. (2017, March). Hydrologic refugia, plants, and climate change. *Global Change Biology*, *23*(8), 2941–2961. Retrieved from `https://doi.org/10.1111/gcb.13629` doi: 10.1111/gcb.13629

Meng, R., Dennison, P. E., Huang, C., Moritz, M. A., & D'Antonio, C. (2015, December). Effects of fire severity and post-fire climate on short-term vegetation recovery of mixed-conifer and red fir forests in the Sierra Nevada mountains of California. *Remote Sensing of Environment*, *171*, 311–325. Retrieved from `https://doi.org/10.1016/j.rse.2015.10.024` doi: 10.1016/j.rse.2015.10.024

Meyer, M. D., North, M. P., Gray, A. N., & Zald, H. S. J. (2007, March). Influence of soil thickness on stand characteristics in a sierra nevada mixed-conifer forest. *Plant and Soil*, *294*(1-2), 113–123. Retrieved from `https://doi.org/10.1007/s11104-007-9235-3` doi: 10.1007/s11104-007-9235-3

Millar, C. I. (1996). Sierra nevada ecosystem project. *Cooperative report of the PSW Research Station, PSW Region, USDA, for the Sierra Nevada Framework Project, Sacramento, CA.*

Millar, C. I., & Stephenson, N. L. (2015, August). Temperate forest health in an era of emerging megadisturbance. *Science*, *349*(6250), 823–826. Retrieved from `https://doi.org/10.1126/science.aaa9933` doi: 10.1126/science.aaa9933

Miller, C., & Urban, D. L. (2000). Connectivity of forest fuels and surface fire regimes. *Landscape Ecology*, *15*(2), 145–154. Retrieved from `https://doi.org/10.1023/a:1008181313360` doi: 10.1023/a:1008181313360

Miller, J., Safford, H., Crimmins, M., & Thode, A. E. (2009). Quantitative evidence for increasing forest fire severity in the sierra nevada and southern cascade mountains, california and nevada, usa. *Ecosystems*, *12*(1), 16–32.

Miller, J. D., Knapp, E. E., Key, C. H., Skinner, C. N., Isbell, C. J., Creasy, R. M., & Sherlock, J. W. (2009, March). Calibration and validation of the relative differenced normalized burn ratio (RdNBR) to three measures of fire severity in the sierra nevada and klamath mountains, california, USA. *Remote Sensing of Environment*, *113*(3), 645–656. Retrieved from `https://doi.org/10.1016/j.rse.2008.11.009` doi: 10.1016/j.rse.2008.11.009

Miller, J. D., Skinner, C. N., Safford, H. D., Knapp, E. E., & Ramirez, C. M. (2012). Trends and causes of severity, size, and number of fires in northwestern california, usa. *Ecological Applications*, *22*(1), 184–203. Retrieved from `http://www.jstor.org/stable/41416752`

Miller, J. D., & Thode, A. E. (2007). Quantifying burn severity in a heterogeneous landscape with a relative version of the delta normalized burn ratio (dNBR). *Remote Sensing of Environment*, *109*(1), 66 - 80. doi: 10.1016/j.rse.2006.12.006

Minnich, R. A., & Padgett, P. E. (2003). Geology, climate and vegetation of the sierra nevada and the mixed-conifer zone: An introduction to the ecosystem. In *Ozone air pollution in the Siera Nevada: Distribution and effects on forests* (pp. 1–31). Elsevier. Retrieved from `https://doi.org/10.1016/s1474-8177(02)02001-6` doi: 10.1016/s1474-8177(02)02001-6

Moghaddas, E., & Hubbert, K. (n.d.). Section 5—soils. *Science Synthesis to Support Socioecological Resilience in the Sierra Nevada and Southern Cascade Range*, 221.

Moghaddas, E. E. Y., & Stephens, S. L. (2007). Thinning, burning, and thin-burn fuel treatment effects on soil properties in a Sierra Nevada mixed-conifer forest. *Forest Ecology and Management*, *250*(3), 156–166. doi: 10.1016/j.foreco.2007.05.011

Monteith, J. L. (1965). Evaporation and environment. In *Symposia of the society for experimental biology* (Vol. 19, pp. 205–234).

Montzka, C., Rötzer, K., Bogena, H., Sanchez, N., & Vereecken, H. (2018, March). A new soil moisture downscaling approach for SMAP, SMOS, and AS-CAT by predicting sub-grid variability. *Remote Sensing*, *10*(3), 427. Retrieved from `https://doi.org/10.3390/rs10030427` doi: 10.3390/rs10030427

Moody, J. A., & Martin, D. A. (2001a). Initial hydrologic and geomorphic response following a wildfire in the colorado front range. *Earth Surface Processes and Landforms*, *26*(10), 1049–1070. Retrieved from `https://doi.org/10.1002/esp.253` doi: 10.1002/esp.253

Moody, J. A., & Martin, D. A. (2001b). Post-fire, rainfall intensity–peak discharge relations for three mountainous watersheds in the western usa. *Hydrological processes*, *15*(15), 2981–2993.

Moody, J. A., & Martin, D. A. (2009). Synthesis of sediment yields after wildland fire in different rainfall regimes in the western united states. *International Journal of Wildland Fire*, *18*(1), 96. Retrieved from `https://doi.org/10.1071/wf07162` doi: 10.1071/wf07162

Mount, J., Hanak, E., Baerenklau, K., Butsic, V., Chappelle, C., Escriva-Bou, A., & Xu, Z. (2018). Managing drought in a changing climate: Four essential reforms. *Public Policy Institute of California, San Francisco*.

Najafi, M. R., Moradkhani, H., & Jung, I. W. (2011, March). Assessing the uncertainties of hydrologic model selection in climate change impact studies. *Hydrological Processes*, *25*(18), 2814–2826. Retrieved from `https://doi.org/10.1002/hyp.8043` doi: 10.1002/hyp.8043

National Fuel Moisture Database. (n.d.). *Fuel moisture graphs and tables.* `www.wfas.net/index.php/national-fuel-moisture-database-moisture-drought-103`. ([Online; accessed 28-Sept-2020])

National Wildfire Coordinating Group. (2019). *NWCG standards for fire weather stations* (Tech. Rep.). Retrieved from `https://www.nwcg.gov/sites/default/files/publications/pms426-3.pdf`

Neary, D. G., Ryan, K. C., & DeBano, L. F. (2005). Wildland Fire in Ecosystems, effects of fire on soil and water. *USDA-FS general technical report*, *4*(September), 250. doi: http://dx.doi.org/10.1111/j.1467-7717.2009.01106.x

Nelson, D. W., & Sommers, L. E. (1965). Total carbon, organic carbon, and organic matter. In *Methods of soil analysis. part 2. chemical and microbiological properties* (p. 539-579). American Society of Agronomy, Soil Science Society of America. Retrieved from `https://doi.org/10.2134/agronmonogr9.2.2ed.c29` doi: 10.2134/agronmonogr9.2.2ed.c29

Nelson, R. M. (2000, July). Prediction of diurnal change in 10-h fuel stick moisture content. *Canadian Journal of Forest Research*, *30*(7), 1071–1087. Retrieved from `https://doi.org/10.1139/x00-032` doi: 10.1139/x00-032

Nimmo, J. (2005). AGGREGATION | physical aspects. In *Encyclopedia of soils in the environment* (pp. 28–35). Elsevier. Retrieved from `https://doi.org/10.1016/b0-12-348530-4/00532-4` doi: 10.1016/b0-12-348530-4/00532-4

Nolan, R. H., Blackman, C. J., de Dios, V. R., Choat, B., Medlyn, B. E., Li, X., . . . Boer, M. M. (2020, July). Linking forest flammability and plant vulnerability to drought. *Forests*, *11*(7), 779. Retrieved from `https://doi.org/10.3390/f11070779` doi: 10.3390/f11070779

Norman, S. P., & Taylor, A. H. (2005, August). Pine forest expansion along a forest-meadow ecotone in northeastern california, USA. *Forest Ecology and Management*, *215*(1-3), 51–68. Retrieved from `https://doi.org/10.1016/j.foreco.2005.05.003` doi: 10.1016/j.foreco.2005.05.003

North, M., Safford, H., & Meyer, M. (2012). *Managing Sierra Nevada forests* (Tech. Rep.). Retrieved from `https://doi.org/10.2737/psw-gtr-237` doi: 10.2737/psw-gtr-237

Oztas, T., & Fayetorbay, F. (2003, May). Effect of freezing and thawing processes on soil aggregate stability. *CATENA*, *52*(1), 1–8. Retrieved from `https://doi.org/10.1016/s0341-8162(02)00177-7` doi: 10.1016/s0341-8162(02)00177-7

Parsons, D. J., & DeBenedetti, S. H. (1979). Impact of fire suppression on a mixed-conifer forest. *Forest Ecology and Management*, *2*, 21–33.

Peng, J., Loew, A., Merlin, O., & Verhoest, N. E. C. (2017, April). A review of spatial downscaling of satellite remotely sensed soil moisture. *Reviews of Geophysics*, *55*(2), 341–366. Retrieved from `https://doi.org/10.1002/2016rg000543` doi: 10.1002/2016rg000543

Pierce, D. W., Barnett, T. P., Santer, B. D., & Gleckler, P. J. (2009). Selecting global climate models for regional climate change studies. *Proceedings of the National Academy of Sciences*(21), 8441–8446. doi: 10.1073/pnas.0900094106

Pierce, D. W., Cayan, D. R., Das, T., Maurer, E. P., Miller, N. L., Bao, Y., . . . Tyree, M. (2013, August). The key role of heavy precipitation events in climate model disagreements of future annual precipitation changes in California. *Journal of Climate*, *26*(16), 5879–5896. Retrieved from `https://doi.org/10.1175/jcli-d-12-00766.1` doi: 10.1175/jcli-d-12-00766.1

Pollet, J., & Brown, A. (2007). Fuel Moisture Sampling Guide. *Bureau of Land Management*(April). Retrieved from `https://www.wfas.net/nfmd/references/fmg.pdf`

Ponisio, L. C., Wilkin, K., M'Gonigle, L. K., Kulhanek, K., Cook, L., Thorp, R., . . . Kremen, C. (2016). Pyrodiversity begets plant–pollinator community diversity. *Global change biology*, *22*(5), 1794–1808.

Pook, E., & Gill, A. (1993). Variation of live and dead fine fuel moisture in pinus radiata plantations of the australian-capital-territory. *International Journal of Wildland Fire*, *3*(3), 155. Retrieved from `https://doi.org/10.1071/wf9930155` doi: 10.1071/wf9930155

Pyne, S. J. (1997). *World fire: The culture of fire on earth.* University of Washington Press. Retrieved from `http://www.jstor.org/stable/j.ctvd7w7dq`

Quinn-Davidson, L. N., & Varner, J. M. (2012). Impediments to prescribed fire across agency, landscape and manager: An example from northern California. *International Journal of Wildland Fire*, *21*(3), 210–218. doi: 10.1071/WF11017

Quintano, C., Fernandez-Manso, A., Marcos, E., & Calvo, L. (2019, October). Burn severity and post-fire land surface albedo relationship in mediterranean forest ecosystems. *Remote Sensing*, *11*(19), 2309. Retrieved from `https://doi.org/10.3390/rs11192309` doi: 10.3390/rs11192309

Quyum, A., Achari, G., & Goodman, R. (2002, September). Effect of wetting and drying and dilution on moisture migration through oil contaminated hydrophobic soils. *Science of The Total Environment*, *296*(1-3), 77–87. Retrieved from `https://doi.org/10.1016/s0048-9697(02)00046-3` doi: 10.1016/s0048-9697(02)00046-3

Raaflaub, L., & Valeo, C. (2009, May). Hydrological properties of duff. *Water Resources Research*, *45*(5). Retrieved from `https://doi.org/10.1029/2008wr007396` doi: 10.1029/2008wr007396

Raffa, K. F., Aukema, B. H., Bentz, B. J., Carroll, A. L., Hicke, J. A., Turner, M. G., & Romme, W. H. (2008, June). Cross-scale drivers of natural disturbances prone to anthropogenic amplification: The dynamics of bark beetle eruptions. *BioScience*, *58*(6), 501–517. Retrieved from `https://doi.org/10.1641/b580607` doi: 10.1641/b580607

Rasband, W., & Ferreira, T. (2012, October). Image j user guide. Retrieved from `https://imagej.nih.gov/ij/docs/guide/user-guide.pdf`

Reeder, C. J., & Jurgensen, M. F. (1979, September). Fire-induced water repellency in forest soils of upper michigan. *Canadian Journal of Forest Research*, *9*(3), 369–373. Retrieved from `https://doi.org/10.1139/x79-062` doi: 10.1139/x79-062

Renkin, R. A., & Despain, D. G. (1992, January). Fuel moisture, forest type, and lightning-caused fire in yellowstone national park. *Canadian Journal of Forest Research*, *22*(1), 37–45. Retrieved from `https://doi.org/10.1139/x92-005` doi: 10.1139/x92-005

Revuelto, J., Billecocq, P., Tuzet, F., Cluzet, B., Lamare, M., Larue, F., & Dumont, M. (2020, November). Random forests as a tool to understand the snow depth distribution and its evolution in mountain areas. *Hydrological Processes*. Retrieved from `https://doi.org/10.1002/hyp.13951` doi: 10.1002/hyp.13951

Richter, C., Rejmánek, M., Miller, J. E. D., Welch, K. R., Weeks, J., & Safford, H. (2019, October). The species diversity×fire severity relationship is hump-shaped in

semiarid yellow pine and mixed conifer forests. *Ecosphere*, *10*(10). Retrieved from `https://doi.org/10.1002/ecs2.2882` doi: 10.1002/ecs2.2882

Riley, K. L., & Loehman, R. A. (2016, November). Mid-21st-century climate changes increase predicted fire occurrence and fire season length, Northern Rocky Mountains, United States. *Ecosphere*, *7*(11). Retrieved from `https://doi.org/10.1002/ecs2.1543` doi: 10.1002/ecs2.1543

Riley, K. L., Williams, A. P., Urbanski, S. P., Calkin, D. E., Short, K. C., & O'Connor, C. D. (2019, February). Will landscape fire increase in the future? a systems approach to climate, fire, fuel, and human drivers. *Current Pollution Reports*, *5*(2), 9–24. Retrieved from `https://doi.org/10.1007/s40726-019-0103-6` doi: 10.1007/s40726-019-0103-6

Robichaud, P. R. (2000). Forest fire effects on hillslope erosion: what we know. *Watershed Management Council Networker*, *9*(1).

Robinne, F.-N., Miller, C., Parisien, M.-A., Emelko, M. B., Bladon, K. D., Silins, U., & Flannigan, M. (2016). A global index for mapping the exposure of water resources to wildfire. *Forests*, *7*(1), 22.

Roche, J. W., Goulden, M. L., & Bales, R. C. (2018, May). Estimating evapotranspiration change due to forest treatment and fire at the basin scale in the sierra nevada, california. *Ecohydrology*, *11*(7), e1978. Retrieved from `https://doi.org/10.1002/eco.1978` doi: 10.1002/eco.1978

Rodríguez-Alleres, M., Varela, M., & Benito, E. (2012, December). Natural severity of water repellency in pine forest soils from NW spain and influence of wildfire severity on its persistence. *Geoderma*, *191*, 125–131. Retrieved from `https://doi.org/10.1016/j.geoderma.2012.02.006` doi: 10.1016/j.geoderma.2012.02.006

Rother, M. T., Veblen, T. T., & Furman, L. G. (2015, November). A field experiment informs expected patterns of conifer regeneration after disturbance under changing climate conditions. *Canadian Journal of Forest Research*, *45*(11), 1607–1616. Retrieved from `https://doi.org/10.1139/cjfr-2015-0033` doi: 10.1139/cjfr-2015-0033

Rothermel, R. C. (1983). *How to predict the spread and intensity of forest and range fires* (Tech. Rep.). Retrieved from `https://doi.org/10.2737/int-gtr-143` doi: 10.2737/int-gtr-143

Rothwell, R., Woodard, P., & Samran, S. (1991). The effect of soil water on aspen litter moisture content. In *Proceedings of the eleventh conference on fire and forest meteorology* (p. 117-123). Society of American Foresters National Convention (USA).

Rundel, P. W. (1975). Primary succession on granite outcrops in the montane southern sierra nevada. *Madroño*, *23*(4), 209–220. Retrieved from `http://www.jstor.org/stable/41424027`

Safford, H., & Stevens, J. T. (2017). Natural range of variation for yellow pine and mixed-conifer forests in the sierra nevada, southern cascades, and modoc and inyo national forests, california, usa..

Saksa, P. C., Bales, R. C., Tague, C. L., Battles, J. J., Tobin, B. W., & Conklin, M. (2020, April). Fuels treatment and wildfire effects on runoff from sierra nevada mixed-conifer forests. *Ecohydrology*, *13*(3). Retrieved from `https://doi.org/10.1002/eco.2151` doi: 10.1002/eco.2151

Samran, S., Woodard, P., & Rothwell, R. (1995, 05). The effect of soil water on ground fuel availability. *Forest Science*, *41*, 255-267.

San Francisco Public Utilities Commission. (2014). *Proposed fy 2015-2018 water and sewer rates.* `https://sfwater.org/modules/showdocument.aspx?documentid=5031`. (Accessed on 12/29/2019)

San Francisco Public Utilities Commission. (2017, November). *Water resources division annual report; fiscal year 2016-17.* `https://sfwater.org/modules/showdocument.aspx?documentid=11472`. (Accessed on 12/29/2019)

San Francisco Public Utilities Commission. (2018). *Proposed fy 2019-2022 water and sewer rates.* `https://sfwater.org/modules/showdocument.aspx?documentid=11886`. ((Accessed on 12/29/2019))

Sanderson, B. M., Wehner, M., & Knutti, R. (2017). Skill and independence weighting for multi-model assessments. *Geoscientific Model Development*, *10*(6), 2379–2395. doi: 10.5194/gmd-10-2379-2017

Schlesinger, W. H., & Jasechko, S. (2014, June). Transpiration in the global water cycle. *Agricultural and Forest Meteorology*, *189-190*, 115–117. Retrieved from `https://doi.org/10.1016/j.agrformet.2014.01.011` doi: 10.1016/j.agrformet.2014.01.011

Schoenherr, A. A. (2017a). *A natural history of california.* Univ of California Press.

Schoenherr, A. A. (2017b). *A natural history of california.* University of California Press. Retrieved from `https://doi.org/10.1525/9780520964556` doi: 10.1525/9780520964556

Scholl, A. E., & Taylor, A. H. (2010, March). Fire regimes, forest change, and self-organization in an old-growth mixed-conifer forest, Yosemite National Park,

USA. *Ecological Applications*, *20*(2), 362–380. Retrieved 2019-06-28, from `http://doi.wiley.com/10.1890/08-2324.1` doi: 10.1890/08-2324.1

Schroeder, M., & Buck, C. (1970). Fire weather: a guide for application of meteorological information to forest fire control operations. *USDA Forest Service: Washington, DC*, *360*, 236.

Schroeder, M. J. (1969). Ignition probability. *U.S. Forest Service Office Report*. Retrieved from `https://www.frames.gov/documents/behaveplus/publications/Schroeder_1969_OR2106-1_ocr.pdf`

Schweizer, D., Nichols, T., Cisneros, R., Navarro, K., & Procter, T. (2020). Wildland fire, extreme weather and society: Implications of a history of fire suppression in california, usa. In *Extreme weather events and human health* (pp. 41–57). Springer.

Serra-Diaz, J. M., Maxwell, C., Lucash, M. S., Scheller, R. M., Laflower, D. M., Miller, A. D., ... Thompson, J. R. (2018, April). Disequilibrium of fire-prone forests sets the stage for a rapid decline in conifer dominance during the 21st century. *Scientific Reports*, *8*(1). Retrieved from `https://doi.org/10.1038/s41598-018-24642-2` doi: 10.1038/s41598-018-24642-2

Shakesby, R. (2011, April). Post-wildfire soil erosion in the mediterranean: Review and future research directions. *Earth-Science Reviews*, *105*(3-4), 71–100. Retrieved from `https://doi.org/10.1016/j.earscirev.2011.01.001` doi: 10.1016/j.earscirev.2011.01.001

Shapiro, S. S., & Wilk, M. B. (1965, December). An analysis of variance test for normality (complete samples). *Biometrika*, *52*(3/4), 591. Retrieved from `https://doi.org/10.2307/2333709` doi: 10.2307/2333709

Simkovic, I., Dlapa, P., Doerr, S. H., Mataix-Solera, J., & Sasinkova, V. (2008). Thermal destruction of soil water repellency and associated changes to soil organic matter as observed by FTIR spectroscopy. *Catena*, *74*(3), 205–211. doi: 10.1016/j.catena.2008.03.003

Skinner, C. N., & Chang, C. (1996). Fire regimes, past and present. In *In: Sierra nevada ecosystem project: Final report to congress. vol. ii. assessments and scientific basis for management options. wildland resources center report no. 37. centers for water and wildland resources, university of california, davis. 1041-1069* (Vol. 2, pp. 1041–1069).

Smith, H. G., Sheridan, G. J., Lane, P. N., Nyman, P., & Haydon, S. (2011, January). Wildfire effects on water quality in forest catchments: A review with implications for water supply. *Journal of Hydrology*, *396*(1-2), 170–192. Retrieved from `https://doi.org/10.1016/j.jhydrol.2010.10.043` doi: 10.1016/j.jhydrol.2010.10.043

Steel, Z. L., Safford, H. D., & Viers, J. H. (2015, January). The fire frequency-severity relationship and the legacy of fire suppression in California forests. *Ecosphere*, *6*(1), art8. Retrieved from `https://doi.org/10.1890/es14-00224.1` doi: 10.1890/es14-00224.1

Stephens, S. L., Collins, B. M., Biber, E., & Fulé, P. Z. (2016, November). U.S. federal fire and forest policy: emphasizing resilience in dry forests. *Ecosphere*, *7*(11), e01584. Retrieved from `https://doi.org/10.1002/ecs2.1584` doi: 10.1002/ecs2.1584

Stephens, S. L., Kobziar, L. N., Collins, B. M., Davis, R., Fulé, P. Z., Gaines, W., . . . Spies, T. A. (2019, July). Is fire "for the birds"? how two rare species influence fire management across the US. *Frontiers in Ecology and the Environment*, *17*(7), 391–399. Retrieved from `https://doi.org/10.1002/fee.2076` doi: 10.1002/fee.2076

Stephens, S. L., Lydersen, J. M., Collins, B. M., Fry, D. L., & Meyer, M. D. (2015, May). Historical and current landscape-scale ponderosa pine and mixed conifer forest structure in the southern Sierra Nevada. *Ecosphere*, *6*(5), art79. Retrieved from `https://doi.org/10.1890/es14-00379.1` doi: 10.1890/es14-00379.1

Stephens, S. L., Martin, R. E., & Clinton, N. E. (2007, November). Prehistoric fire area and emissions from californias forests, woodlands, shrublands, and grasslands. *Forest Ecology and Management*, *251*(3), 205–216. Retrieved from `https://doi.org/10.1016/j.foreco.2007.06.005` doi: 10.1016/j.foreco.2007.06.005

Stephens, S. L., & Ruth, L. W. (2005, April). Federal Forest-Fire Policy in the United States. *Ecological Applications*, *15*(2), 532–542. Retrieved from `https://doi.org/10.1890/04-0545` doi: 10.1890/04-0545

Stephens, S. L., Westerling, A. L., Hurteau, M. D., Peery, M. Z., Schultz, C. A., & Thompson, S. (2020, June). Fire and climate change: conserving seasonally dry forests is still possible. *Frontiers in Ecology and the Environment*, *18*, 354–360. Retrieved from `https://doi.org/10.1002/fee.2218` doi: 10.1002/fee.2218

Stevens, J. T. (2017, July). Scale-dependent effects of post-fire canopy cover on snowpack depth in montane coniferous forests. *Ecological Applications*, *27*(6), 1888–1900. Retrieved from `https://doi.org/10.1002/eap.1575` doi: 10.1002/eap.1575

Stevens, J. T., Boisramé, G. F., Rakhmatulina, E., Thompson, S. E., Collins, B. M., & Stephens, S. L. (2020). Forest vegetation change and its impacts on soil water following 47 years of managed wildfire. *Ecosystems*, 1–19.

Stevens, J. T., Boisramé, G. F. S., Rakhmatulina, E., Thompson, S. E., Collins, B. M., & Stephens, S. L. (2020, February). Forest vegetation change and its impacts on soil water following 47 years of managed wildfire. *Ecosystems*. Retrieved from `https://doi.org/10.1007/s10021-020-00489-5` doi: 10.1007/s10021-020-00489-5

Stevens-Rumann, C. S., Kemp, K. B., Higuera, P. E., Harvey, B. J., Rother, M. T., Donato, D. C., ... Veblen, T. T. (2017, December). Evidence for declining forest resilience to wildfires under climate change. *Ecology Letters*, *21*(2), 243–252. Retrieved from `https://doi.org/10.1111/ele.12889` doi: 10.1111/ele.12889

Stewart, I. T., Cayan, D. R., & Dettinger, M. D. (2004, January). Changes in snowmelt runoff timing in western north america under a business as usual climate change scenario. *Climatic Change*, *62*(1-3), 217–232. Retrieved from `https://doi.org/10.1023/b:clim.0000013702.22656.e8` doi: 10.1023/b:clim.0000013702.22656.e8

Stoof, C. R., Ferreira, A. J., Mol, W., Van den Berg, J., De Kort, A., Drooger, S., ... Ritsema, C. J. (2015). Soil surface changes increase runoff and erosion risk after a low–moderate severity fire. *Geoderma*, *239*, 58–67.

Stoof, C. R., Moore, D., Ritsema, C. J., & Dekker, L. W. (2011). Natural and fire-induced soil water repellency in a portuguese shrubland. *Soil Science Society of America Journal*, *75*(6), 2283–2295.

Swain, D. L., Langenbrunner, B., Neelin, J. D., & Hall, A. (2018, April). Increasing precipitation volatility in twenty-first-century california. *Nature Climate Change*, *8*(5), 427–433. Retrieved from `https://doi.org/10.1038/s41558-018-0140-y` doi: 10.1038/s41558-018-0140-y

Syphard, A. D., Sheehan, T., Rustigian-Romsos, H., & Ferschweiler, K. (2018, August). Mapping future fire probability under climate change: Does vegetation matter? *PLOS ONE*, *13*(8), e0201680. Retrieved from `https://doi.org/10.1371/journal.pone.0201680` doi: 10.1371/journal.pone.0201680

Tague, C. L., & Band, L. E. (2004). RHESSys: Regional hydro-ecologic simulation system—an object-oriented approach to spatially distributed modeling of carbon, water, and nutrient cycling. *Earth Interactions*, *8*(19), 1-42. doi: 10.1175/1087-3562(2004)8¡1:RRHSSO¿2.0.CO;2

Tague, C. L., Moritz, M., & Hanan, E. (2019, May). The changing water cycle: The eco-hydrologic impacts of forest density reduction in mediterranean (seasonally dry) regions. *Wiley Interdisciplinary Reviews: Water*, e1350. Retrieved from `https://doi.org/10.1002/wat2.1350` doi: 10.1002/wat2.1350

Tarroja, B., AghaKouchak, A., & Samuelsen, S. (2016, September). Quantifying climate change impacts on hydropower generation and implications on electric grid greenhouse gas emissions and operation. *Energy*, *111*, 295–305. Retrieved from `https://doi.org/10.1016/j.energy.2016.05.131` doi: 10.1016/j.energy.2016.05.131

Taylor, A. H., & Beaty, R. M. (2005, March). Climatic influences on fire regimes in the northern sierra nevada mountains, lake tahoe basin, nevada, USA. *Journal of Biogeography*, *32*(3), 425–438. Retrieved from `https://doi.org/10.1111/j.1365-2699.2004.01208.x` doi: 10.1111/j.1365-2699.2004.01208.x

Templer, P. H., Reinmann, A. B., Sanders-DeMott, R., Sorensen, P. O., Juice, S. M., Bowles, F., . . . Grant, N. (2017, February). Climate change across seasons experiment (CCASE): A new method for simulating future climate in seasonally snow-covered ecosystems. *PLOS ONE*, *12*(2), e0171928. Retrieved from `https://doi.org/10.1371/journal.pone.0171928` doi: 10.1371/journal.pone.0171928

Tepley, A. J., Thomann, E., Veblen, T. T., Perry, G. L. W., Holz, A., Paritsis, J., . . . Anderson-Teixeira, K. J. (2018, March). Influences of fire-vegetation feedbacks and post-fire recovery rates on forest landscape vulnerability to altered fire regimes. *Journal of Ecology*, *106*(5), 1925–1940. Retrieved from `https://doi.org/10.1111/1365-2745.12950` doi: 10.1111/1365-2745.12950

Thomas, D., Butry, D., Gilbert, S., Webb, D., & Fung, J. (2017, November). *The costs and losses of wildfires: a literature survey* (Tech. Rep.). Retrieved from `https://doi.org/10.6028/nist.sp.1215` doi: 10.6028/nist.sp.1215

Thompson, K. L., Zuckerberg, B., Porter, W. P., & Pauli, J. N. (2018, June). The phenology of the subnivium. *Environmental Research Letters*, *13*(6), 064037. Retrieved from `https://doi.org/10.1088/1748-9326/aac670` doi: 10.1088/1748-9326/aac670

Thompson, P. D. (1977). How to improve accuracy by combining independent forecasts. *Monthly Weather Review*, *105*(2), 228-229. doi: 10.1175/1520-0493(1977)105¡0228:HTIABC¿2.0.CO;2

Thompson, S. E., Harman, C. J., Troch, P. A., Brooks, P. D., & Sivapalan, M. (2011, May). Spatial scale dependence of ecohydrologically mediated water balance partitioning: A synthesis framework for catchment ecohydrology. *Water Resources Research*, *47*(10). Retrieved from `https://doi.org/10.1029/2010wr009998` doi: 10.1029/2010wr009998

Tiedemann, A. R. (1979). *Effects of fire on water: a state-of-knowledge review* (Vol. 10). Department of Agriculture, Forest Service.

Toms, J. D., & Lesperance, M. L. (2003, August). Piecewise Regression: A Tool For Identifying Ecological Thresholds. *Ecology*, *84*(8), 2034–2041. Retrieved from `https://doi.org/10.1890/02-0472` doi: 10.1890/02-0472

Trevitt, A. (1988). Weather parameters and fuel moisture content: standards for fire model inputs. In *Proceedings of the conference on bushfire modelling and fire danger rating systems* (pp. 11–12).

Tubbesing, C. L., York, R. A., Stephens, S. L., & Battles, J. J. (2020, March). Rethinking fire-adapted species in an altered fire regime. *Ecosphere*, *11*(3). Retrieved from `https://doi.org/10.1002/ecs2.3091` doi: 10.1002/ecs2.3091

USGS. (2016). *LANDFIRE existing vegetation cover layer.* `http://landfire.cr.usgs.gov/viewer/`. ([Online; accessed 15-Sept-2020])

Vankat, J. L., & Major, J. (1978, December). Vegetation changes in sequoia national park, california. *Journal of Biogeography*, *5*(4), 377. Retrieved from `https://doi.org/10.2307/3038030` doi: 10.2307/3038030

van Mantgem, P. J., & Stephenson, N. L. (2007, October). Apparent climatically induced increase of tree mortality rates in a temperate forest. *Ecology Letters*, *10*(10), 909–916. Retrieved from `https://doi.org/10.1111/j.1461-0248.2007.01080.x` doi: 10.1111/j.1461-0248.2007.01080.x

van Mantgem, P. J., Stephenson, N. L., Byrne, J. C., Daniels, L. D., Franklin, J. F., Fule, P. Z., ... Veblen, T. T. (2009, January). Widespread increase of tree mortality rates in the western united states. *Science*, *323*(5913), 521–524. Retrieved from `https://doi.org/10.1126/science.1165000` doi: 10.1126/science.1165000

Van Wagtendonk, J. W. (1977). *Refined burning prescriptions for yosemite national park* (No. 2). US National Park Service.

van Wagtendonk, J. W. (2007, Dec 01). The history and evolution of wildland fire use. *Fire Ecology*, *3*(2), 3–17. doi: 10.4996/fireecology.0302003

van Wagtendonk, J. W., van Wagtendonk, K. A., & Thode, A. E. (2012, April). Factors associated with the severity of intersecting fires in Yosemite national park, California, USA. *Fire Ecology*, *7*(1), 11–31. doi: 10.4996/fireecology.0801011

Watson, C., & Letey, J. (1970, 11). Indices for characterizing soil-water repellency based upon contact angle-surface tension relationships. *Soil Sci. Soc. Am., Proc.; (United States)*. doi: 10.2136/sssaj1970.03615995003400060011x

Westerling, A. L. (2018). Wildfire simulations for California's fourth climate change assessment: Projecting changes in extreme wildfire events with a warming climate. , 1–29. (online: https://www.energy.ca.gov/sites/default/files/2019-11/Projections $CCCA4 - CEC - 2018 - 014ADA.pdf$)

Westerling, A. L., & Bryant, B. P. (2008, Mar 01). Climate change and wildfire in California. *Climatic Change*, *87*(1), 231–249. doi: 10.1007/s10584-007-9363-z

White, H. (1980, May). A heteroskedasticity-consistent covariance matrix estimator and a direct test for heteroskedasticity. *Econometrica*, *48*(4), 817. Retrieved from `https://doi.org/10.2307/1912934` doi: 10.2307/1912934

Wildland Fire Assesment System. (n.d.). *Processing.* U. S. Forest Service. Retrieved from `https://www.wfas.net/index.php/processing-mainmenu-28`

Williams, A. P., Abatzoglou, J. T., Gershunov, A., Guzman-Morales, J., Bishop, D. A., Balch, J. K., & Lettenmaier, D. P. (2019, August). Observed impacts of anthropogenic climate change on wildfire in california. *Earths Future*, *7*(8), 892–910. Retrieved from `https://doi.org/10.1029/2019ef001210` doi: 10.1029/2019ef001210

Williams, C. J., McNamara, J. P., & Chandler, D. G. (2009, July). Controls on the temporal and spatial variability of soil moisture in a mountainous landscape: the signature of snow and complex terrain. *Hydrology and Earth System Sciences*, *13*(7), 1325–1336. Retrieved from `https://doi.org/10.5194/hess-13-1325-2009` doi: 10.5194/hess-13-1325-2009

Wine, M. L., Cadol, D., & Makhnin, O. (2018, January). In ecoregions across western USA streamflow increases during post-wildfire recovery. *Environmental Research Letters*, *13*(1), 014010. Retrieved from `https://doi.org/10.1088/1748-9326/aa9c5a` doi: 10.1088/1748-9326/aa9c5a

Witty, J. H., Graham, R. C., Hubbert, K. R., Doolittle, J. A., & Wald, J. A. (2003, June). Contributions of water supply from the weathered bedrock zone to forest soil quality. *Geoderma*, *114*(3-4), 389–400. Retrieved from `https://doi.org/10.1016/s0016-7061(03)00051-x` doi: 10.1016/s0016-7061(03)00051-x

Wood, C. M., & Jones, G. M. (2019, oct). Framing management of social-ecological systems in terms of the cost of failure: the Sierra Nevada, USA as a case study. *Environmental Research Letters*, *14*(10), 105004. Retrieved from `https://doi.org/10.1088%2F1748-9326%2Fab4033` doi: 10.1088/1748-9326/ab4033

Woods, S. W., & Balfour, V. N. (2010, November). The effects of soil texture and ash thickness on the post-fire hydrological response from ash-covered soils. *Journal of Hydrology*, *393*(3-4), 274–286. Retrieved from `https://doi.org/10.1016/j.jhydrol.2010.08.025` doi: 10.1016/j.jhydrol.2010.08.025

Writer, J. H., Hohner, A., Oropeza, J., Schmidt, A., Cawley, K. M., & Rosario-Ortiz, F. L. (2014, April). Water treatment implications after the High Park Wildfire, Colorado. *Journal - American Water Works Association*, *106*(4), E189–E199. Retrieved from `https://doi.org/10.5942/jawwa.2014.106.0055` doi: 10.5942/jawwa.2014.106.0055

Yanai, Y., Toyota, K., & Okazaki, M. (2004). Effects of successive soil freeze-thaw cycles on soil microbial biomass and organic matter decomposition potential of soils. *Soil science and plant nutrition*, *50*(6), 821–829.

Yoon, J.-H., Wang, S.-Y. S., Gillies, R. R., Kravitz, B., Hipps, L., & Rasch, P. J. (2015, October). Increasing water cycle extremes in california and in relation to

ENSO cycle under global warming. *Nature Communications*, *6*(1). Retrieved from `https://doi.org/10.1038/ncomms9657` doi: 10.1038/ncomms9657

Young, D. J. N., Werner, C. M., Welch, K. R., Young, T. P., Safford, H. D., & Latimer, A. M. (2019, January). Post-fire forest regeneration shows limited climate tracking and potential for drought-induced type conversion. *Ecology*, *100*(2), e02571. Retrieved from `https://doi.org/10.1002/ecy.2571` doi: 10.1002/ecy.2571

Yue, X., Mickley, L. J., & Logan, J. A. (2013, December). Projection of wildfire activity in southern california in the mid-twenty-first century. *Climate Dynamics*, *43*(7-8), 1973–1991. Retrieved from `https://doi.org/10.1007/s00382-013-2022-3` doi: 10.1007/s00382-013-2022-3

Zavala, L. M., García-Moreno, J., Gordillo-Rivero, Á. J., Jordán, A., & Mataix-Solera, J. (2014, August). Natural soil water repellency in different types of mediterranean woodlands. *Geoderma*, *226-227*, 170–178. Retrieved from `https://doi.org/10.1016/j.geoderma.2014.02.009` doi: 10.1016/j.geoderma.2014.02.009

Zhang, Z., Ma, W., Feng, W., Xiao, D., & Hou, X. (2016, April). Reconstruction of soil particle composition during freeze-thaw cycling: A review. *Pedosphere*, *26*(2), 167–179. Retrieved from `https://doi.org/10.1016/s1002-0160(15)60033-9` doi: 10.1016/s1002-0160(15)60033-9

Zhao, J., Chen, J., Wu, Q., & Hou, X. (2018, December). Snow cover influences the thermal regime of active layer in urumqi river source, tianshan mountains, china. *Journal of Mountain Science*, *15*(12), 2622–2636. Retrieved from `https://doi.org/10.1007/s11629-018-4856-y` doi: 10.1007/s11629-018-4856-y

Appendix A

Supporting Information for Chapter 2

Introduction

This Supplementary Information provides additional detail on sampling site, modeling analysis, and alternative models presented in Chapter 2.

A.1 Blodgett Research Forest Sampling Locations

All fuel sampling was collected at Blodgett Research Station which is a a 4,270 acre property of University of California, Berkeley and supports different research objectives. The forest is generally divided into 110 main compartments of which some are ecological reserves that have no management objectives, young-growth reserves, even age reserves, and uneven age reserves (Blodgett Forest Research Station, 2012). Excluding young-growth compartments, we have sampled across 15 compartments with a mix of reserve types (Table A.1 and Figure A.1). However our sampling location was focused on compartments that did not have a recently prescribed burn and where soil was not disturbed wither by fire or equipment. To get a soil moisture and fuel moisture gradient, we have sampled in topographical transects throughout compartments and along the Gaddis Creek. Due to different age of vegetation across compartments, we were also focused our sampling to include arange of canopy cover above collected fuels. Figure A.1 shows the 100 sampling locations along with the compartments. Satellite imagery clearly shows different vegetation structure across the compartments.
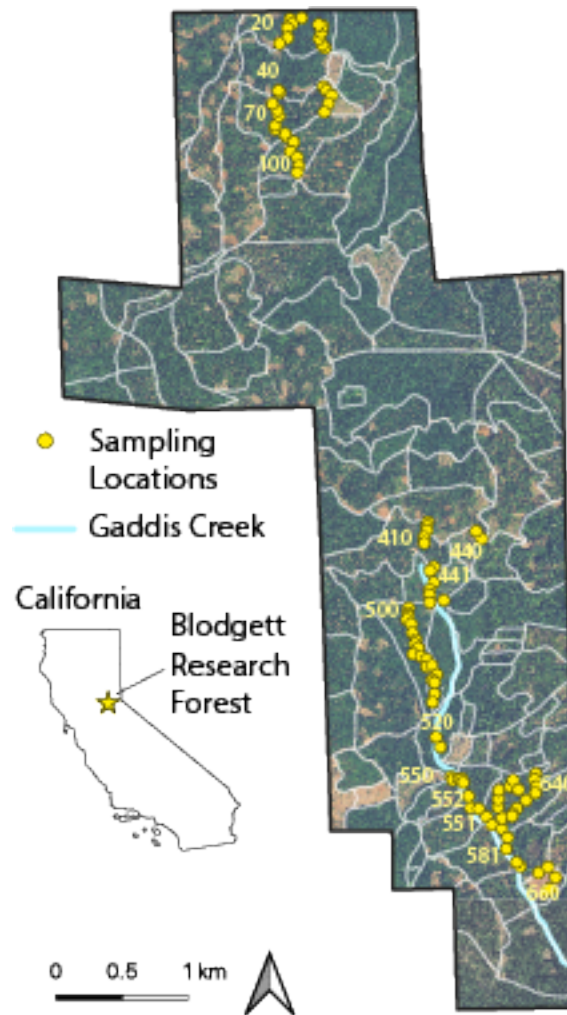
Figure A.1: One hundred and one sampling locations of 1-hr and 10-hr fuels in Blodgett Research Forest in the foothills of Sierra Nevada. Forest research compartments are shown as white perimeters along with the compartment numbers. Gaddis Creek is the main year-round creek at Blodgett

Table A.1: Blodgett compartment numbers along with the number of samples taken of 1-hr and 10-hr fuels within each compartment, and the designated compartment forest treatment. As the names imply, an even-age is comprised of trees of the same age/size and in uneven-age group, tree age/size varies across the compartment. Young-growth forests undergo full regeneration every 90 years. Compartment 520 is a reserve and is left unmanaged. Refer to Blodgett Forest Research Station (2012) for detailed explanation of management objectives and methodologies.

Compartment Number	Number of Samples	Treatment Type
20	12	young-growth
40	2	young-growth
70	12	even-age
100	4	uneven-age
410	6	uneven-age
440	3	even-age
441	6	even-age
500	19	uneven-age
520	2	no management
550	3	even-age
551	2	even-age
552	4	even-age
581	5	even-age
640	16	even-age
660	5	young-growth

A.2 Model Selection

In this section, we provide additional detail on the relationship of all collected and derived variables that were used to explain variation in FMC. Once variables were selected for the final regression forms for 1-hr and 10-hr fuels, we provide the model fit of these regressions

Variable Correlations

Before fitting different regressions to data, we looked at correlations among the collected variables. Figure A.2 shows a correlation coefficient matrix among all the variables, both collected in the field and derived from topographical information.
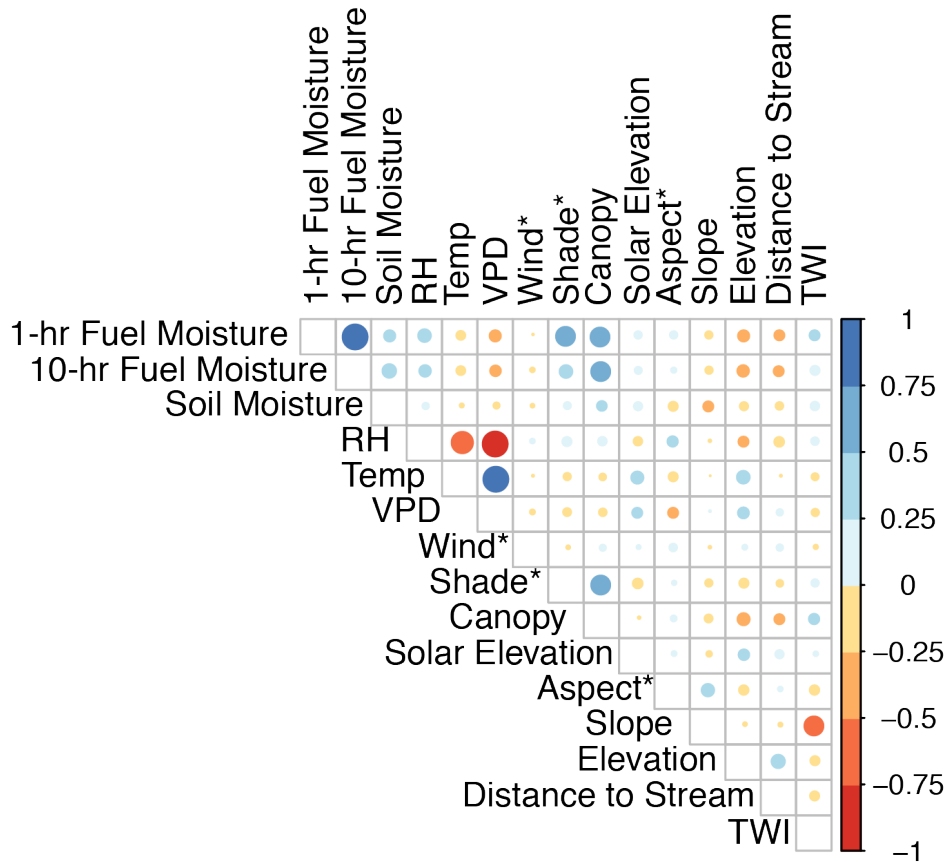
Figure A.2: Correlation coefficient matrix among variables collected in the field and derived from topographical information (marked with an asterisk) Positive correlation is in blue and negative correlation in red. Strength of the correlation is represented by the size of the circle, where the bigger the circle, the stronger is the correlation

Both 1-hr and 10-hr FMC is strongly correlated to (r=0.68 and 0.61 respectively) to above fuel percent canopy. There is also a strong positive correlation between shade (binary value signifying fuels being in the shade at the time of collection) and FMC for both fuel categories, though its more string for finer 1-hr fuels. Unsurprisingly, shade and percent canopy variables are also correlated. Both fuel categories are also somewhat responsive to atmospheric conditions by having weak correlation to relative humidity (1-hr r=0.42 and 10-hr r=0.34) and vapor pressure deficit (1-hr r=-0.34 and 10-hr r=-0.29). Some topographic/geographic variables weakly correlated to FMC as well; elevation, distance to stream were weakly correlated to both fuels, and TWI also weakly correlated to 1-hr fuels, but the relationship was weaker with 10-hr fuels. We do not believe that elevation itself is a meaningful predictor of FMC and instead it correlates to percent canopy cover and soil moisture, where low elevations generally drain more water and have more vegetation that provides shading for fuels. Both 1-hr and 10-hr FMC have a positive correlation to SMC of 0.34 and 0.49 respectively. Interestingly, SMC and TWI are poorly correlated (r=0.25), meaning that TWI is not a good proxy for SMC at the scales measured at Blodgett Research Station.

As described in the Methods Section of Chapter 2, we have used backward stepwise selection to eliminate variables from model formulation. For 1-hr fuels, the final form of the model took the form of ordinary least squares (OLS) regression, however for 10-hr fuels, we fitted data using weighted least squares regression since non-weighted OLS had heteroscedasticity and non-linearity in the residuals. In addition to tabular model fit statistics presented in Results Section, Figure **??** provides a visual of the model fit by plotting fitted values vs studentized residuals and showing a quantile-quantile plot.
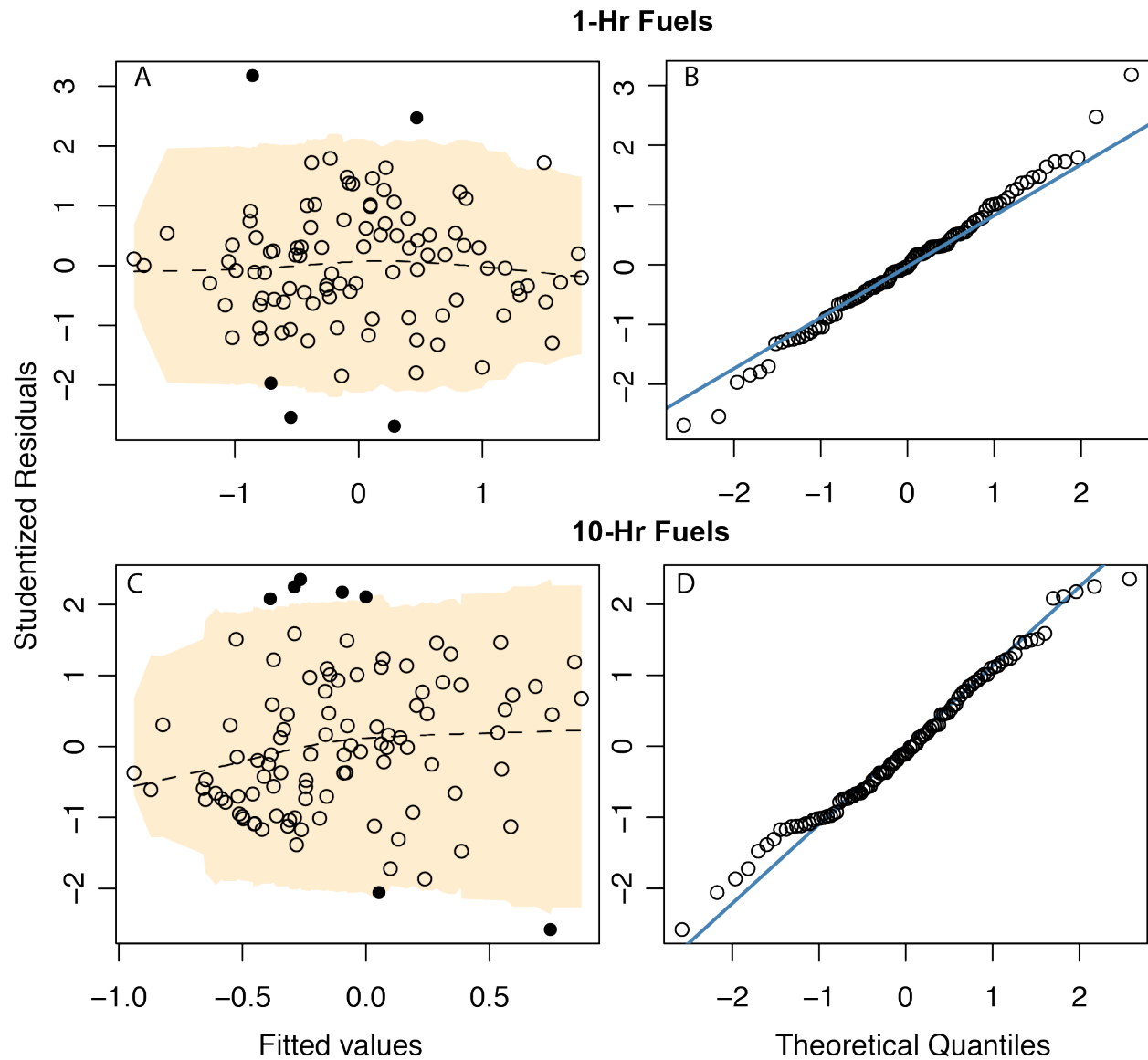
Figure A.3: Linear regression fit for 1-hr FMC (top) and weighted linear regression for 10-hr FMC (bottom). Plots on the left show fitted values against studentized residuals (circles). The orange area represents the 97.5th percentile of the studentized residuals. The more rectangular this area is, the more homoscedastic are the residuals. The dashed line shows the smoothed mean of the studentized residuals. The closer this line is to zero, the more linear is the model fit. Quantile-quantile plots are shown on the right. The closer the points are to the 1:1 blue line), the more normal is the distribution of the model residuals

Both fuel models have relatively equal variance in the residuals. Each model has a number of predicted values with very high absolute residuals (filled circles in Figure A.2), these data points were not removed from model formulation, because we do not believe that there was an error in the measurement. Both models have approximately normal distributions since residual quantiles match normal distribution quantiles. Though it appears that the 10-hr model is somewhat biased at low fuel moisture values since it tends to under-predict low fuel moisture contents, as seen by a below zero mean of the studentized residuals (dashed line in Figure A.2).

Models Without Soil Moisture

As described in detail in Section 2.2, in addition to fitting models using SMC as a predictor for both 1-hr and 10-hr FMC, we have also fitted regressions to predict 1-hr and 10-hr FMC in the absence of SMC. For 1-hr fuels, the regression is fitted on the dataset spanning the entire measured SMC range; model coefficients for 1-hr OLS without SMC are described in Table A.2.

Unlike the 1-hr OLS that excludes SMC, the 10-hr model without SMC was broken into two regression. The first regression was fit on data observations below SMC of 20.9% (A in Table A.2) and the second regression was fit on observations above SMC of 20.9% (B in Table A.2).

Table A.2: Scaled regression coefficients for 1-hr FMC regression. Regression intercept is α and regression residuals are represented by ϵ. Significance level of each coefficient is based on robust p-values. Model performance is assessed by AIC and RMSE. P-values of homoscedasticity test (BP) and residuals' normality (SW) test are provided, where the null hypothesis is the assumption of homoscedasticity and normality of the studentized residuals. Lastly, expected value of studentized residuals is reported as $E[\epsilon]$

Coefficient	Estimate	Robust p-value	Significance
$FMC_{1-hr} = \alpha + \beta_{VPD}VPD + \beta_C C + \beta_{SE}SE + \beta_W W + \epsilon$			
α	0.000	1.000	
VPD	-0.345	0.000	***
C	0.609	0.000	***
SE	0.224	0.000	***
W	-0.100	0.108	
AIC=202 RMSE=0.62			
SW p-value=0.65 BP p-value= 0.50 E[ϵ]=0.00			
Significance Level: · 0.1, * 0.05, ** 0.01, *** 0.001			

Table A.3: Scaled regression coefficients for 10-hr FMC regression fitted on data observations below SMC of 20.9% (A) and on observations above SMC of 20.9% (B). Regression intercept is α and regression residuals are represented by ϵ. Significance level of each coefficient is based on robust p-values. Model performance is assessed by AIC and RMSE. P-values of homoscedasticity test (BP) and residuals' normality (SW) test are provided, where the null hypothesis is the assumption of homoscedasticity and normality of the studentized residuals. Lastly, expected value of studentized residuals is reported as $E[\epsilon]$.

Coefficient	Estimate	Robust p-value	Significance
$FMC_{10-hr} = \alpha + \beta_{VPD}VPD + \beta_C C + \beta_{SE}SE + \beta_W W + \epsilon$			
A. Data corresponding to SMC $< 20.9\%$			
α	-0.140	0.006	**
VPD	-0.155	0.006	**
C	0.423	0.000	***
SE	0.080	0.152	
W	-0.089	0.047	*
AIC=110 RMSE=0.76			
SW p-value=0.02 BP p-value= 0.06 $E[\epsilon] = 0.00$			
B. Data corresponding to SMC $\geq 20.9\%$			
α	0.240	0.331	
VPD	-0.422	0.008	**
C	0.627	0.001	**
SE	0.480	0.137	
W	-0.279	0.177	
AIC=79.8 RMSE=0.85			
SW p-value=0.01 BP p-value= 0.34 E[ϵ]=0.03			
Significance Level: · 0.1, * 0.05, ** 0.01, *** 0.001			

Alternative 10-Hr Regression Models

In Section X, we fitted WLS regression to quantify the effect of soil moisture on 10-hr FMC. In this section we present other statistical models that quantify the effect of SMC on FMC. Namely, these models are: OLS with robust errors, log-transformed FMC, and polynomial

OLS with robust errors

When fitting OLS to 10-hr FMC data, the residuals were non-normally distributed and heteroscedastic. Though the coefficients are unbiased in the presence of heteroscedasticity, their standard errors cannot be estimated because OLS assumes equal variance of the residuals. Heteroscedasticity consistent standard errors (HCE, aka standard errors) is a

Table A.4: Scaled coefficients for 10-hr FMC OLS. Regression intercept is α and regression residuals are represented by ϵ. Significance level of each coefficient is based on robust p-values. Model performance is assessed by AIC and RMSE. P-values of homoscedasticity test (BP) and residuals' normality (SW) test are provided, where the null hypothesis is the assumption of homoscedasticity and normality of the studentized residuals. Lastly, expected value of studentized residuals is reported as $E[\epsilon]$

Coefficient	Estimate	Robust p-value	Significance
α	0.000	1.000	
SMC	0.380	0.000	***
VPD	-0.210	0.003	**
C	0.453	0.000	***
SE	0.122	0.082	.
W	-0.114	0.096	.

AIC=212   RMSE=0.645
SW p-value=0.00   BP p-value= 0.00   E[ϵ]=0.01

Significance Level: · 0.1,   * 0.05,   ** 0.01,   *** 0.001

method to correct for the heteroscedasticity and to obtain error estimates, thus allowing to test coefficients for their significance without changing their estimates (White, 1980). Of course if the underlying model is not correct, than the coefficients cannot be trusted in the first place. Table A.2 provides a summary of 10-hr OLS with robust errors. We can see that the regression is heteroscedastic, since the BP test has a p-value of 0.00, where the null hypothesis is that the residuals are homoscedastic. However, using robust errors, we can conclude that SMC is a significant predictor of FMC, explaining larger variance in FMC than VPD. Though canopy percentage remains the best predictor. Though, the OLS model is not the most appropriate model to describe the SMC-FMC relationship, because the residuals have big deviations from a normal distribution and are non-linear.

Log-transformed

If data analysis shows non-linear relationship between variables, variable transformation may result in a better model fit. Both explanatory and response variables can be transformed and there are different transformation functions that can be applied. In the following section we present log-transformed FMC model, where we fit a regression using the same explanatory variables as described in the Methods Section X, however the response variable, FMC, is log-transformed. Table A.2 provides a summary of 10-hr OLS with log-transformed FMC. The model passes homoscedasticity, normality, and linearity tests. In this model formulation, SMC is a significant predictor of FMC. The magnitude of the SMC coefficient is slightly lower than that of the VPD, but overall canopy percentage

Table A.5: Scaled coefficients for 10-hr log-transformed FMC OLS. Regression intercept is α and regression residuals are represented by ϵ. Significance level of each coefficient is based on robust p-values. Model performance is assessed by AIC and RMSE. P-values of homoscedasticity test (BP) and residuals' normality (SW) test are provided, where the null hypothesis is the assumption of homoscedasticity and normality of the studentized residuals. Lastly, expected value of studentized residuals is reported as $E[\epsilon]$

Coefficient	Estimate	Robust p-value	Significance
$log(FMC_{10-hr}) = \alpha + \beta_{SMC}SMC + \beta_{VPD}VPD + \beta_C C + \beta_{SE}SE + \beta_W W + \epsilon$			
α	0	1.000	
SMC	0.202	0.012	*
VPD	-0.277	0.000	***
C	0.564	0.000	***
SE	0.166	0.010	*
W	-0.157	0.010	*

AIC=195   RMSE=1.66
SW p-value=0.48   BP p-value= 0.19   E[ϵ]=0.00

Significance Level: · 0.1,   * 0.05,   ** 0.01,   *** 0.001

explains the largest portion of variation in FMC. A disadvantage of transforming variables is that it is difficult to interpret different model coefficients and some of the physical relationships may become less clear, therefore this model was not selected by us to explain the role of SMC on FMC in the main text. Nonetheless, log-transformed model supports the conclusions made by the WLS regression.

Polynomial Regression

Since the relationship between 10-hr FMC and SMC appears to be non-linear (Figure XX), we have fit a piecewise regression to describe the relationship between SMC and FMC in the main text. This relationship is based on the discontinuous relationship between soil moisture and soil evaporative flux. To assess other non-linear relationships, we have fit a second order (quadratic) orthogonal polynomial regression to explain variation in FMC. Orthogonal polynomials were selected over raw polynomials to reduce collinearity. The regression coefficients are summarized in Table A.6. Since the quadratic term is insignificant, we do not expect a quadratic regression to be a good model to describe SMC-FMC relationship.

Table A.6: Scaled regression coefficients for 10-hr FMC orthogonal polynomial regression. Regression intercept is α and regression residuals are represented by ϵ. $P_1(SMC)$ and $P_2(SMC)$ are 1st and 2nd order orthogonal polynomials of SMC. Significance level of each coefficient is based on robust p-values. Model performance is assessed by AIC and RMSE. P-values of homoscedasticity test (BP) and residuals' normality (SW) test are provided, where the null hypothesis is the assumption of homoscedasticity and normality of the studentized residuals. Lastly, expected value of studentized residuals is reported as $E[\epsilon]$

Coefficient	Estimate	Robust p-value	Significance
$FMC_{10-hr} = \alpha + \beta P_1(SMC) + \beta P_2(SMC) + \beta_{VPD}VPD + \beta_C C + \beta_{SE}SE + \beta_W W + \epsilon$			
α	0.000	1.000	
$P_1(SMC)$	3.930	0.003	**
$P_2(SMC)$	1.715	0.113	
VPD	-0.177	0.001	***
C	0.433	0.000	***
SE	0.093	0.109	
W	-0.130	0.019	*
AIC=207 RMSE=0.62			
SW p-value=0.00 BP p-value= 0.50 E[ϵ]=0.00			

Significance Level: · 0.1,   * 0.05,   ** 0.01,   *** 0.001

A.3   Spatial Soil Moisture and Ignition Probabilities

In Section 3.3.2, we discuss the spatial distribution of probability of ignition that is based on 10-hr FMC. To derive probability of ignition across ICB, we relied on spatially distributed vegetation cover, soil moisture, temperature, and vapor pressure deficit maps. Some of these are shown in Figure A.4. Both vapor pressure deficit and temperature maps not shown) were spatially scaled from the temporary weather station location (lat -119.57, lon 37.68, elevation 2,136 m) to the rest of the ICB using a temperature lapse rate of $-0.007^oC/m$ (Boisramé et al., 2019b), where ICB elevation is shown in Figure A.4-A. Percent canopy map used for ICB (Figure A.4-C) is based on LANDFIRE 2016 canopy product. LANDFIRE reports percent canopy for both forest and shrubland vegetation. In Figure A.4-B, we set all percent canopy for all shrubland cover types to 0%, since we do not expect sufficient shading to affect fuel moisture. In reality, there is likely to be an effect, but we assume that shading provided by the shrub cover is a lot lower than the shading provided by forest cover type for an equivalent percent canopy value. Lastly, used spatial soil moisture maps for ICB for spring (end of May) and fall (beginning of August) of 2017 which were derived based on Boisramé et al. (2017) methodology. These soil moisture maps are shown in Figure A.4-C and D).
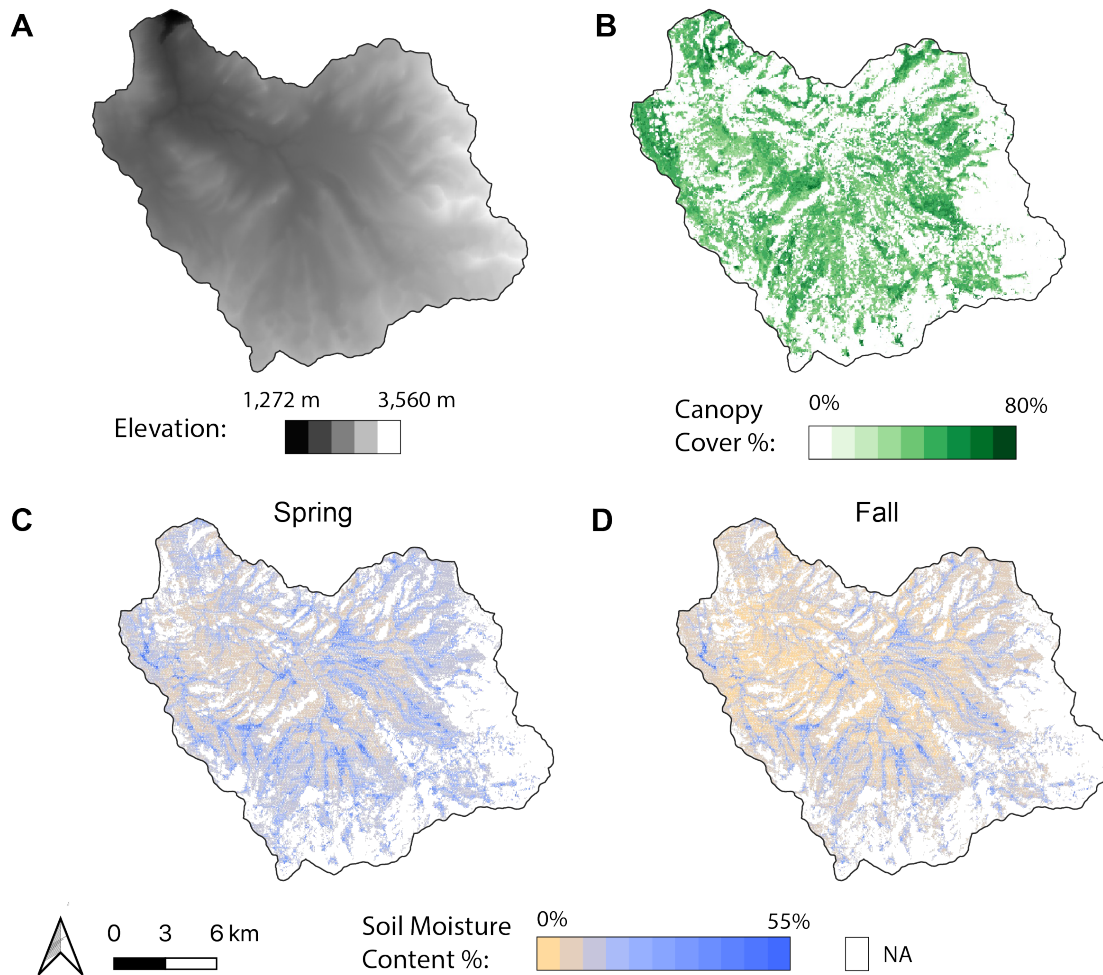
Figure A.4: Spatial variables that were used as inputs to calculate fuel moisture content and associated probabilities of ignition. Digital elevation model (DEM) of the ICB (A) was used to scale weather station temperature VPD measurements across the basin; percent canopy maps were derived from LANDFIRE's 2016 existing vegetation cover. All non-forest vegetation canopy cover and exposed rock (white color) was set to zero; Volumetric soil moisture content in the Illilouette Creek Basin representative of the spring (C) and fall (D) conditions in 2017. The soil moisture maps are representative of the top 12 cm mineral soil water content. Areas that do not have associated soil moisture values (white color) are either exposed rock or bodies of water.

Probability of ignition maps for spring and fall of 2017 are based on 10-hr FMC (Figure A.5). Two methods were used to derive spatial probability of ignition: 1) regression that does not include SMC as a predictor (A.5-A and B), and 2) regression that uses SMC as

a predictor (A.5-C and D).

Probability of Ignition Without Soil Moisture

Probability of Ignition With Changing Soil Moisture

Figure A.5: Probability of ignition maps based on 10-hr FMC are shown for spring and fall of 2017. The top figures are derived based on regression that excludes SMC from FMC predictions, and the bottom set of figures calculates FMC based on piecewise regression with SMC as a predictor

Appendix B

Supporting Information for Chapter 4

B.1   Sugarloaf Creek Basin Site Information

Table B.1: All fires from FRAP (2017) perimeter database that burned within SCB. Percent and area burned at high severity is based on the relative differenced normalized burn ratio (RdNBR) using the thresho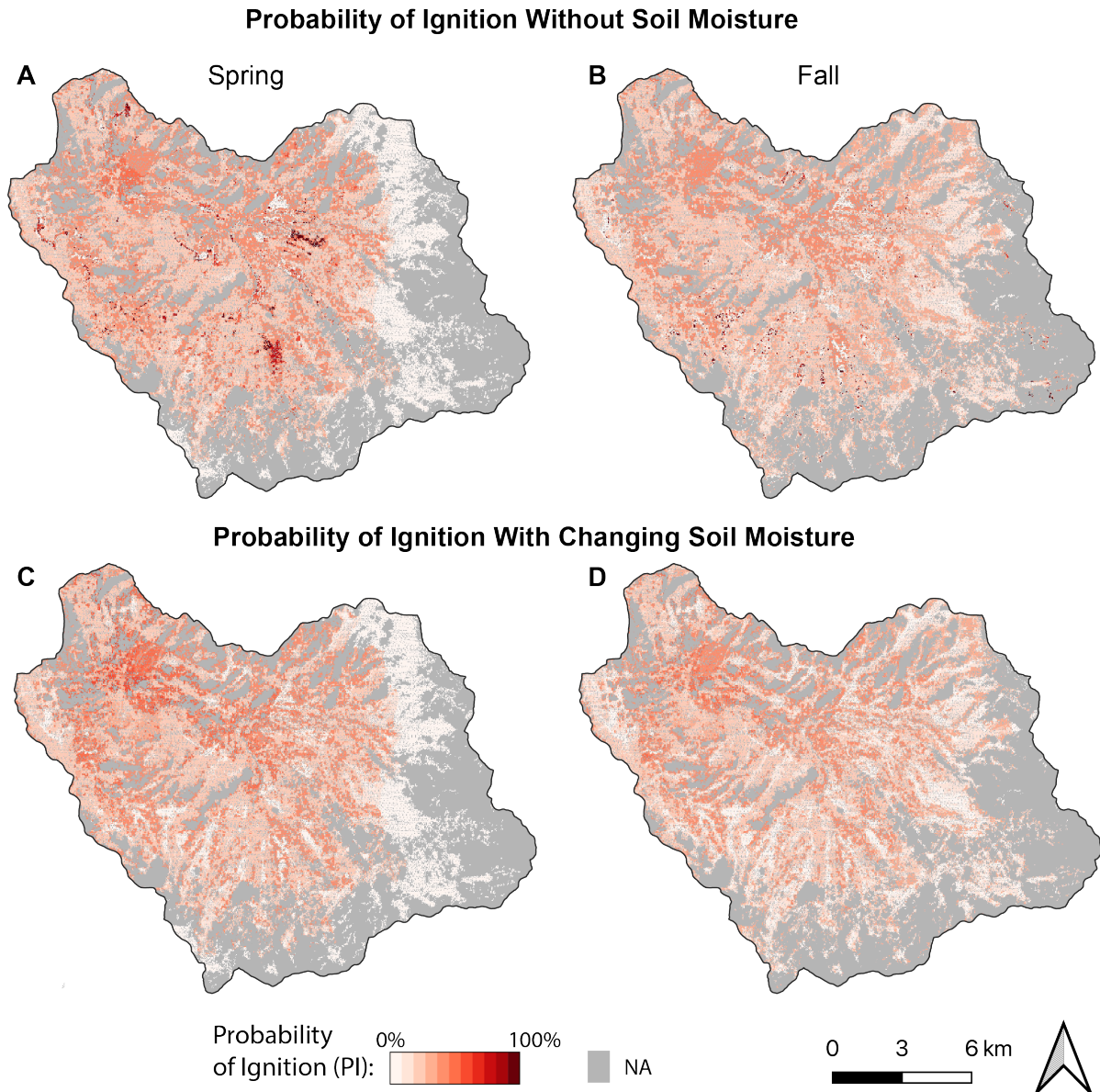ld from Miller and Thode (2007). The satellite imagery used to compute RdNBR is only available from 1984 on. RdNBR assessments were not available for fires smaller than 20 ha.

Year	Name	Report date	Total area (ha)	Area of watershed burned (ha)	Percent high-severity (%)	Area high-severity (ha)	Included in analyses?
1952	Sugarloaf	19-Jun	15	15	NA	NA	N
1964	Williams	2-Oct	5	5	NA	NA	N
1971	Ball Dome	13-Aug	99	99	NA	NA	N
1972	Sugar Valley	15-Sep	16	5	NA	NA	N
1973	So. Sentinel	28-Aug	1084	1038	NA	NA	Y
1974	Comanche	22-Jul	1219	1219	NA	NA	Y
1976	In Between	29-Jul	13	13	NA	NA	Y
1977	Sugarloaf	20-Jul	264	264	NA	NA	Y
1977	Ferguson	26-Jun	4219	1594	NA	NA	Y
1980	Roaring	1-Aug	170	72	NA	NA	Y
1985	Sugarloaf	28-Jul	1153	1152	1	12	Y
1988	Sugarbaby	20-Jun	3	3	NA	NA	Y
1992	Ellis Meadow	2-Jun	57	57	0	0	Y
1997	Sugarloaf	15-Aug	114	114	6	7	Y
1999	Williams	18-Sep	232	232	0	0	Y
2003	Williams	28-Jul	1429	1427	3	50	Y
2004	Ferguson	7-Jul	1	1	NA	NA	N
2006	Pond	13-Aug	5	0	NA	NA	N
TOTAL			**10,098**	**7310**	**2**	**69**	

Table B.2: Specific discharge (total streamflow volume divided by watershed area) from the Merced Watershed (which contains ICB) and South Fork Kings River Watershed (which contains SCB) illustrate drier conditions in the region including SCB. IRMA = irma.nps.gov/AQWebPortal Large Watershed Sub-Watershed Measurement

Large Watershed	Sub-Watershed Measurement Point	Gage or Data Source	Lat/Lon	Sub-watershed Area	Years Used for Mean	Mean Annual Specific Discharge (Flow/Area)
South Fork Kings	SF Kings River Near Cedar Grove, CA[1]	USGS 11212500	36o48'25"N 118o44'55" W	1056 km^2	1950-1957	0.55 m/yr
South Fork Kings	Kings River near Hume, CA[1]	USGS 11213000	36o50'50" N 118o53'50" W	2160 km^2	1921-1958	0.4 m/yr
Merced	Illilouette Creek at Ill. Falls Bridge	IRMA	37º42'43" N 119º33'35" W	150 km^2	2011-2017	0.8 m/yr
Merced	Illilouette Creek at base of Illilouette Falls	Modeled[3]	37º43'32" N 119º33'27" W	150 km^2	1972-2017	0.9 m/year
Merced	Merced River at Happy Isles Bridge nr Yosemite CA[2]	USGS 11264500	37º43'53" N 119º33'33" W	469 km^2	1921-1958	0.66 m/yr
Merced	Merced River at Pohono Bridge nr Yosemite CA[1]	USGS 11266500	37º43'01" N 119º39'55" W	831 km^2	1921-1958	0.65 m/yr

1: These two gages on the Merced River are located downstream of where flow from ICB enters the Merced River (although they measure flow draining
2: These two gages on the Merced River are located downstream of where flow from ICB enters the Merced River (although they measure flow draining
3: Model based on Boisramé et al. (2017)

B.2 Sugarloaf Creek Basin and Illilouette Creek Basin weather station sites

We installed three temporary weather stations in Sugarloaf Creek Basin (SCB) in September 2016, with one weather station each in dense meadow, shrub, and mature mixed conifer vegetation types, and all sites located within 200m of each other at an elevation of approximately 2400 m (Figure B.1). All stations are located at least 30 m from the nearest edge of their respective vegetation patches. The dense meadow weather station site has dense grass cover with some conifer regeneration, but no overstory above the weather station. It is situated in an area that burned at high severity in 2003. The shrub weather station consists of whitethorn ceanothus (Ceanothus cordulatus) interspersed with grasses, some conifer regeneration, and no overstory above the station. The SCB shrub site also burned at high severity in 2003. The mixed conifer site has little herbaceous vegetation, and mature mixed conifers form the overstory. This site burned at low severity in 2003. Fire severity characterizations are based on remote sensing, aerial photography and visual observations of tree mortality at each site. Three similar weather stations were installed in 2015 at ICB (station elevation 2100 m; Figure B.2). The ICB wetland site contained less conifer regeneration than SCB, and was predominantly vegetated with tall grasses. The shrub site in ICB was comprised mostly of whitethorn ceanothus (Ceanothus cordulatus) when weather stations were installed, but burned at high severity during the 2017 Empire Fire, resulting in bare soil with little live vegetation during the 2018 WY. The SCB shrub site by contrast contained a dense growth of young conifers with a mix of ceanothus and grass. The forest sites in the two basins were similar in terms of tree density, tree species. Topographic variables between the sites were also generally similar (Table B.3), and all sites were forested prior to being burned.

Table B.3: Topographic attributes of each weather station, including slope, aspect, elevation and topographic wetness index (TWI). All of these values were calculated from digital elevation models (obtained from Kane et al. (2015) for ICB, and USGS for SCB).

	May 23rd, 2017			August 5th / 9th 2017		
	Wetland	Forest	Shrub	Wetland	Forest	Shrub
Spatial average	48%±13%	8.7%±2.3%	7.5%±1.8%	41%±14%	1.3%±1.2%	1.0%±0.6%
12cm weather station	49%	11%	10%	49%	2.2%	2.9%

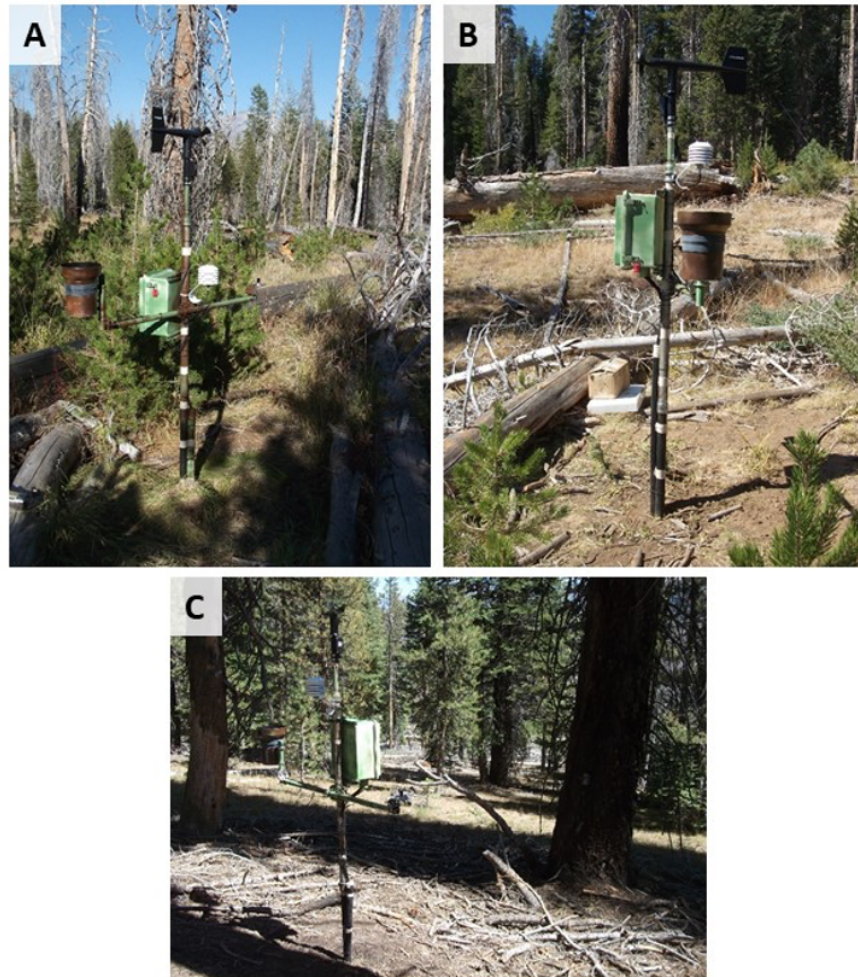Figure B.1: Images of weather stations in Sugarloaf Creek Basin. These stations are located in three nearby areas: one relatively wet site dominated by grasses and conifer recruitment (A; referred to as "wetland" in the main text), one drier site with sparse conifer recruitment and shrub growth (B; referred to as "shrub" in the main text), and one with an intact mature conifer canopy (C; referred to as "forest" in the main text).
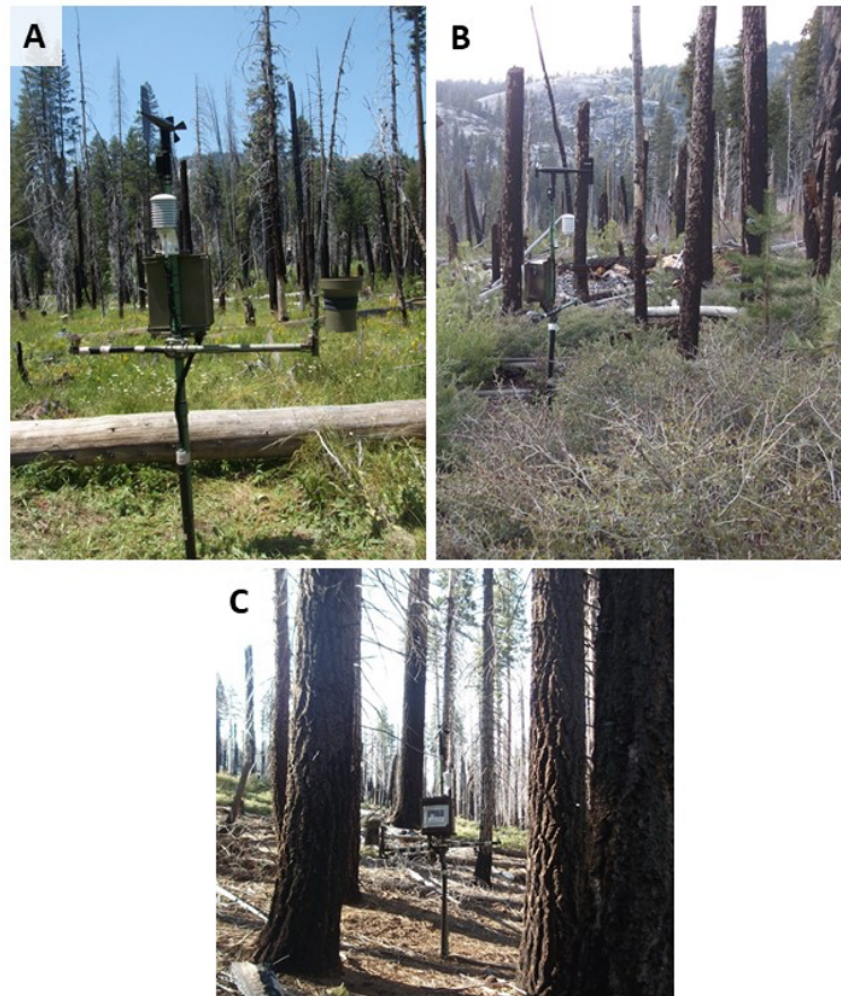
Figure B.2: Images of weather stations in Illilouette Creek Basin. These sites are dominated by wetland vegetation (A; "wetland"), shrubs and conifer recruitment (B; "shrub"), and a mature conifer canopy (C; "forest").

Soil samples were collected during the installation of the sub-surface TDR probes, and analyzed for soil texture properties at the UC Davis Analytical Laboratory (Davis, CA, USA). Soils were loamy sand or sand at all sites and depths, with the wetland sites containing more silt and organic content (at shallow depth) than the others. Shallow wetland soils (top 10cm) in both ICB and SCB had higher organic matter and silt content compared to both deeper wetland soils and all shrub/forest soils, although soil texture at both SCB and ICB did not vary greatly with depth. Precipitation at SCB was measured at 10-minute intervals by a 0.1-inch Campbell Scientific TE525 tipping bucket rain gauge (6-inch diameter orifice). The rain gauges were not heated, and the weather stations generated incomplete precipitation records due to frozen tipping buckets, downtime for station maintenance, and damage by wildlife. Where possible, we gap-filled precipitation at one station using predictive mean matching (R package "MICE") to perform multiple imputations of the missing data. Predictive mean matching (Little, 1988) is an advantageous technique for large datasets having non-normal distributions, and discrete values with physical bounds (in our case precipitation cannot be less than zero). When all three stations were missing precipitation data (only the case at SCB), we first identified periods of snowmelt using increases in shallow soil moisture, and then gap-filled these periods using snowmelt (as determined by a decrease in snow depth observed from field cameras). Snow depth was converted to snow water equivalent (SWE) using snow density measurements taken at Rowell Meadow (station RWM, cdec.water.ca.gov), a nearby snow course: 0.30 cm water / cm snow in January/February of 2017, and 0.52 in May/June of 2017 (the two periods when precipitation gap-filling was necessary). All calculations were rounded to the nearest 0.1 inch (2.54 mm), the smallest increment in the rain gauge. Soil moisture was measured at 10-min intervals by horizontally installed Campbell Scientific 300 mm two-prong TDR probes (CS650) at 12, 60, and 100 cm depths. We compared soil moisture observations from the weather stations to the average of a spatially-distributed grid of local measurements made with the hand-held soil moisture meter (Table B.2). Spatial averages were calculated from 25 measurements made in a 100 x 100 ft (30.48 m) grid centered on each weather station site, and compared to the 12 cm deep TDR at the weather stations. The consistency between the results indicates both that the weather stations were representative of their local area and that the mobile and in-situ instrumentation performed similarly. The slightly wetter measurements found at the weather stations are due to the spatially-distributed measurements averaging soil water content vertically from the surface 12 cm depth, and the buried moisture probes averaging soil water content horizontally at a depth of 12 cm. To investigate another metric of relative water balance differences between the three vegetation sites, we calculated cumulative shallow soil moisture gain at each site, defined as the cumulative increase in shallow soil moisture over the duration of the study. We averaged the two soil moisture measurements at 12 cm and 60 cm depths ("shallow soil") at every 10-minute measurement interval, and then calculated a six-hour moving-window average soil moisture for each measurement interval using all measurements on three hours on either side of the target measurement interval to eliminate signal noise. An increase between two consecutive 10-minute average soil moisture records was considered

Table B.4: Comparison of spatially averaged (±1 standard deviation) shallow soil moisture readings and the time averaged in-situ TDR soil moisture readings at 12cm at the SCB weather stations. In the late summer campaign, wetland and forest sites were measured on August 5th, and the shrub site on August 9th.

	WY 2016	WY 2017	WY 2018
Weather Station, ICB	580 mm	1102 mm	563 mm
PRISM, ICB	1028 mm	2017 mm	797 mm
Weather Station, SCB	NA	761 mm	487 mm
PRISM, SCB	843 mm	1491 mm	673 mm
ICB/SCB, Weather Stations.	NA	1.45	1.16
ICB/SCB, PRISM	1.22	1.35	1.19
PRISM/Station, ICB	1.77	1.83	1.42
PRISM/Station, SCB	NA	2.65	1.63

to be water gain in the shallow soil column. To convert percent volumetric water content (VWC) measured by the probes to a depth of water accumulated at each time step, we multiplied the increase in VWC between two measurements by 48 cm (the depth of the shallow soil moisture column; decreases and zero values between intervals were ignored). Cumulative soil moisture gain is thus the sum of soil moisture gains for each individual 10-minute timestep over the course of the recorded water year. Data are shown in Table 4.1.

The weather stations reported more precipitation in ICB than SCB (Table B.4), with the differences being larger (1.3-1.6 times more precipitation in ICB than SCB) in 2017 (a wet year) than 2018 (1.1-1.2 times more precipitation in ICB), a dry year. Precipitation totals for ICB are conservative for 2017 WY because of the removal of the weather stations prior to the Empire Fire (September through the end of November 2017). At least two precipitation events occurred during this time. Comparing the weather station precipitation estimates to PRISM data (http://www.prism.oregonstate.edu) at the same locations shows the same general trends in space and time, giving us confidence in our estimates of the relative differences in precipitation between the basins, even if the exact values do not agree (Table B.4). PRISM precipitation is highly uncertain in the Sierra Nevada, and the differences in annual total precipitation do not indicate that ICB/SCB measurements are erroneous (Henn et al., 2018).

Table B.4. Annual precipitation estimates for water years (WY) 2016 through 2018. Weather station estimates are averaged between the non-forest stations at each watershed (ICB and SCB) as these stations should not experience interception losses. The ratio of precipitation between sites and between datasets show that for 2016-2018 ICB always received more annual precipitation than SCB (regardless of dataset), and PRISM always estimated higher precipitation than our weather stations.

Most precipitation in both basins is in the form of snow, and the basins had different

snowpack depths (Figure B.3). Snow data in 2017 are incomplete for SCB because of periods of time when the snowpack covered the cameras. Nonetheless, we estimate that snow depth was similar between the two sites during the 2017 and 2018 WYs. In ICB manual snow depth measurements were taken in a grid around each weather station in March 2016, January and April 2017, and March 2018 (points and error bars on Figure B.3 for ICB), but manual measurements were not made at SCB because the site was inaccessible in the winter. For both locations and all water years, the wetland station had the greatest snowpack depth and the latest melt date, and the forest station had the lowest snowpack depth and earliest melt date.
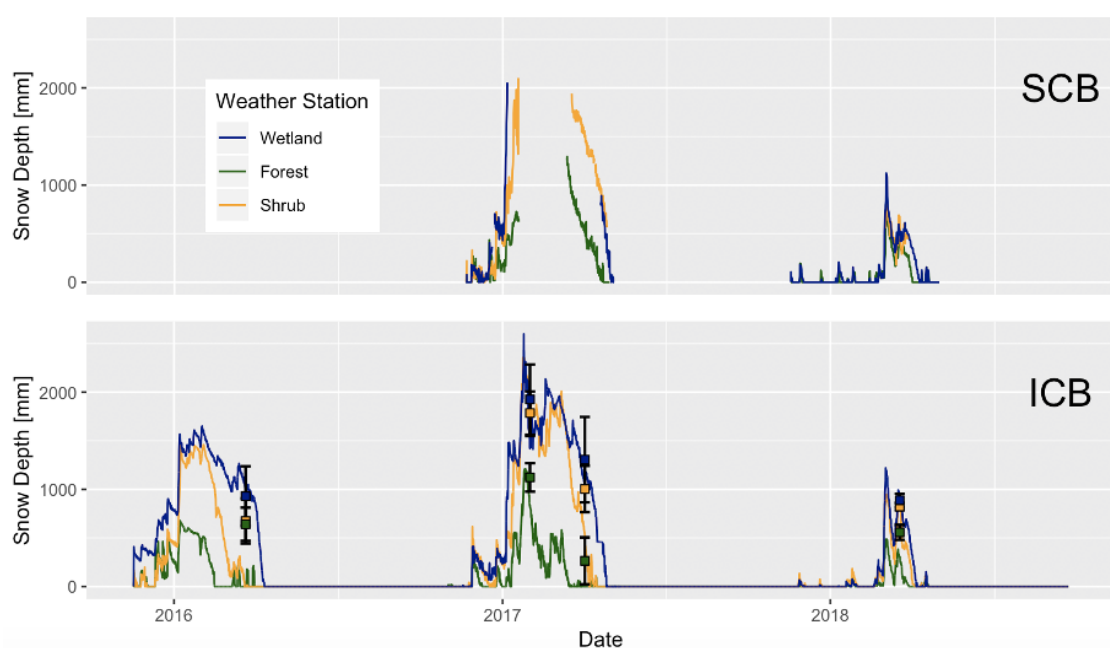

Figure B.3: Snow depth (in mm) for Sugarloaf Creek Basin (top) and Illilouette Creek Basin (bottom) as measured from images taken four times each day at wetland, shrub, and forest weather station sites. Additionally, error bars (squares indicating mean, and bars indicating standard deviation) are shown for manually measured snow depths in ICB. In SCB, cameras were covered during peak snowpack for 2017-18 winter, and the shrub camera stopped working before full snowmelt, resulting in missing data.

B.3 Details of landscape changes

Methods

To assess vegetation transitions within SCB, we used our classified images from 1973 and 2014 to calculate the number of pixels that underwent each possible transition among those four categories (including pixels that remained the same). Our null expectation of vegetation change was that a transition between two vegetation types was equally likely in each direction, with this transition probability estimated by summing the number of pixels in each direction of change between a given pair of vegetation types, and dividing by two. We then compared the distribution of pixels in each of the resulting sixteen potential vegetation transition classes against an expected distribution (holding the number of unchanged pixels constant) using a chi-squared test. We determined the residual proportion of expected change, compared to the null expectation, as a percentage (increase or decrease) from the null expectation for a given transition class. To calculate and compare vegetation patch metrics for ICB and SCB, we used FRAGSTATS software (https://www.umass.edu/landeco/research/fragstats/fragstats.html) to analyze vegetation maps created from images taken in 1973 and 2014 (SCB) and from images taken in 1969/70, 1987, 1997, 2005, and 2012 for ICB. For both watersheds, the first year of imagery (either 1973 or 1969/70) coincided with the end of a long period of fire exclusion and suppression, and represents vegetation before the first fire in the managed wildfire era. The vegetation maps divided land cover into four vegetation classes: forest, shrub, sparse meadow, and dense meadow. For SCB, areas south of the southernmost extent of historical fires were removed from the landscape change analysis, since this area consisted mostly of isolated patches of vegetation surrounded by rock and caused misleading values (this was not necessary for ICB, which contained very little mapped vegetation in the rocky high-elevation areas). Isolated pixels surrounded by different vegetation types were removed from the maps before processing by merging them with the surrounding vegetation type, which minimized differences caused by small isolated patches that were likely due to classification error or would be difficult to capture the same way using two sets of imagery. Diversity indices describe heterogeneity by measuring how patches of vegetation are distributed spatially across the landscape and capture fire-related landscape changes well (Romme, 1982). We evaluated the following diversity metrics:

1. *Shannon's Evenness Index* (SHEI) is the Shannon's Diversity Index (calculated using information theory) divided by the maximum diversity given the number of cover types present (McGarigal et al., 2012). An evenness index of 1 means that all vegetation types are equally represented in the landscape; higher evenness indicates greater landscape diversity.

2. *Simpson's Evenness Index* (SIEI) is similar, but is calculated using the probability that any two cells selected at random would be different patch types (McGarigal et al., 2012). Again, a value of 1 means all patch types cover an equal area, while a

value near 0 means that one type dominated nearly all of the landscape. We include both evenness indices in order to verify that the exact method of calculating evenness does not affect our results.

3. *Aggregation Index* (AI) is a measure of how much each vegetation type is clumped into a few large groups (high aggregation) or spread into many small groups (low aggregation).

Patch properties describe local-scale heterogeneity and the size and shape of individual vegetation patches. For this study, we used metrics which have been shown to be consistent across many different landscapes (Cushman et al., 2008): 1. Largest patch percent area (LPI) gives the percent of the total vegetated area taken up by the largest contiguous vegetation patch within each vegetation class. This metric gives an idea of the maximum area dominated by a single type of overstory. 2. Fractal dimension (FRAC) measures how complex and plane-filling the shapes are by using the relationship between the area and perimeter of a patch. As the dimension approaches 2, perimeter is maximized for a given area of coverage, while for simple geometries such as squares or circles the dimension is 1 (McGarigal et al., 2012). For example: a vegetation class with a low fractal dimension whose largest patch covers a large area indicates a spatially homogeneous region. On the other hand, a high fractal dimension suggests an increase in the total length of boundaries between patches of different types, thus increasing local heterogeneity. We also calculated the mean and standard deviation of the areas of all patches within each vegetation class. These measures help capture the changes in the distribution of patch sizes. All calculations were made on a rasterized vegetation map with a spatial resolution of 5 meters. This spatial resolution was chosen to match with calculations made on ICB vegetation (Boisramé et al., 2017).

SCB Landscape Change Results

As described in the main text results, transitions from shrub and mixed-conifer to sparse and to a lesser extent dense meadow were more strongly overrepresented in the burned areas than in the unburned areas (Figure B.4 c,d). Dense meadow area is limited in this watershed and saw limited expansion or contraction in absolute terms (Figure B.4).
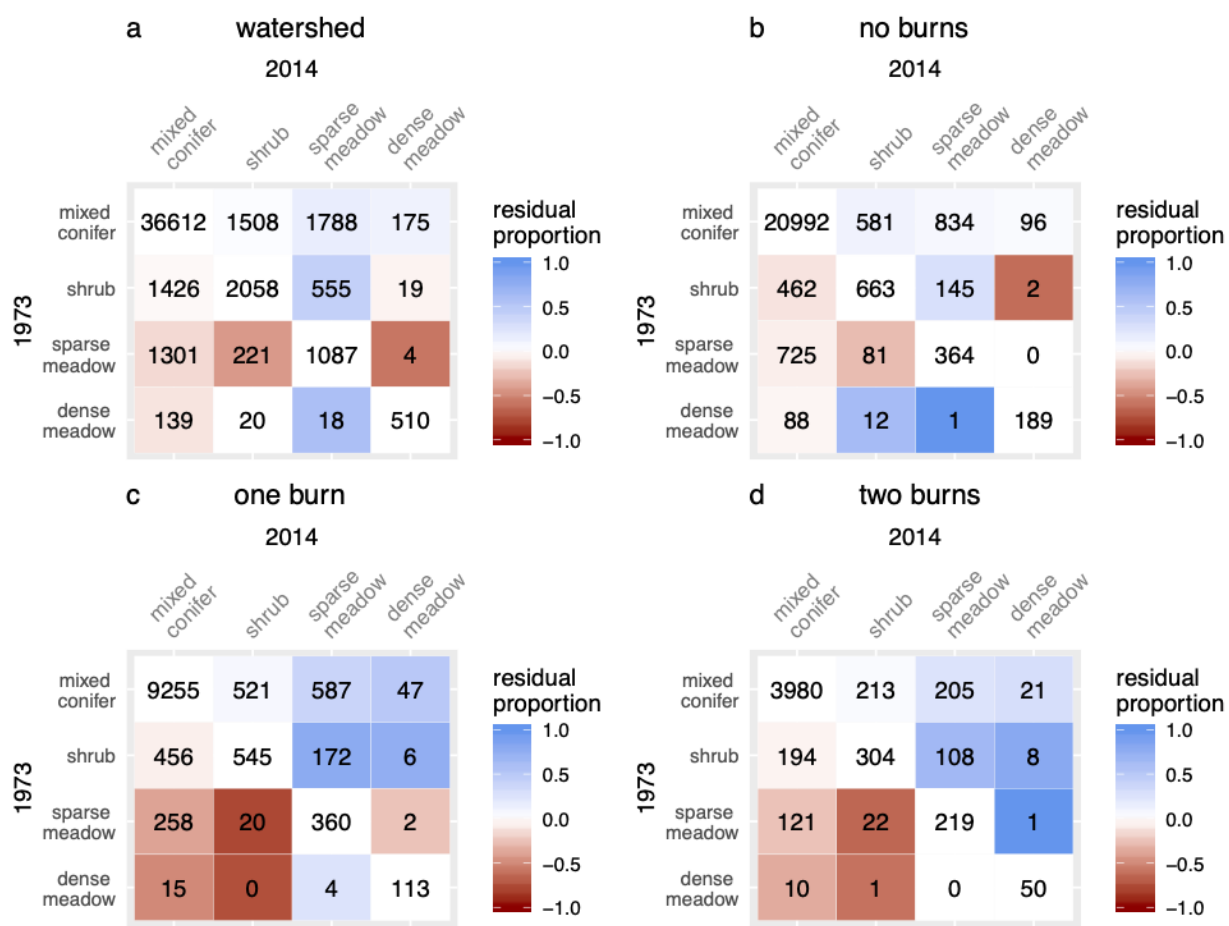
Figure B.4: Image change analysis. Colors indicated change in observed vegetation transitions relative to a null expectation of equally likely change in each direction. Color scale the proportion of the null expectation at which a given transition occurred, either more (blue) or less (red) than expected. Cell numbers indicate the number of 0.16 ha pixels in each transition category. Transitions occur from vegetation type in row (from 1973) to vegetation type in column (from 2014).

Vegetation Patch Metrics Results

Sugarloaf Creek Basin (SCB) showed a much smaller degree of landscape change than Illilouette Creek Basin (ICB). Diversity indices increased over time for both watersheds, but the change was negligible for SCB, demonstrating that landscape diversity rose only very slightly in response to fire (Figure B.5). The landscape-scale aggregation index increased slightly over time in SCB, in contrast to a decrease in ICB (Figure B.6). This could be due to fires creating larger areas of sparse meadow that are more aggregated

than pre-burn meadow areas (Figure B.7 b). The size of the largest vegetation patches did not vary appreciably in SCB between 1973 and 2014, with the exception of sparse meadows (Figure B.7). The mean and standard deviation of patch sizes, however, showed similar trends to ICB (Figure B.8). Most notably, conifer patches got smaller and less varied in size following 4 decades of fire (Figure B.8). While fractal dimension increased for all vegetation types in ICB, it remained flat or decreased slightly in SCB (Figure B.9). This may partially be due to fires creating a small number of new fairly homogeneous patches with simple geometries, but the small amount of change demonstrates that patch properties varied very little in response to fire in SCB. Relative proportions of each vegetation type were similar between the two watersheds (Figure 4.6; note that these proportions do not account for exposed rock). Both watersheds also had similar Shannon's Evenness Index values in their pre-fire/post-suppression states (Figure B.5). These similarities show that, despite differences discussed in the main text, the large-scale land cover types and distributions are comparable between these watersheds, making them useful to use as two case studies demonstrating how fire affects two similar landscapes in areas with slightly different climatology and geology.
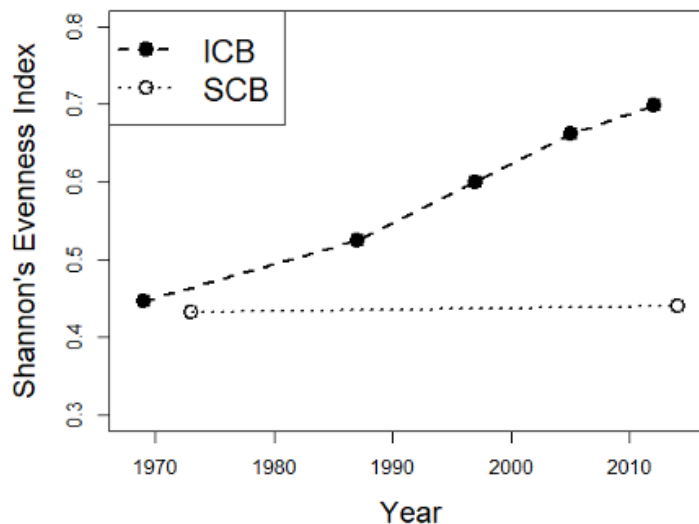

Figure B.5: Shannon's Evenness Index calculated for both ICB and SCB for each year that we created vegetation maps from aerial imagery
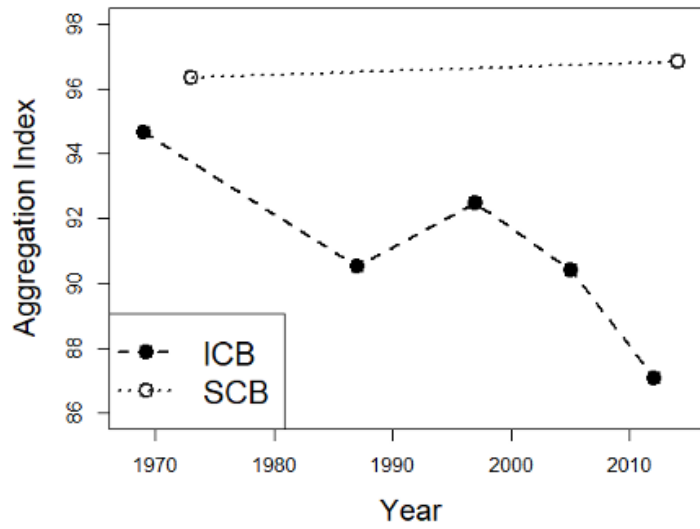
Figure B.6: Aggregation Index calculated for both ICB and SCB for each year that we created vegetation maps from aerial imagery.
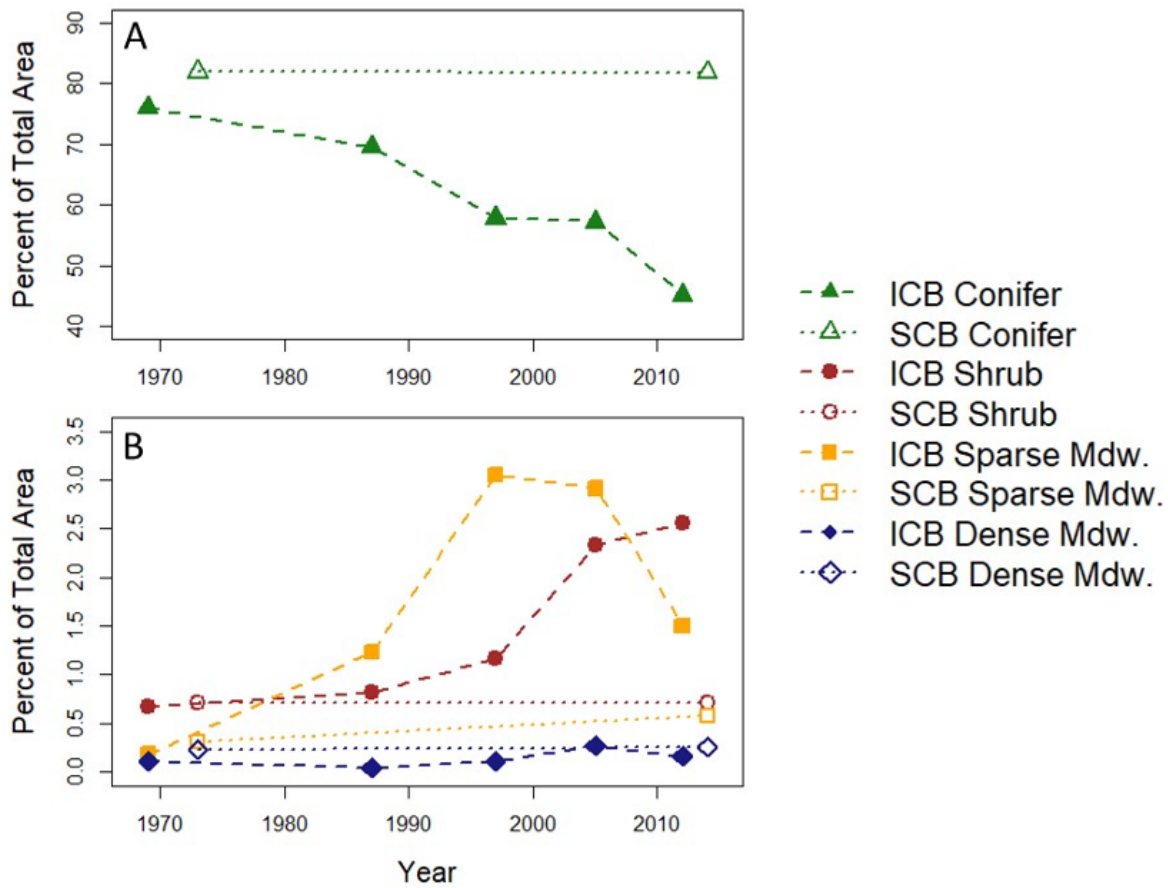
Figure B.7: Largest patch index (LPI; the percent of the total area occupied by the largest contiguous patch of vegetation) for each vegetation class for both ICB and SCB. Conifer (A) is shown separately from the other vegetation classes (B) due to large differences in scale.
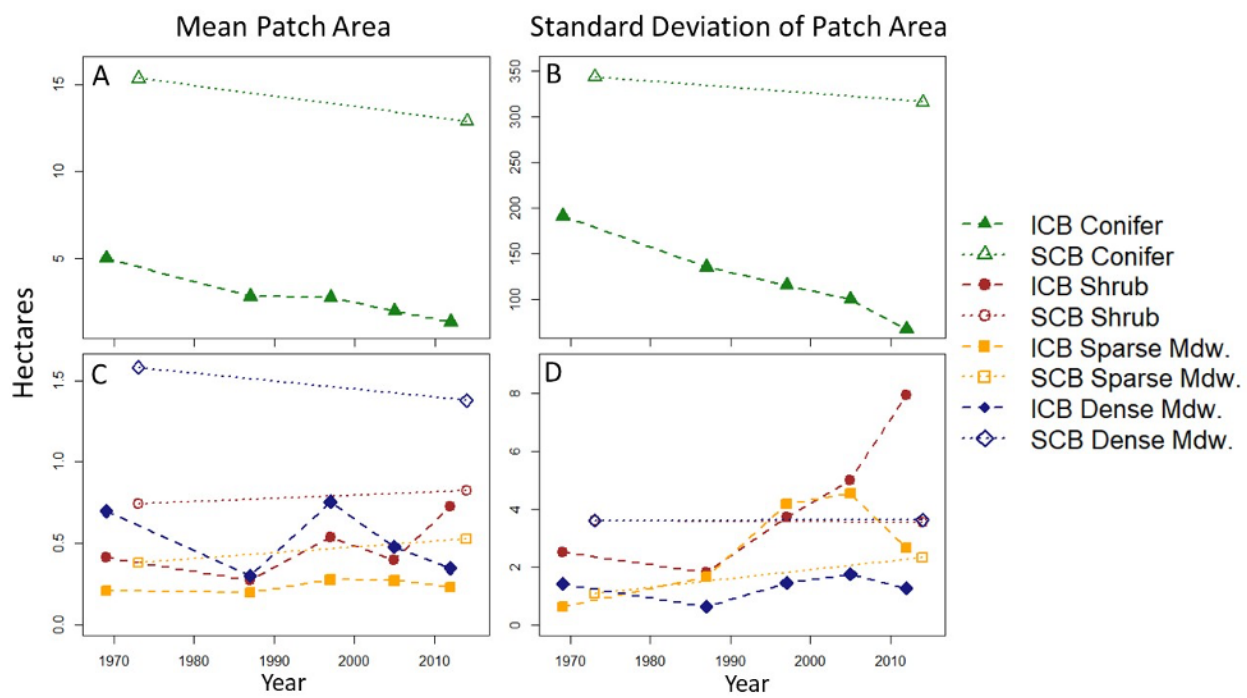
Figure B.8: Mean (A,C) and standard deviation (B,D) of patch size for each vegetation class for both ICB (dashed lines) and SCB (dotted lines). Conifer is shown separately (A,B) from the other vegetation classes due to large differences in scale.
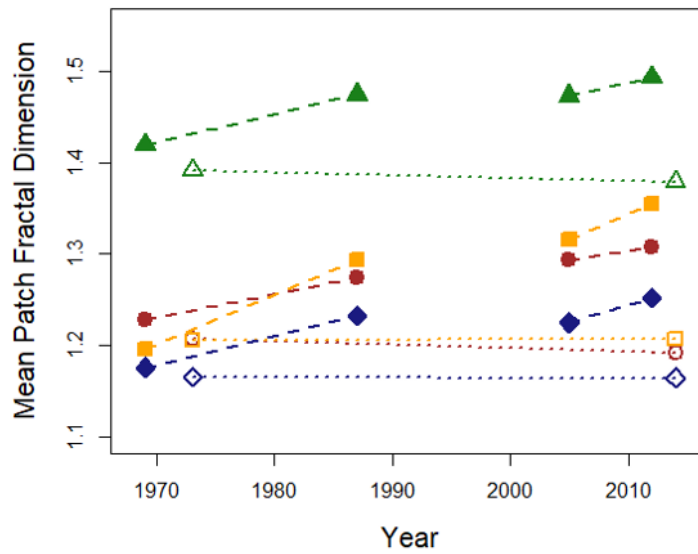
Figure B.9: Mean area-weighted fractal dimension of patches for each vegetation class for both ICB and SCB. 1997 is omitted due to small differences in mapping protocol affecting patch fractal dimension.
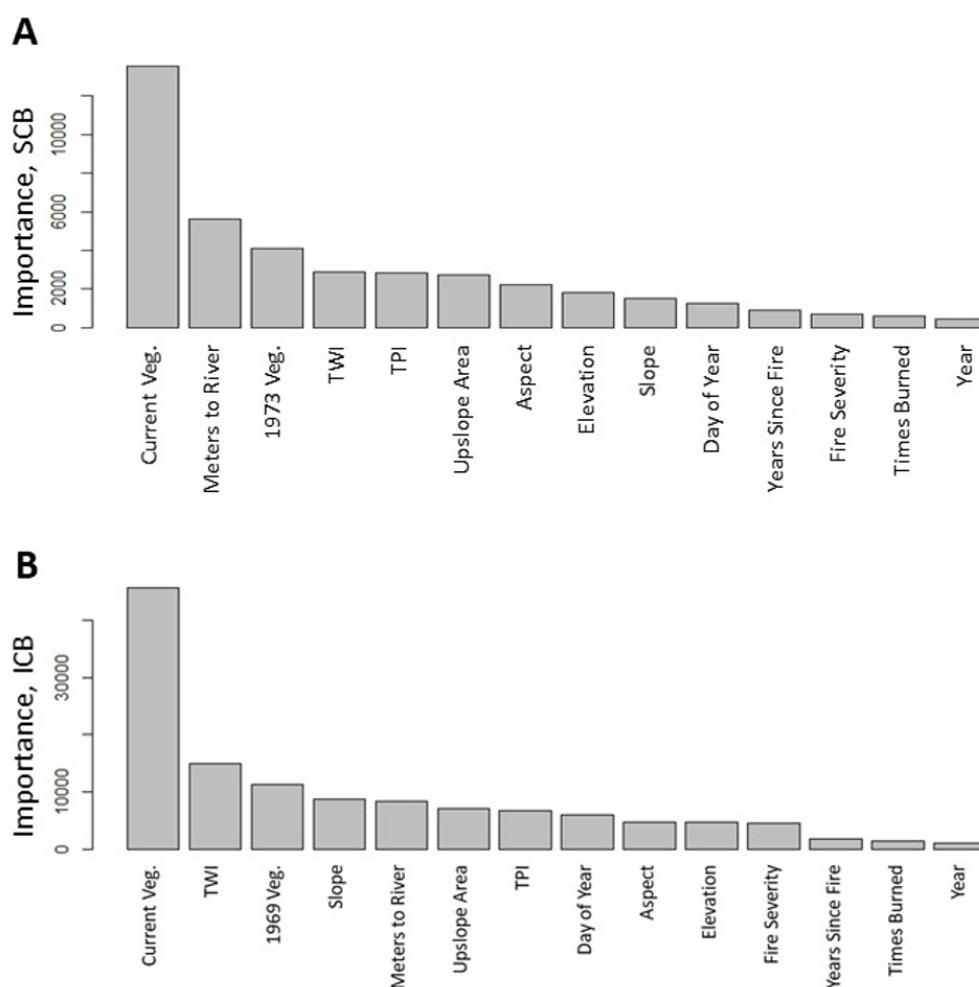
B.4 Detailed soil moisture model results

Figure B.10: Relative importance of each variable in predicting plot-level soil moisture for Sugarloaf Creek Basin (A) and Illilouette Creek Basin (B). Variables include 2014 vegetation (Current Veg), Distance from nearest stream, 1973 vegetation, topographic wetness index at a 10m resolution (TWI), Upslope contributing area, topographic position index calculated at a scale of 300m (TPI), aspect, elevation, slope, maximum fire severity, days since January 1 for the measurement (Day of Year), years since fire, times burned, and year of the measurement. A higher importance value indicates that including the given variable in the model leads to a larger reduction in model error (Liaw and Wiener, 2002).
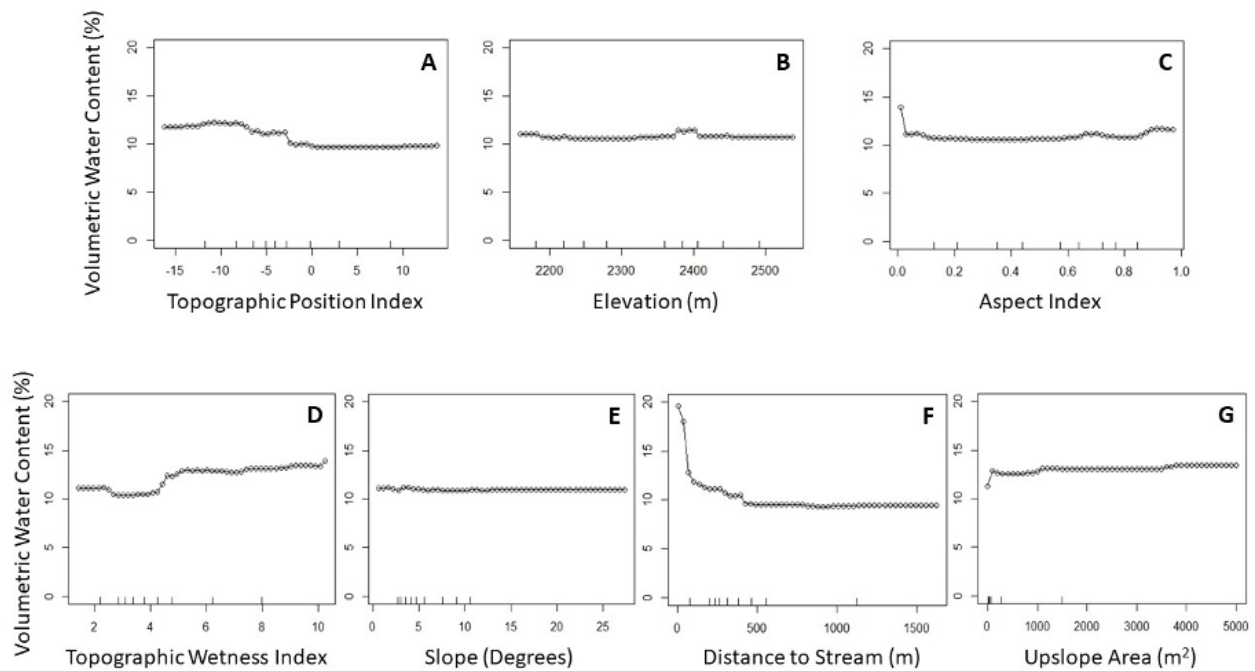
Figure B.11: Partial plots showing how the mean soil moisture (across all other possible variable values) varies with each topographic variable. These plots were created using the *randomForest* R package.
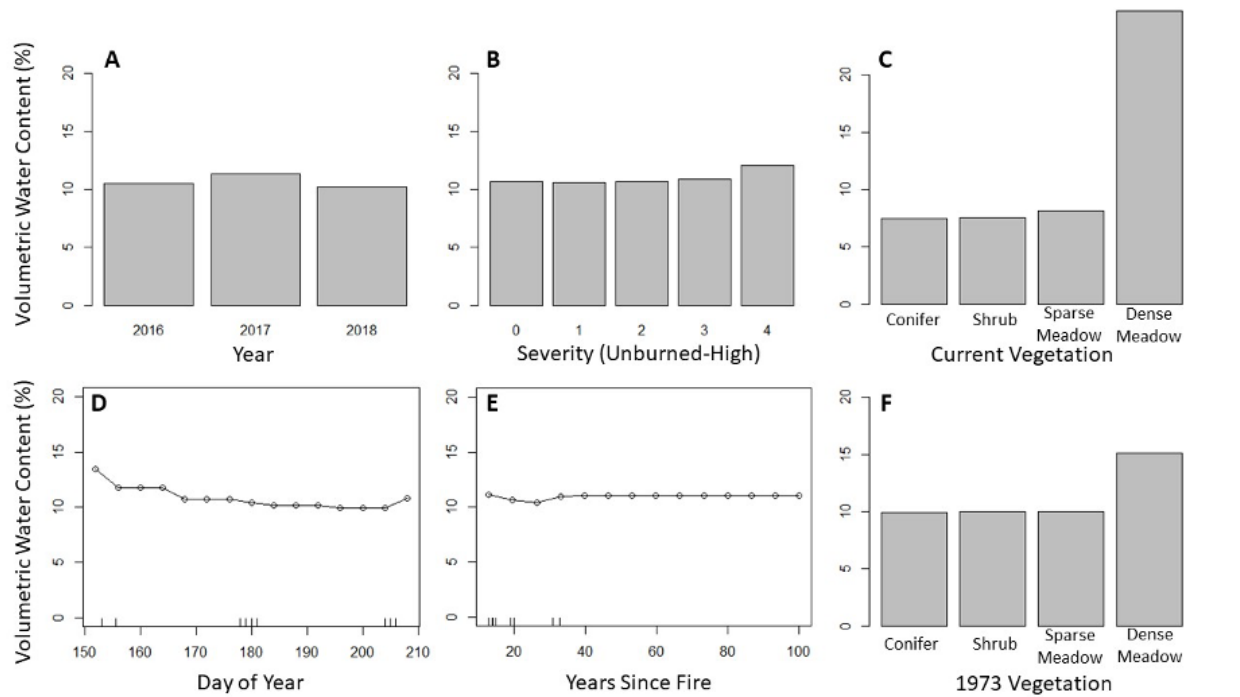
Figure B.12: Partial plots showing how the mean soil moisture (across all other possible variable values) varies with each non-topographic variable. Those variables treated as factors rather than continuous values in the model are shown as bar plots. Number of fires varied moisture by less than 0.4%, and is not shown. Current vegetation (C) is different from Figure 4.7 in the main text because Figure 4.7 modeled each measurement site explicitly, whereas the means shown here are taken across the entire range of possible covariates from all sites, regardless of whether a given site actually contained a given vegetation class. The difference occurs because meadows are more likely to be found in sites that are topographically prone to high moisture.
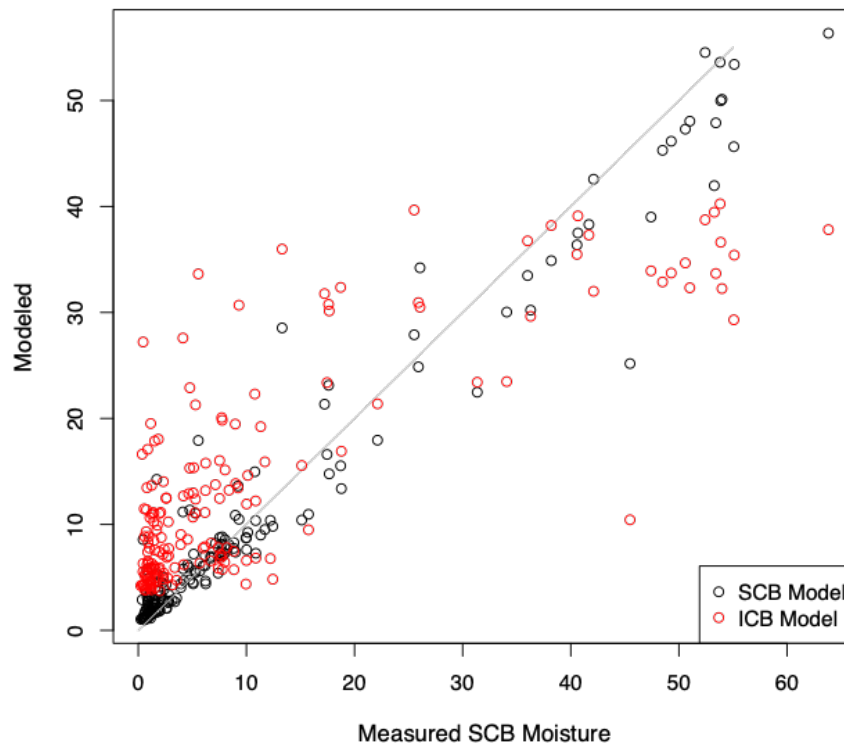
Figure B.13: Modeled versus measured soil moisture in SCB (site means). Red points are calculated using a model trained on ICB data; black points are from a model trained on SCB data.
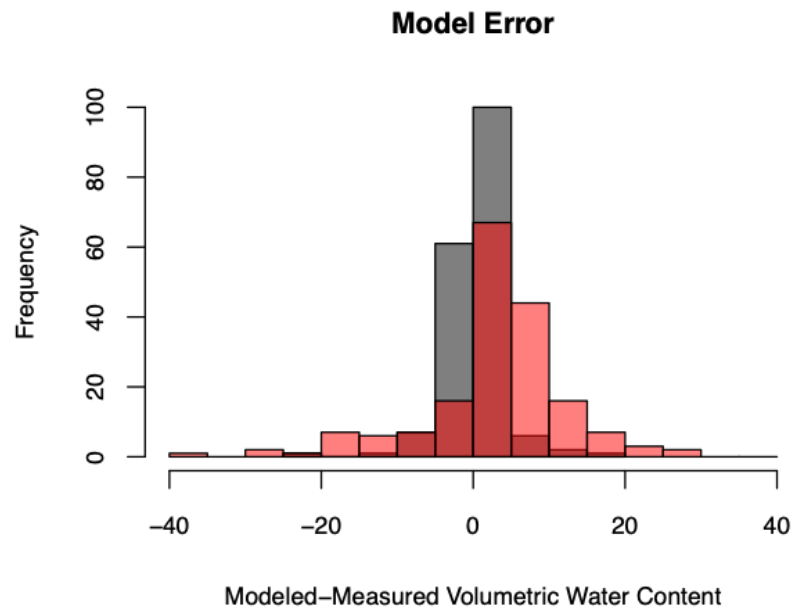
Figure B.14: Errors in predicting SCB soil moisture using a model trained on SCB data (grey) and on ICB data (red)
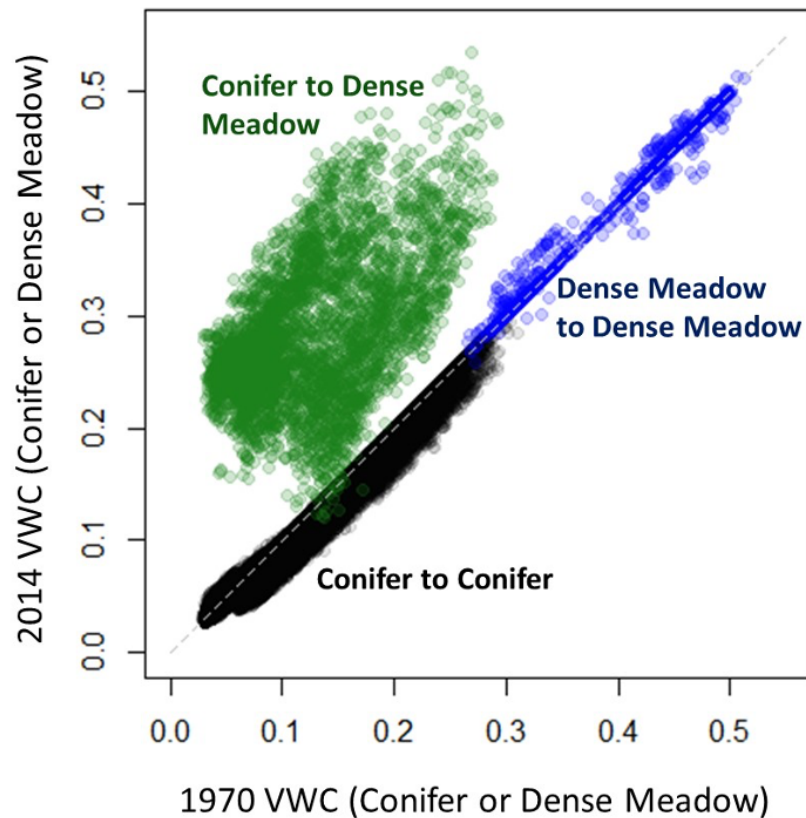
Figure B.15: Model results for Illilouette Creek Basin (ICB) showing volumetric water content (VWC, as a proportion between 0 and 1) at many points across the watershed using 2014 vegetation (after 40+ years of wildfires) versus 1970 vegetation (after nearly a century of fire suppression). Green points represent locations which were conifer-dominated in 1970 but converted to dense meadow by 2014. Black and blue represent locations which remained conifer or meadow, respectively. These model results suggest a much greater impact of fires on soil moisture in ICB compared to SCB (See Figure 4.8 in the main document). This figure is reproduced from Boisrame2018.

Appendix C

Supporting Information for Chapter 5

Introduction

This Supplementary Information provides additional detail on modeling results, including modeling assumptions, climate data, model uncertainty, post-fire vegetation transitions, and water supply and hydropower revenue calculations

C.1   Assumptions

The following table provides a summary of fire regime characteristics. We have considered how these can be affected in future climates and provided justifications for each characteristic.

Fire regime characteristics	Are future changes accounted for?
Individual fire area	No change expected in ICB Collins & Stephens (2007)
Individual fire severity proportions	No change expected in ICB Collins et al. (2009); Kolden et al. (2015)
Fire frequency	Historical and 2 future scenarios addressed Westerling & Bryant (2008) Batllori et al. (2013)
Post fire regeneration vegetation type	Provided uncertainty bounds (Section C.6)
Post fire rate of vegetation regeneration	RHESSys accounts for this

C.2   Climate Data

The minimum requirements for RHESSys inputs are precipitation and maximum and minimum temperature time series. The following section provides additional details about climate data used in historical and future climate modeling.

Weather Stations

Precipitation and temperature data from the Yosemite Headquarters (CDEC station YHQ; http://cdec.water.ca.gov/) weather station were used for historical modeling and to bias-correct future climate ensemble. Station YHQ has been operating at daily resolution since 1926 (elevation 1,225 m), however it has some missing records and gap filling was necessary. From January 1926 to October 2017, HQ station was missing 7.8% of its record. These gaps are largely covered by data recorded at adjacent stations (CDEC stations SEY at 1560 m, TUM at 2620 m, YOW at 1510 m, and GML at 2790 m). Only 0.1% of the total length of record is missing at all stations. Using the MICE package in R, precipitation and temperature data were gap-filled using the predictive mean matching algorithm in MICE (Little, 1988). Predictive mean matching works well with non-normally distributed data and draws from observed data, avoiding non-realistic values (such as negative precipitation).

RHESSys uses temperature and precipitation lapse rates to spatially distribute singular weather station inputs to the entire basin based on elevation. Boisramé et al. (2019a) provides details of how lapse rates were calculated. In addition to weather stations operated by the US National Park Service that are located at different elevations and have a long operating record, there are also temporary weather stations installed directly in ICB that have measured temperature and precipitation since the fall of 2015. Figure C.1 provides a comparison between the temperature profile recorded by station YHQ and one of the temporary weather stations installed in ICB (elevation 2,136 m). On average, the temperature in ICB is 7°C cooler than in Yosemite Valley, which is 911 m lower in elevation than the temporary weather station in ICB.

Global Circulation Models

Global circulation models (GCMs) were selected to represent possible future climates based on the criteria of having enough models to produce a range of possible hydrological outcomes in the future of ICB. Due to the high computational cost of including all of the available models in CMIP5, we sub-selected ten GCMs (step 1 in Figure C.2). The sub-selection process followed work by Knutti et al. (2013), which created a "family tree" of CMIP5 GCM models based on the pairwise distance of precipitation and temperature fields. The models were also color coded based on their similarity in code. We focused our model selection on those that were from different institutions and had dissimilar underlying atmospheric models while having high prediction skill. Table C.1 presents a summary of
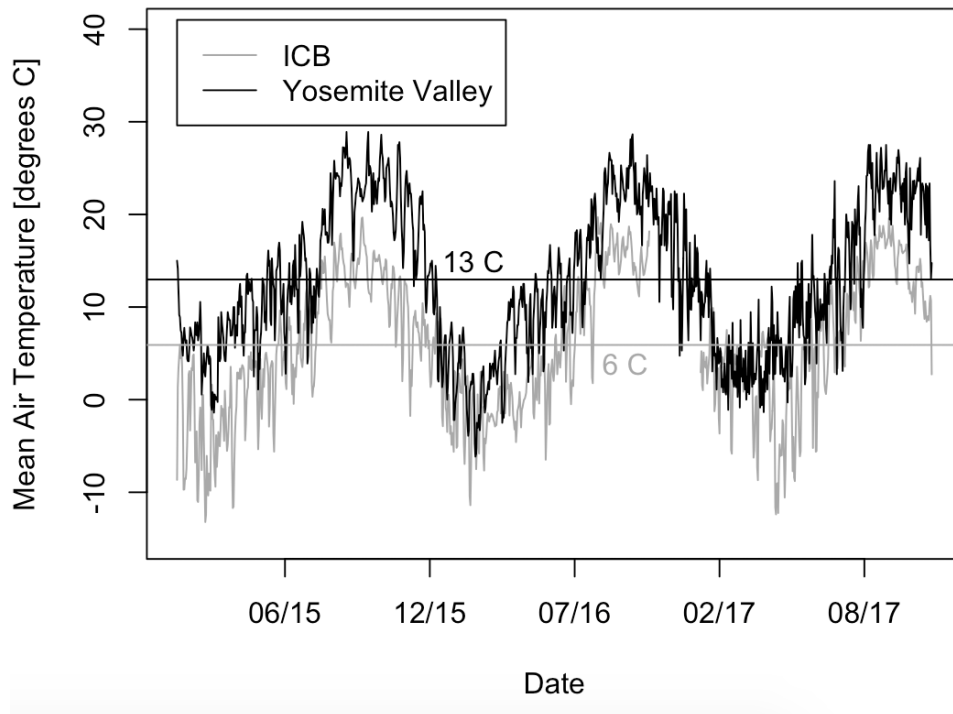
Figure C.1: Yosemite Valley weather station (YHQ) was used for both bias-correction of Global Circulation Models and for historical model simulation. Average daily temperature recorded by Yosemite Valley station is on average 7°C warmer than the temperature recorded by the temporary weather station that was installed in ICB in 2015 in a shrubland vegetation cover. RHESSys spatially downscales YHQ's climatic inputs to sub-units within ICB using lapse rates.

the 10 GCMs that were used in our modeling for both RCP 4.5 and RCP 8.5 climate scenarios.
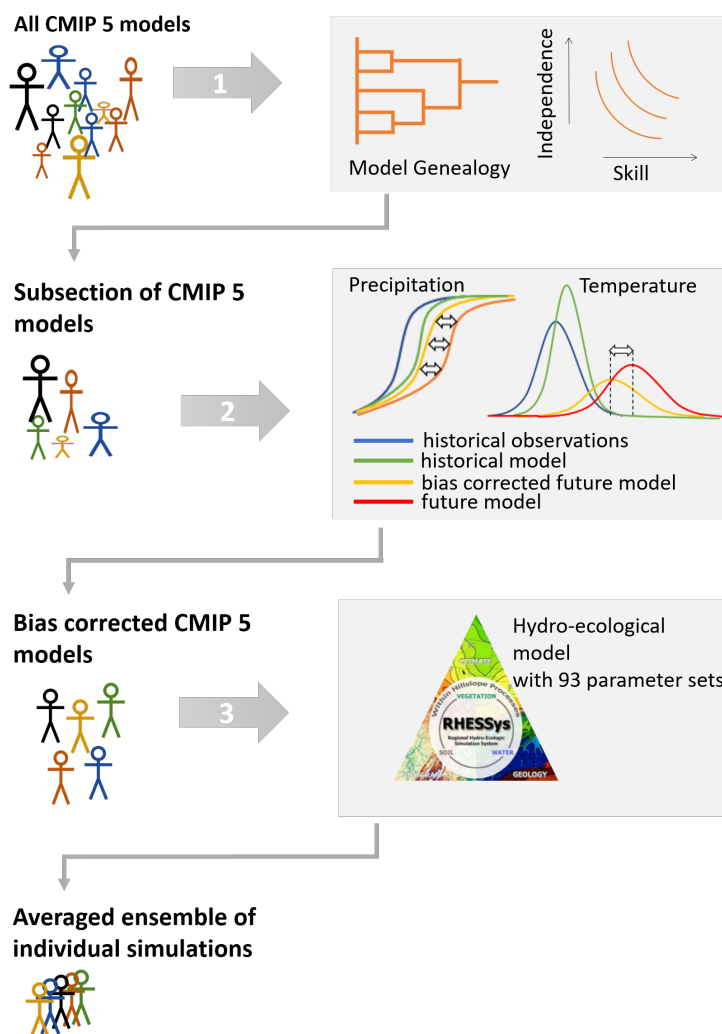
Figure C.2: A subset of 10 models (each model is represented pictorially as a stick person) is chosen based on skill and independence from all CMIP5 models with daily resolution for both RCP 4.5 and 8.5 scenarios (step 1), bias-correction is performed via quantile delta mapping (step 2), and the bias-corrected climate timeseries are individually used as inputs into RHESSys (step 3). The output from individual model runs is then averaged and confidence bounds obtained associated with both model parameter sets and the climate ensemble.

Table C.1: List of 10 GCMs used in the ICB climate ensemble, showing the modeling agency that produced each GCM, and the grid resolution available from the CMIP5 ensemble (Gregory Flato, 2013)

Model	Country	Organisation	Resolution (Lat x Lon)
ACCESS 1-3	Australia	Commonwealth Scientific and Industrial Research Organization (CSIRO) and Bureau of Meteorology (BOM)	1.25° x 1.875°
CanESM2	Canada	Canadian Center for Climate Modelling and Analysis	2.8° x 2.8°
CMCC-CM	Italy	The Centro Euro-Mediterraneo sui Cambiamenti Climatici	0.75° x 0.75°
CSIRO Mk3.6	Australia	Queensland Climate Change Centre of Excellence and Commonwealth Scientific and Industrial Research Organisation	1.875° x 1.875°
GFDL-ESM2M	USA	NOAA Geophysical Fluid Dynamics Laboratory	2° x 2.5°
inmcm4	Russia	Russian Institute for Numerical Mathematics	1.5° x 2.0°
IPSL-CM5A-MR	France	Institut Pierre Simon Laplace	2.5° x 1.25°
MIROC5	Japan	University of Tokyo, National Institute for Environmental Studies, and Japan Agency for Marine-Earth Science and Technology	1.4° x 1.4°
MRI-CGM3	Japan	Meteorological Research Institute	1.1° x 1.1°
NorESM1-M	Norway	Norwegian Climate Centre	2.5° x 1.9°

Temperature and precipitation data series from the GCMs shown in Table C.1 were extracted for the GCM cell containing the Yosemite Headquarters weather station. These data series were bias-corrected to the datasets described in Section C.2 using the quantile delta mapping approach (Cannon et al. (2015), step 2 in Figure C.2). Yearly sums and means of bias-corrected precipitation and air temperature averaged across 10 GCMs along with the historical record are shown in Figure C.3
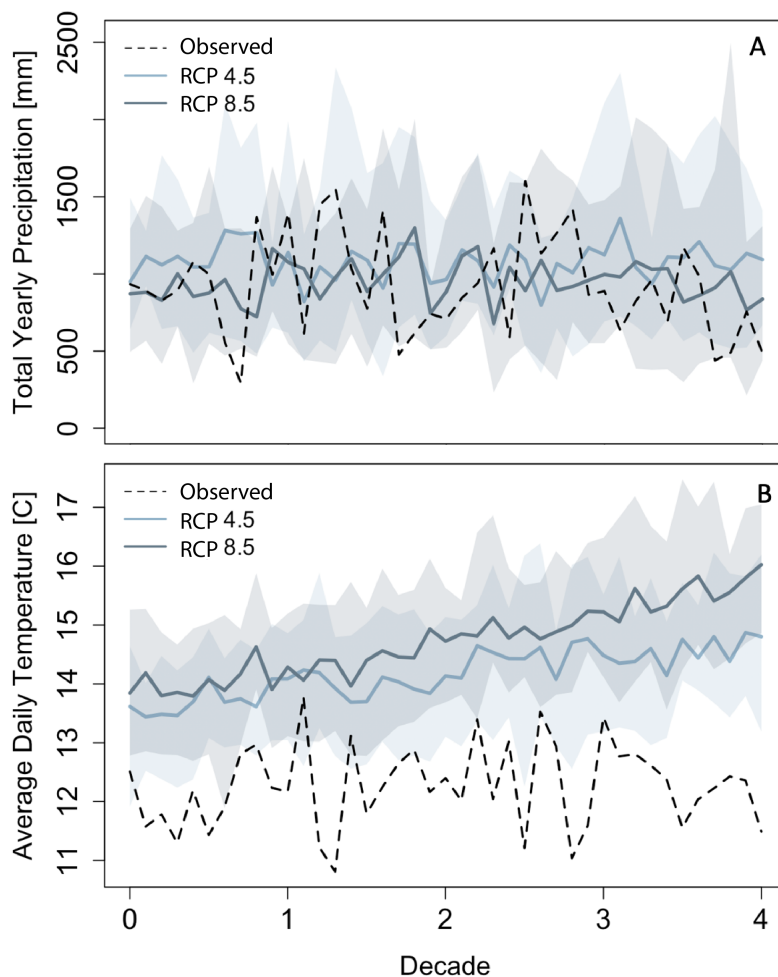

Figure C.3: Timeseries of yearly precipitation sums [mm] (A) and average daily temperatures [^{0}C] (B) for historical, RCP 4.5 and RCP 8.5 for the Yosemite Head Quaters location. Mean and 95th percentile of 10 GCMs is shown. Basin averaged historical precipitation timeseries is shown in dashed black. The x axis shows the decades from 1970-2010 for the historical data and 2030-2070 for the future climate scenarios.

Mean daily temperature is consistently greater for both future climate scenarios when

compared to the historical record, with the highest temperatures observed for the RCP 8.5 climate scenario. The historical climate data do not show obvious trends in time, but the RCP 4.5 and RCP 8.5 climate scenarios have a continuously rising temperature record (Figure C.3-B). The means of the daily precipitation for the RCP 4.5 climate scenario are similar to the mean of the daily precipitation for the observed historical climate C.4-A. For the RCP 8.5 climate scenario, the shape of the distributions varies vastly among climate models and when compared to the observed historical distribution. There are many peaks at the high end of the precipitation totals, suggesting an occurrence of extreme events (Figure C.4-B).
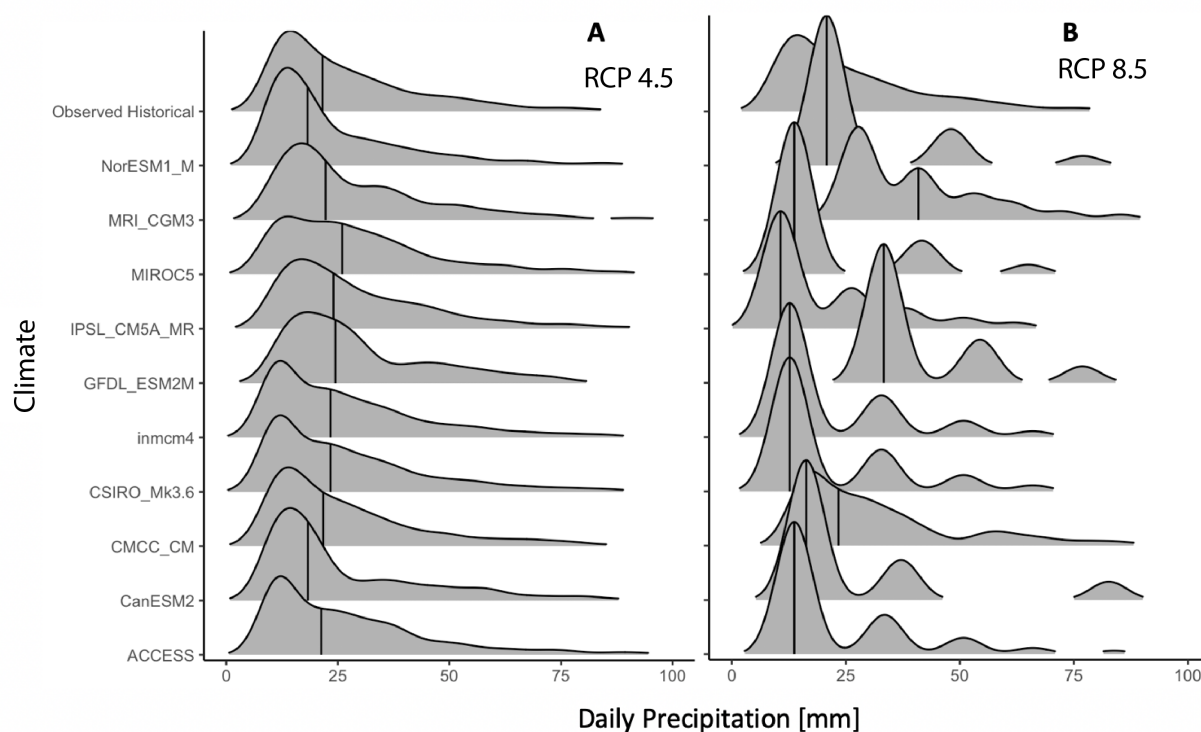

Figure C.4: Distribution of downscaled (to the location of Yosemite Headquarters weather station) daily precipitation [mm] for RCP 4.5 (A) and RCP 8.5 (B) climate scenarios for 10 GCM models (2030-2070) and the observed historical climate (1970-2010). Vertical dashes are means of the distribution

C.3 Wildfire Effects on Recent Vegetation and Streamflow

Wildfires burning with increasing high severity fractions could result from hotter and drier conditions in future climate. In turn, vegetation burning at high severity can have post-fire transition to vegetation prone to continue burning at high severity (i.e. shrubs) (Cornwell et al., 2012; Serra-Diaz et al., 2018). Fire severity and fire size have not been increasing throughout the wildfire management period (1972-2017) in ICB (Figure 3); we examine potential severity changes in more detail by comparing the re-burn severities of the Empire Fire of 2017 (most recent wildfire in ICB), to the Meadow Fire of 2004 (Figure C.5). The two fires have an overlapping burn area of 515 ha in ICB. Based on the Landsat-derived RdNBR maps, within the overlapping fire area, Meadow Fire on average burned at RdNBR of 585 while Empire Fire burned at a lower average of 466 RdNBR. Within the overlapping fire area, 26% of high severity (>650 RdNBR) fire area re-burned at low to moderate severity (<650 RdNBR), 14% of high severity also re-burned at high severity, and only 8% of low to moderate severity area re-burned at high severity in 2017. The non-overlapping RdNBR distribution for both fires was very similar (RdNBR of 252 Empire vs 272 Meadow).
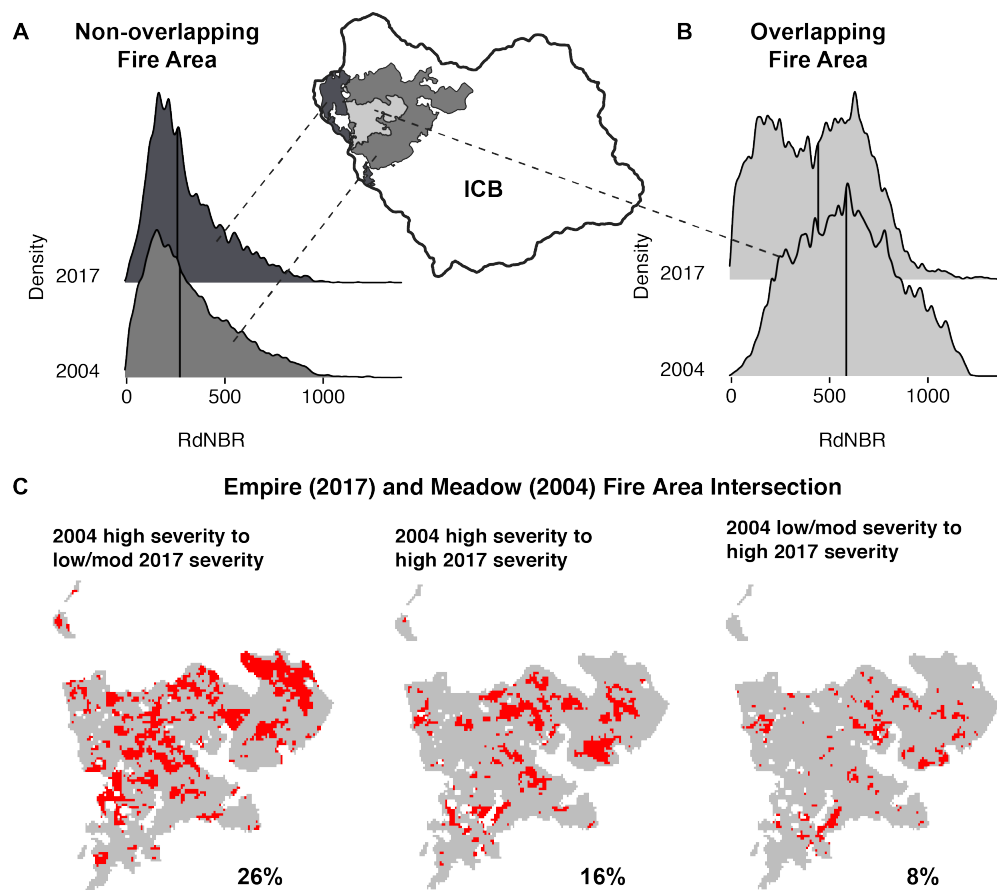
Figure C.5: The two most recent fires, Meadow in 2004, and Empire in 2017, had an overlapping fire area of 515 ha in ICB. RdNBR distribution for both the overlapping (A) and non-overlapping fire area (B) shows that the re-burned area in 2017 experienced lower severity than in 2004. Within the fire overlap area re-burn severity generally decreased from 2004 to 2017 (C). Pixels with an RdNBR<640 are classified as low/moderate severity, and pixels with RdNBR>640 are classified as high severity. Median of the RdNBR distributions is shown as a vertical line.

Even though there were multiple drought years and record high temperatures in the Sierra Nevada in the in the 2010's, based on Figure C.5, the high severity areas are not increasing in size and the fuel limiting fire behavior is apparent with lower re-burn severities.

C.4 Uncertainty Analysis

In this section we present a mathematical representation of how uncertainty was calculated for the differences between climate and fire scenarios.

In order to determine whether a modeled fire scenario had a significant impact on a given output variable (e.g., streamflow) compared to the fire exclusion scenario, the difference (D) between the scenarios would be given by:

$$D_{i,j} = f(p_i, c_j, fire_f) - f(p_i, c_j, fire_s) \quad \text{for } i = 1, ..., 93, \ j = 1, ..., 10 \quad \text{(C.1)}$$

where D is the difference between two RHESSys model scenarios and $f(p, c, fire)$ represents the RHESSys model output created using one of the 93 parameter sets (p_i), one of the 10 climate models (c_j), and a fire regime scenario ($fire_f$ for representing either historical frequency or a frequency increase of 30% or 60%, and $fire_s$ representing the scenario without fires). The climate scenario (observed, RCP 4.5, or RCP 8.5) would be held constant. A 95% confidence interval of the difference between fire scenarios would then be calculated by finding the middle 95% range of these 930 D values. Note that for the unique case of comparing fire scenarios under observed climate, there are only 93 D values in the ensemble since there is only one historical climate timeseries (c) rather than ten.

Similarly, in order to determine whether a future climate scenario (RCP 4.5 or RCP 8.5) combined with a given future fire scenario would cause a significant change compared to the observed climate and fire frequency, we would determine whether the 95% confidence interval of the following following 930 differences encompass zero:

$$D_{i,j} = f(p_i, c_j, fire_f) - f(p_i, c_{obs}, fire_h) \quad \text{for } i = 1, ..., 93, \ j = 1, ..., 10 \quad \text{(C.2)}$$

where c_{obs} is the observed climate, c_j is the future climate from one of the 10 climate models, and $fire_f$ refers to a potential future fire frequency. When $fire_f$ represents fire exclusion, then $fire_h$ is the excluded scenario; if $fire_f$ is historical, 30% increased frequency, or 60% increased frequency then $fire_h$ instead refers to the historical fire frequency in order to better compare the impact of future fire-climate scenarios versus actual observed scenarios.

C.5 RHESSys Outputs

This section provides additional RHESSys outputs and analysis of the different climate and fire regime scenarios that are useful for understanding the change observed in the water balance. This section discusses LAI, seasonality of water balance variables and snowpack, and changes in the maximum streamflow.

Table C.2: Decadally-averaged LAI (leaf area per ground area; dimensionless) for the four fire scenarios: fire excluded, historical frequency, 30% increase, and 60% increase in fire frequency and three climate scenarios: historical, RCP 4.5, and RCP 8.5 climate scenarios. Decades 1, 2, 3, and 4 refer to the time periods 1971-1980, 1981-1990, 1991-2000, and 2001-2010 for the observed climate, while for future climate scenarios (RCP 4.5 and 8.5) these decades refer to 2031-2040, 2041-2050, 2051-2060, and 2061-2070 respectively. Grey highlighting indicates a significant difference between modeled LAI in the future climate and the historically observed climate (Using Equation C.2). An asterisk indicates that wildfires significantly affected the modeled LAI (Using Equation C.1).

Scenario		Decade			
Fire	Climate	1	2	3	4
		LAI			
Fire Excluded	Observed	0.4	0.42	0.41	0.38
	RCP 4.5	0.52	0.48	0.49	0.5
	RCP 8.5	0.41	0.43	0.43	0.45
Historical Frequency	Observed	0.4*	0.41	0.4*	0.32*
	RCP 4.5	0.51*	0.48	0.47*	0.43*
	RCP 8.5	0.41*	0.42*	0.41*	0.37*
30% Increase	RCP 4.5	0.51*	0.44*	0.43*	0.4*
	RCP 8.5	0.41*	0.38*	0.36*	0.34*
60% Increase	RCP 4.5	0.51*	0.43*	0.42*	0.42*
	RCP 8.5	0.41*	0.37*	0.35*	0.35*

LAI

Leaf Area Index (LAI) is a proxy for the amount of canopy present in the basin, and places important constraints on the land surface energy budget and how vapor fluxes are partitioned between transpiration and evaporation. As fires remove vegetation, they reduce the total basin LAI and its distribution through the ICB. However, RHESSYs will model canopy growth and recovery and associated changes to LAI. Table C.2 shows LAI change under fire excluded, historical fire use and 30% and 60% future fire frequency scenarios for each climate case. In the fire excluded scenarios, LAI is maximal under RCP 4.5. The CO_2 levels are constant throughout all scenarios, therefore, precipitation and temperature differences are the drivers of the observed increase.

The response of LAI to changing climate and fire frequency is shown graphically in Figure C.6. The right hand-side plot (red colors) shows the effect of the historical wildfire use scenario for each climate. The greatest change in LAI due to fire the historical fire regime is observed for RCP 8.5 climate scenario, followed by RCP 4.5, and historical climate. This can be explained by the post-fire recovery rate of LAI, where LAI recovers faster in the historical climate.

Looking at the effects of the varying fire regimes (historical, 30%, and 60%) for both future

climate scenarios (RCP 4.5 and RCP 8.5) in the two left hand-side plots (blue colors) in Figure C.6, we observe that the more frequent fire regimes (30% and 60% increase in fire frequency) increases observed change in LAI by the final simulated decade and decrease the amount of time it takes to observe maximum change. Though by the final simulated decade, LAI does not change much due to fire because the carbon stores for the re-burn areas are sufficiently low (data not shown).
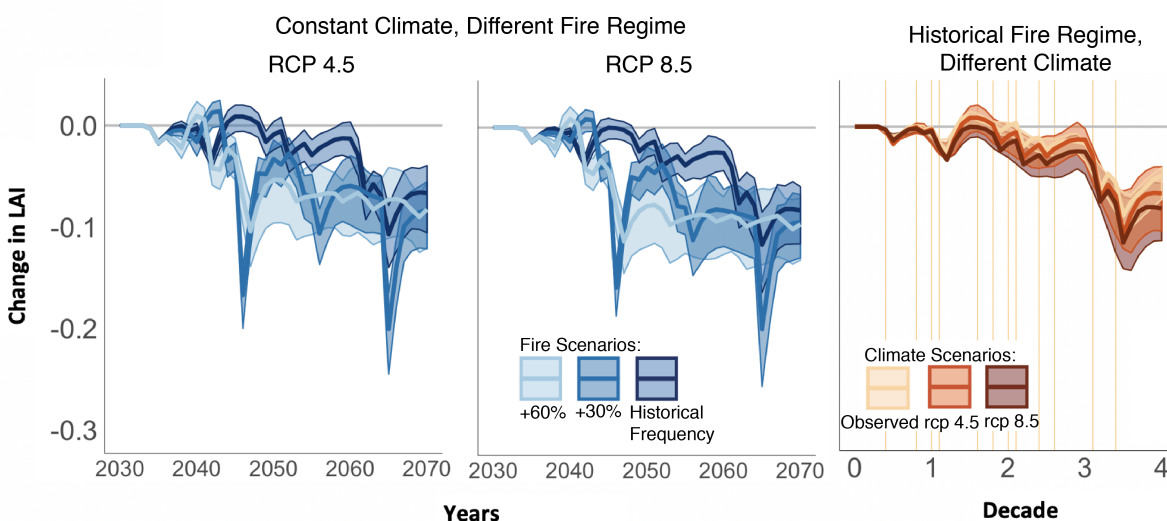

Figure C.6: Change in LAI due to fires for different climates and fire regimes (blues) and climate and historical fire regime only (reds). Vertical orange lines represent occurance of fires in the historical fire regime.

Seasonal Change in Water Balance

The seasonality of changes in the water balance due to fire activity is important to the ecology of the ICB and of Illilouette Creek itself. Figure C.7 shows the seasonality of observed changes due to the historical fire regime for the last modeling decade. Streamflow gain represents the largest change in the water balance and is concentrated around winter months under historical climates, and broadens throughout the fall - spring for RCP 4.5 and RCP 8.5. Transpiration change is the greatest around July for the historical climate, and June for RCP 4.5 and RCP 8.5 climates. Evaporation decreases slightly and near-uniformly from October to March. Soil storage change is highly uncertain (expected, since subsurface routing parameters formed the calibration parameters for RHESSys in this modeling exercise) and generally increases slightly during winter months.
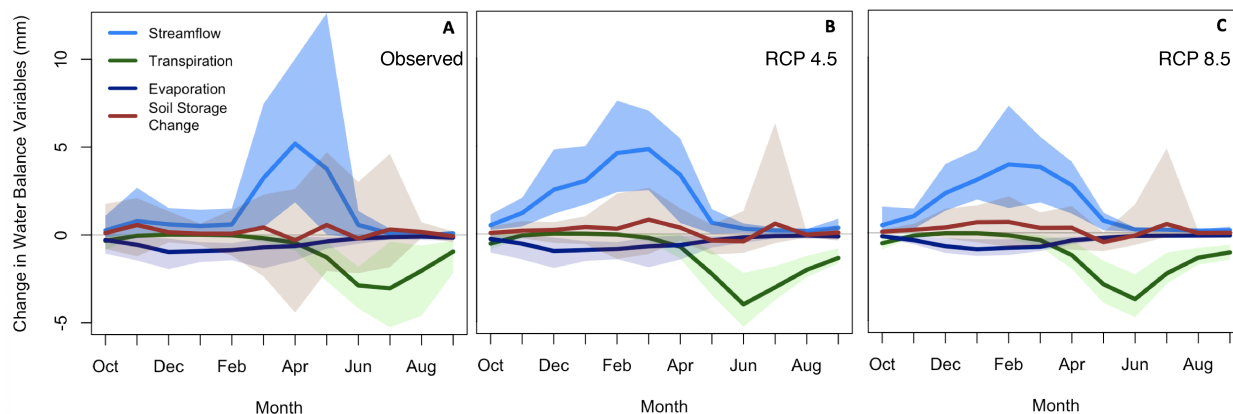
Figure C.7: Seasonality of the change in streamflow, transpiration, evaporation, and change in soil storage due to the historically observed fire frequency regime for the historical (A), RCP 4.5 (B) and RCP 8.5 (C) climate scenarios for the final simulated decade. Shading indicates 95 percentiles.

Snowpack

Snowmelt is a big contributor to streamflow in snow-dominated basins, such as the ICB. Hotter climates will decrease snowpack and that has implications on both seasonality of streamflow and streamflow amounts. In the absence of fires, snowmelt represents 95% of the peak streamflow volume. This number decreases to 83% and 75% for RCP 4.5 and RCP 8.5 climate scenarios, respectively (Figure C.8-A,B,C). Adding the effect of the historical fire regime, the maximum change in streamflow coincides with the timing of maximum change in snowmelt. Though there is a relatively larger change in streamflow than in snowmelt; the change in snowmelt is 47%, 31%, and 38% of the change in streamflow at the time peak streamflow (Figure C.8-D,E,F). This indicates that snowmelt is an important contributor to the total streamflow volume, though this contribution is less in the future climate.

Canopy sublimation accounts for 23-70% (average 48%) of total basin sublimation. Wildfires reduce canopy storage, causing snow sublimation to decrease across all climate and fire regime scenarios (Figure C.9). Changing sublimation affects both the evaporative budget (Figure 6 of the main text) and total snowpack. Change in sublimation depends largely on precipitation, temperature, and LAI. Even though there is more overall snowpack historically in 2000-2010 (517 mm SWE) vs 514 mm SWE (RCP 4.5) and 472 mm SWE (RCP 8.5) in 2060-2070, sublimation change due to the historical fire regime is greatest for RCP 4.5 climate scenario and lowest for RCP 8.5 climate scenario. Increasing fire frequency (blue plots in Figure C.9), decreases the time it takes to observe maximum change in sublimation due to fire.
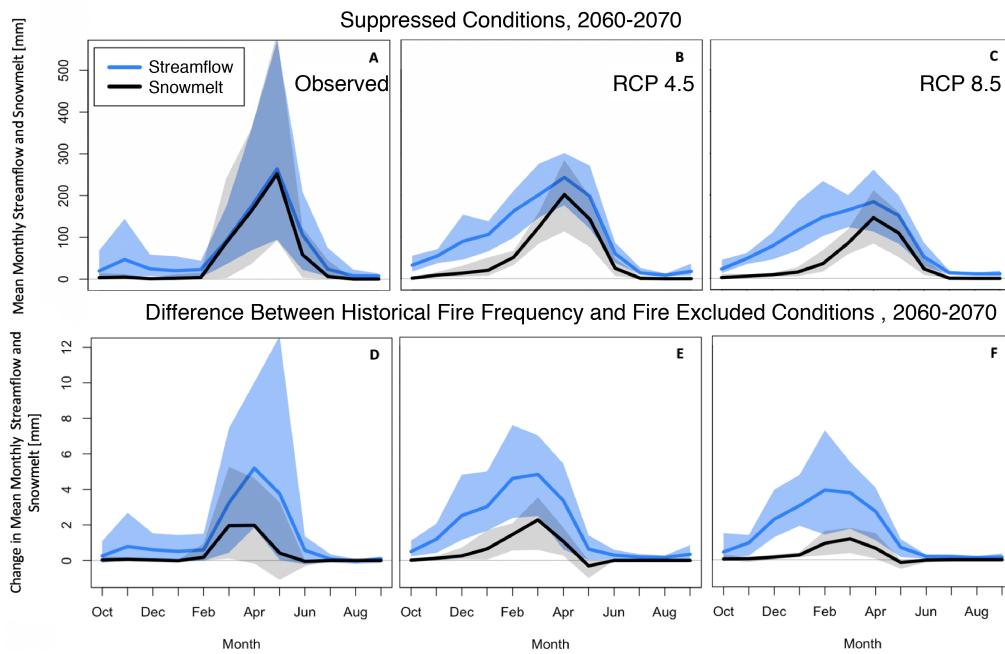
Figure C.8: Mean monthly total streamflow and snowmelt for fire excluded conditions for historical (A), RCP 4.5 (B) and RCP 8.5 (C) climate scenarios. Mean monthly total stream-flow and snowmelt change due to the historical fire regime for historical (D), RCP 4.5 (E) and RCP 8.5 (F) climate scenarios for years 2000-2010 (A and D) and 2060-2070 (B,C,E, and F). Shading indicates 95-percentile of all years and parameter sets
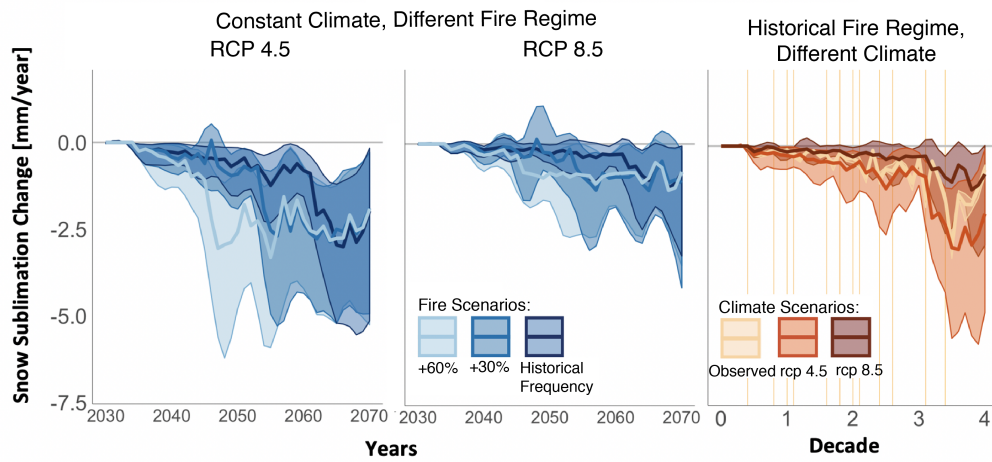
Figure C.9: Change in annual snow sublimation as a result of different climate and fire regime scenarios. Shading indicates a 95% confidence interval, vertical orange lines are observed historical fires.

Peak Streamflow

Any benefits associated with increasing streamflow could be offset if peak streamflow - i.e. flood casuing flows - are also increased. If wildfires increase high flows, dams might reach capacity faster and floods can be more likely, more dangerous and more extensive. To investigate the effects of wildfires on peak streamflow, we looked at maximum streamflow event of the year for all climate scenarios and compared it to the same day in the fire excluded ICB. Wildfire management causes on average a 1.1 mm, or a 3.2% increase in the volume of the maximum streamflow event by the final simulated decade. The increase is modest, but is not statistically significant across all fire and climate scenarios (Figure C.10). Due to the lack of high spatial resolution data over the ICB domain, RHESSys was not calibrated well to extreme streamflow events, however, so these findings are preliminary in nature.
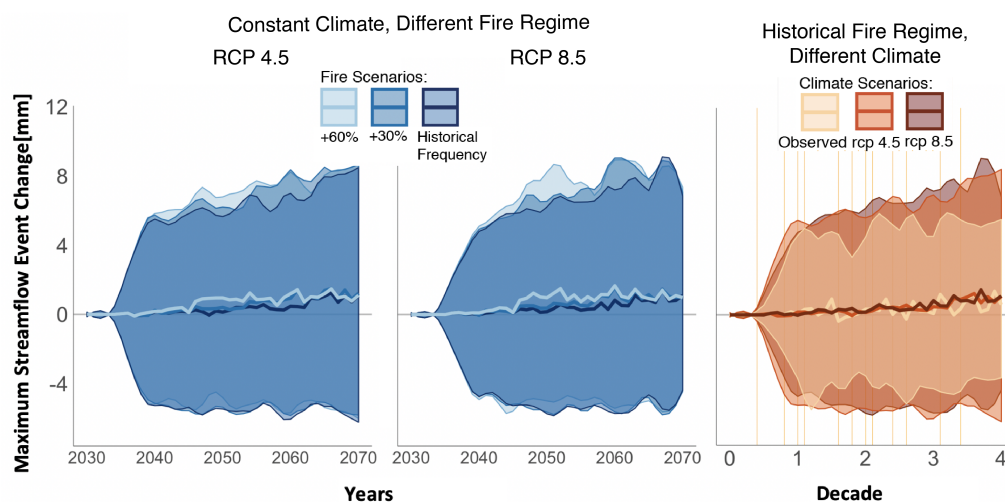

Figure C.10: Change in maximum streamflow of the water year as a results of different climate and fire regime scenarios.Vertical lines indicate occurrence of the historical fires. Shading indicates a 95% confidence interval.

C.6   Hydrological Modeling with Different Post-fire Vegetation Transitions

Wildfires in future climate are expected to cause different vegetation transitions from the observed historical transitions (see Appendix F). The model setup used here includes spatially-varying transitions to either new forest, shrubland, or meadow following high

severity fire, based on observed past transitions. However, in reality drier/hotter climates mean that vegetation is more likely to transition to shrubs (Cornwell et al., 2012). While we cannot couple post-fire vegetation transitions to climate within the RHESSys framework, we did perform additional analysis to determine the magnitude of uncertainty that the different vegetation transitions would impose on the hydrology of ICB. For this analysis, we compared model results from the historically observed post-fire vegetation transitions to the results from hypothetical situations in which every high severity fire patch transitioned entirely to either 1) shrub, 2) forest, or 3) wetland. Specifically, we compare hydrological outputs for the historical fire frequency regime to the fire excluded ICB hydrology for the RCP 4.5 and RCP 8.5 future climate ensembles. Though these vegetation transitions are not realistic in the future climate, they do provide additional bounds of uncertainty around the effects of the fire regime in the future climate.

All vegetation transitions resulted in similar hydrological outcomes as the historically observed vegetation transitions, though the magnitudes of change have some deviations (Figure C.11). Streamflow and subsurface storage are insensitive to the different vegetation transitions with little deviation from the mean and 95% confidence interval of the historical vegetation transition. Transpiration, evaporation, and maximum snowpack are more sensitive to the type of vegetation transition, though the difference between vegetation scenarios remains small.

The largest deviation from historical transitions was observed for vegetation conversion to all forest cover type, which is the least likely vegetation transition given climate change predictions. Forest LAI declined most rapidly and approached the LAI of wetland cover types, indicating that trees are not re-growing after disturbance under modeled future climates (likely due to higher water stress). On the other hand, shrubland cover types have the quickest post fire recovery rates.

In summary, our model results are not highly sensitive to the fact that we are not able to couple post-fire vegetation transitions to climate, given an extreme range of possible vegetation transitions. Modeling suggests that the hydrological outcomes of wildfire management in future climate will be similar to the historically observed outcomes for a given fire regime even if post-fire vegetation types shift. However, we want to acknowledge that post-fire vegetation transitions can in turn influence the fire regime itself (Syphard et al., 2018), thereby creating feedbacks that cause the fire regime to shift. Such vegetation-fire feedbacks are beyond the scope of the current study, but will be explored in future work.
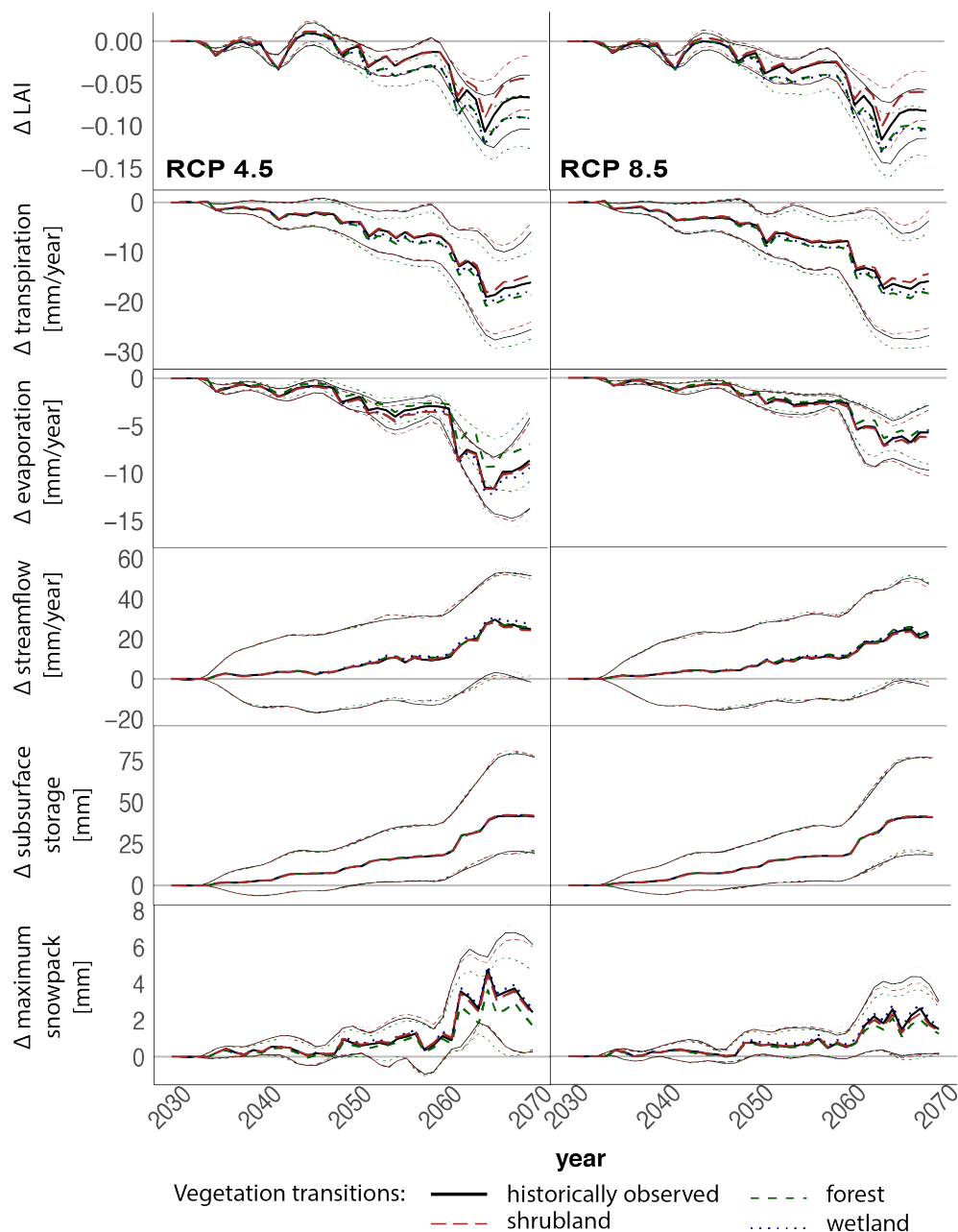
Figure C.11: All plots show the difference between the historical and excluded fire scenarios in ICB. Post-fire vegetation scenarios are shown with different dashed lines for transitions to all forest, wetland, and shrubland. Historically observed post-fire vegetation scenario is shown as a solid line. Hydrological outputs are representative of the RCP 4.5 and RCP 8.5 climates in the left and right column respectively. Thin lines indicate 95% confidence interval of the 930 model runs (93 parameter sets for each of the 10 GCMs), while thick lines represent average difference.

C.7 Hydropower and Water Supply Calculations

The following section provides supporting calculations for the revenue from water sales and hydropower generation.

Water Supply

Low-high bounds of modeled streamflow gain from ICB under the historical fire scenario are 19-29 mm of additional streamflow per year when compared to fire excluded ICB (Table 2 and Figure 5). The following calculation corresponds to ICB's entire area of 150 km^2. Using 2017 water year reports for the city of San Francisco, the cost of water for single-family residency for the first tier was 6$ per ccf (one-hundred cubic-feet) of water delivered (San Francisco Public Utilities Commission, 2014). This is the most conservative estimate of water use, and actual prices charged are higher for higher water use tiers and multi-family residential categories. Based on the above data, the cost of additional streamflow gain in ICB translated to San Francisco water sales is:

$$Water\ Sales =$$

$$19\ \text{to}\ 29\ mm * \frac{10^{-6}\ km}{mm} * 150\ km^2 * \frac{6\ \$}{ccf} * \frac{ccf}{2.83149\ m^3} * \frac{m^3}{10^{-9}\ km^3}$$

$$= 6.0 - 9.2\ million\ \$/year$$

Considering a proposed price of 9.6 $/ccf for 2020 WY (San Francisco Public Utilities Commission, 2018), the income from ICB's water gain will increase to 9.6 -14.7 million$ (an additional 3.6-5.5 million $/year). In 2017 WY, on average 36 million gallons per day (MGD) of water were delivered to residential customers (San Francisco Public Utilities Commission, 2017). ICB's additional water gain is:

ICB streamflow gain =

$$\frac{19\ \text{to}\ 29\ mm * \dfrac{10^{-6}\ km}{mm} * 150\ km^2 * 1\ \dfrac{1MGD}{3.78541178 \times 10^{-6}\ km^3}}{36\ MGD/day * 365\ days/year} * 100\%$$

$$= 5.7 - 8.7\%\ \text{of annual San Francisco residential water consumption}$$

Hydro Power

O'Shaughnessy Dam releases water from Hetch Hetchy reservoir and channels it into Canyon Power Tunnel, which is one of the forks that connects with the Hetch Hetchy Aqueduct. Kirkwood power station is the first power station below O'Shaughnessy Dam which generated 524 million KWh in 2017 from the flow from Canyon Power Tunnel (California Energy Commission, 2019a). Water flows into Mountain Tunnel and Moccassin power station below generating 324 million kWh in 2017 (California Energy Commission,

2019b). Therefore total power generation in 2017 from the flow coming directly from Hetch Hetchy reservoir was 849 million kWh. The flow through the Hetch Hetchy aqueduct is relatively stable year to year, equalling 265,000 acre feet per year (Aquafornia, 2008). Average residential electricity cost was .204 dollars per kWh in 2017 (Bureau of Labor Statistics, 2018). Using these numbers, the potential hydropower revenue from an increase in streamflow equal to that seen in ICB:

Hydropower revenue =

$$19 - 29 \ mm * 150 \ km^2 * \frac{10^{-6} \ km}{mm} * \frac{849 \ million \ kWh}{265,000 \ acre \ feet}$$
$$* \frac{acre \ foot}{1.23 \times 10^{-6} \ km^3} * \frac{0.204 \ \$}{kWh}$$
$$= 1.5 \text{ - } 2.3 \text{ million \$/year}$$